VIRAL AND CELLULAR TARGETS FOR THE VARICELLA-ZOSTER VIRUS ORF66 PROTEIN KINASE

by

Amie J. Eisfeld

Bachelor of Arts, University of Minnesota—Morris Campus, 1999

Submitted to the Graduate Faculty of

The School of Medicine in partial fulfillment

of the requirements for the degree of

Doctor of Philosophy

University of Pittsburgh

2007

UNIVERSITY OF PITTSBURGH

SCHOOL OF MEDICINE

This dissertation was presented

by

Amie J. Eisfeld

It was defended on

August 23, 2007

and approved by

Neal A. DeLuca, Professor
Department of Molecular Genetics and Biochemistry

Robert L. Hendricks, Professor
Departments of Ophthalmology, Molecular Genetics and Biochemistry, and Immunology

Russell D. Salter, Professor
Department of Immunology

Thomas E. Smithgall, Professor
Department of Molecular Genetics and Biochemistry

Paul R. Kinchington, Associate Professor
Departments of Ophthalmology and Molecular Genetics and Biochemistry
Dissertation Director

VIRAL AND CELLULAR TARGETS FOR THE VARICELLA-ZOSTER VIRUS ORF66 PROTEIN KINASE

Amie J. Eisfeld, PhD

University of Pittsburgh, 2007

Varicella-zoster virus (VZV) is a human alphaherpesvirus that causes two important diseases, chickenpox and herpes zoster, separated by a prolonged period of latent infection in which no disease occurs. VZV remains a serious public health concern despite the availability of licensed vaccines for the prevention of chickenpox during childhood and zoster in the elderly. The VZV ORF66 protein kinase is a well-established mediator of VZV tropism and pathogenesis *in vivo*, but information regarding the molecular mechanisms of ORF66 function is limited. ORF66 is orthologous to the alphaherpesvirus U_S3 kinase family, which is involved in regulating diverse aspects of the host environment. ORF66 has been implicated in nuclear exclusion of the VZV principle transcriptional regulator and tegument protein, IE62, during late-stage VZV infection; and in downmodulation of class I major histocompatibility complex surface expression, which is critical for the identification and elimination of infected cells by the adaptive immune system. However, the mechanisms underlying these processes are not well-resolved. In this work, I have significantly extended our understanding of known ORF66 functions during VZV infection, and I have established novel functions for both ORF66 and the IE62 protein. Purification of ORF66 allowed the development of an *in vitro* kinase assay, and I used this to prove that ORF66 directly phosphorylates IE62 adjacent to its nuclear localization signal to mediate nuclear exclusion. Additional investigations of IE62 nucleocytoplasmic trafficking revealed a novel nuclear export activity, which was multi-dimensionally regulated by intrinsic IE62 nuclear retention and

phosphorylation by kinase(s) other than ORF66. With regard to the ORF66 role in the regulation of MHC-I surface presentation, I developed assays with recombinant VZV expressing enhanced green fluorescent protein-tagged ORF66 to establish that ORF66 affects the cellular environment such that early MHC-I biogenesis is delayed, resulting in a reduction in total surface MHC-I. MHC-I studies indicated highly novel ORF66 nuclear distribution patterns, and a further examination of these revealed that ORF66 may regulate nucleocapsid morphogenesis or trafficking in VZV-infected nuclei. In sum, this work represents a major contribution to VZV biology and provides insights into a multi-functional mediator of VZV persistence and pathogenesis.

TABLE OF CONTENTS

LIST OF FIGURES

PREFACE

My decision to enter graduate school was spurred by my love of science, a desire to independently study in my field of choice, and an aspiration to make the world a better place for all humankind. The challenges of graduate study have only served to deepen my conviction that I have the strength to affect the world in a positive manner, and I consider this momentous academic achievement only the beginning of what I will learn, create and apply as a scientist and as a human being.

I thank all of the scientists at the University of Pittsburgh who influenced my education: Dr. Steven Phillips, who told me to learn to perturb the system; Dr. Ora Weisz for telling me to keep an open mind; Drs. Neal DeLuca, Gerard Apodaca and Jack Yalowich for their high expectations and skill in teaching me critical review; Dr. Joanne Flynn for her honesty and for setting such an excellent example for women in science; and the members of my thesis committee for their guidance and ideas throughout my dissertation research. Additionally, I owe gratitude to multiple technical specialists, without whom I would not have been able to succeed in many of my endeavors: Stephanie Turse, Karen Fite, Jean-Paul Vergnes, Nancy Zurowski, Kira Lathrop and Michael Yee.

My accomplishments would not have been possible without the careful guidance of my dissertation advisor, Paul "Kip" Kinchington. His critical mind, humility, and caring nature are inspiration for the type of scientist I hope to be. In him, I have gained a life-long friend.

Equally important to my success has been my husband, Curtis Fenney. He is my soul-mate, my best friend, and a continuous reminder that things are not always what they seem. It is impossible to put into words all of the ways that Curtis is an inspiration to me.

Finally, I thank all of my friends and family, both in Pittsburgh and throughout the world. You make life so colorful, and your influences on me as a scientist and a person are too enumerable to elaborate upon here. I love you all!!

1.0 INTRODUCTION

1.1 VARICELLA-ZOSTER VIRUS DISEASE AND PUBLIC HEALTH IMPACT

Varicella-zoster virus (VZV) causes two clinically significant syndromes in humans: varicella (chickenpox) during initial infection and herpes zoster (shingles) following reactivation from neuronal latency. Varicella is characterized by a highly contagious, but typically self-resolving, disseminated vesicular skin rash that erupts ~10-21 days following initial inoculation. Replication in skin results in the establishment of latent infection in the dorsal root ganglia of sensory neurons. In response to age or stimuli that induce cellular immune dysfunction (e.g., acquired immunodeficiency syndrome or immunosuppression due to transplantation), latent infections may reactivate, replicate in the ganglia, and cause herpes zoster: an often painful skin rash in the dermatome associated with the reactivated neuron (11, 102). VZV spreads to naïve hosts through respiratory inoculation, which can result from exposure to an infectious individual with either primary varicella or reactivated zoster disease.

Serious morbidity and mortality are associated with both varicella and herpes zoster. Previous to the licensing of the live, attenuated varicella vaccine in 1995 (Varivax, Merck), complications arising from varicella disease resulted in ~11,000 hospitalizations and ~100 deaths in the United States (US) annually (33). The most common cause for hospitalization is bacterial (*Staphylococcal* or *Streptococcal*) super-infection of VZV skin lesions. However, more serious

complications including invasive group A *Streptococcal* secondary infections, viral or bacterial pneumonia, or encephalitis may lead to mortality (92, 130). Reactivated VZV disease (herpes zoster) occurs once in a lifetime in ~30% infected individuals (102). A particularly excruciating and poorly understood complication associated with zoster is chronic pain at the epidermal site of replication, a condition known as post-herpetic neuralgia (PHN). PHN may persist for greater than a year following resolution of zoster skin lesions, and currently no efficacious treatment is available (70). Herpes zoster infection can involve ocular tissues, with serious manifestations resulting in vision problems, blindness and ophthalmic PHN (169). Disseminated varicella and zoster infections can occur in immunocompromised patients, such as transplant recipients, children with leukemia or lymphoma, and individuals with acquired immunodeficiency syndrome (AIDS) (9). Although VZV can be successfully treated with the herpesvirus-specific anti-virals (acyclovir, valacyclovir), extended treatments in AIDS patients have resulted in emergence of acyclovir-resistant VZV strains (77).

The serious nature of varicella and zoster disease provided the impetus for the development of the live, attenuated varicella vaccine, which was licensed in the in the United States (US) in 1995 for use in children 12 months of age or older (33). Varivax represents the first and only successful introduction of a herpesvirus vaccine among the human population. Varivax is estimated to be 70-90% effective in preventing VZV infection, and 90-100% effective against moderate to severe varicella disease. Despite the success of Varivax, several concerns remain: 1) Varivax maintains the ability to establish life-long latent infection and vaccine-associated herpes zoster has been observed (78). Over the long-term, the potential for Varivax reactivation, vaccine-associated herpes zoster, and serious complications is not known. 2) For reasons that are not yet completely clear, primary VZV infection acquired during adulthood

results in more severe varicella disease and a higher incidence of serious complications (33). The reduction in childhood varicella cases and opportunities for initial exposure due to implementation of the vaccine may result in an increased number of adult varicella cases among people who do not receive childhood vaccination. 3) The Hope-Simpson model of VZV pathogenesis postulates that immunological boosting against VZV occurs from repeated exposure to primary varicella infection throughout a lifetime, and suggests that zoster occurs when immunological boosts are lacking and VZV-specific immunity wanes (102). Thus, the elimination of the boosting population through vaccination against varicella may inordinately decrease the age at which initial zoster episodes appear and increase the incidence of zoster in the population in general, possibly giving rise to a higher incidence of serious zoster complications (29, 81). In 2006, the zoster vaccine (Zostervax; Merck) was approved for use in the US in people aged 60 years and older. However, Zostervax does not provide complete protection from herpes zoster episodes, and has been reported to reduce the incidence by only 51%, although cases of PHN were reduced by 66% (190).

Taken together, these observations accentuate the role of VZV as a significant human pathogen and important public health concern, and underscore the requirement for a more detailed understanding of the molecular basis of viral replication and the host-pathogen relationships that regulate VZV pathogenesis. A better understanding of VZV biology will ultimately assist in both prevention and treatment of VZV disease.

1.2 VZV TROPISM AND PATHOGENESIS

VZV is spread to naïve individuals by inoculation of the airway or conjunctiva with aerosolized droplets of infectious cell-free VZV derived from skin vesicles or respiratory secretions of persons exhibiting either varicella or zoster disease. VZV DNA is detected in peripheral blood mononuclear cells (PBMC) a few days after exposure, and secondary cell-associated viremia occurs just before eruption of vesicles at the skin surface (158). Varicella lesions are disseminated in skin throughout the infected host, and this differs markedly from the localized infection observed at the primary inoculation site during herpes simplex virus type 1 (HSV-1) infection. Interestingly, VZV preferentially infects human tonsillar $CD4^+$ T cells that exhibit memory and skin homing markers, implying that T cell infection may occur directly after initial inoculation, and that these cells may be required for the transfer of virus to epidermal cell layers (138). Additionally, monocyte-derived dendritic cells (DC) are susceptible to VZV infection *in vitro*, and can efficiently transfer infectious virus to co-cultured T cells, suggesting that DC could also be an initial target during primary infection (3, 179). In a third possibility, VZV may undergo limited replication in the respiratory epithelium around the tonsils, and these cells may mediate subsequent infection of T cells. In the skin, VZV replicates primarily in keratinocytes and works its way to the epidermal surface to result in infectious lesions, but also gains access to the axons of innervating sensory neurons. VZV infects sensory neurons, presumably travels by retrograde transport into neuronal cell bodies of the dorsal root (255), and establishes latent infection. In contrast with latency of HSV-1, in which only the latency associated transcript (LAT) is abundantly expressed, several VZV lytic antigen transcripts have been detected at abundant levels in latently infected human ganglia (44, 45, 170). Some evidence also exists for the expression of viral regulatory proteins during VZV latency, although these may aberrantly

localize to the cytoplasm (156). Although it is well-known that waning cell-mediated immunity contributes to reactivation of VZV, the molecular mechanisms that initiate this process remain largely unknown.

The exquisite host specificity of VZV has severely limited our ability to understand VZV pathogenesis, as no robust animal model of VZV infection exists. However, the development of a severe combined immunodeficient (SCID)-hu model of VZV infection, in which human tissue xenografts are implanted underneath the kidney capsule, has recently been developed to begin to unravel this process ((173) and reviewed in (10)). In SCID-hu mice, VZV transfer to skin xenografts can be mediated by release of infectious virus by infected tonsillar $CD4^+$ T lymphocytes (139). VZV replication in the epidermis is slow and spread occurs by cell-to-cell contact and fusion of adjacent cell membranes. A robust interferon α (IFNα) response occurs in the cells surrounding the site of VZV inoculation, providing an innate barrier that VZV must overcome to cause infectious lesions at epidermal surfaces. The extended period of growth required to overcome the IFNα barrier in skin correlates with the VZV incubation period in humans, and suggests that skin may become infected shortly after the initial inoculation. VZV can also mediate infection of dorsal root ganglia implants in the SCID-hu model, and establishes latent infections characterized by some viral transcript expression and no replication (255). One major disadvantage intrinsic to the SCID-hu model is the lack of an intact host immune system. Thus, the contributions of VZV genes involved in evasion of adaptive immunity cannot be readily assessed using this model of *in vivo* infection.

1.3 VZV VIROLOGY

1.3.1 Classification

Herpesviridae is a family of highly successful viruses that are widely disseminated in nature. More than one hundred viral species have been identified and diverse animal groups are affected, including mammals, birds, reptiles, fish, amphibians and bivalves (192). A single herpesvirus typically infects a single natural host. All herpesviruses encode linear, double-stranded (ds) DNA genomes ranging from 125-230 kbp in length, and express multiple enzymes involved in nucleotide metabolism, viral genome replication, and post-translational protein modification. Herpesviruses utilize the host cell nucleus for viral gene expression and genome replication and packaging; and progeny virions are assembled in the cytoplasm. In their natural reservoirs herpesviruses establish latent infections, in which only a sub-set of viral genes is expressed and no progeny virus is released. Importantly, latent viral genomes persist for the life of the host and maintain the capacity to replicate, cause disease and spread to uninfected hosts in response to stimuli that induce reactivation.

Herpesviridae is divided into three sub-families—*Alphaherpesvirinae*, *Betaherpesvirinae*, and *Gammaherpesvirinae*—based on biological properties, although more recent genome sequencing data validate these sub-classifications at the genetic level (192). Alphaherpesviruses have relatively short replication cycles, cause visible cytopathic effect in cultured cells, and establish latent infections primarily in ganglia. Beta and gammaherpesviruses have longer replication cycles, and betaherpesviruses establish latency in secretory glands, lymphoreticular cells or kidneys; while gammaherpesviruses are T or B lymphocyte-trophic and establish latency in lymphoid tissue. Humans are the natural reservoir for eight herpesviruses, including species

representing each sub-family, and these viruses are responsible for a wide array of clinically important diseases (summarized in Figure 1-1).

Virus	Sub-family	Clinical Manifestations
Herpes simplex virus type 1 (HSV-1)	alpha	oral* and genital herpes, HSK
Herpes simplex virus type 2 (HSV-2)	alpha	oral and genital* herpes
Varicella-zoster virus (VZV)	alpha	chickenpox and herpes zoster
Epstein-Barr Virus (EBV)	gamma	mononucleosis, cancers (BL, NPC)
Human Cytomegalovirus (HCMV)	beta	birth defects, pneumonia, retinitis
Human Herpesvirus 6 (HHV-6)	beta	roseola
Human Herpesvirus 7 (HHV-7)	beta	roseola
Kaposi's sarcoma virus (KSHV)	gamma	Kaposi's sarcoma, other cancers

* The predominant clinical manifestation observed.
BL= Burkitt's lymphoma
NPC= nasopharyngeal carcinoma

Figure 1-1 Human herpesviruses

The eight human herpesviruses are shown, along with the corresponding sub-family classification and the major clinical manifestation.

VZV is a human restricted alphaherpesvirus that is further classified into the genus *Varicellovirus*, which includes simian varicella virus and several agriculturally significant herpesviruses, such as pseudorabies virus (PrV) and bovine herpesvirus 1 (BHV-1). Varicelloviruses share the ability to cause widely disseminated infections in the skin, mucous membranes, viscera and nervous system tissues of natural reservoirs; and have similar genome arrangements with predominant isomeric forms (41). VZV is the only human varicellovirus, and is the prototype virus of the *Varicellovirus* genus. Among the human herpesviruses, VZV is most similar to herpes simplex virus types 1 and 2 (HSV-1 and HSV-2), which belong to the genus *Simplexvirus*. Despite their evolutionary digression, the VZV and HSV genomes are

remarkably co-linear in arrangement, and only five VZV gene products do not have corresponding orthologs in the HSV-1 genome (ORFs 1, 2, 13, 32 and 57) (48, 161-163, 197). Thus, many aspects of VZV replication classically have been assumed to emulate those of the better studied HSV-1. However, VZV and HSV-1 pathogenesis differ markedly, and accumulating molecular evidence suggests that many aspects of VZV replication are governed in a unique manner. The viral protein functions that underlie these differences are only beginning to be elucidated.

1.3.2 Structure and Assembly

Herpesviruses are structurally indistinguishable by negative staining in electron microscopy (EM). The herpesvirus particle is spherical in shape, and consists of a central nucleocapsid housing the electron-dense viral genome core, a host-derived lipid envelope studded by viral glycoproteins and an intermediate proteinaceous layer, known as the tegument, which resides between the nucleocapsid and the envelope (Figure 1-2).

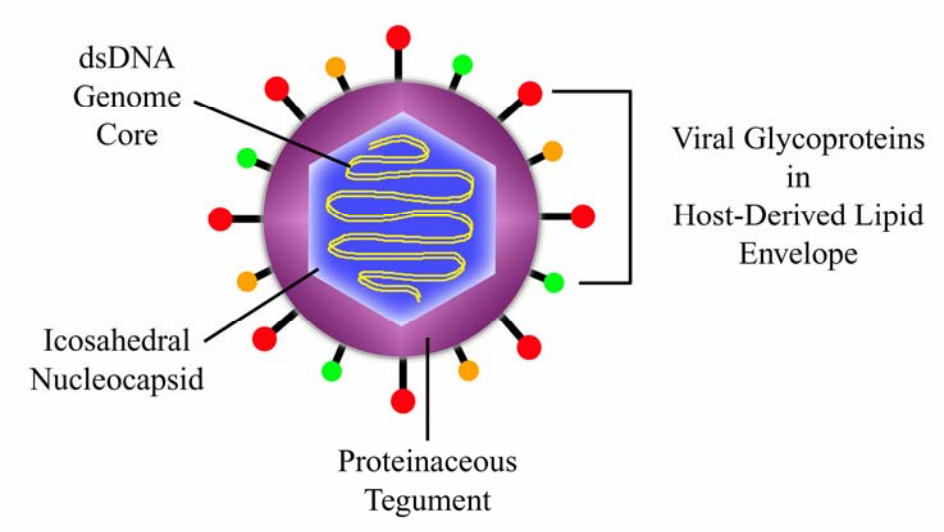

Figure 1-2 Graphical representation of the herpesvirus structure

The herpesvirus nucleocapsid (blue) contains one linear, double-stranded DNA genome (yellow) packaged in concentric spherical shells. The tegument (purple) resides between the nucleocapsid and the host-derived lipid envelope (grey). Viral glycoproteins associated with the envelope stud the virion surface (red, green, orange). The drawing is not to scale.

Genome: The VZV genome is the smallest of all the herpesviruses and consists of 125 kbp of dsDNA, which encodes at least 69 unique open reading frame (ORF)s (48). The genome is arranged into Unique long (U_L) and Unique short (U_S) regions, each bounded by terminal repeat sequences (Figure 1-3). The terminal repeats of the U_L segment (TR_L, IR_L) are short (~88.5 nt), while the terminal repeats of the U_S segment (TR_S, IR_S) are much longer (~ 7000 nt), code for three viral ORFs in duplicate (ORFs 62/71, ORFs 63/70 and ORFs 64/69), and include the origins of replication. Packaged VZV DNA exists predominantly in two equimolar isomeric forms, which differ in the inversion of the U_S region with respect to the nearly invariant configuration of the U_L region (128). The arrangement of VZV DNA within the nucleocapsid is not currently known. However, in HSV-1 the nucleocapsid core contains one linear dsDNA molecule, which is arranged in concentric spherical shells within the capsid (259).

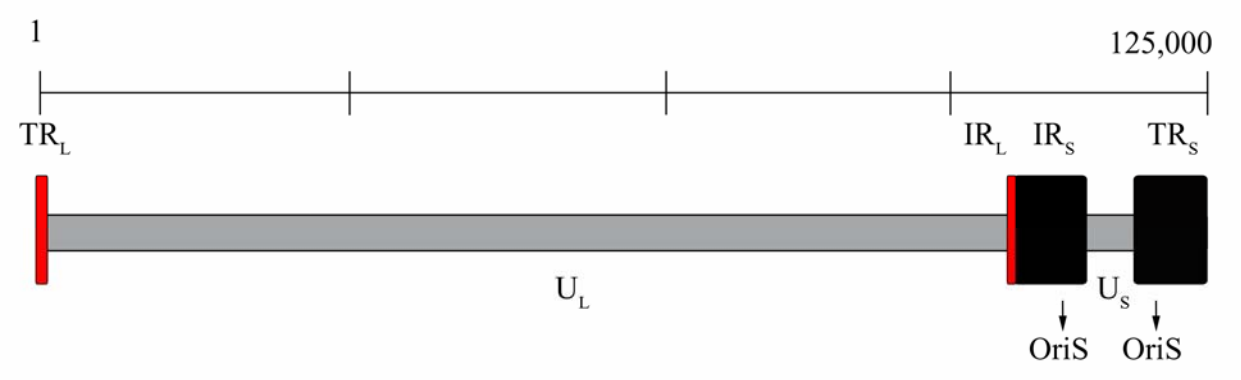

Figure 1-3 The VZV genome

The VZV genome consists of 125 kbp of double-stranded DNA, arranged into unique long (U_L) and unique short (U_S) regions (gray), bounded by internal and terminal repeats (TR_L and IR_L, red; TR_S and IR_S black). The unique regions are indicated by labels below the genome, while the repeat regions are indicated by labels above. The lengths of each segment are drawn to scale, except for the TR_L, IR_L, which have been enlarged slightly for ease of visualization. The scale bar at the top facilitates estimation of the approximate length of each genome segment in nucleotides. The two origins of replication are indicated.

Nucleocapsid: VZV capsids exhibit icosahedral symmetry, contain 162 capsomeres and have a diameter of 80-120 nm (41). The VZV ORF33 protein is the predicted VZV assembly protein, and has demonstrated serine protease auto-cleavage activity, which releases the ORF33.5 product presumably to act as scaffolding for capsid morphogenesis (72, 165). ORF33 can replace its HSV-1 counterpart (VP24) in a baculovirus expression system to promote assembly of HSV-1 capsid shell proteins (204), indicating that HSV-1 and VZV mechanisms of capsid assembly may be similar. The VZV ORF40 gene encodes the major capsid protein (MCP; HSV-1 ortholog VP5), which is expressed as a 155 kDa nuclear antigen in infected cells (236). By homology with HSV-1, the additional VZV capsid proteins are likely those encoded by ORF23 (minor capsid protein; HSV-1 VP26), and ORF20 and ORF41 (triplex proteins; HSV-1 VP19C and VP23, respectively). Studies have shown that nucleocapsids are detected in VZV-

infected cell nuclei at 24-48 hours post-infection (hpi), and greatly increase in number by 72 hpi (89). They are observed both individually and in small clusters.

Tegument: The herpesvirus tegument consists of upwards of 20 viral protein products, which are released into the cytoplasm upon entry and uncoating and are immediately available to assist in the establishment of a pro-viral replication state. Some recent evidence also suggests the presence of cellular proteins and viral mRNAs (16, 17, 27, 222, 230, 239). The total protein complement of the VZV tegument is not known, but many reports indicate that the VZV tegument is very different from that of HSV-1. HSV virions carry a tegument associated non-specific RNase (U_L41 or *v*irion *h*ost *s*hutoff, vhs) that is responsible for cleaving host mRNA to prevent new host protein synthesis (60, 66, 141). One vital result of *vhs* activity is the inhibition of interferon production in newly infected cells (35, 56, 183). The VZV ortholog of *vhs* is not detected in purified VZV particles (217). In HSV-1, an essential tegument protein is the α-*trans*-inducing factor (α-TIF), which is a transcriptional transactivator critical for the expression of immediate early viral genes in the absence of *de novo* viral protein synthesis (248). The VZV ortholog to α-TIF, the ORF10 protein product, is associated with VZV particles (125), but is not essential for viral replication in culture (42), although it is necessary for pathogenesis in skin in the SCID-hu model (34). Several other VZV transcriptional regulators are tegument-associated, and these may assist in activation of VZV gene expression in the absence of ORF10 protein expression. Specifically, the principle VZV transcriptional transactivator, IE62, is an abundant tegument protein (125), whereas its HSV-1 counterpart (ICP4) is present only in minor amounts (24, 252). The VZV ORF4 (HSV-1 ortholog = ICP27) and ORF63 (HSV-1 ortholog = ICP22) protein products are also associated with the VZV tegument, but the ORF61 (HSV-1 ICP0) protein is not (122). It is unknown whether HSV-1 ICP22 is a tegument protein; however, while

ICP27 is not a tegument component, small amounts of ICP0 have been detected in the HSV-1 virion particle (251). The VZV-encoded ORF47 and ORF66 serine/threonine (Ser/Thr) protein kinases have both been reported to be associated with the VZV tegument, although the ORF47 kinase is more abundant and may be responsible for virion kinase activity (123, 226).

Envelope and glycoproteins: VZV encodes 9 putative and known viral glycoproteins that are presumed to be involved in mechanisms of attachment and entry, envelopment, cell-to-cell spread and egress (127). The most abundant VZV glycoprotein expressed at the infected cell surface is gE, which is also present in the TGN, and is a component of the virion envelope (119, 171, 242, 261). gE is responsible for binding the VZV receptor for cell-to-cell fusion in culture, the insulin-degrading enzyme (150, 151). VZV glycoproteins traffic into the Golgi apparatus, initially independent of the maturation of the VZV nucleocapsid, in preparation for virion assembly in modified cisternae of the *trans*-Golgi network (TGN) (79, 89, 260).

1.3.3 Regulation of Viral Gene Expression

Herpesvirus gene expression during lytic infection occurs in a transcriptional cascade regulated by both cellular factors and viral proteins, characterized by temporally-defined waves referred to as α, β, and γ (100, 101). Upon infection with HSV-1, the essential α-TIF protein is released from the tegument and enters the nucleus to activate expression of a sub-set of viral genes, known as the Immediate Early (IE) or α genes. α-TIF forms a complex with the cellular Oct-1 and HCF-1 transcription factors, and together this complex binds to a specific motif (TAATGARAT) in the enhancer region of IE promoters (248). IE transcripts accumulate in the absence of *de novo* protein synthesis, and have roles in regulating the viral transcriptional program and suppression of mechanisms of host defense against infection. The next wave of

viral gene expression (Early; E or β genes) is activated by the IE genes, and these mainly include factors involved in DNA metabolism and viral genome replication. As E genes require IE genes for expression, they are not made in the absence of *de novo* protein synthesis. Late (L or γ) genes are viral structural (capsid, tegument or envelope) proteins or those that facilitate genome packaging and egress from the infected cell. L gene expression predominantly ensues following initiation of viral genome replication, and L genes are divided into two classes: γ1 and γ2. γ1, or "leaky late", genes are made to low levels before genome replication but peak in expression after replication begins; while γ2, or "true late", genes are only expressed after genome replication. Thus, γ1 genes are made in the presence of genome replication inhibitors, while γ2 genes are not expressed in this situation.

The highly cell-associated nature of VZV infection does not permit high multiplicity synchronous infection, and thus classification of the vast majority of viral gene products into specific temporal classes of expression has not been performed. Exceptionally low titer "cell-free" VZV can be prepared by mechanical disruption of infected cell membranes, and this combined with immunofluorescence-based methods has been used to demonstrate that proteins from ORFs 4, 62 and 63 (orthologs of HSV-1 ICP4, ICP27 and ICP22, respectively) are IE genes (50, 52, 67). In the absence of experimental data, the regulation of most VZV gene expression is assumed to mirror that of corresponding HSV-1 orthologs, although it should be noted that some differences have been experimentally identified. For example, the VZV α-TIF ortholog, ORF10, does not encode an acidic C-terminal activation domain as is observed with HSV-1 (164), is a non-essential protein in culture (42), and may utilize different *cis*-acting elements to control IE gene expression (176).

1.3.4 Cosmid-based system for generation of VZV recombinants

The highly cell-associated nature of VZV also makes isolation of pure populations of mutant virus by standard homologous recombination methods very difficult. However, cosmid-based vectors encoding overlapping segments of the VZV genome have been extensively used to generate mutations in specific VZV genes within both the VZV vaccine strain (vOka) and the parent of the vaccine strain (pOka) (14, 34, 39, 43, 107, 187, 219, 220, 254). Isolation of cosmid DNAs allows specific manipulation of the VZV genome, and once the intended mutations are generated, cosmids are co-transfected into melanoma cells for derivation of isogenic virus expressing these mutations. The cosmid-based recombination system has substantially improved our understanding of several VZV protein functions in the context of infection, and is facilitating our appreciation of the molecular basis for differences in VZV and HSV-1 pathogenesis.

1.4 THE VZV ORF66 PROTEIN KINASE

The goal of this dissertation was to expand our knowledge of the molecular mechanisms of function of a VZV-encoded S/T protein kinase, ORF66. ORF66 was putatively identified as a protein kinase based on significant sequence similarity at the primary amino acid level with known eukaryotic protein kinases (ePKs), following the initial sequencing of the VZV genome (48, 226). In the proceeding sections, I give an overview of ePKs, an introduction to the VZV protein kinases encoded by ORFs 47 and 66, and a more detailed discussion of the fundamental molecular properties of ORF66.

1.4.1 Context: Eukaryotic Protein Kinases

Protein kinases (PKs) are enzymes that catalyze the reversible, covalent addition of a phosphate group from a high-energy donor molecule (e.g., ATP) to the –OH group in a serine (Ser or S), threonine (Thr or T) or tyrosine (Tyr or Y) side chain of a substrate protein, in a reaction termed phosphorylation. A single substrate phosphorylation event adds two negative charges, which induces an overall change in protein structure that ultimately may affect catalytic activity or protein:protein interactions. PKs may be dedicated to a single or related group of substrate proteins, or may be multi-functional and modify diverse targets. The specificity of kinase-mediated substrate phosphorylation is constrained by the ability of the kinase to recognize the specific contextual amino acid residues that surround the target S/T/Y phosphorylation site. However, additional levels of constraint reside in the expression pattern and spatial distribution of the kinase and the substrate within the cell, and their ability to physically associate under physiological conditions. ePKs regulate signaling pathways induced by both extracellular and intracellular signals, and are involved in diverse cellular processes including metabolism, transcription, cell cycle progression, immune activation, regulation of cellular shape and apoptosis.

The ePK catalytic domain consists of a contiguous stretch of approximately 250 amino acids, which are divided into 11 major conserved sub-domains that are partially defined by a set of nearly invariant amino acids (86, 87). Some universal structural characteristics include an N-terminal glycine loop motif, which stabilizes nucleotide binding; a nearby invariant lysine residue, which is involved in phospho-transfer; and downstream central catalytic core, which contains residues involved in ATP interaction, Mg^{2+} (salt) bridge formation, and phospho-

transferase activity. Specific sequences in the C-terminal portion of the ePK catalytic domain distinguish S/T kinases from Y kinases.

1.4.2 VZV Protein Kinases: ORF47 and ORF66

VZV encodes two genes, ORF47 and ORF66, which contain motifs consistent with catalytic domains of eukaryotic S/T PKs (226). Much is known with regard to the function of the ORF47 kinase, which is the VZV ortholog to the U_L13 protein kinase family conserved among all herpesviruses. ORF47 is critical for VZV replication in both human skin xenografts and thy/liv implant-derived T lymphocytes in the SCID-hu model *in vivo*, and it serves important structural and catalytic roles in the viral life cycle (21, 22, 174). Conditions under which the ORF47 kinase is active *in vitro* have been determined, and these include a requirement for poly-amines; stimulation in the presence of Mn^{2+} over Mg^{2+}; the ability to exchange GTP for ATP as a phosphate donor; and activity in the presence of heparin, an effective inhibitor of the cellular casein kinase II (CKII) (121, 185, 186). The minimum ORF47 consensus sequence has been derived through extensive analysis of ORF47 *in vitro* targets: S/T-X-D/E-D/E, (D=aspartic acid; E= glutamic acid; X=any amino acid except for arginine/R or lysine/K) (120). While this is similar to motifs recognized by CKII (166), ORF47 kinase activity has been differentiated from that of CKII both *in vitro* and in VZV-infected cells (119, 120, 186). Several viral protein targets have been identified for the ORF47 kinase, including gE and the VZV IE62 transactivator. ORF47 phosphorylates the gE cytoplasmic tail, thereby regulating its cellular distribution and fusogenic properties in VZV-infected cells (21, 119). ORF47 phosphorylates IE62 *in vitro* (121, 185, 186); mediates phosphorylation of co-precipitated IE62 from infected cells, and may

facilitate IE62 nuclear exclusion during late-stage infection in a kinase activity dependent manner (22).

Much less is known with regard to the functions of the ORF66 kinase during VZV infection, although its role in pathogenesis has been firmly established. The ORF66 gene resides within the U_S region of the VZV genome, and is an ortholog of the U_S3 kinase family, members of which are expressed only among the alphaherpesviruses. Recombinant VZV lacking ORF66 expression are minimally impaired for replication in melanoma cells in culture (91, 220), but are significantly impaired for replication in cultured T lymphocytes (224). *In vivo* data reflect this cell-type-specific effect on VZV tropism, in that VZV lacking ORF66 reaches similar titers as wild-type virus in skin xenografts in the SCID-hu model, but is severely attenuated for replication in thy/liv implant-derived T lymphocytes (174, 220). Since T cells are critical for VZV viremia and dissemination in the infected host, these data indicate that ORF66 expression is a major determinant of VZV virulence and pathogenesis *in vivo.*

1.4.3 ORF66: Fundamental Molecular Properties

In the context of infection, ORF66 is likely expressed with early kinetics, similar to orthologous U_S3 kinases from other herpesviruses. However, this has not been experimentally established, and no current literature regarding the regulation of the ORF66 promoter by viral or cellular factors is available. In HSV-1 and PrV infections, long and short U_S3 transcripts are expressed (202, 238), but only the full-length ORF66 transcript has been detected during VZV infection (219). ORF66 is a 393 amino acid protein, encoded by nucleotides 113,037-112,333 in the VZV Dumas reference genome sequence. Early studies identified ORF66 as a 48 kDa phosphoprotein when expressed in VZV-infected cells, and demonstrated that ORF66 expressed from a vaccinia

virus vector was exclusively cytoplasmic (226). In contrast with this, studies in our lab have shown that HA-tagged ORF66 transiently expressed from a plasmid in the absence of additional exogenous protein expression is localized to both the nucleus and the cytoplasm in transfected human melanoma cells (124). More recent studies have identified ORF66 in the cytoplasmic fraction during VZV infection, as well as detectable amounts in the soluble nuclear fraction (219). Thus, it ORF66 is both a nuclear and a cytoplasmic protein. Other than phosphorylation, no additional post-translational modifications have been reported for ORF66.

The ORF66 catalytic domain resides between amino acids 93-378, as determined through a query of the Conserved Domain Architecture Retrieval Tool (CDART) (75). Specific motifs within this domain are highlighted in Figure 1-4. There have been no reports of any mutations in ORF66 N-terminal or C-terminal regions that lie outside of the kinase motif, and it is currently unknown the extent to which these contribute to ORF66 functions. I consider it likely they are involved in specific protein:protein interactions.

ORF66 Primary Amino Acid Sequence:

```
  1 MNDVDATDTF VGQGKFRGAI STSPSHIMQT CGFIQQMFPV EMSPGIESED DPNYDVNMDI
 61 QSFNIFDGVH ETEAEASVAL CAEARVGINK AGFVILKTFT PGAEGFAFAC MDSKTCEHVV
121 IKAGQRQGTA TEATVLRALT HPSVVQLKGT FTYNKMTCLI LPRYRTDLYC YLAAKRNLPI
181 CDILAIQRSV LRALQYLHNN SIIHRDIKSE NIFINHPGDV CVGDFGAACF PVDINANRYY
241 GWAGTIATNS PELLARDPYG PAVDIWSAGI VLFEMATGQN SLFERDGLDG NCDSERQIKL
301 IIRRSGTHPN EFPINPTSNL RRQYIGLAKR SSRKPGSRPL WTNLYELPID LEYLICKMLS
361 FDARHRPSAE VLLNHSVFQT LPDPYPNPME VGD
```

Figure 1-4 ORF66 primary amino acid sequence

The ORF66 primary amino acid sequence is represented in single letter code. The consensus catalytic motif is shown in green, with the conserved regions involved in ATP-binding and phosphor-transfer indicated: ATP-stabilizing glycine loop (orange); invariant ATP-binding lysine (red); and catalytic core (purple). Letters in black are the terminal sequences likely involved in specific protein:protein interactions. The relative amino acid numbers (every 60) is indicated to the left.

ORF66 induces kinase activity in VZV-infected cells, either due to intrinsic catalytic activity, or by activation of cellular kinases (91). ORF66 is highly insoluble and inefficiently immunoprecipitated from VZV-infected or transiently expressing cells (unpublished observations). For this reason, high level purification of ORF66 for the establishment of an *in vitro* kinase assay has not been possible, and thus the specific consensus motif phosphorylated by ORF66 has not been determined. Related U_S3 kinases preferentially target highly basic consensus motifs and phosphorylate S/T residues downstream of these (47, 116, 145, 206, 207). The preferred phosphorylation motifs for HSV-1 and -2 are shown in Figure 1-5.

Known U_S3 Phosphorylation motifs	
HSV-1 Consensus	$(R)_N$-X-(S/T)-Y-Y
HSV-1 Preferred	R-R-R-R-X-S
HSV-2 Most preferred	R-R-R-R-Y-S-V-A

N= >2; X= absent or any amino acid, with preference for Arg, Ala, Val, Pro, Ser; Y= X, but not absent, Pro or acidic amino acid

Figure 1-5 Known U_S3 phosphorylation motifs

Phosphorylation motifs for HSV-1 and HSV-1 are shown on single letter amino acid code, with the phosphorylated residue underlined.

Recent reports have provided evidence that ORF66 transcripts and possibly proteins are expressed in latently infected human ganglia (44, 45). While ORF66 is not required for the establishment of latency (218), its expression during latent infection may imply a role in the regulation of the neuronal environment or other latency-associated VZV antigens to contribute to the maintenance or persistence of latent viral genomes.

1.5 VIRAL AND CELLULAR TARGETS FOR ORF66

While the literature regarding specific functions of the ORF66 protein kinase is somewhat limited, U_S3 orthologs have been studied quite extensively. This group of kinases is highly multi-functional and well known to modulate the cellular environment to promote various aspects of infection. In the sections below, I outline well-characterized U_S3 kinase functions, and describe the proteins and pathways that are known to be affected by ORF66.

1.5.1 U_S3 kinases affect diverse aspects of the host environment

U_S3 kinases have been primarily implicated in regulation of the cellular environment during infection. Several viral protein targets are known, but the role of these phosphorylations in the context of infection have not been clearly defined, and thus are not included here.

i) Regulation of apoptosis. U_S3 kinases from HSV-1 and PrV are involved in preventing apoptosis induced by exogenous stimuli, pro-apoptotic cellular proteins, and infection with mutant viruses (53, 71, 74, 112, 149, 188). Studies with HSV-1 U_S3 indicate that this may occur through activation of the cellular PKA pathway (19), and may be partially dependent on inhibitory phosphorylation of the cellular pro-apoptotic protein BAD (18, 32). In PrV, inhibition of apoptosis has been shown to be dependent on U_S3 kinase activity, as a point-mutated inactive version expressed in the context of infection failed to protect cells from apoptosis or induce BAD phosphorylation (53). Very recent studies in VZV-infected T lymphocytes demonstrate that the ORF66 protein kinase prevents activation of caspases in VZV-infected T-cells in a kinase activity dependent manner (219, 220).

ii) Regulation of capsid egress from the nucleus. U_S3 null viruses from HSV-1, PrV, and an avian alphaherpesvirus, Marek's Disease Virus (MDV), accumulate enveloped virions in the peri-nuclear space (between the inner and outer nuclear membranes), implying a role in efficient capsid egress (131, 212, 215, 221, 241). Peri-nuclear virions were not evenly distributed in these mutants, and rather accrued in clusters. Recent studies suggest that U_S3 proteins mediate phosphorylation of cellular proteins of the nuclear lamina, including lamins and emerin, and that these phosphorylations induce subtle changes in protein localization at the nuclear membrane (144, 181) (178). Such changes may assist in capsid nuclear egress by uncoupling interactions between the nuclear lamina, the actin cytoskeleton and chromosomes. In one study comparing VZV expressing or lacking ORF66, fewer capsids were apparent in infected T-cell nuclei, but capsid clusters were not observed in the space between the inner and outer nuclear membranes (220). No differences were observed between the two viruses in melanoma cells.

iii) Regulation of cell-to -cell spread. The PrV U_S3 kinase is sufficient to induce actin stress fiber breakdown in both transfected and PrV-infected cells (237). Elegant experiments demonstrated that actin stress fiber breakdown was concomitant with the formation of actin and microtubule-containing projections in PrV-infected cells, and these contained viral particles that moved towards the projection tip (63). In low-density cells, the ability of U_S3 to induce projections was important for cell-to-cell spread. Similar effects on actin stress fiber formation have been described for MDV (221). The cellular protein targeted by U_S3 kinases to induce this effect is currently unknown, and it is also not known whether VZV ORF66 can induce these effects.

iv) Regulation of HDAC. Serendipitously, Poon, et. al. made the discovery that HSV-1 U_S3 expression could substitute for the histone deacetylase (HDAC) inhibitor, sodium butyrate,

to promote *trans*-gene expression in eukaryotic cells infected with baculoviruses (201). This suggests that this U_S3 kinase is involved in the negative regulation of HDACs, and it was hypothesized that this may be for the purpose of promoting viral gene expression in HSV-1 infected cells. It was subsequently determined that HDAC1 and 2 are differentially post-translationally modified and possibly translocated to the cytoplasm in a U_S3-dependent fashion (84, 201). It is not currently known whether ORF66 has the capacity to affect HDACs, either alone of in the context of VZV infection.

v) Regulation of the cellular response to viral infection. The deletion of U_S3 in the context of HSV-1 infection resulted in increased sensitivity to type I interferon (198). ORF66 was reported to have the ability to attenuate cellular signaling in VZV-infected T cells treated with γ-interferon, in that the levels of phosphorylated Stat1 were reduced (220).

vi) Known ORF66 targets are unique compared to other U_S3 kinases. At the outset of this project, it was unknown whether ORF66 affected any of these processes. However, two unique roles had been identified for the ORF66 kinase, including: 1) nuclear exclusion of the VZV principle transcriptional transactivator, IE62, in late-stage VZV infection (127); and 2) the possible downregulation of class I major histocompatibility complex (MHC-I) surface expression (2).

1.5.2 A viral target for ORF66: VZV IE62

Studies in our lab have identified the only known viral protein target affected by the ORF66 protein kinase: the principle transcriptional regulator and major tegument protein, IE62 (124). IE62 is completely nuclear during early VZV infection, but becomes predominantly cytoplasmic in late-stage infected cells as a result of the expression of ORF66. In transiently expressing cells,

ORF66 co-expression is sufficient to mediate IE62 nuclear exclusion, establishing that additional VZV gene expression is not required for this ORF66 function.

IE62 is a 1310 amino acid, heavily phosphorylated protein in VZV-infected cells, which is resolved at ~175 kDa by SDS-PAGE analysis. The IE62 gene is encoded in duplicate in the VZV genome at ORFs 62 and 71, residing in the U_S region internal and terminal repeats. Based on sequence similarity with ICP4 and IE62 truncation mapping studies, five distinct functional domains have been assigned within the IE62 primary sequence (15, 162). A scheme of these regions and a summary of domains involved in transactivation activities are summarized in Figure 1-6. Significant homology with HSV-1 ICP4 is observed in region 2, the DNA-binding and dimerization domain (DBDD); and the C-terminal region 4, for which no specific function has been determined. Lesser homology is observed in regions 1, 3 and 5. Region 1 contains a potent N-terminal activation domain (aa 1-86), and a poly-serine/acidic tract (pSAT; aa 353-371). The function of the pSAT is not known, but is likely a major substrate for phosphorylation by the cellular casein kinase II (CKII) or the VZV ORF47 kinase (58, 119, 120, 186). Region 3 contains the IE62 nuclear localization signal (NLS), which is of the classic type and is arginine/lysine (R/K)-rich ($_{677}$RLRTPRKRK$_{685}$) (129). Interestingly, region 5 contains a unique repeat of the N-terminal pSAT, which is not encoded by ICP4, and which may represent an additional CKII or ORF47 phosphorylation site (aa 1285-1295). A segment at the joint of regions 4-5 may be involved in both transactivation and repression activities (15), but no other function has been assigned to regions 4 or 5.

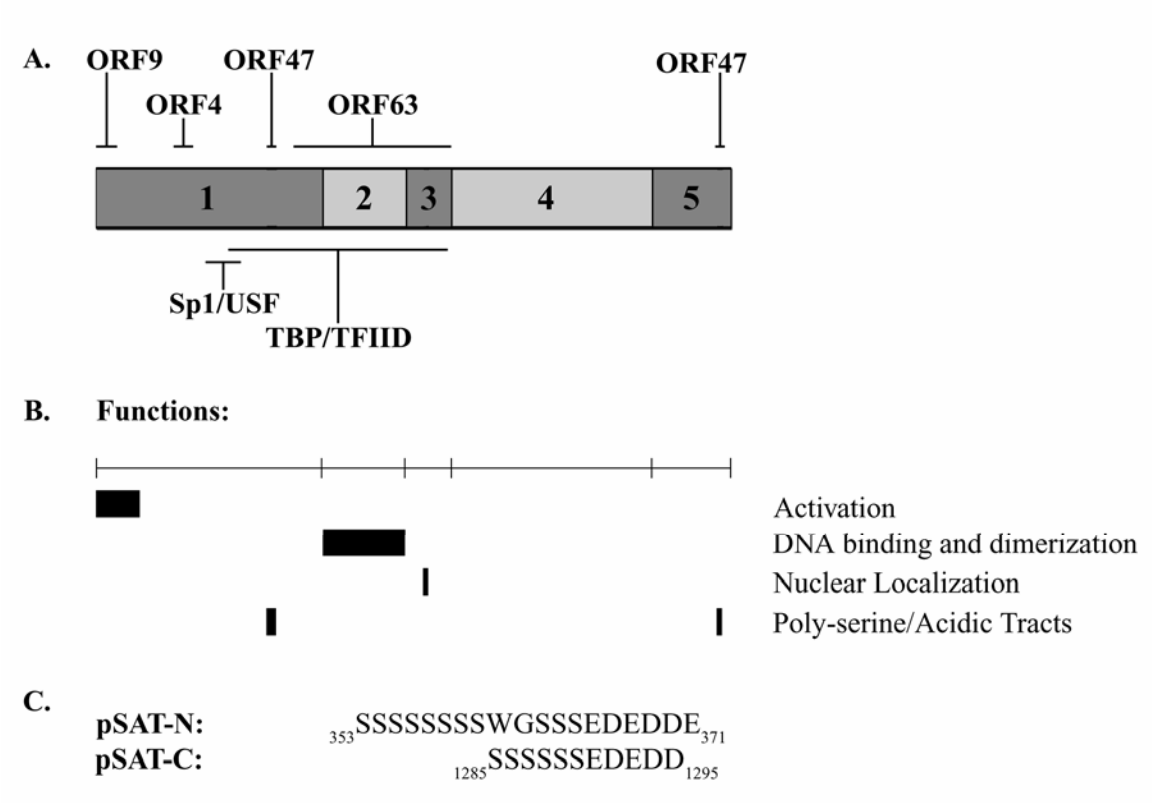

Figure 1-6 IE62 functional and protein interaction domains

A. IE62 homology with ICP4: dark gray regions are representative of low homology, while light gray regions have high homology. Regions involved in binding specific viral or cellular proteins are indicated above and below, respectively. **B.** Known IE62 functions and the regions to which they map are represented by the black boxes. IE62 functions are indicated to the right. **C.** Poly-serine/Acidic tract (pSAT) amino acid sequences in single letter code, with the position within the IE62 annotated. All components of the drawing are to scale.

At the primary amino acid level, IE62 exhibits homology with the HSV-1 ICP4 transcriptional regulator, and the IE62 gene can complement HSV-1 expressing ICP4 mutants or replace ICP4 in the HSV-1 genome (54, 64). Since HSV-1 carrying IE62 in place of ICP4 exhibits reduced replication relative to wild-type HSV-1, the mechanism of ICP4 and IE62 transactivation may involve slightly different processes. IE62 transactivates expression from all putative classes of VZV promoters (15, 40, 195), positively and negatively influences its own

promoter activity (55, 196), and substantially enhances the infectivity of VZV DNA (177). The specific mechanism whereby IE62 transcriptional regulation occurs is not known, but is likely similar to that of ICP4, involving recruitment and stabilization of components of the general transcription machinery on viral promoters (31, 253). IE62 is phosphorylated by viral and cellular protein kinases (124, 125), is an abundant tegument protein (125), and has multiple experimentally mapped protein:protein interactions with both viral and cellular factors (summarized in Figure 1-6A) (22, 37, 157, 194, 209, 225). IE62 is also an abundant VZV tegument protein (125). Studies performed in our lab have clearly demonstrated that the expression of the VZV ORF66 protein kinase was responsible for most of the IE62 tegument association (123), and this occurred due to aberrant retention of IE62 in the nucleus in the absence of ORF66 expression. Thus, through regulation of IE62 cellular distribution, the ORF66 kinase mediates a critical switch in IE62 function, from a transcriptional regulator in the nucleus in early infection to a virion structural protein in the cytoplasm during late infection.

Interestingly, IE62 transcripts have been detected by multiple groups in latently-infected human ganglia (118, 170), and some evidence suggests that IE62 proteins are also expressed with aberrant localization to the cytoplasm (156). The authors of the latter study suggested that IE62 nuclear exclusion in neurons may contribute to the maintenance of VZV latency, given that IE62 has powerful transactivation activities and the VZV genome persists in the nucleus. Recent evidence suggests that ORF66 protein is also expressed in latently infected neurons (44, 45). Thus, ORF66 may contribute to the maintenance of VZV latency by inducing IE62 nuclear exclusion and compartmental separation of the VZV genome and this powerful transcriptional activator. The mechanisms underlying ORF66-mediated IE62 nuclear exclusion have not been defined in detail.

1.5.3 Overview of the classical nuclear import and export pathways

The double membrane of the nuclear envelope (NE) provides a basic structural barrier between the nucleus and the cytoplasm, and restricts the nucleocytoplasmic exchange of macromolecules by means of the nuclear pore complex (NPC). Molecules <40 kDa can freely diffuse across the NPC, while larger molecules (>40 kDa) must be recognized and actively transported by soluble receptors of the karyopherin family (i.e., importins and exportins).

Classical nuclear import, the pathway likely used by the VZV IE62 protein to enter the nucleus, is mediated by the importin α (IMPα) adaptor, which recognizes a basic R/K-rich NLS in a cargo protein and is, in turn, recognized by the importin β1 (IMPβ1) transport receptor (Figure 1-7A) (reviewed in (143, 180, 193)) . IMPβ1 interacts transiently with the F/G repeats of nucleoporins that line the NPC to facilitate movement of the ternary complex into the nucleus. Once in the nucleus, the activated form of Ran (RanGTP) binds IMPβ1 to dissociate and release IMPα and the cargo protein. Additional factors mediate the final release of cargo, and IMPα is recycled back into the cytoplasm by the specific exportin receptor, CAS, via the RanGTP-regulated nuclear export pathway. Human cells express 9 IMPβ proteins in addition to IMPβ1, and these recognize their cargoes without the assistance of the IMPα adaptor (143).

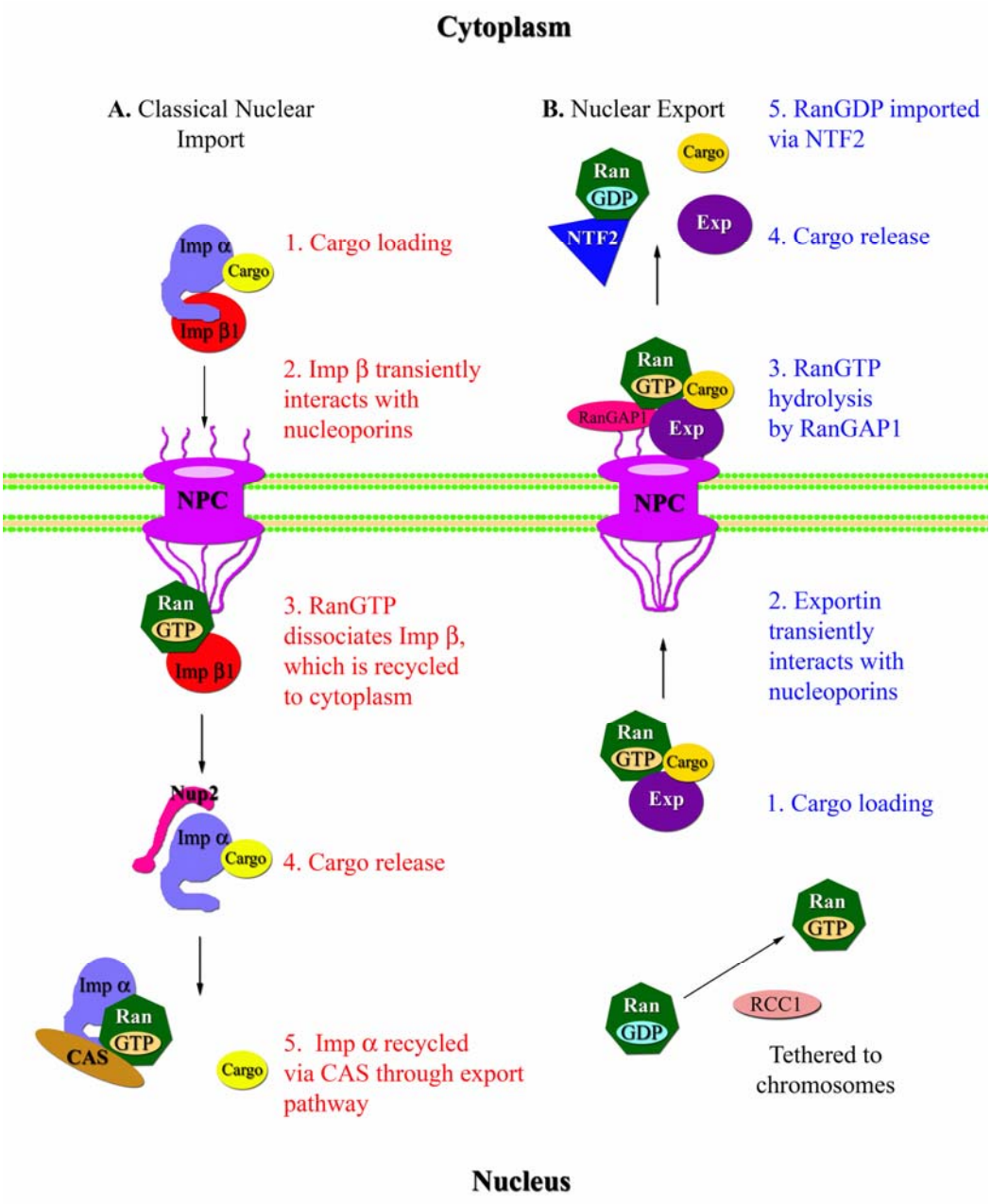

Figure 1-7 Nucleocytoplasmic transport

Overview of classical nuclear import (A) and nuclear export (B). All components are labeled, and brief descriptions of each step in import (red) and export (blue) are shown.

In humans, 7 karyopherin receptors are known to deliver cargoes into the cytoplasm, but only 5 of these have been shown to carry proteins: Crm1, exportin 4, exportin 6, exportin 7, and CAS (140, 193). Of these, only the Crm1 nuclear export receptor recognizes an identifiable motif in cargo proteins, characterized by an abundance of leucine or other bulky hydrophobic residues: φ-x_{2-3}-φ-x_{2-3}-φ-x-φ; φ=[L,I,V,F,M], where x=any amino acid (140). Nuclear export occurs after cargo is recognized in the nucleus by exportin (Figure 1-7B). Following association with RanGTP, the entire complex moves across the NPC in a manner similar to the IMPα/β1/cargo complex. The Ran GTPase activating protein (RanGAP) is tethered to nucleoporins on the cytoplasmic face of the NPC, and RanGTP hydrolysis to GDP facilitates the release of the cargo and the exportin protein into the cytoplasm. RanGDP is recycled back into the nucleus via the specific NTF2 receptor, and once inside the nucleus, the GDP is exchanged for GTP by the Ran guanylnucleotide exchange factor, RCC1, to facilitate another round of nuclear import or export. Interestingly, recent reports have also indicated that many nuclear hormone receptors are exported from the nucleus by calreticulin in a Ca^{2+}-dependent manner, via export motifs localized in the DNA-binding domains (25, 98, 99).

One of the most common mechanisms for the regulation of nuclear trafficking is through intra- or intermolecular masking of the NLS or NES. Intramolecular masking may occur if the NLS/NES is not accessible due to the addition of a charge (e.g., phosphorylation) or a change in the conformation of the protein. Intermolecular masking occurs through the binding of a heterologous protein to prevent the recognition of the NLS/NES by its specific receptor. Many examples of both NLSs and NESs that are regulated by these mechanisms exist, and are thoroughly reviewed in (203).

1.5.4 A cellular target for ORF66: MHC-I

A screen of a plasmid library of VZV regulatory proteins for affects on MHC-I surface expression revealed that cells expressing the ORF66 protein kinase had reduced levels of surface MHC-I compared to vector-transfected negative controls and cells transfected with plasmids expressing six other VZV regulatory proteins (2). A similar function has not been described for any other U_S3 kinase, thus implying a highly novel ORF66 interaction with the cellular environment, and a possible new mechanism for herpesvirus mediated immune evasion.

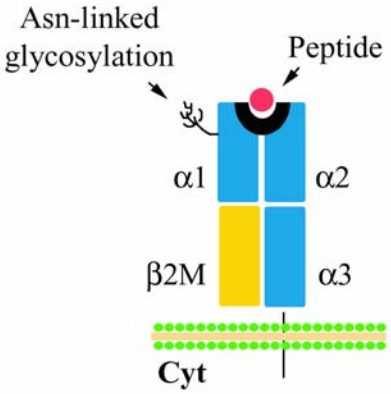

Figure 1-8 MHC-I Structure

MHC-I expressed at the cell surface consists of a heavy chain with a single transmembrane domain and three luminal domains referred to as α1, α2, α3 (blue); the non-covalently associated β_2-microglobulin (yellow); and a proteasome-derived peptide (pink). In transit to the surface, MHC-I is core glycosylated at a highly conserved residue in the α1 region of the heavy chain.

MHC-I is an integral molecule of the adaptive immune system, which signals intracellular infection to $CD8^+$ T lymphocytes. MHC-I expressed at the cell surface is a heterotrimeric complex, consisting of a 44 kDa type I membrane protein referred to as class I heavy chain (HC), a 12 kDa non-covalently associated protein known as β_2-microglobulin (β2M), and an 8-11mer intracellularly-derived peptide (Figure 1-8A). The MHC-I HC consists

of three highly variable globular luminal regions (α1, α2, and α3), a transmembrane domain, and a short cytoplasmic tail. The peptide-binding cleft is formed by the α1 and α2 regions, and the α3 region is membrane-proximal and exhibits structure similar to the immunoglobulin (Ig) constant domain (216). MHC-I protein bearing a foreign peptide, expressed at the cell surface, is recognized by CTL bearing a cognate T cell receptor (TCR). The consequence of TCR:MHC-I ligation is induction of TCR signaling pathways and subsequent activation of an antiviral response, which may include production of γ-interferon and/or the release of exocytic granules designed to instigate infected cell lysis. Because this is detrimental to viral replication, and ultimately to the establishment and persistence of latent viral genomes, herpesviruses have evolved an impressive repertoire of mechanisms directed at inhibition of MHC-I surface expression and the resultant evasion of CTL-mediated adaptive immunity.

1.5.5 MHC-I antigen presentation

Class I HCs are co-translationally inserted into the membrane of the ER via the Sec61p translocon (189), and are core-glycosylated at a single highly conserved asparagine residue (N_{86}) in the α1 domain (Figure 1-9) (257). HC molecules associate with the ER-resident chaperones, immunoglobulin binding protein (BiP) and calnexin, which assist with folding since HCs are not stable in the absence of β2M and peptide (257). Subsequently, calnexin dissociation occurs, followed by association with β2M in the presence of calreticulin and the protein disulfide isomerase Erp57 (132). Erp57 mediates the formation of disulfide bridges, which stabilize the maturing HC molecule. β2M, which also displays an Ig-like fold, makes several contacts with the HC α3 region.

Peptides for loading onto the MHC-I binding groove are continuously generated by the multi-catalytic protease complex, the proteasome, from substrate proteins that have been tagged with poly-ubiquitin, and are transported into the ER by the transporter associated with antigen processing (TAP). Substrates are primarily derived from unwanted proteins and defective ribosomal products (DRiPs) (146) and can be of either nuclear or cytoplasmic origin. The TAP is an ER-resident, heterodimeric ATP-binding cassette (ABC) transporter, consisting of one molecule each of TAP1 and TAP2 (1). The TAP1 and TAP2 proteins have 10 and 9 transmembrane domains, respectively, which associate to form a pore in the ER membrane. Proteasomeally-derived peptides are processed by cytosolic peptidases, and 8-12mer peptides are selectively transported into the ER lumen by the TAP in a manner dependent on ATP-binding and hydrolysis mediated by the cytosolic nucleotide binding domains.

To form the peptide loading complex (PLC), the MHC-I specific chaperone, tapasin, binds the TAP and recruits the HC- β2M-Erp57-calreticulin complex. Tapasin is necessary for the proper function of the PLC, and performs multiple roles including bridging TAP to MHC-I, stabilizing TAP, coordinating peptide transfer to the MHC-I binding groove, and selection of high-affinity peptides for MHC-I (132). Following peptide binding, MHC-I is released from the PLC and is transported to the cell surface where it is surveyed by CTL for the presence of foreign peptides.

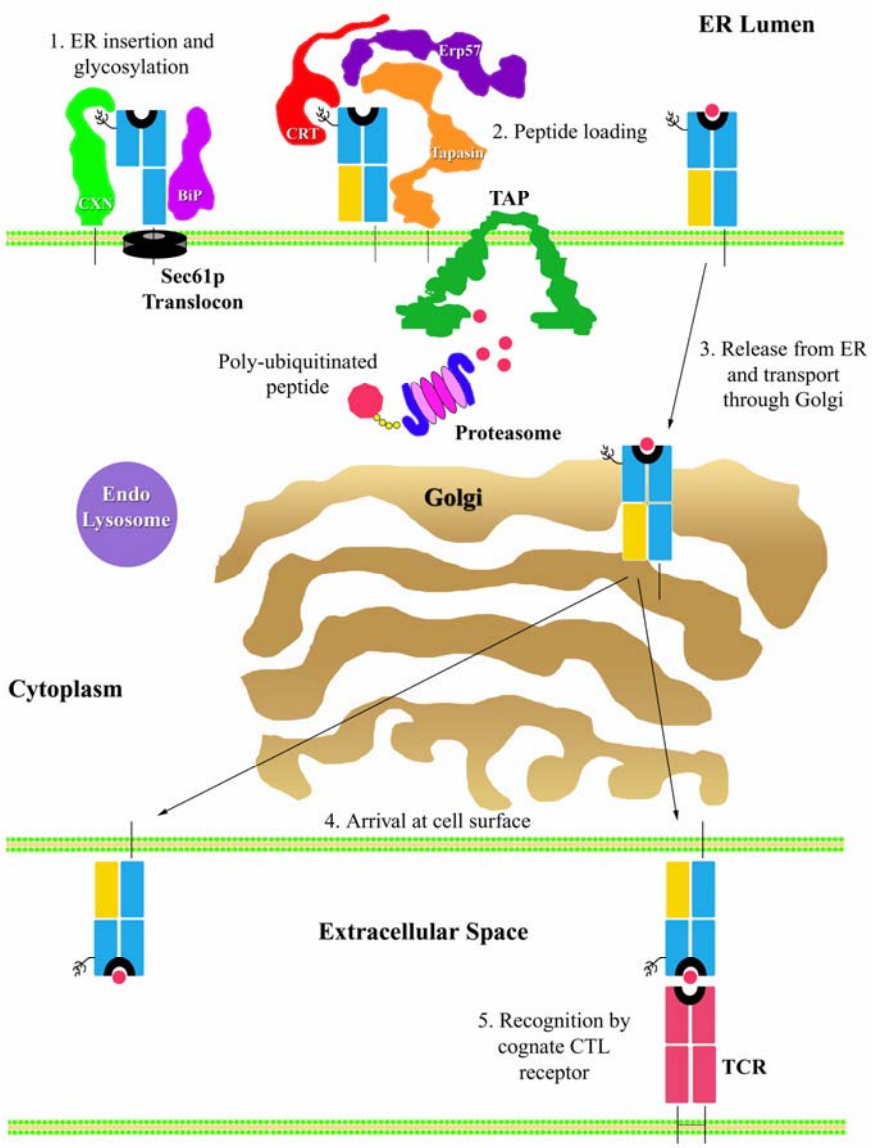

Figure 1-9 MHC-I antigen presentation

Overview of the MHC-I antigen presentation pathway. All proteins and cellular domains, as well as a brief numbered description of each step in the pathway, are summarized in the body of the image.

1.5.6 Herpesvirus subversion of MHC-I antigen presentation

Since there was no precedence for MHC-I downregulation mediated by a viral protein kinase, I looked to the extensive body of literature regarding herpesvirus subversion of MHC-I surface expression as a starting point for understanding the mechanism of ORF66's effect on this pathway. Herpesviruses target MHC-I by a variety of mechanisms, and these can be grouped according to the strategy used to disrupt MHC-I biosynthesis. These are described below, and are summarized in Figure 1-10. As there is an abundance of review articles dedicated to the various mechanisms of herpesvirus-mediated immune evasion, these were used to reference specific interactions, when possible, to save bibliographic space.

i) Host protein synthesis shutoff: In alphaherpesviruses, a non-specific RNase (U_L41 or virion host shutoff, vhs) mediates cleavage of host mRNA and induces a global reduction in host protein synthesis. *vhs* activity contributes to downregulation of MHC-I surface expression in several viruses (76, 82, 135), and has been shown to diminish recognition of infected cells by virus-specific CTL (97). The VZV ortholog to *vhs*, the ORF17 gene, can induce mRNA degradation (217), but its role in the reduction of host protein synthesis is currently unknown.

ii) Peptide loading complex inhibition: HC-β2M heterodimers lacking peptide are not stable, and are not released from the ER for transport to the cell surface. Thus, peptide translocation by the TAP complex represents a rate-limiting step in the efficiency of MHC-I maturation, and not surprisingly, TAP function is targeted by representatives of the alpha-, beta- and gammaherpesvirus sub-families (reviewed in (95, 175, 210)). In cells infected with the human alphaherpesviruses HSV-1 and HSV-2, the 10 kDa soluble immediate early protein, ICP47, binds to the cytosolic domain of TAP with high affinity to competitively inhibit the binding of proteasomeally-derived peptides. Additionally, ICP47 prevents ATP hydrolysis and

conformational changes in TAP that are required for peptide transport. Other alphaherpesviruses of agricultural importance (BHV-1, EHV-1 and PrV) have also been shown to inhibit the TAP complex (5-7, 136). For these viruses, the 9 kDa U_L49.5 ER-localized type I membrane glycoprotein has been implicated, which operates by arresting TAP in a functionally incompetent conformation and promoting TAP degradation by the proteasome (134). In the betaherpesvirus HCMV, the 21 kDa ER-resident membrane protein, U_S6, binds to TAP in the ER lumen by means of its own luminal domain and indirectly and specifically interferes with ATP binding on the TAP cytosolic tail, but does not inhibit peptide binding. Human gammaherpesviruses have also been shown to inhibit TAP-mediated peptide transport (211). The HCMV U_S3 ER-resident glycoprotein (unrelated to the alphaherpesvirus U_S3 kinase) utilizes a slightly different approach to impede peptide loading. It specifically targets tapasin, which is required to bridge TAP and MHC-I, resulting in inhibition of high affinity peptide loading and MHC-I retention in the ER (191).

iii) HC degradation. In lymphotrophic beta- and gammaherpesvirus infections, viral proteins mediate active degradation of MHC-I HCs. HCMV encodes two proteins, U_S2 and U_S11, sharing 20% sequence identity at the amino acid level, which hijack the ER-associated protein degradation pathway (ERAD) to induce retro-translocation of ER-localized immature HCs, lacking β2M, through the Sec61p translocon (153). Retro-translocation results in HC deglycosylation, poly-ubiquitination and degradation by the proteasome. This process requires the presence of the HC cytoplasmic tail, which may be used to pull HC molecules into the cytoplasm. In KSHV two proteins, kK3 and kK5, also related by sequence homology (~40%), target MHC-I molecules for degradation. kK3 and kK5 are PHD/LAP zinc finger domain-containing E3 ubiquitin ligases that attack mature, peptide-bearing MHC-I expressed at the cell

surface, promoting ubiquitination of HC cytoplasmic tails (reviewed in (147). Ubiquitination results in clathrin-mediated endocytosis of MHC-I and subsequent sorting into the acidic late endosomal/lysosomal compartment, where degradation is mediated by acidic proteases. The related mK3 protein of murine gammaherpesvirus 68 is also an ubiquitin ligase, but mediates ER-associated HC ubiquitination and disposal via the the proteasome. Interestingly, mK3 also promotes degradation of the TAP (147).

iv) Aberrant MHC-I trafficking. In HHV-6 and -7 infections, the 60 kDa U21 membrane protein binds properly folded MHC-I molecules and diverts them directly from the Golgi complex for sequestration in a peri-nuclear endo/lysosomal compartment (95). Murine cytomegalovirus, another betaherpesvirus, encodes three viral chaperones (m152/gp40, m06/gp48, and m04/gp34) that negatively influence MHC-I surface presentation (94). The m06/gp48 protein functions similar to U21, in that it binds mature class I molecules and diverts them to a lysosomal compartment. The m152/gp40 proteins retains class I molecules in the ER-*cis*-Golgi intermediate compartment (ERGIC). The m04/gp34 protein utilizes a unique mechanism, binding MHC-I in the ER and escorting it to the cell surface where it cannot be sufficiently recognized by CTL. The HCMV U_S10 gene encodes a glycoprotein that binds MHC-I and impairs its transport through the endoplasmic reticulum (95). Finally, the HCMV soluble pp71 tegument protein mediates MHC-I downregulation by promoting its retention in infected cells, and is critical for downregulation immediately upon infection (233).

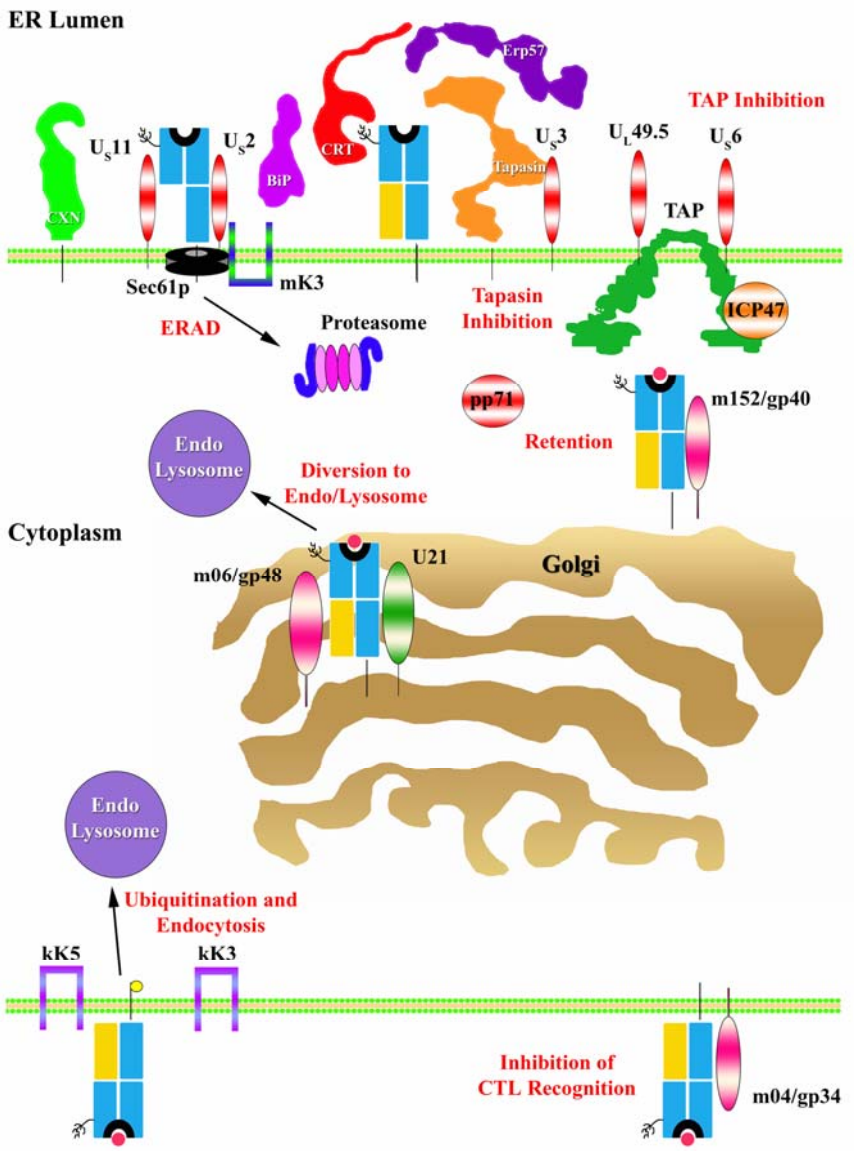

Figure 1-10 Herpesvirus subversion of MHC-I antigen presentation

Overview of herpesvirus effects on MHC-I biogenesis and surface presentation. All viral and cellular components are labeled in the document, and viral proteins are represented by striped objects. Generalized mechanisms of subversion are indicated in red.

1.5.7 MHC-I subversion in VZV-infected cells

VZV does not encode an HSV-1 ICP47 ortholog, and yet maintained the ability to induce MHC-I downregulation in HFF, MRC-5 fibroblasts and melanoma cells in culture, as well as T lymphocytes *in vivo* and in culture (2). In HFF, folded MHC-I accumulated in the Golgi apparatus. This mechanism of subversion of MHC-I surface expression has not been observed for any other human herpesvirus studied to date. VZV-infected cells incubated with an inhibitor of late gene synthesis revealed that either an immediate early or early protein was involved. As described above, the ORF66 kinase was implicated in this process, as HFF cells transiently expressing ORF66 exhibited reduced MHC-I surface levels. It is currently unknown whether ORF66 is responsible for the observed Golgi accumulation, and the mechanism of ORF66 mediated MHC-I downregulation is not known.

2.0 RATIONALE AND SPECIFIC AIMS

2.1 OVERALL RATIONALE

ORF66 is a critical mediator of VZV pathogenesis *in vivo*, but the molecular mechanisms of ORF66 function remain largely unresolved. A firmly established role for ORF66 in VZV-infected cells is the nuclear exclusion of the VZV IE62 protein. IE62 is an essential viral gene that regulates many aspects of the VZV transcriptional program, and is also a major virion tegument component. In the absence of ORF66 expression IE62 aberrantly accumulates in the nucleus and fails to incorporate into the tegument, thus providing a functional link between ORF66-induced nuclear exclusion and an IE62 cytoplasmic structural role during late-stage infection. A similar relationship has not been described for U_S3 kinase proteins of other alphaherpesviruses. One additional function for ORF66 in VZV infection is suggested by the report that ORF66 can induce a reduction in MHC-I surface expression in the absence of additional VZV gene expression. MHC-I is a cellular protein involved in the activation of adaptive immunity in response to intracellular infection. As this function has not been attributed to any U_S3 kinase, or any other viral protein kinase, it may represent a highly novel mechanism of immune evasion. In this work, my original aims were targeted at understanding the specific mechanisms underlying the ORF66 roles in IE62 nuclear exclusion and MHC-I surface downregulation. However, new observations and hypotheses derived from these were extended

into a third and a fourth aim that addressed aspects of IE62 and ORF66 cellular trafficking. These are described in brief below and are further delineated in Chapters 3-6.

2.2 SPECIFIC AIM 1

Development of an ORF66 in vitro kinase assay to establish whether the IE62 protein is a direct phosphorylation target, and to delineate any IE62 residues phosphorylated by ORF66 to mediate nuclear exclusion.

While there are several possible explanations for the functional significance of ORF66-mediated IE62 nuclear exclusion in VZV-infected cells, the molecular mechanisms that govern this process have only been partially elucidated. Point mutations in the predicted ORF66 ATP-binding lysine (K122) or two critical catalytic loop residues (D206 and K208), which putatively render ORF66 catalytically inactive, abolished the ability of ORF66 to mediate IE62 nuclear exclusion, suggesting this function is dependent on ORF66 kinase activity (124). In addition, orthophosphate labeling analyses of truncated IE62 peptides in ORF66-co-transfected or VZV-super-infected cells narrowed the region of IE62 affected by ORF66 to amino acids 602-730. Within this region, only two possible sequences exhibit similarity to the consensus derived for other US3 kinases (see Figure 1-5), with multiple basic amino acid residues preceding a S/T residue: 1) the IE62 NLS (RLRTPRKRKS$_{686}$); and 2) a motif just downstream of the IE62 NLS (KAKRRVS$_{722}$). From this, I hypothesize that a direct ORF66-mediated phosphorylation of IE62 in the region containing its NLS leads to its inability to undergo nuclear import, thus inducing IE62 cytoplasmic accumulation during late-stage VZV infection.

To identify any ORF66-mediated specific IE62 phosphorylation events, it was essential to develop an ORF66 *in vitro* kinase assay and establish that ORF66 is catalytically active. As previously mentioned, the ORF66 protein is highly insoluble and could not be expressed and immunoprecipitated to sufficient levels in transfected cells to allow for use in an *in vitro* assay. Thus, I chose to express hemagglutinin (HA) epitope-tagged ORF66 from a baculovirus vector in insect cells. While ORF66 remained ≥95% insoluble in this system, the tremendous level of ORF66 overexpression allowed for immunopurification of significant levels of ORF66 using an antibody to the HA epitope tag (data not shown). I then used intrinsic ORF66 autophosphorylation to define the optimal conditions for kinase activity. For the identification of IE62 residues phosphorylated by ORF66, I also developed multiple IE62 peptide substrates fused to maltose binding protein (MBP) and affinity purified these substrates, after expression in bacteria, for use in the *in vitro* kinase assay. These results are presented in their entirety in Chapter 3.

2.3 SPECIFIC AIM 2

Determine whether IE62 is a nuclear shuttling protein, and if so, map regions involved in nuclear export.

In the preceding study, we clearly established that ORF66 mediates IE62 phosphorylation at two serine residues (S686 and S722), with phosphorylation at S686 being sufficient for IE62 nuclear exclusion. Based on its similarity with other U_S3 kinases, it is generally assumed that ORF66 is expressed with early kinetics, after the expression and nuclear import of the IE62 protein at immediate early times post-infection. Thus, ORF66 phosphorylation may not be

sufficient for the efficient IE62 nuclear clearance observed in many late-stage VZV-infected cells. From these observations, I hypothesize that efficient IE62 nuclear exclusion is dependent on a combination of direct ORF66 phosphorylation and intrinsic IE62 nuclear export activities.

Initially, I used recombinant VZV expressing enhanced green fluorescent protein tagged ORF66 (discussed in more detail in Aim 3) in a cell-free infection/immunofluorescence-based assay to investigate the IE62/ORF66 spatio-temporal expression relationship, identify potential cellular sites of interaction, and obtain information regarding the timing of IE62 cytoplasmic accumulation and nuclear exclusion. To determine the ability of IE62 to undergo nuclear export, I developed an interspecies heterokaryon assay with an intrinsic control for the assessment of the nuclear membrane integrity. I used an existing panel of IE62 truncation mutants and developed several additional mutations within the IE62 sequence, and tested these in the heterokaryon assay to delineate specific structural determinants involved in IE62 nuclear export. These results are presented in their entirety in Chapter 4.

2.4 SPECIFIC AIM 3

Characterize the role of the ORF66 kinase in MHC-I downregulation during VZV infection.

VZV mechanisms of MHC-I downregulation must differ from that of HSV-1, since VZV does not encode an ortholog to the HSV-1 ICP47 TAP inhibitor. A previous study of the effects of VZV on MHC-I surface expression identified a possible role for ORF66 in this process in transiently expressing cells lacking any additional VZV gene expression (2). I confirmed this using a transient co-transfection assay in which an EGFP reporter gene was used to identify

expressing cells (data not shown). While no other U_S3 kinase has been shown to mediate this effect, U_S3 kinases are well-established modulators of the host-cell environment. From this, I hypothesized that ORF66 may have a unique role in the regulation of MHC-I surface expression during VZV infection.

A variety of novel reagents and methods were developed for this Aim. Specifically, we generated recombinant VZV expressing EGFP-tagged ORF66 under the control of the native ORF66 promoter, or a truncated version lacking the C-terminal catalytic domain; and replication defective adenovirus vectors expressing EGFP-66 or a point-inactivated version that lacks specific kinase activity. VZV expressing EGFP-tagged ORF66 kinase proteins provided a superior method for determining the percentage of infected cells, and enabled me to establish the required multiplicity of cell-associated VZV to achieve similar end-points for viruses either expressing or lacking the ORF66 catalytic domain. I chose to use replication defective adenoviruses because they efficiently infect VZV-permissive MRC-5 cells, which are a non-transformed diploid cell line and are likely more representative of *in vivo* infection with respect to the melanoma cells used in many other studies. I used these novel reagents to comparatively assess the effects of ORF66 kinase proteins on MHC-I surface expression, biosynthetic trafficking in the early secretory compartment, and general cellular distribution. These results are presented in their entirety in Chapter 5.

2.5 SPECIFIC AIM 4

Utilize VZV expressing EGFP-tagged ORF66 kinase proteins to investigate novel ORF66 nuclear trafficking as a function of kinase activity and time.

Studies with VZV expressing EGFP-tagged ORF66 kinase proteins revealed highly novel ORF66 distributions in the nucleus, including the appearance of nucleoplasmic and putative nucleolar speckles during late-stage VZV infection. A similar distribution pattern has not been observed for prototypical U_S3 kinases expressed by HSV-1 and PrV, and I considered that this distribution may be reflective of a novel ORF66 process in VZV infected cells. Furthermore, I hypothesize that a better understanding of ORF66 spatio-temporal trafficking will facilitate identification of novel ORF66 functions in VZV-infected cells.

I used fixed and live-cell microscopy assays to study ORF66 trafficking in VZV-infected cells as a function of time and kinase activity. Co-localization analyses were performed with antibodies against major cellular nuclear bodies that are known to associate with the nucleolus, as well as VZV proteins that demarcate nuclear genome replication and capsid assembly compartments. Additonally, live-cell time lapse microscopy was employed to provide a clearer understanding of the dynamic process of ORF66 nuclear trafficking. These results are presented in Chapter 6.

3.0 PHOSPHORYLATION OF THE VARICELLA ZOSTER VIRUS (VZV) MAJOR TRANSCRIPTIONAL REGULATORY PROTEIN IE62 BY THE VZV ENCODED OPEN READING FRAME 66 PROTEIN KINASE

Amie J. Eisfeld[2,3], Stephanie E. Turse[1], Sara Jackson[4], Edwina C. Lerner[2] and Paul R. Kinchington[1,2]

Departments of Ophthalmology[1] and of Molecular Genetics and Biochemistry[2], Graduate Programs in Molecular Virology and Microbiology[3] and Biochemistry and Molecular Genetics[4], School of Medicine, University of Pittsburgh, Pittsburgh PA 15213

Note: For this study, I developed the ORF66 *in vitro* kinase assay. This included derivation of baculovirus constructs for expression of the ORF66 and the IE62/MBP peptide substrates, and determination of optimal conditions for ORF66 *in vitro* kinase activity. In addition, I performed all the experiments requested by the reviewers of *Journal of Virology*. Thus, my contributions are represented in Figs. 1-3, 1-5, 1-8, and 1-9. All of the writing was done by me.

3.1 ABSTRACT

IE62, the major transcriptional regulatory protein encoded by varicella zoster virus (VZV), is nuclear at early times of VZV infection, but then becomes predominantly cytoplasmic as a result of expression of the protein kinase encoded by open reading frame (ORF) 66. Cytoplasmic forms of IE62 are required for its inclusion as an abundant VZV virion tegument protein. In this work, we show that ORF66 directly phosphorylates IE62 at two residues, with phosphorylation at S686 being sufficient to regulate IE62 nuclear import. Phosphotryptic peptide analyses established an ORF66 kinase mediated phosphorylation of complete IE62 protein in transfected and VZV infected cells. Using truncated and point-mutated IE62 peptides, ORF66 directed phosphorylation was mapped to residues S686 and S722, immediately downstream of the IE62 nuclear localization signal. IE62 protein carrying an S686A mutation retained efficient nuclear import, even in the presence of functional ORF66 protein kinase, but IE62 protein containing S686D alterations imported to the nucleus inefficiently. In contrast, nuclear import of IE62 carrying S722A was still modulated by ORF66 expression, and IE62 with S722D mutation imported efficiently to the nucleus. An *in vitro* phosphorylation assay was developed using bacterially expressed IE62-maltose binding protein fusions as substrates for immunopurified ORF66 protein kinase from recombinant baculovirus infected insect cells. ORF66 kinase phosphorylated the IE62 peptides with similar specificity for residues S686 and S722. These results indicate that IE62 nuclear import is modulated as a result of direct phosphorylation of IE62 by ORF66 kinase. This represents an interaction that is so far unique among the alphaherpesviruses.

3.2 INTRODUCTION

Varicella zoster virus (VZV) is the human herpesvirus that causes chickenpox upon primary infection and herpes zoster following reactivation from a latent state. These diseases are separated by a prolonged period of neuronal latency in which no clinical disease is apparent, but a few select viral genes are expressed (83, 118). In a VZV lytic infection, approximately 70 VZV proteins are expressed in a temporally regulated manner (214), most likely in a typical α–β–γ cascade which is transcriptionally regulated in a manner similar to that seen in herpes simplex virus type 1 (HSV-1) infected cells (100, 101). Several VZV proteins have been implicated to regulate VZV gene expression, based on studies demonstrating their influence on viral promoter-reporter activities in transfection assays. These include the proteins encoded by open reading frames (ORFs) 4, 61, 62, 63, 10 and 29 (127).

Of these, the principal transcriptional transactivator of VZV transcription is IE62, encoded by VZV ORF62. This 1310 amino acid, heavily phosphorylated protein (124, 125) is expressed with immediate early kinetics (67, 124), stimulates transcription from VZV promoters in transfection assays and enhances the infectivity of VZV DNA (15, 40, 177, 195). It also positively and negatively regulates its own transcription, depending on cell type (55, 196). While the exact mechanisms underlying IE62-mediated transactivation of viral genes have not been well defined, they are likely similar to those of ICP4 of HSV-1, as IE62 can complement ICP4 HSV-1 mutants and functionally replace ICP4 in the HSV-1 genome (54, 64). ICP4 has been shown to interact with and recruit specific components of the general transcription machinery to viral promoters and stabilize their formation for transcriptional initiation (31, 253). VZV IE62 has also been shown to co-operate and interact with both cellular and viral proteins in

gene regulation, including USF (209) and SP-1 (194), and the viral regulatory proteins from ORFs 4 (225), 47 (22, 186) and 63 (157).

The extensive phosphorylation of IE62 has led to several investigations of its possible interactions with cellular and viral encoded kinases. IE62 is phosphorylated by cellular kinases in the absence of other viral proteins (124, 186). It has two poly-serine tracts, one located internally and the other near the C terminus, which are strongly predicted to be sites for casein kinase II. The internal serine tract is conserved in other alphaherpesvirus orthologues and in HSV-1 ICP4, it is a site for phosphorylation by casein kinase II, protein kinase A and protein kinase C (249, 250). IE62 is also the target of the VZV ser/thr specific protein kinase encoded by ORF 47. ORF47 directly phosphorylates IE62 *in vitro,* and targets sequences resembling those phosphorylated by casein kinase II (121, 186). Whether ORF47 phosphorylates IE62 *in vivo* and what the consequences of ORF47 directed phosphorylation are on IE62 functions have yet to be defined. While not essential (90), the ORF47 kinase is a tegument protein that is required for efficient virion assembly (21, 22, 137) and efficient growth and viral pathogenesis in the SCID-hu mouse model (177). IE62 is also a possible target for the ORF66 protein kinase, as ORF66 expression affects the cellular distribution of IE62. In VZV infected cells, IE62 expressed at early times of infection enters the cell nucleus using a single classical arginine/lysine rich nuclear localization signal (NLS) mapping to amino acids 677-685 (129). However, at late stages of infection, IE62 accumulates predominantly in the cytoplasm (127, 129). This activity is mediated by ORF66 protein kinase, as IE62 remains nuclear in cells infected by recombinant VZV that do not express ORF66. Furthermore, progeny virus from VZV infected cells not expressing ORF66 do not incorporate IE62 as an abundant virion protein (123). Thus, either IE62 cytoplasmic accumulation and/or its targeting by ORF66 are required

for virion inclusion of IE62 as an abundant tegument protein (123, 125). Co-transfection studies indicate the ORF66 kinase is sufficient to induce the cytoplasmic accumulation of IE62 independent of other VZV proteins (124, 129). As VZV recombinants lacking ORF66 expression demonstrate considerable impairment for growth in human T lymphocytes (174, 220, 224), the ORF66 induced effects on IE62 cellular distribution and IE62 inclusion into the virion structure may be important in the pathogenesis of VZV. Furthermore, a single report has suggested that ORF66 is expressed during VZV latency in human ganglia (45). While not yet confirmed, this could mechanistically explain reports of a predominantly cytoplasmic distribution of IE62 found in latently infected neurons (83, 156). The cytoplasmic accumulation of IE62 induced by ORF66 requires the integrity of the ORF66 kinase activity, suggesting that phosphorylation is a necessary step to affect IE62 cellular redistribution. In agreement with this, small IE62 peptides responsive to ORF66 mediated cytoplasmic redistribution were found to be preferentially phosphorylated in cells co-expressing the ORF66 kinase (124).

It has not been determined whether IE62 phosphorylation occurs as a result of ORF66 activation of cellular pathways, or if IE62 represents a direct target for the ORF66 protein kinase. In this work, we precisely map ORF66 mediated phosphorylation of IE62, show that ORF66 directly phosphorylates the IE62 protein *in vitro* and demonstrate that one of the phosphorylation events leads to IE62 cytoplasmic accumulation. Thus, IE62 represents a new viral target for the U_S3 kinase group.

3.3 MATERIALS AND METHODS

3.3.1 Cells and virus

VZV was grown on the human melanoma cell line MeWo (obtained from C. Grose, University of Iowa) as detailed previously (123). 293T cells (ATCC) were maintained in DMEM supplemented with 5% FBS, 100 U penicillin, 100 μg/ml streptomycin and 0.25 μg/ml amphotericin B. Cosmid-derived recombinant VZV ROka, ROka47S (not expressing ORF47) and ROka66S (not expressing ORF66) have been detailed previously (90, 91) and were a kind gift of J. I. Cohen (Laboratory of Clinical Investigation, NIH). VZV stocks were prepared and stored as previously described (122, 125). For transient expression studies, MeWo cells at 70% confluence were transfected using Lipofectamine with the PLUS reagent (InVitrogen Corp. Carlsbad, CA), as detailed previously (124). 293T cells were transfected at 50-70% confluence using either a modified calcium phosphate co-precipitation method, with 30 μg total plasmid DNA transfected in 1 ml total of HEPES buffered saline, divided between two 60 mm dishes containing 5 ml of media/dish. Cells were exposed to the precipitate in media overnight, followed by media replacement. In all comparative transfection studies, the total amount of the human cytomegalovirus major IE promoter used to drive gene expression was equalized by adding a corresponding amount of empty vector. Baculoviruses were grown in SF9 cells (InVitrogen Corp.) at 28^{o}C in Grace's insect media supplemented with 5% FBS and antibiotics, as detailed by the supplier.

3.3.2 Antibodies and immunological methods

Polyclonal rabbit antibodies that recognize IE62 and the ORF66 protein kinase have been described previously (45, 123, 124). Antibodies to the nine amino acid epitope YPYDVPDYA of the influenza virus hemagglutinin (HA) protein were initially obtained from Santa Cruz Biotechnologies, Inc. (Santa Cruz, CA) or were later derived using a monoclonal antibody (48EC) developed against the synthetic peptide by the Hybridoma Core Facility of the University of Pittsburgh Department of Ophthalmology. Immunofluorescence, immunoblotting and immunoprecipitations were carried out as detailed previously (124), except that bound antibodies in immunoblotting studies were detected using secondary goat anti-rabbit or goat anti-mouse antibodies coupled to horseradish peroxidase (ICN/Cappel, Aurora, OH), followed by detection with West Dura chemiluminescent substrate (Pierce, Inc., Rockford, IL). Quantitation of protein band signal was achieved either by a Biorad GS525 phosphorimager, or by densitometry of autoradiographs exposed to be in the linear range of the film.

3.3.3 Plasmids and DNAs for transfection

The following constructs have been detailed previously (124, 129): pG310 expression vector, pGK2-HA expression vector, pKCMV62, pKCMV47, pGK2-HA47, pKCMV66, pGK2-HA66 and pGK2-HA66-K122A. Briefly, the pG310 or pGK2-HA vectors contain the complete HCMV IE promoter, followed by EcoRI and BamHI sites for gene insertion, and a polyadenylation signal derived from the HCMV IE1 gene. pGK2-HA is similar to pG310 but additionally contains an initiating methionine, followed by the sequence encoding the HA epitope, followed by the same cloning sites. Plasmid pKCMV66 and pKCMV66 K122A express wild-type ORF66

or a point inactivated kinase dead ORF66 altered at K122A, the residue suspected to be required for binding ATP, respectively; pGK2-HA66 and pGK2-HA66-K122A express the same proteins as N terminal HA tagged forms. Plasmid pGK2-HA47 expresses HA tagged ORF47 and pKCMV62 expresses untagged, full-length IE62 protein.

The following new IE62 peptide-expressing constructs were developed using PCR amplification with the proof-reading polymerase Expand (Roche Biochemicals, Inc.): pGK2-HA846, pGK2-HA825, pGK2-HA819, pGK2-HA821, pGK2-HA823, pGK2-HA810, pGK2-HA828, and pGK2-HA811. pGK2-HA846 was generated by EcoRI linker addition (New England Biolabs, Inc., Beverly, MA) to an EcoRV-BstXI DNA fragment of IE62 (122,010 to 123,232, residues 414 to 823 of IE62 with respect to the Dumas VZV sequence), followed by digestion with EcoRI and BamHI (BamHI site is at 122,962, residue 735 of IE62). Cloning this fragment into the pGK2-HA vector resulted in expression of IE62 residues from 414-735 in frame with the HA epitope tag. Additional constructs from pGK846 were derived by replacement of a DNA fragment defined by a unique KpnI site at 122,475 (residue 571 of IE62) and the unique BamHI site, with either double-stranded complementary oligonucleotide primers, or with KpnI- and BamHI digested PCR amplification products. Accordingly, pGK2-HA810 expressed residues 414-687; pGK2-HA828 expressed residues 414-571 fused in frame to 673 to 735; pGK2-HA825 expressed residues 414-571 fused in frame to residues 656-735; pGK2-HA811 expressed residues 414-571 fused to 677-735; pGK2-HA819 expressed residues 414-571 fused to the nuclear localization signal of IE62, defined by residues 677-686 (129); pGK2-HA821 expressed residues 414-571 fused to residues 386-394 of the VZV ORF61 protein, corresponding to the ORF61 nuclear localization signal (ARGAKRRL) (227); pGK2-HA823 expresses 414-571 fused in frame to the nuclear localization signal for SV40 (PPKKKRKV)

(213). A second set of constructs was derived from the plasmid pGK2-HA846, containing point mutations resulting in substitution of alanines at specific serine /threonine residues between amino acids 680-735 of IE62. Mutations were carried out by site-specific mutagenesis using the Gene Editor system (Clontech Corp., Palo Alto, CA). To derive IE62 full length proteins with select amino acid changes, the KpnI-BamHI fragment from pKCMV62 was replaced with the corresponding KpnI-BamHI fragment derived from the site-specifically altered pGK2-HA846 derivative, resulting in plasmids pKCMV62-S686A, pKCMV62-S686D, pKCMV62-S722A and pKCMV62-S722D. All DNAs were prepared for transfection using Qiagen columns.

To derive maltose binding protein (MBP) IE62 fusions, the portion of the IE62 gene defined by the KpnI-BamHI sites in IE62 (residues 571 to 735) was inserted into the KpnI and BamHI sites of pMalcR1 (New England Biolabs), followed by in-frame alignment of the maltose binding protein and IE62 ORF by digestion with KpnI, treatment with T4 DNA polymerase and dNTPs, and subsequent re-ligation. For expression of forms of MBP- IE62 fusion proteins containing mutations, the corresponding NotI-BamHI fragments (encoding residues 602-735) were switched between the pGK2-HA846 based constructs and the maltose binding protein-IE62 residue 571-735 derivative.

3.3.4 Phosphorylation analyses

[^{32}P]-labeled IE62 peptides for phosphotryptic peptide analysis were generated from transfected cells incubated in growth media containing 5% serum, 1/20th the normal phosphate and [^{32}P]-orthophosphate at 500 μCi/ml for 8 to 12 h, initiating at 16 h post transfection. Immunoprecipitations were carried out as detailed previously (124) using a modified buffer to solubilize proteins (50 mM HEPES-KOH pH[7.4], 150 mM NaCl, 1% Nonidet-P 40, 0.5%

sodium desoxycholate, 1 mM EDTA and 1 mM DTT) containing protease inhibitor cocktail (Complete miniEDTA free, Roche Applied Sciences, Indianapolis, IN) and the phosphatase inhibitors 2 mM $NaVO_4$ and 25 mM NaF. Labeled proteins were separated by SDS polyacrylamide gel electrophoresis (SDS PAGE) and identified by autoradiography.

Two dimensional phosphopeptide analyses were carried out as detailed previously (26). Briefly, immunoprecipitated, SDS PAGE separated, [^{32}P]-phosphate labeled IE62 proteins were transferred to Immobilon-P membrane, identified by autoradiography and the membrane fragments containing the labeled proteins were excised. Membranes were washed sequentially in 0.5% polyvinyl pyrolodone in 100 mM acetic acid for 30 min, water for 10 min and then 50 mM ammonium bicarbonate for 10 min. IE62 peptides were released by two sequential digestions in 200 µl of 5 mM ammonium bicarbonate containing 10-20 µg TPCK-treated trypsin at 37^{o}C for 24 h and then again for 4 h. Released peptides were concentrated by freeze drying and then spotted onto silica TLC sheets in a 1-3 mm spot. Resolution of peptides in the first dimension was by electrophoresis in pH 1.9 buffer of formic acid:glacial acetic acid:water at a ratio of 25:78:897. TLC sheets were dried and peptides were subsequently resolved in the second dimension by ascending chromatography in phosphochromatography buffer (15:10:3:12 ratio of n-butanol:pyridine:glacial acetic acid:water). [^{32}P]-labeled IE62 peptides were then identified by autoradiography, using Kodak Biomax imaging screens and film.

3.3.5 Baculovirus construction and *in vitro* phosphorylation analyses

Baculoviruses expressing the HA-tagged ORF66 protein kinase were derived using the BaculoGold system (BD Pharmingen, San Diego, CA). The complete HA-tagged ORF66 gene with the HCMV-IE1 polyadenylation signal was excised from pGK2-HA66 and cloned into the

baculovirus transfer vector pVL1392 (BD Pharmingen). Following co-transfection with BaculoGold DNA into SF9 cells, progeny virus was isolated and amplified. Expression of the HA-ORF66 protein kinase in infected SF9 cells was verified by immunoblot analyses with HA specific antibodies. The baculovirus generated ORF66 protein of 55 KDa was the same size as HA-ORF66 protein present in extracts of pGK2-HA66 transfected 293T cells. For *in vitro* kinase activity and *in vitro* phosphorylation, immunoprecipitates were prepared from SF9 cells infected with either a baculovirus expressing HA-tagged ORF66 (Bac-HA66) or a control baculovirus expressing glutathione-S-transferase (Bac-GST). Proteins were solubilized using a radio-immunoprecipitation buffer (RIPA) (20mM Tris HCl [7.4], 50mM KCl, 1% NP40, and 0.5% desoxycholate) plus protease inhibitor cocktail and phosphatase inhibitors (as just detailed) and ORF66 was precipitated using monoclonal antibodies specific for the HA epitope tag. An unrelated, non-specific control monoclonal antibody was used for control immunoprecipitates where indicated (a gift of N. Sundar-Raj, Department of Ophthalmology, University of Pittsburgh). In some studies, competing HA peptide or a non-specific peptide derived from the VZV ORF29 C terminal domain (126) were added to the SF9 cell extracts at a final concentration of 0.2 mg/ml prior to addition of monoclonal antibody. Following extensive washing in the RIPA buffer, beads were washed in a kinase buffer (20 mM HEPES [7.5], 50 mM KCl, 0.1 mM EDTA, 10 mM $MgCl_2$ or 50 mM $MnCl_2$ as indicated in the text), and then incubated in 50 µl kinase buffer containing 10 µg/ml heparin and 5 µCi of [γ-^{32}P] ATP (6000 Ci/mmol), at 35^{o}C for 30 min. Reactions were halted by addition of SDS sample buffer, proteins were separated by SDS PAGE, and phosphorylated bands were detected by autoradiography.

MBP-IE62 protein substrates for the *in vitro* phosphorylation reactions were expressed in *E. coli* and purified as detailed previously (122) and as by the manufacturer (New England

Biolabs, Inc.), except that induction of MBP fusion proteins was carried out at 30^{o}C for 3 hours, and pellets were sonicated 4 x 30 seconds at 4^{o}C to release fusion proteins. *In vitro* kinase assays were performed using approximately 5 μg of MBP fusion substrates with an equally divided HA-ORF66 immunoprecipitate, so that each reaction received identical kinase amounts.

3.4 RESULTS

3.4.1 Phosphopeptide analysis of IE62 expressed with and without the VZV encoded protein kinases

Previously, we showed that the dramatic redistribution of the VZV IE62 nuclear localizing protein to the cytoplasm was dependent on the integrity of the VZV-encoded ORF66 kinase activity (124, 129). However, it was difficult to demonstrate specific ORF66-mediated IE62 phosphorylation within full-length IE62 protein, because the extensive phosphorylation of IE62 protein by cellular kinases masked any ORF66 mediated events (124, 125, 186). Increased phosphorylation induced by ORF66 could only be demonstrated on IE62 peptides missing large regions that are strong targets for cellular protein kinases (124). While these data implied that the ORF66 kinase influenced phosphorylation of IE62, we considered it important to demonstrate differential phosphorylation induced by ORF66 in the context of the complete IE62 protein. We also reasoned that similar approaches might reveal whether the ORF47 kinase can mediate novel phosphorylation of IE62 *in vivo*, as suggested by *in vitro* (121, 186) studies.

To characterize the complexity of IE62 phosphorylation, we used a tryptic phosphopeptide mapping procedure detailed previously (26). Phosphorylation of IE62 was first

examined in the presence of the VZV protein kinases (at a 1:1 ratio) in co-transfected 293T cells. Following metabolic labeling in media containing [^{32}P]-orthophosphate for 8 h, IE62 was immunoprecipitated, separated by SDS PAGE, and transferred to Immobilon P membranes. The amount of [^{32}P] label incorporated into IE62 proteins obtained under all conditions was similar, and the mobility of [^{32}P]-IE62 in SDS PAGE was not detectably different in each condition (data not shown). Tryptic phosphopeptides released from membrane-immobilized IE62 proteins were extracted, separated in two dimensions and detected by autoradiography as detailed in Materials and Methods. As the technique shows some variability in separate runs, all comparative studies were carried out in parallel and under identical conditions. Autoradiographs revealed complex tryptic phosphopeptide maps for IE62, even in the absence of any VZV protein kinases, substantiating IE62 as a target for cellular kinases. At least 11 peptides could be readily identified (Figure 3-1A). The peptide maps for IE62 expressed alone and IE62 expressed in the presence of ORF47 were very similar, with most peptides migrating to similar positions (Figure 3-1B). Only very minor differences were apparent, suggesting that ORF47 did not greatly affect the phosphorylation state of IE62 *in vivo*. In contrast, the peptide map of IE62 expressed in the presence of ORF66 showed numerous changes, both in the relative abundance of several phosphopeptides (spots 5, 8, 9 and 10 were reduced), and in the appearance and/or movement of at least two novel phosphopeptide spots (Figure 3-1C, arrows). In particular, peptide 11 in the map of IE62 expressed in the absence of any kinase was altered in maps of ORF66 co-expressed IE62 to at least two, possibly three peptides (indicated by arrows), and peptide 7 migrated further in the electrophoresis direction from the origin. We conclude that ORF66 induces a differential phosphorylation state of the complete IE62 protein.

Similar approaches were used to address IE62 phosphorylation in the context of VZV infected MeWo cells, using recombinant VZV that do not express the kinases (Figure 3-2). Following equivalent infection with VZV-ROka, ROka47S (not expressing ORF47) or ROka66S (not expressing ORF66) at a ratio of 1 infected cell per 20 uninfected cells, and a 12 h metabolic labeling period with [^{32}P] orthophosphate initiating at 18 h post infection, IE62 was immunoprecipitated and analyzed by phosphotryptic peptide mapping. The phosphopeptide map of ROka66S IE62 (produced in the absence of ORF66 expression) exhibited a general reduction in many of the IE62 phosphopeptides compared to Roka IE62, despite equal loading of counts on to the TLC plates (Figure 3-2C). Furthermore, we observed one IE62 peptide spot (labeled 7b) that was abundant in both ROka and ROka47s IE62, which demonstrated a considerably reduced signal in ROka66S IE62 (arrowed, Figure 3-2C). These observations indicated that ORF66 induced novel phosphorylation events of the whole IE62 protein in the context of VZV infection. Comparison of ROka and ROka47S IE62 protein maps revealed very minor differences in the resolved phosphopeptide maps (Figure 3-2A and B), indicating that ORF47 does not grossly affect most of the phosphorylation events that occur on IE62 in the context of VZV infection in MeWo cells.

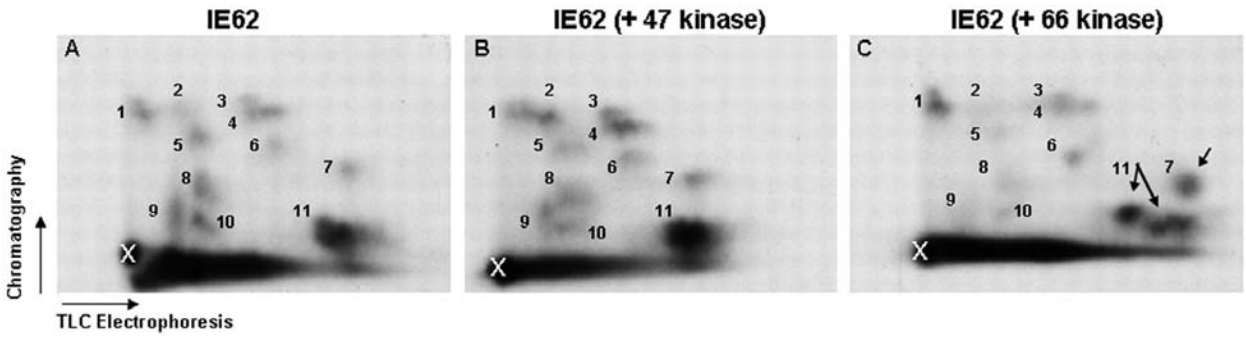

Figure 3-1 Full-length IE62 is differentially phosphorylated in the presence of ORF66 kinase

IE62 was expressed in the absence (A) or presence of ORF47 (B) or ORF66 kinase (C) in transfected 293T cells, metabolically labeled with [^{32}P]orthophosphate, immunoprecipitated, and subjected to tryptic phosphopeptide mapping as described in Materials and Methods. The X in the lower left corner of each map indicates the origin of spotting of the peptides. The horizontal axes represent electrophoresis of the peptides on TLC plates, and the vertical axes represent the chromatography step. Phosphopeptide spots are labeled with numbers to facilitate reference from panel to panel, and arrows in panel C indicate the differences in spots generated by co-expression of IE62 with the ORF66 kinase that are discussed in the text.

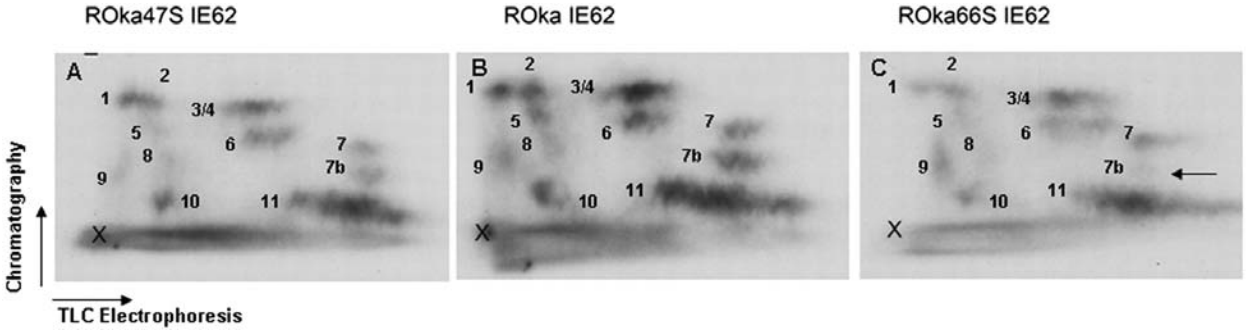

Figure 3-2 IE62 is differentially phosphorylated in the presence of ORF66 in the context of VZV infection

Tryptic phosphopeptide maps were generated from IE62 obtained from ^{32}P-labeled VZV-infected cells by immunoprecipitation, as described in Materials and Methods and in the legend to Figure 1. IE62 was derived from MeWo cells infected with VZV ROka47S (not expressing ORF47) (A), VZV ROka (B), and VZV ROka66S (not expressing ORF66) (C). The X in the lower left corner of each map indicates the origin of spotting of the peptides. The arrow in panel C indicates a phosphopeptide which is reduced in ROka66S IE62.

3.4.2 Fine mapping of ORF66 mediated phosphorylation of IE62

Because novel phosphorylation of IE62 induced by ORF66 has not been reported for the corresponding orthologous proteins in other alphaherpesviruses, we took approaches to map the phosphorylation sites in detail. We were unable to unambiguously identify the novel ORF66 induced peptides seen in the ORF66 co-transfection IE62 peptide map (Figure 3-1C) using peptide mass spectrometry approaches. Therefore, we used a series of IE62 deletion and peptide expression plasmids to map the ORF66 mediated phosphorylation of IE62. In previous studies, ORF66 induced the phosphorylation of a peptide of IE62 of residues 571-735, although much more efficient phosphorylation occurred with IE62 peptides spanning residues 414-823 (124). The more efficient phosphorylation of the larger peptide was suspected to be a consequence of the presence of the predicted DNA binding and dimerization domains of IE62, which may act to stabilize the IE62 peptide in transfected cells. We therefore used a larger peptide, and deletions of it, as a basis for further mapping (Figure 3-3A). Each HA-tagged IE62 peptide was co-expressed in transfected 293T cells with either functional untagged ORF66 protein kinase or empty vector control, metabolically labeled with [^{32}P]-orthophosphate and immunoprecipitated with HA antibody. The immunoprecipitated IE62 peptide of residues 414-735 expressed from plasmid pGK2-HA846 demonstrated strong phosphorylation in cells co-expressing the ORF66 protein kinase and little detectable phosphorylation in the absence of the kinase, confirming that this domain contained sites of ORF66 directed phosphorylation (Figure 3-3B, lane 2). An IE62 peptide that contained an in-frame deletion of the residues between 571 and 656 (HA825) was also efficiently and preferentially phosphorylated in ORF66 co-expressing cells (Figure 3-3B, lane 4). However, IE62 peptides containing residues 414-571 fused to only the IE62 nuclear localization signal (HA819) did not show [^{32}P] incorporation in ORF66 co-expressing or control

cells (Figure 3B, lane 6), and a peptide representing residues 414 to 687 (HA810) showed only minor labeling in both ORF66 expressing and not expressing cells (lane 16). Of note, the HA810 peptide contains a predicted cdk2 consensus site at T680, and cdk2 regulates the nuclear import of SV40 T antigen (109). The implied phosphorylation of residues C terminal to the nuclear localization signal was strengthened by examining IE62 peptides containing amino acids 414-571 fused to 673-735 (HA828) containing T680, and a peptide containing residues 414-571 fused to 677-735 (HA811), which lacks the residues preceding T680 (Figure 3-3B, lanes 14 and 12). Both of these peptides were efficiently phosphorylated, suggesting ORF66 mediated phosphorylation events occur between residues 686 to 735, which are carboxyl to the IE62 NLS (Figure 3-3A). In other studies, we noted that the peptide expressed from HA810, terminating at residue 687, was not efficiently imported into the nucleus (data not shown). As it was possible that the lack of phosphorylation of the peptide may have been a consequence of nuclear import, we examined two additional IE62 peptides in which the 414-571 peptide was fused to residues encoding NLSs from either ORF61 (HA821) or SV40 T antigen (HA823). These peptides were predominantly nuclear (data not shown), yet both were poor phosphorylation substrates (Figure 3-3B, lanes 8 and 10). Thus, the differential phosphorylation events identified reflect the presence or absence of target motifs for phosphorylation, rather than differences in cellular localization. Finally, it was possible that the observed phosphorylation differences could be due to unstable peptides, so we examined the expression of the peptides in transfected cells. All the IE62 peptides used in this study were found to be efficiently expressed in transfected cell extracts, although we noticed a somewhat more efficient expression of most peptides in the presence of the kinase in some studies (Figure 3-3C). However, the differences in expression do not account for the differences in phosphorylation seen in Figure 3-3B. Thus, the different

phosphorylation levels more likely reflect presence or absence of phosphorylation sites. We additionally note that an ORF66-specific phosphorylated protein of approximately 17 KDa was found in many (Figure 3-3B, indicated by a hatched circle, lanes 2, 4, 6, 8, 10 and 16) but not all (Figure 3-3B lanes 12 and 14) IE62 peptide immunoprecipitates from ORF66 kinase positive cells. The identity of this protein has not yet been resolved.

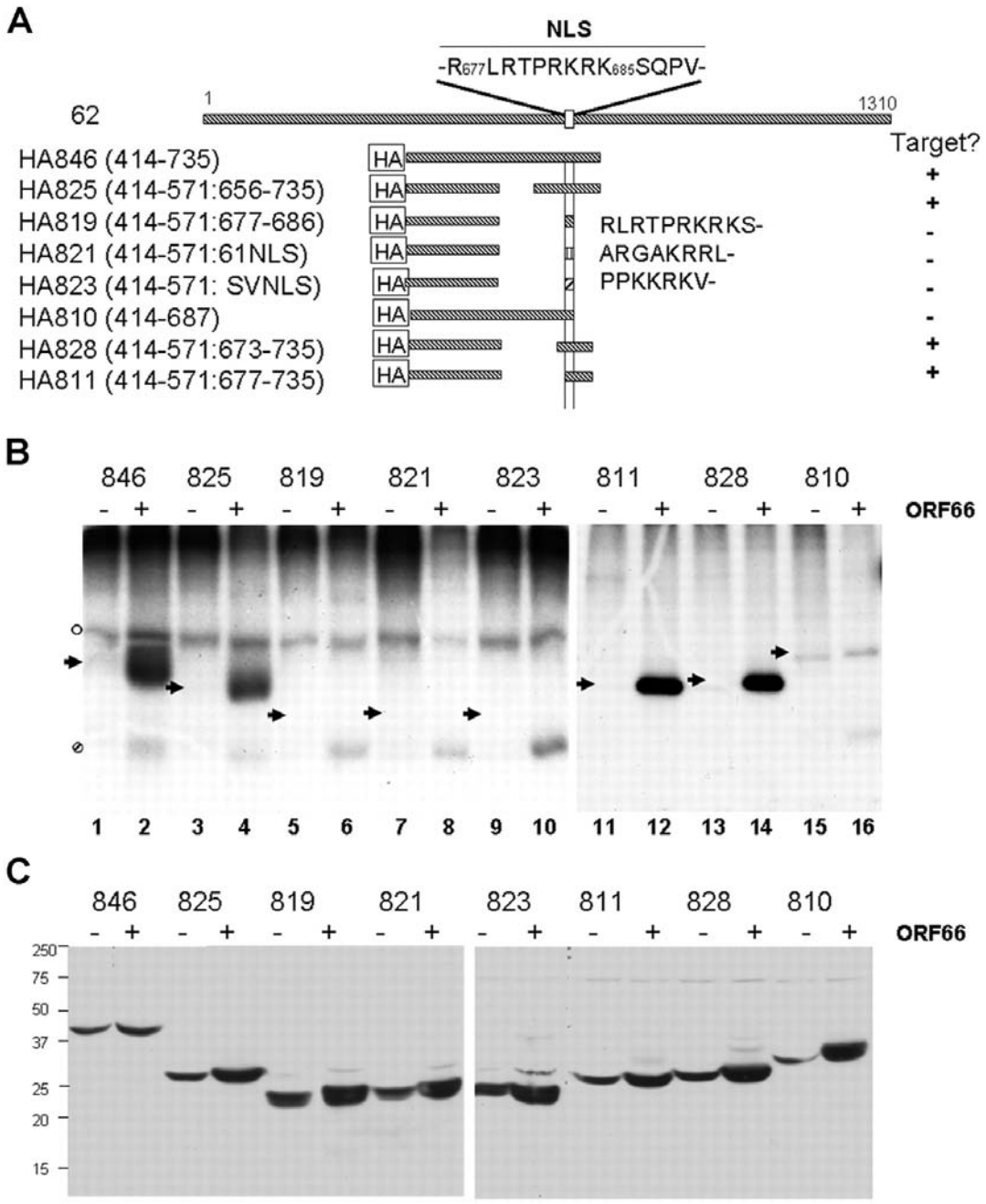

Figure 3-3 Mapping of VZV ORF66 kinase-induced phosphorylation of IE62 peptides

(A) Schematic representation of IE62 peptides used for this work. The top line represents the full-length IE62 protein and the relative position of its NLS (33), which is shown above the line in single-letter code, with key residues numbered according to their positions in IE62. Lines beneath full-length IE62 represent the peptides expressed relative to the complete IE62 protein. The precise residues expressed from each construct are indicated to the left of each representation, and for constructs expressing NLSs of other proteins in conjunction with a 414-571 IE62 peptide, the NLS sequences are indicated in single-letter code to the right of the

representations. ORF66-specific phosphorylation of the peptide (Target?) is indicated to the right. (B) SDS-PAGE-separated, immunoprecipitated, ^{32}P-labeled IE62 peptides expressed from the constructs shown in panel A, either in the presence (+) or in the absence (–) of ORF66 kinase. Arrowheads indicate the expected sizes of the expressed IE62 peptides for reference in the text. Nonspecific phosphopeptides detected in both the presence and absence of ORF66 in some studies are indicated by an open circle, and an unidentified protein co-precipitating with the IE62 peptide expressed in ORF66 kinase-positive cells is identified by a hatched circle. Lane numbers are indicated at the bottom of the radiograph. (C) Immunoblot detection of the same respective peptides expressed in 293T cell extracts obtained from a similar transfection, showing the relative levels of peptides expressed in the absence (–) or presence (+) of a 1:1 ratio of the ORF66 protein kinase. The peptides were detected with an HA-specific antibody. Molecular masses of marker proteins and their relative mobilities are shown to the left of the blots.

To further delineate the ORF66-specific target residues within IE62, a site-specific mutagenesis approach was used, in which single or clusters of the nine candidate threonine and serine residues between the IE62 NLS and amino acid 735 were mutated to alanine (Figure 3-4A). Each point mutated construct was generated in the background of the 414-735 peptide and then co-expressed and metabolically labeled in transfected 293T cells with either functional ORF66 protein kinase or dead kinase expressed from the plasmid pCMV66-K122A (111). In this study, we detected a low level of IE62 peptide labeling in the absence of the functional ORF66 kinase, reflecting a weak activity of cellular protein kinases on the 414-735 peptide. This was also observed for peptide expressed from construct 810 (Figure 3-3B). In the presence of the ORF66 protein kinase, there was enhanced labeling of the wild-type peptide, as expected (Figure 3-4B, lane 11). In peptides containing serine to alanine mutation of residues 691/693/701 as a group, and of residues 726/728/729 as a group, there was ORF66-specific phosphorylation comparable to the wild type peptide (Figure 3-4B, lanes 1 and 7). However, in peptides that contained S722A or S686A mutations, either alone or with other residues, there was a significant reduction of the level of phosphorylated peptides found, although in no circumstance was all phosphorylation abrogated by a single point mutation. These results

suggested that both S686 and S722 are target residues in IE62 for the phosphorylation induced by the ORF66 protein kinase. Densitometric analyses from this experiment indicated that the S686A and S722A mutations abrogated 64% and 54% of the IE62 peptide phosphorylation in the presence of the ORF66 kinase, respectively, as compared to the unaltered peptide. Similar results were obtained from peptides expressed in transfected MeWo cells, although the level of basal phosphorylation of the peptides in the absence of the ORF66 kinase, presumably representing activity of cellular kinases, was found to be higher (data not shown).

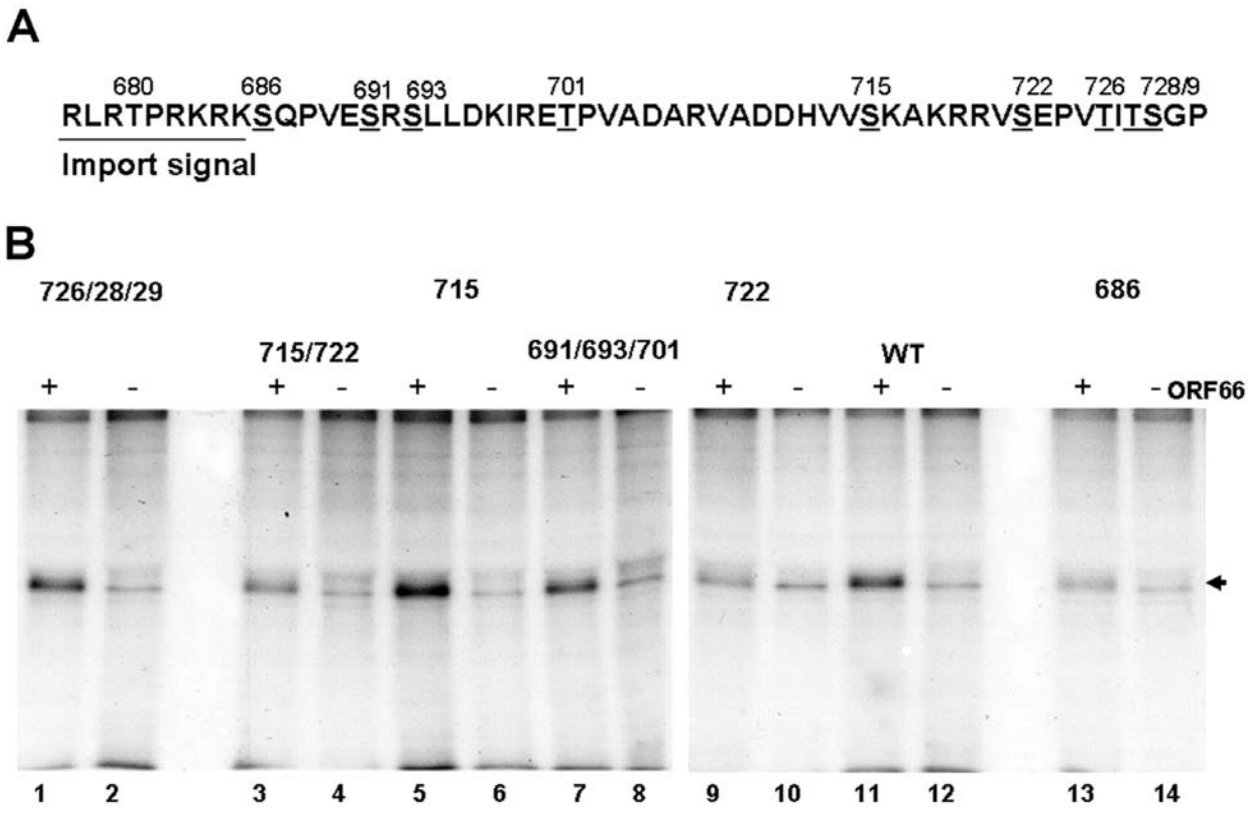

Figure 3-4 Identification of ORF66-induced phosphorylation of IE62 peptides

(A) Representation of the region of IE62 containing ORF66-directed phosphorylation sites, with the amino acid sequence in single-letter code and the position of each serine or threonine residue indicated with the residue number above. (B) Radiograph showing SDS-PAGE-separated immunoprecipitates of ^{32}P-labeled IE62 peptides expressed in the absence (–) and presence (+) of a 1:1 ratio of functional ORF66 protein kinase. All peptides contain residues 414 to 735 of the IE62 peptide, but with specific serine/threonine transitions to alanine, as indicated above each

pair of lanes. The arrowhead indicates the expected size of the phosphorylated IE62 peptides. Lane numbers are indicated at the bottom of the radiograph for reference in the text.

To further evaluate the ORF66 protein kinase-induced phosphorylation at IE62 S686 and S722, we carried out *in vivo* labeling studies of peptides lacking one or both targets in the IE62 414-735 residue peptide background; wild type, S686A, S722A and a double mutated peptide S686A/722A. MeWo cells were transfected with ORF66:IE62 plasmid ratios of 0:1, 1:1, 3:1, and 5:1 to determine if higher levels of phosphorylation could be achieved with more transfected kinase. The IE62 wild-type peptide exhibited an increase in phosphorylation of 3.7 fold at the 1:1 ratio over the peptide expressed in ORF66 negative conditions (0:1). At higher ratios of kinase to peptide, this level of phosphorylation did not increase significantly (peptide HA846, Figure 3-5A). Peptides containing either S722A or S686A single mutations exhibited an overall reduction in their level of phosphorylation when expressed with ORF66, although ORF66 induced phosphorylation was still apparent at all ratios of ORF66:IE62 peptide, as compared to no kinase. In contrast, when both S686 and S722 were altered to alanines, IE62 peptide phosphorylation in the presence of ORF66 was reduced to background phosphorylation levels seen in the absence of transfected ORF66. Densitometric analyses of the level of the phosphorylation of the double mutant IE62 peptide indicated only a 1.3X increase in phosphorylation at the 1:1 and 3:1 ratios and no relative phosphorylation increase at the 5:1 ratio, as compared to peptide expressed in the absence of ORF66 (0:1). Immunoblot analyses of the IE62 peptides expressed in transfected cells with different levels of the protein kinase indicated that they were efficiently expressed (Figure 3-5B). Overall, the differences seen in Figure 3-5A were concluded to reflect [^{32}P] incorporation levels and not peptide expression levels. These

data support the conclusion that ORF66 mediated phosphorylation of the IE62 peptide is largely restricted to two sites carboxyl to the IE62 NLS, namely residues S686 and S722.

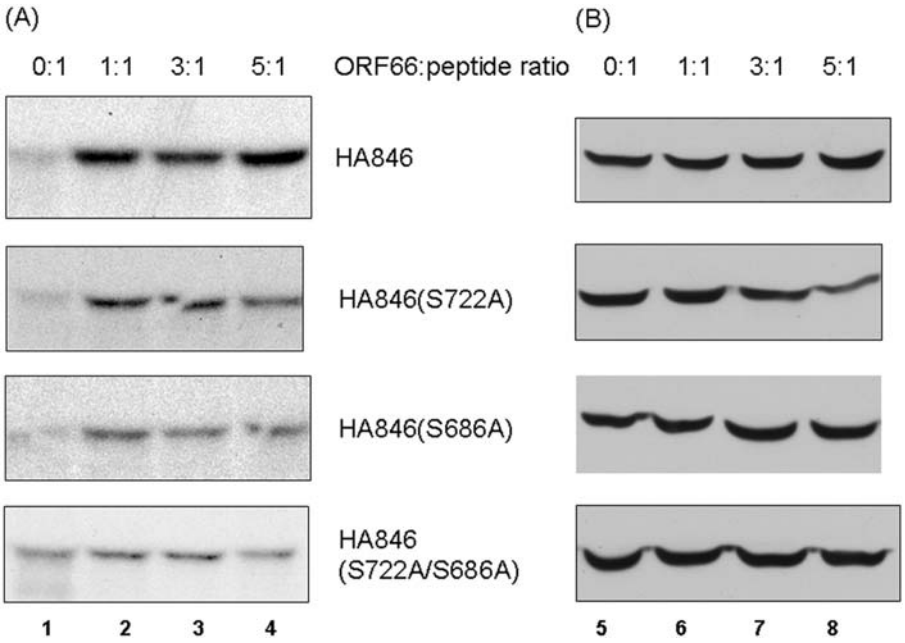

Figure 3-5 Expression and [32P]orthophosphate labeling of IE62 wild-type and serine mutant peptides expressed in the absence or presence of different levels of ORF66

(A) Autoradiograph showing SDS-PAGE-separated, [^{32}P]orthophosphate-labeled, immunoprecipitated peptides expressed from plasmid pGK2-HA846 (HA846) or similar plasmids with S686A, S722A, or S686A/S722A mutations. Immunoprecipitates were prepared from cells transfected with equal levels of plasmid expressing the IE62 peptide and with an empty vector or plasmid expressing ORF66, adjusted to give ORF66-to-IE62 peptide ratios of 0:1, 1:1, 3:1, and 5:1, as indicated at the top of the figure. The exposures of the autoradiographs were equivalent, except for that of the IE62 double mutant (S686A/S722A), which was overexposed approximately threefold compared to the others to show the minor level of phosphorylation by cellular kinases. (B) Immunoblots showing the expression of each HA-tagged IE62 peptide expressed in cells following similar transfections to those performed for panel A in order to show expression of the peptides at the different IE62 peptide-to-ORF66 ratios. The peptides were identified with HA-specific antibodies. Numbers at the bottom refer to lanes discussed in the text.

3.4.3 Identification of the ORF66 induced phosphorylation events affecting nuclear import of IE62

Both of the IE62 residues S686 and S722 are carboxyl to the mapped NLS of IE62 (127, 129), and have similarities in contextual sequence (see Figure 3-4A). Both are preceded by 3 basic amino acids at the -4, -3 and -2 positions, and are followed by a proline at the +2 position and a valine at the +3 position. Interestingly, only the arginine/lysine rich region preceding S686 acts as an NLS in MeWo cells (129). If phosphorylation of IE62 at S686 (immediately adjacent to the NLS) or S722 (37 residues downstream of the NLS) affects IE62 nuclear import, the alteration of the key target serine should result in the generation of a nuclear IE62 protein in the presence of the ORF66 kinase. To this end, the cellular distribution of wild-type and mutant full-length IE62 proteins containing serine to alanine mutations were analyzed (Figure 3-6). In these studies, functional, HA-tagged ORF66 kinase was used to facilitate the identification and cellular location of the protein kinase in transfected cells by immunofluorescence. All co-transfections were performed with a 1:1 ratio of ORF66:IE62. Two hundred IE62 positive cells were scored for the cellular distribution of IE62 under each condition.

Full-length, wild-type IE62 expressed in the absence of ORF66 showed typical nuclear localization in greater than 94% of IE62 positive cells, with both a diffuse nuclear staining, negative nucleolar staining and a sub-nuclear concentration to distinct dots adjacent to the nucleolus (Figure 3-6A). Rare cells (less than 5% of the total positive) showed some cytoplasmic distribution of IE62, and these were suspected to represent cells with poorly defined nuclear membranes that may have recently undergone cell division. Only one cell of 200 counted showed an exclusively cytoplasmic form of IE62. Virtually identical nuclear distribution patterns were found in IE62 S686A (Figure 3-6B) and IE62 S722A (Figure 3-6C) proteins in the

absence of ORF66 kinase expression. In the presence of the ORF66 kinase, approximately 70% of the wild-type IE62 positive cells demonstrated a predominantly cytoplasmic staining for the IE62 protein, with the remaining cells demonstrating both nuclear and cytoplasmic forms of IE62 (Figure 3-6D). No cells expressing both wild-type IE62 and ORF66 demonstrated a predominantly nuclear phenotype for the IE62 protein, and nuclear IE62 was only detected in those few transfected cells which failed to co-express ORF66. The ORF66 protein demonstrated a predominantly nuclear speckled localization in many cells in the presence of wild-type IE62, with some cytoplasmic distribution, similar to that observed in previous studies (124). Like wild-type IE62, IE62 containing S722A co-expressed with the ORF66 protein kinase resulted in predominantly cytoplasmic localization of the IE62 protein in all ORF66 co-expressing cells (Figure 3-6E). In contrast, IE62 carrying the S686A mutation demonstrated predominantly nuclear localization both in the presence and the absence of the ORF66 protein kinase in nearly all cells, similar to wild type IE62 expressed alone (Figure 3-6C and F). The ORF66 kinase showed a mostly nuclear distribution but nucleolar exclusion, and confocal analyses indicated a predominant overlap of the signals of the two proteins. IE62 S686A remained nuclear even in the presence of higher ratios of ORF66:IE62, suggesting that the kinase insensitivity of nuclear localization could not be overcome by expressing higher levels of protein kinase (data not shown). These results strongly suggest that ORF66 mediated phosphorylation of S686 is the event that causes the cytoplasmic accumulation of IE62.

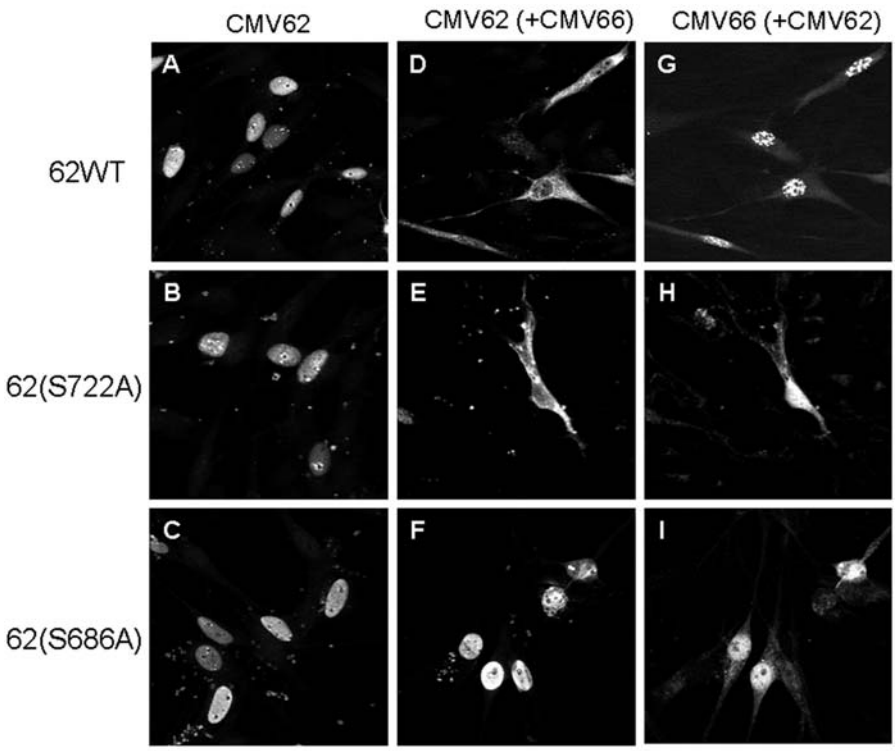

Figure 3-6 IE62 protein containing S686A, but not S722A, mutation is resistant to ORF66-mediated nuclear exclusion

IE62 proteins carrying either the wild-type residues or an S686A or S722A mutation were expressed in the presence or absence of functional HA-tagged ORF66 in VZV-permissive MeWo cells, and their cellular distributions were determined using indirect immunofluorescence at 24 h, as described in Materials and Methods. IE62 was detected using rabbit anti-IE62 with secondary Alexa fluor 488-conjugated antibodies, and ORF66 was detected using mouse anti-HA with secondary Alexa fluor 546-conjugated antibodies. The left panels exhibit full-length IE62 proteins transfected in the absence of ORF66 (A to C), the middle panels display IE62 protein staining in cells co-expressing the live HA-tagged ORF66 kinase (D to F), and the right panels (G to I) show the expression of HA-tagged ORF66 in the same cells as those shown in the middle panels.

To further support this interpretation, we derived and expressed IE62 proteins that contained S686D or S722D mutations, designed to place a permanent, primary structure-based negative charge at S686 or S722, to mimic the negative charges exerted by phosphorylation. In transfected MeWo cells, IE62 S722D protein showed a nuclear distribution similar to wild type protein, including a sub-nuclear concentration adjacent to nucleoli (Figure 3-7B). In contrast,

S686D IE62 proteins demonstrated an inefficient nuclear import, with most cells displaying at least some cytoplasmic accumulation. Some cells expressing the IE62 S686D protein had little nuclear distribution (upper left, Figure 3-7C), but many demonstrated some nuclear accumulation with obvious cytoplasmic accumulation (lower right, Figure 3-7C). Confocal sectioning indicated that there was nuclear import of IE62 S686D protein in these cells. These results are consistent with the ORF66 mediated phosphorylation and addition of a negative charge at IE62 residue S686, which negatively regulates the activity of the immediately adjacent NLS. The partially inhibited nuclear import phenotype likely resulted from the inability of the aspartate residue to fully mimic the negative charge exerted by phosphorylation.

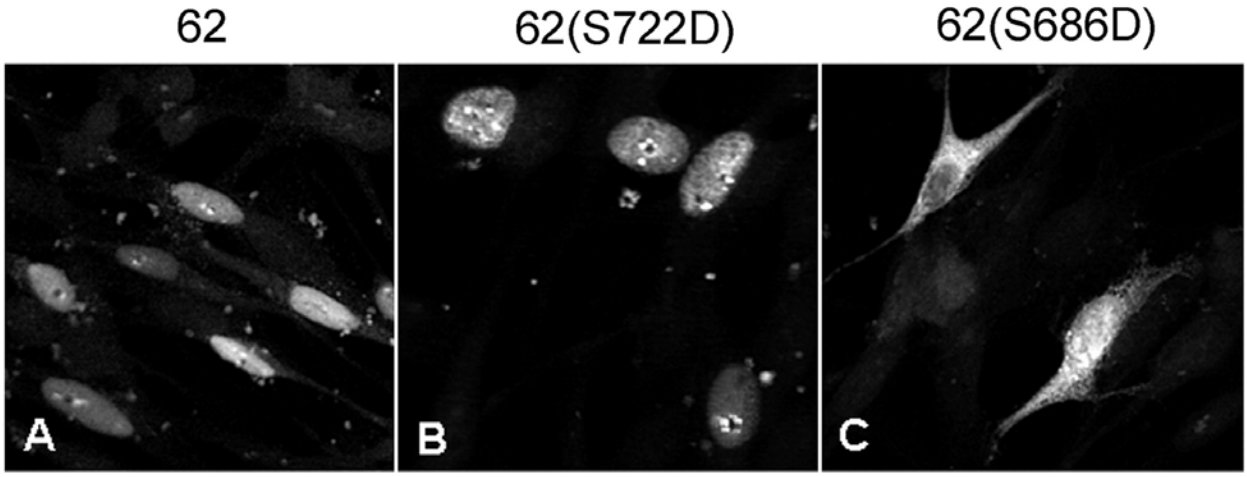

Figure 3-7 Mimicking phosphorylation through aspartic acid replacement of S686, but not S722, results in partial inhibition of nuclear import

Full-length IE62 proteins with the wild-type sequence or with an S686D or S722D mutation were individually transfected into MeWo cells, and cells were fixed and stained for IE62 expression using anti-IE62 and Alexa fluor 488-conjugated secondary antibodies as described in Materials and Methods. Representative cells are shown. The specific S→D mutation is indicated above each panel.

3.4.4 Baculovirus mediated expression and *in vitro* autophosphorylation of the ORF66 kinase

The observed phosphorylation of IE62 in ORF66 expressing cells could be either a consequence of direct phosphorylation by the ORF66 kinase or the result of an indirect mechanism, such as ORF66 activation of a cellular kinase or pathway that leads to IE62 phosphorylation. We therefore considered it necessary to determine if the ORF66 kinase could directly phosphorylate IE62. Extensive attempts to develop an *in vitro* kinase assay with ORF66 obtained from VZV infected cells were not successful, because the ORF66 protein kinase has proven to be highly insoluble in buffers designed to solubilize the kinase and retain its kinase activity. Therefore, we expressed the HA tagged ORF66 protein kinase in SF9 cells using a recombinant baculovirus (Bac-HA66). Following high multiplicity infection and 48 hours of expression, approximately 5% of the total HA-ORF66 protein was soluble after cell lysis in a mild RIPA buffer. Immunoblotting of HA-ORF66 with HA specific antibodies resulted in identification of two closely migrating but distinct forms on SDS-PAGE, as seen in transfected cells (124) (data not shown).

We first examined autophosphorylation of the SF9 expressed protein kinase. ORF66 autophosphorylation was implied from the observation that point inactivated ORF66 kinases do not exhibit the slower migrating form on SDS PAGE gels (124). Extracts of SF9 cells expressing either the HA-ORF66 kinase or glutathione-S-transferase (GST) control were immunoprecipitated with HA specific or non-specific antibodies, either in the presence or absence of blocking HA peptide or an unrelated peptide. The washed immunoprecipitates were incubated with a standard kinase buffer containing 10 mM $MgCl_2$, [γ–^{32}P] ATP and 10 µg/ml heparin (to block casein kinase II activity (186). The latter was found through preliminary

studies not to affect ORF66 kinase activity. SDS-PAGE and autoradiography revealed a heavily phosphorylated band of 55 KDa, consistent with the size of HA-tagged ORF66, only in immunoprecipitates from SF9 cells infected with the Bac-HA66 (Figure 3-8, lane 2). This band was efficiently detected when a non-specific peptide was used with the antibody-antigen mix, and its immunoprecipitation was inhibited by addition of HA peptide (Figure 3-8, lane 4). There was no equivalent 55 KDa phosphorylated band in extracts immunoprecipitated from Bac-GST infected cells under any conditions (Figure 3-8, lanes 5-8). These data show that the HA-ORF66 kinase is specifically precipitated from Bac-HA66 infected cell extracts and can autophosphorylate.

The optimal conditions for ORF66 *in vitro* kinase activity were determined by evaluating cation choice (Mn^{2+} or Mg^{2+}) and concentration (2 to 100 mM), different pH (pH 6.0 to 9.0), and variable salt concentrations (0 to 1M KCl). These were performed for auto-phosphorylation activities, but the optimal conditions were found to be suitable for trans-phosphorylation of a highly purified IE62-MBP 571-735 peptide. Kinase activity was found to be optimal with 50 mM Mn^{2+}, physiological pH [7.5], 50 mM KCl and was not inhibited by 10 μg/ml heparin. As such, the optimized buffer was used for all remaining kinase assays. We note the preference for Mn^{2+} ions was also found for the phosphorylation activity of the VZV ORF47 kinase (186). While sites for autophosphorylation of ORF66 have not yet been determined, two ORF66 candidate sequences ($KRS_{331}SRKPGSR$ and $RHRPS_{368}$) have serines proximal to multiple basic residues, as found for the target residues for ORF66 directed phosphorylation in IE62.

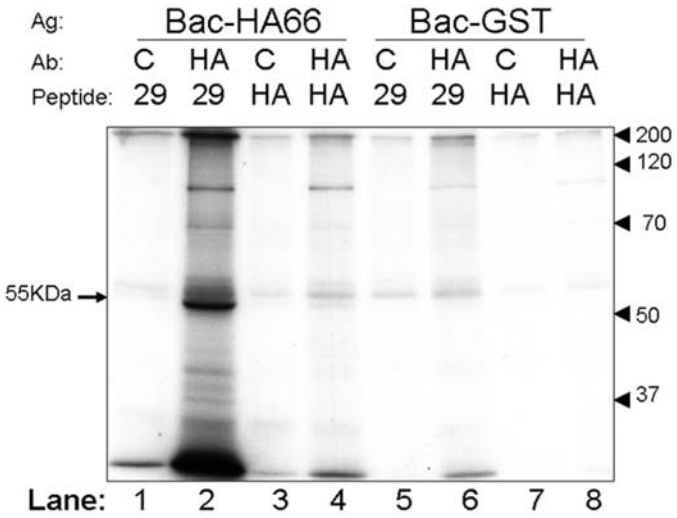

Figure 3-8 Development of immunocomplexed ORF66 in vitro kinase assay

Protein antigens (Ag) from SF9 insect cells infected with Bac-HA66 or control Bac-GST were solubilized in a modified RIPA buffer and immunoprecipitated with either anti-HA (HA) or a nonspecific (C) antibody in the presence of either 0.2 mg/ml specific (HA) or nonspecific (29) competitor peptide. Washed immunoprecipitates were then incubated with [γ-^{32}P]ATP in kinase buffer as described in Materials and Methods. Proteins were resolved by SDS-PAGE and detected by autoradiography. SDS-PAGE standards are marked at the right, and lanes are marked at the bottom of each panel for reference in the text. The 55-kDa HA-ORF66 autophosphorylated protein band is indicated by an arrow to the left of the autoradiograph.

3.4.5 ORF66 phosphorylates IE62 peptides *in vitro* with the same specificity as *in vivo*

To determine if ORF66 could directly phosphorylate IE62, immunoconjugated HA ORF66 was incubated with purified MBP-IE62 peptide fusion substrates under optimal kinase conditions (Figure 3-9). Four purified MBP-fusion proteins containing IE62 amino acid region 571-733 fused to MBP were analyzed, with or without changes at the specific serine residues identified in the *in vivo* phospholabeling studies (WT, S686A, S722A, and S686A/S722A; Figure 3-9A). Equal amounts of these fusion proteins (Figure 3-9B, lanes 11-14) were incubated with HA-immunoprecipitates from Bac-HA66 (Figure 3-9B, lanes 1-5) or Bac-GST-infected cell lysates (Figure 3-9B, lanes 6-10) and analyzed by SDS PAGE. In the Bac-GST control

immunoprecipitates, virtually no phosphate labeling was detected for any of the IE62 peptides (Figure 3-9B, lanes 6-10; the first and second panels represent equally exposed autoradiographs). However, incubation of MBP-IE62 fusion proteins with Bac-HA66 immunoprecipitates resulted in strong phosphorylation of the wild-type MBP-IE62 fusion (Figure 3-9B, lane 1). Importantly, the MBP-IE62 fusion with point mutations in both S686 and S722 was a much poorer substrate for the HA-ORF66 kinase, despite loading of equivalent levels of each MBP-IE62 peptide into the assay. Furthermore, individual mutation of one serine to alanine resulted in reduced phosphorylation of the peptide, but not to the extent of wild type IE62-MBP fusions (Figure 3-9B, lanes 3 and 4). The phosphorylated protein of 55 KDa was the autophosphorylated protein kinase, as it was present in the immunoprecipitates lacking any MBP fusions and was not present in Bac-GST control immunoprecipitates. Similar results were obtained in two replicate experiments.

Phosphorimaging analysis of phosphorylated MBP-IE62 peptides was performed for three replicate experiments, and the average percent optical density (compared to wild-type) of each phosphorylated band is plotted in Figure 3-9C. A marked ~75% decrease in signal was observed with the double mutant peptide, and a reduced signal was seen with single mutation of either S686 or S722 individually. We conclude that IE62 is a direct substrate for the ORF66 protein kinase, and that the activity observed in our *in vitro* reactions reflects a direct ORF66-mediated IE62 phosphorylation event. Thus, IE62 represents a new target for the US3 group of kinases.

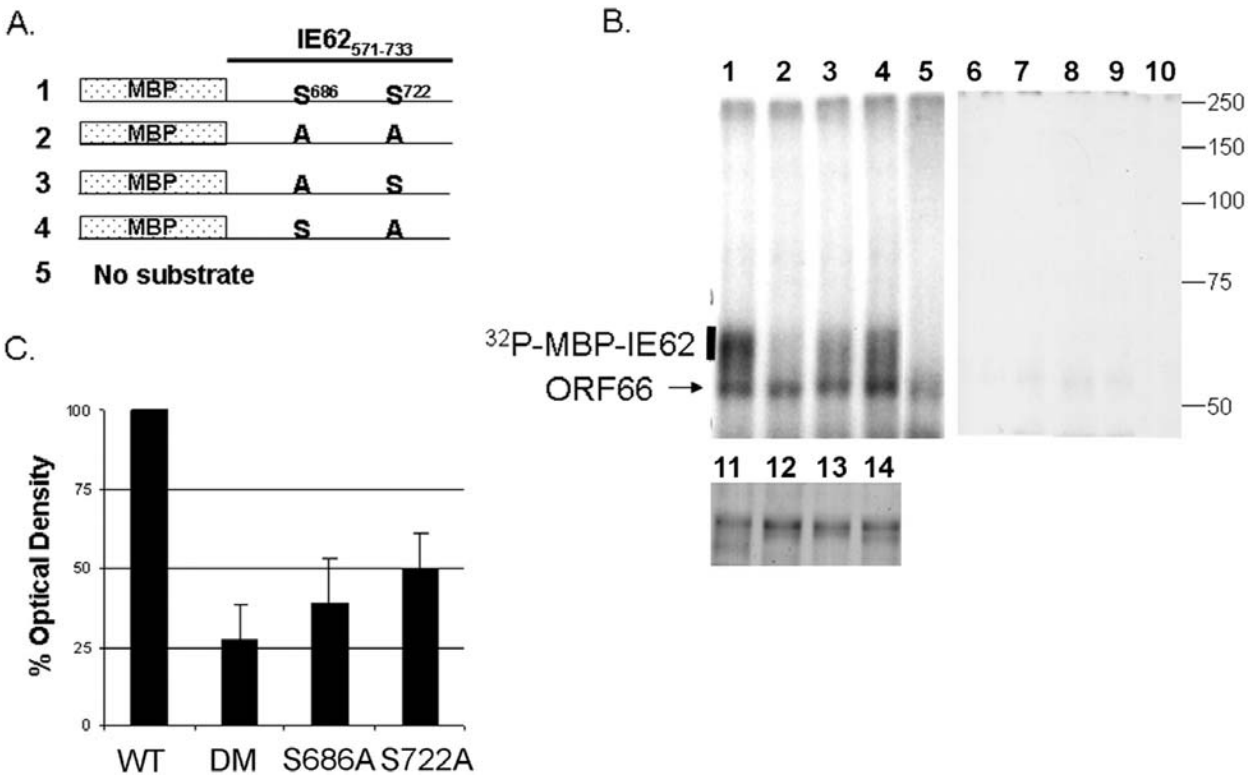

Figure 3-9 Immunopurified ORF66 specifically phosphorylates MBP-IE62 peptides at S686 and S722 in vitro

(A) Representation of MBP-IE62 fusion proteins that were constructed and purified for the in vitro kinase assay. The residues at positions 686 and 722 are shown in single-letter code for the IE62 portion of the fusion peptide. (B) Autoradiographs of in vitro kinase assays using equivalent amounts of each purified MBP-IE62 substrate protein shown in panel A. The purified proteins were incubated in optimal kinase buffer with immunocomplexed HA-ORF66 (lanes 1 to 5) or with similar HA-tagged immunoprecipitates obtained from Bac-GST-infected cell lysates (lanes 6 to 10). Lanes 1 and 6 contain the wild-type IE62 peptide, lanes 2 and 7 contain the double mutant peptide, lanes 3 and 8 contain the S686A mutant peptide, lanes 4 and 9 contain the S722A mutant peptide, and lanes 5 and 10 contain the respective baculovirus immunoprecipitates with no added maltose binding protein fusions. Both autoradiographs were exposed equally. The lower panel (lanes 11 to 14) shows SDS-PAGE-separated input MBP-IE62 substrate proteins used for lanes 1 to 4 and 6 to 10 following staining with Coomassie brilliant blue to show the purified proteins. To the right of the radiographs are shown the approximate positions of molecular mass markers, in kDa. (C) Average values from densitometric quantification of autoradiographs of three replicate experiments, including that shown in panel B. Densitometric values of phosphorylated MBP-IE62 fusion proteins were normalized to the wild-type MBP-IE62 peptide densitometry value (set to 100%) after subtracting the background signal for each lane. Error bars represent standard deviations from the means. Only the region of the gel indicated by a bar to the left of the autoradiograph in panel B was evaluated. DM, double mutant.

3.5 DISCUSSION

Taken together with previous results (123, 124, 129), we have now shown that VZV IE62, the principal transcriptional transactivator and a major component of the VZV virion tegument, is a direct target for phosphorylation by the VZV ORF66 protein kinase. Phosphorylation occurs at two residues, but the targeting of residue S686 is sufficient to induce IE62 to become cytoplasmic. These observations are consistent with a model in which one role of the ORF66 protein kinase is to directly phosphorylate IE62, negating its nuclear import to possibly negatively regulate IE62 mediated transcriptional activation of viral gene expression, and/or to potentially enable virion inclusion of a preformed transactivator into the VZV virion tegument. As ORF66 negative viruses are impaired for growth in T lymphocytes and in the SCID-hu thy/liv model of VZV infection (174, 220, 224), the interaction of ORF66 with IE62 may be an important for efficient viral pathogenesis.

Several lines of evidence were presented to support the conclusion that the ORF66 protein kinase phosphorylates IE62. Previously, nuclear exclusion of the IE62 protein by the ORF66 protein was shown to occur only if the protein kinase activity of ORF66 was intact and this correlated with enhanced phosphorylation of IE62 peptides by the ORF66 kinase in the context of both transfection and VZV infection (124). In a second study, IE62 demonstrated slightly different mobilities in SDS PAGE if the ORF66 kinase was not expressed (123). Here we used tryptic phosphopeptide mapping studies to further establish that ORF66 directs new phosphorylation events in full length IE62, in both co-transfections and in VZV infections. Two novel IE62 phosphopeptides were observed when IE62 was co-expressed with ORF66 transiently, and one IE62 phosphopeptide spot that was abundant in both ROka and ROka47S IE62 peptide maps was considerably reduced in IE62 from ROka66S. These differential levels

of phosphopeptide spots do not discriminate between direct phosphorlyation and ORF66 induced cellular kinase activity. We also note there was an overall reduction in many other IE62 phosphopetides found in the presence of ORF66, although they migrated to the same relative positions. One possible reason for the reduction is that IE62 is phosphorylated by compartmentalized cellular kinases, which act differentially on IE62 as a result of the ORF66 induced cellular re-localization of IE62. Another possibility is that ORF66 activates host cell signaling cascades and the activities of cellular kinases that subsequently lead to an increased level of IE62 phosphorylation. Other alphaherpesvirus US3 kinases have been implicated to affect host signaling cascades, because they have multiple effects on host cell function, such as multiple cytoskeletal reorganization effects (74, 221, 237). Studies are currently under way to determine the general phosphoprotein state of the cell expressing the ORF66 kinase.

IE62 peptides demonstrated the same phosphorylation specificity in both *in vivo* phospho-labeling studies in the presence of ORF66 and the *in vitro* ORF66 kinase assay, strongly suggesting IE62 is a direct target. Individually mutated IE62 peptides with S686A or S722A showed reduced phosphorylation, and mutation of both residues resulted in peptides that were much less sensitive to ORF66 phosphorylation. For an intermediate cellular kinase to act as the go-between for ORF66 mediated phosphorylation of IE62, it would have to efficiently co-purify with the baculovirus-expressed immunopurified ORF66 and have activity in the same buffer used for the kinase assays. The use of the divalent cation Mn^{2+} and heparin exclude activity of contaminating cellular CKII, and we consider that other cellular kinase contamination seems highly unlikely. Further proof will require high-level purification of the ORF66 protein kinase and demonstration of its affinity for its substrates. A suitable approach for this was recently elegantly demonstrated with the HSV-1 U_S3 kinase of HSV-1, in which purified GST-

U_S3 protein specifically phosphorylated several viral and cellular target–MBP protein fusion substrates (117). For ORF66, this has proven to be quite difficult because the protein kinase is very insoluble from VZV infected cells, and we have found that GST addition to the N terminus of ORF66 appears to inactivate or interfere with the kinase activity of ORF66 (A. Erazo, K, Fite, and P. R. Kinchington, unpublished data). Nevertheless, strategies to purify ORF66 may enable a more rigorous *in vitro* phosphorylation assay to be developed.

Of the two IE62 residues phosphorylated by ORF66, only S686 was shown to be involved in the nuclear exclusion of IE62. In conventional nuclear import, a basic arginine/lysine-rich NLS is recognized by one or more of the six importin α proteins, which in turn complex with importin β and are translocated through the nuclear pore via the GTP-binding protein Ran (reviewed in references (110, 180)). IE62 S686 is immediately adjacent to the IE62 NLS (aa 677-685) (129), and the close proximity strongly suggests an underlying mechanism in which phosphorylation inhibits nuclear import. Nuclear import of many proteins is highly regulated by phosphorylation close to their NLSs (reviewed in references (88, 110). Recent studies have shown that either direct phosphorylation or mutations mimicking phosphorylation through acidic residue replacement of the target residue at a site immediately N terminal to an NLS results in decreased affinity of the NLS for importin α (88). N-terminal phosphorylation events that impair nuclear import of proteins are common, and occur in proteins such as SV40 T antigen, parathyroid hormone-related protein (PTHrP), and v-jun (109, 142, 213, 229). As far as we are aware, IE62 is one of a much rarer group of proteins that are nuclear import regulated by phosphorylation at a residue carboxyl to the NLS. One other such protein is the adenomatous polyposis coli (APC) protein (256). Mechanistically, the simplest explanation is that the strong negative charge exerted by phosphorylation at a site proximal to the NLS reduces importin

binding affinity. However, there are some suggestions that more complex issues affect nuclear distribution of IE62. In transfected cells, the majority of ORF66 protein localizes to the nucleus, with only a fraction remaining cytoplasmic (124). With the simple model, phosphorylation of newly translated IE62 at S686 would be mediated by the small fraction of cytoplasmic ORF66. In an alternative explanation, the phosphorylation of IE62 by ORF66 would occur in the nucleus, and coupled with a possible nuclear export mechanism of phosphorylated IE62, IE62 would exit and be unable to re-enter the nucleus. In a VZV infection, the latter scenario would enable nuclei to empty of IE62 at late stages of VZV infection, and we and others have observed that many late stage nuclei in wild-type VZV plaques appear devoid of IE62 (unpublished data; see also figures in reference (22)). The possible nucleocytoplasmic shuttling capability of IE62 in VZV infection is currently under investigation.

The functional significance of phosphorylation at residue S722 is not yet clear. While residues immediately amino terminal to S722 have similarity to canonical NLSs (see Figure 3-4A), the sequence cannot act as an NLS in the absence of the 677-685 NLS sequence in MeWo cells (129). Furthermore, phosphorylation of S722 (in S686A mutants of IE62) does not inhibit IE62 nuclear import in multiple cell types tested. However, we postulate that the IE62 716-720 basic residue region may function as an NLS in specific cell type(s) not yet identified. The six known importin α proteins each demonstrate variable binding specificity to cargoes and also show cell-type dependent regulation of expression (180, 208). VZV infects multiple cell types during the natural course of infection, including epithelial cells, T-lymphocytes, dendritic cells (179), skin cells and sensory neurons (138, 139), and it is possible that the IE62 716-720 region may be a functional or preferred NLS in one of these cell types. Therefore, we suggest that the phosphorylation of both S686 and S722 is maintained to abrogate IE62 nuclear import at later

stages of VZV infection in multiple host cell types with different importin α expression characteristics.

IE62 is the first viral target reported for the VZV ORF66 kinase, and the corresponding interaction demonstrated in this work has not been reported in other alphaherpesviruses. We previously postulated that IE62's role as a tegument protein may be, in part, to supplement transactivation of IE viral gene expression (123), as VZV that does not express ORF10, the HSV-1 VP16 homolog, can still grow well in culture (42). Several viral targets of the orthologous US3 kinase have been identified, but it is not yet clear whether these are conserved in VZV. While ORF66 is not "essential" for tissue culture growth, disruption of ORF66 expression results in low virus production and poor capsid assembly (220). Recent data suggests that ORF66 may affect additional functions in the host cell in addition to IE62. ORF66 induces the downregulation of MHC-I surface expression ((2) and A. Eisfeld, P. Kinchington, unpublished data). In addition, comparison of ORF66 expressing and not expressing viruses in T cells has suggested that ORF66 may have roles in resistance to interferon as well as inhibition of virally induced apoptosis (220). Both of these activities have been attributed to US3 protein kinases (182, 188, 198). It thus seems that US3 kinases may share some common host cell targets, but that viral targets have differentiated as VZV and other alphaherpesviruses have evolved and separated from a presumed common ancestor. The effects of ORF66 on the host cell are now under investigation.

4.0 THE VARICELLA-ZOSTER VIRUS PRINCIPLE TRANSCRIPTIONAL REGULATOR, IE62, IS A NUCLEAR SHUTTLING PROTEIN

Amie J. Eisfeld[1,2] and Paul R. Kinchington[2,3,*]

Graduate Program in Molecular Virology and Microbiology[1] and Departments of Ophthalmology[2] and Molecular Genetics and Biochemistry[3], School of Medicine, University of Pittsburgh, PA, 15213

4.1 ABSTRACT

The varicella-zoster virus (VZV) IE62 protein is a critical nuclear transcriptional regulator that is re-distributed to the cytoplasm as a result of direct phosphorylation by the VZV ORF66 protein kinase. Based on the putative early expression kinetics of the ORF66 protein, we hypothesized that IE62 may require both ORF66 phosphorylation and nuclear export activities to account for its efficient nuclear exclusion in late-stage infected cells. Here, we utilized the recently described VZV.GFP-66 in cell-free time-course infections to establish for the first time that ORF66 expression ensues following that of IE62, and that ORF66 nuclear localization is not sufficient for IE62 nuclear exclusion. We assessed IE62's nuclear export abilities using interspecies heterokaryon analyses, which revealed IE62 shuttling into murine nuclei in both transfected cells expressing only IE62 and VZV infected cells where IE62 was insensitive to ORF66-mediated nuclear exclusion. Shuttling was specific, as a human nuclear resident protein remained associated only with human nuclei; and Crm1-independent, as it occurred in the presence of leptomycin B. Similar analyses of IE62 truncation peptides identified amino acids 733-995 as critical for nuclear export. Interestingly, disruption of the DNA-binding and dimerization domain resulted in enhanced shuttling, suggesting that IE62 nuclear retention may occur by recognition of cellular DNA or a dimerization-induced nuclear protein interaction. These studies also indicated a possible role for phosphorylation of the N-terminal poly-serine tract in facilitating nuclear export. In sum, IE62 nuclear exclusion is a complex process, likely regulated through phosphorylation by multiple kinases and active nuclear export through a Crm1-independent pathway.

4.2 INTRODUCTION

Varicella-zoster virus (VZV) is a human alphaherpesvirus, closely related to herpes simplex virus type 1 (HSV-1), that causes chickenpox upon primary infection and herpes zoster (shingles) following reactivation from latency. The VZV genome consists of ~125 kbp of dsDNA, and codes for ~70 unique open reading frame (ORF)s that are expressed during lytic infection. Gene expression likely occurs in a typical α-β-γ transcriptional cascade similar to that of HSV-1 (100, 101), and is regulated by the viral proteins from ORFs 4, 10, 29, 61, 62/71 and 63/70 (127). Of these, the principal transcriptional regulator of VZV gene expression is the immediate early protein encoded in duplicate by ORFs 62 and 71 (known as IE62).

IE62 activates expression from all putative temporal classes of VZV promoters (15, 40, 177, 195), positively and negatively influences its own promoter activity (55, 195), and substantially enhances the infectivity of VZV DNA (177). The IE62 primary sequence is similar to that of the HSV-1 ICP4 protein, and IE62 can partially complement ICP4 mutants and replace ICP4 in the HSV-1 genome (54, 64). However, HSV-1 carrying the IE62 gene exhibits an impaired replication phenotype, implying that unique processes govern IE62 and ICP4-mediated viral gene expression. The specific mechanism of IE62-mediated transactivation is not known, but likely involves recruitment and stabilization of components of the general transcription machinery on viral promoters (31, 253). IE62 structural motifs that contribute to its transactivation abilities include a potent N-terminal activation domain (aa 1-83) (40, 195), a DNA-binding and dimerization domain (DBDD; aa 486-641) (23, 234, 235, 247), and a nuclear localization signal (NLS; aa 677-685) (129). In marked contrast with ICP4, IE62 is major component of purified viral particles and is associated with the VZV tegument (123). This

implies a unique virion structural role and/or an important function during the initial stage of infection following entry and uncoating.

IE62 undergoes temporally defined spatial re-distribution, from the nucleus during early-stage infection to the cytoplasm during late-stage infection (124). This change in IE62 compartmentalization divides known roles of IE62 as a transcriptional regulator in the nucleus and as a viral structural protein assembled into virions in the cytoplasm. IE62's mass (175 kDa in VZV-infected cells) precludes free diffusion across the size-constrained nuclear pore complex (NPC), and IE62 nuclear import relies upon its arginine (R)/lysine (K)-rich NLS ($_{677}$RLRTPRKRK$_{685}$) (129). The IE62 NLS is likely recognized by a karyopherin α adaptor and actively transported into the nucleus after karyopherin β1 association, followed by release into the nucleoplasm as a result of Ran-GTP binding at the nucleoplasmic face of the NPC. IE62 cytoplasmic accumulation in late-stage VZV infection is dependent upon expression and functional catalytic activity of the VZV ORF66 protein kinase (123, 124, 219). Specifically, ORF66 mediates a direct phosphorylation of IE62 at the serine residue immediately downstream of the IE62 NLS, (S686), which may sterically inhibit karyopherin α binding to impede IE62 nuclear import (58). Importantly, ORF66 expression is required for the abundant tegument association of IE62 (123).

ORF66 is expressed in the nucleus and the cytoplasm in VZV-infected cells (58, 219), and thus IE62 phosphorylation may occur in either compartment. Assuming that ORF66 is expressed with early kinetics during infection, similar to its HSV-1 ortholog U_S3, phosphorylation of IE62 restricted to the cytoplasmic compartment would result in nuclear forms of IE62 throughout infection, since IE62 is expressed with immediate early kinetics (67) and can enter the nucleus in the absence of ORF66 expression. Alternatively, ORF66-mediated IE62

phosphorylation may occur in the nucleus, and combined with a mechanism of nuclear export, may result in more efficient nuclear clearance of IE62 during late-stage VZV infection. Coincidentally, we and others have reported quite efficient IE62 nuclear exclusion in late-stage VZV infections in multiple cell types, supporting the latter scenario and implying that IE62 may undergo nuclear export to facilitate nuclear exclusion (58).

In this study, we sought to further delineate the processes involved in IE62 nuclear exclusion during VZV infection. Utilizing the recently described VZV.GFP-66, we demonstrate for the first time that ORF66 is expressed with early kinetics, and that ORF66 expression and nuclear localization are not sufficient for IE62 nuclear exclusion. Interspecies heterokaryon analyses revealed that IE62 undergoes Crm1-independent nuclear export, and IE62 amino acids 733-995 were critical for this. Similar analyses also uncovered IE62 DNA-binding and dimerization domain (DBDD)-dependent nuclear retention and poly-serine tract phosphorylation-dependent nuclear export. These results begin to elucidate a complex cycle of IE62 nuclear import, retention and export during VZV infection, which ultimately controls the switch in IE62 function between transcriptional regulation and virion assembly.

4.3 MATERIALS AND METHODS

4.3.1 Cells, viruses and antibodies

HEK-293T cells and MRC-5 human lung fibroblasts (ATCC, Manassas, VA), human melanoma (MeWo) cells (kindly provided by C. Grose, University of Iowa, Iowa City, IA) and the B6WT3 murine fibroblast cell line (kindly provided by R. Hendricks, University of Pittsburgh,

Pittsburgh, PA) were maintained as previously detailed (58). VZV.GFP-66 and VZV-S686A$_2$ have been described elsewhere (58, 61). Briefly, VZV.GFP-66 was created using VZV-pOka cosmids, and expresses EGFP-tagged ORF66 in place of wild-type ORF66. VZV-S686A$_2$ was derived using the VZV bacterial artificial chromosome and encodes IE62 proteins (from both the ORF62 and ORF71 genes) carrying a point mutation (S686A), which renders IE62 resistant to ORF66-mediated nuclear exclusion (58).

Polyclonal rabbit antiserum directed against the IE62 protein (124) was used at 1:800 for immunofluorescence or 1:2500 for immunoblotting. For primary detection of cellular antigens in immunofluorescence, we used a mouse monoclonal antibody against p230, a marker of the trans-Golgi network (BD-Biosciences, Pharmingen; used at 1:500), and a mouse monoclonal antibody specific for the human nuclear protein, Ku86 (Santa Cruz Biotechnology, Santa Cruz, CA; used at 1:200). Alexa Fluor conjugated Fab fragments (goat anti-mouse or goat anti-rabbit; used at 1:400; Invitrogen Corp.) were used for secondary detection by immunofluorescence. Excitation spectra are indicated in the Figure Legends.

4.3.2 Plasmids

All plasmids were purified using Qiagen columns (Qiagen, Inc., Valencia, CA), according to the manufacturer's instructions. All IE62 ORF coordinates described here correspond to the sequenced and annotated VZV-Dumas strain. pKCMV62, which expresses the full-length IE62 protein under the control of the minimal HCMV IE promoter, has been previously described (58, 124). Several derivatives of this plasmid expressing truncated IE62 protein forms have been previously described: pKCMV62Δ26-602, pKCMV62Δ161-506 and pKCMV62Δ733-end pCMV62Δ733-995, pCMV62Δ968-end, pCMV62Δ865-end pCMV62Δ161-272 (127).

Additional IE62 internal truncation mutants were derived from pKCMV62 using primers with restriction endonuclease overhangs corresponding to natural restriction sites within the IE62 ORF. For these, one primer per set was designed to include a restriction site overhang attached to sequences internal to the native site, taking into account the open reading frame, to generate PCR fragments lacking specific regions. Following PCR amplification, these were cloned into the pKCMV62 backbone. These plasmids include: pCMV62Δ272-347 using Mfe I (nt 814) → Eco RV (nt 1246), with Eco RV internal; pCMV62Δ735-853 using Bam HI (nt 2199) → Pml I (nt 2901), with Pml I internal; and pCMV62Δ942-968 using Bam HI → Pml I, with Bam HI internal. In some cases, the restriction sites used were not unique in the pKCMV62 backbone. For these, we prepared pKCMV62 by performing limiting digestion with ethidium bromide. To generate a deletion of the IE62 N-terminal poly-serine/acidic tract pSAT (pCMV62ΔpSAT), we used a splicing by overlap extension (SOE) method (103). In the first step, 5' and 3' overlapping IE62 fragments were generated by PCR amplification using external primers corresponding to the 5' Mfe I and the 3' Kpn I site (nt 1712), and extended internal complementary primers that lacked IE62 amino acids (aa) 352-375 ($_{352}$VSSSSSSSSWGSSSEDEDD EPRRV$_{375}$) (nt 1054-1125). Internal primers also carried a novel Eco RI site that was inserted by silent mutagenesis. The products from the first reaction were used to self-prime in a second PCR reaction, and the resultant fragment was cloned into pKCMV62 using the Mfe I and Kpn I restriction sites. To generate pSAT mutations in which all serine residues were replaced with alanine ($_{352}$VAAAAAAAAWGAAAEDEDDE PRRV$_{375}$) (pCMV62pStoA) or glutamic acid ($_{352}$VEEEEEEEEWGEEEEDEDDEPRRV$_{375}$) (pCMV62pStoA), we inserted hybridized complementary oligonucleotides at the novel Eco RI site after ethidium bromide-mediated partial digestion of pCMV62ΔpSAT. Importantly, no changes other than the specific S→A or S→E

mutations described above were inserted in the IE62 sequence at this site. A similar SOEing approach to used to generate a partial deletion of the DNA-binding and dimerization domain, pCMV62Δ484-515 ($_{484}$PSGETREGHWEDEAVRAARARYEASTEPVPLY$_{515}$) (nt 1449-1545), using 5' Eco RV and 3' Kpn I primers in the first PCR step. For this mutant, an internal Sac I site was inserted by silent mutagenesis in the internal primers. All oligonucleotide primers were obtained from IDT Inc. (Coralville, IA), and PCR reactions were carried out using the proofreading polymerase Expand (Roche Applied Science, Indianapolis, IN). The accuracy of all truncations and mutations of IE62 was verified by sequencing.

4.3.3 Infections and transfections

Cell-free VZV was prepared from VZV.GFP-66-infected MeWo cells exhibiting >75% EGFP-66 fluorescence and CPE as follows: infected cells were harvested in the absence of trypsin; resuspended in ice-cold SPGA buffer (218 mM sucrose, 3.8 mM KH_2PO_4, 7.2 mM K_2HPO_4, 4.9 mM sodium-glutamate, 1% BSA, 10% FBS; pH 8.0) to stabilize infectivity; vortexed 3 x 15 s with 0.5 mm glass beads; transferred to a fresh, pre-chilled tube; and cleared by centrifugation at 4ºC. Resultant supernatents were used to directly infect confluent MRC-5 fibroblasts on 24 x 30 mm coverslips. Each coverslip was exposed to cell-free VZV extract equivalent to ~1/6 of one T_{175} flask for 1 h at 37ºC, followed by medium replacement and fixation at the times indicated in the text. For heterokaryon analyses in VZV-infected cells, VZV-S686A$_2$ was used to infect MeWo cells grown on coverslips at a ratio of 1 infected cell to 50 uninfected cells. All transfections were performed in slightly sub-confluent MeWo or HEK-293T cell cultures using the Lipofectamine 2000 reagent (Invitrogen Corp., Carlsbad, CA), according to the manufacturer's instructions.

4.3.4 Interspecies heterokaryon assay

All medium, buffers and solutions used in heterokaryon formation were warmed to 37ºC prior to use. Transfected or infected human melanoma cells grown on coverslips were overlaid with an equal number of briefly trypsinized murine B6WT3 fibroblasts. B6WT3 cells were allowed to settle and adhere, and then co-cultures were incubated in medium containing 100 μg/ml cycloheximide (CHX; Sigma-Aldrich, St. Louis, MO) for one hour at 37ºC, to inhibit protein expression. To fuse cells and form interspecies heterokaryons, coverslips were first washed with 1X PBS, and then subjected to 50% polyethylene glycol (PEG; Hybri-Max molecular weight 3000-3700, Sigma-Aldrich, St. Louis, MO) in medium for exactly two minutes, followed by extensive washing with 1X PBS to remove PEG. Subsequently, heterokaryons were incubated for an additional 3-4 hours at 37ºC in the presence of 100 μg/ml CHX to allow protein shuttling in the absence of additional protein expression, and then fixed with 4% paraformaldehyde for 15 minutes. In some experiments, the Crm1 inhibitor leptomycin B (LMB; LC Laboratories, Woburn, MA) was included in the pre- and post-fusion incubation media, and was used at 20 ng/ml. Pre-incubation in LMB experiments was performed for two hours to ensure efficient disruption of Crm1-mediated nuclear export.

4.3.5 Immunological methods

Indirect immunofluorescence, two-dimensional microscopy and image processing and immunoblotting was performed as previously described (58, 59). Nuclei were identified and differentiated using Hoechst 33258 (Sigma-Aldrich).

4.4 RESULTS

4.4.1 IE62 and ORF66 spatio-temporal dynamics in VZV-infected cells suggest both nuclear retention and nuclear export activities for IE62

Recent reports have indicated that ORF66 is localized to both the nucleus and the cytoplasm during VZV infection (59, 219), but compartment-specific interactions with IE62 and the precise point of IE62 nuclear exclusion have not been assessed. Additionally, while it assumed that ORF66 is expressed with early kinetics after the expression of IE62, this has not been experimentally demonstrated. Such studies have been impeded, in part, by the lack of availability of a highly specific ORF66 antibody (127). However, we have recently described a novel recombinant VZV, which expresses EGFP-tagged ORF66 in place of the wild-type gene under the control of the native promoter (VZV.GFP-66) (59). Here, we utilized VZV.GFP-66 in cell-free infections to study ORF66 expression kinetics and the IE62-ORF66 spatio-temporal distribution relationship during VZV infection. MRC-5 human lung fibroblasts were infected with cell-free VZV.GFP-66; fixed at 4, 8, 12, 16 and 24 hours post-infection (hpi); and stained with polyclonal rabbit anti-IE62 and monoclonal mouse anti-p230, a protein marker of the *trans*-Golgi network (TGN). As expected, initial inspection of IE62 and ORF66 localizations suggested some variability at time-points beyond 4 hpi, likely due to cell-to-cell variation in multiplicity of infection (MOI) or cell cycle stage upon viral entry. Thus, to monitor the progression of VZV infection and quantitate IE62 and ORF66 localization dynamics, we assessed the specific cellular distribution patterns of IE62 and ORF66 in 20 individual cells from each time point. This analysis revealed 5 progressive phenotypes of IE62-ORF66 distribution, and representative cells exhibiting each phenotype are shown in Figure 4-1.

At 4 hours post-infection (hpi), cellular debris from cell-free VZV extracts were detectable in the cytoplasm of all cells, and were both EGFP-autofluorescent and reactive with anti-IE62 antibodies. Scattered individual cells displayed specific diffuse IE62 staining throughout the nucleoplasm, with 3-10 prominent nuclear foci that were distributed in a non-polar manner, frequently in the vicinity of the nucleolus (Figure 4-1A; "62Nuc/No66"). These cells did not express detectable levels of EGFP-66, establishing that IE62 is expressed and localizes to the nucleus in the absence of ORF66 expression at immediate early times post-infection. The TGN appeared normal in cells at 4 hpi, exhibiting peri-nuclear cisternal distribution. Only ~20% of cells displayed IE62 nuclear localization in the absence of ORF66 expression at 8 hpi, and the presentation of this distribution phenotype progressively declined by 12 and 16 hpi. At 8 hpi, the majority of cells (~80%) expressed detectable levels of GFP-66, which was distributed in one of two manners: 1) in fine, grainy foci evenly distributed throughout the nucleoplasm, with no apparent cytoplasmic distribution (Figure 4-1B; "62Nuc/66Nuc"); or 2) similar grainy nuclear distribution combined with diffuse cytoplasmic localization and some accumulation in the TGN (Figure 4-1C; "62Nuc/66Nuc high-Cyt low"). In both cases, IE62 exhibited nucleoplasmic staining with bright nuclear foci, and lacked the diffuse cytoplasmic forms observed in late-stage VZV-infected cells, similar to what was observed at 4 hpi. The majority of ORF66 did not appear to co-localize with IE62 in these cells, although two slightly enlarged GFP-66 nuclear foci were observed in association with IE62 nuclear foci in Figure 4-1B; and both IE62 and ORF66 were observed in one bright peri-nuclear focus at the opposite side of the nucleus from the TGN in Figure 4-1C. Similar minor sub-populations of co-localization were observed in many cells with these distribution phenotypes, suggesting these regions may be sites for an IE62-ORF66 interaction. Interestingly, in cells

where cytoplasmic ORF66 expression was observed, IE62 nuclear foci appeared to have expanded and frequently localized near each other at one side of the nucleus (Figure 4-1C). These data clearly demonstrate that ORF66 expression and nuclear localization is not sufficient for IE62 nuclear exclusion at early times post-infection.

A significant transformation in IE62 distribution was observed in 36% of cells at 12 hpi and 77% of cells by 16 hpi (Figure 4-1D; "62RC-Cyt/66Nuc high-Cyt high"). Namely, abundant levels of IE62 accumulation were observed in the cytoplasm, and high levels of IE62 were recruited into large nuclear globules, which were identified as viral replication compartments (RCs) in other studies (Chapter 6). Almost no IE62 signal was detected in nucleoplasmic areas that were not shrouded by the RC. Concurrent with IE62 recruitment into RCs and accumulation of cytoplasmic forms, GFP-66 exhibited enhanced nuclear localization and accrual in bright foci in a circular arrangement, possibly surrounding the nucleolus. The GFP-66 grainy nuclear distribution was no longer apparent, and nucleoplasmic GFP-66 displayed no specific accumulation in the RC compared to other regions of the nucleus. In the cytoplasm, both GFP-66 and IE62 co-localized with the TGN, which was no longer distributed in a peri-nuclear manner and was completely independent of the nucleus. While GFP-66 was evenly distributed across the TGN cisternae, IE62 appeared to preferentially accumulate at one side, and did not completely overlap with GFP-66 fluorescence. Notably, in the displayed micrograph, a cell adjacent to the late-stage VZV-infected cell exhibits IE62 nuclear foci in the absence of IE62 nucleoplasmic staining or GFP-66 auto-fluorescence, indicating that this cell is newly infected (Figure 4-1D, arrowheads). By 24 hpi, individually-infected cells were observed with high levels of cytoplasmic IE62 that did not co-localize with the TGN, and little or no nuclear IE62 (Figure 4-1E; "62Cyt/66NucCyt"). In these cells, GFP-66 was localized diffusely in the nucleus,

in putative nucleolar foci, diffusely in the cytoplasm and in the TGN, which formed a ring-shaped structure similar to previously described Golgi reorganization in VZV-infected cells (59). Many newly infected cells were observed at the periphery of the late-stage infected cell boundaries, and these exhibited IE62 and GFP-66 localizations reminiscent of the phenotype shown in Figure 4-1D. Syncytia exhibiting high levels of IE62 in the cytoplasm and nuclear RC were also observed at 24 hpi (Figure 4-1F; "Multi-Nucleate Syncytium"). Interestingly, in some syncytial nuclei, ORF66 appeared to co-localize with early RC, further indicating a possible interaction with IE62 in this compartment (Figure 4-1F, arrowhead).

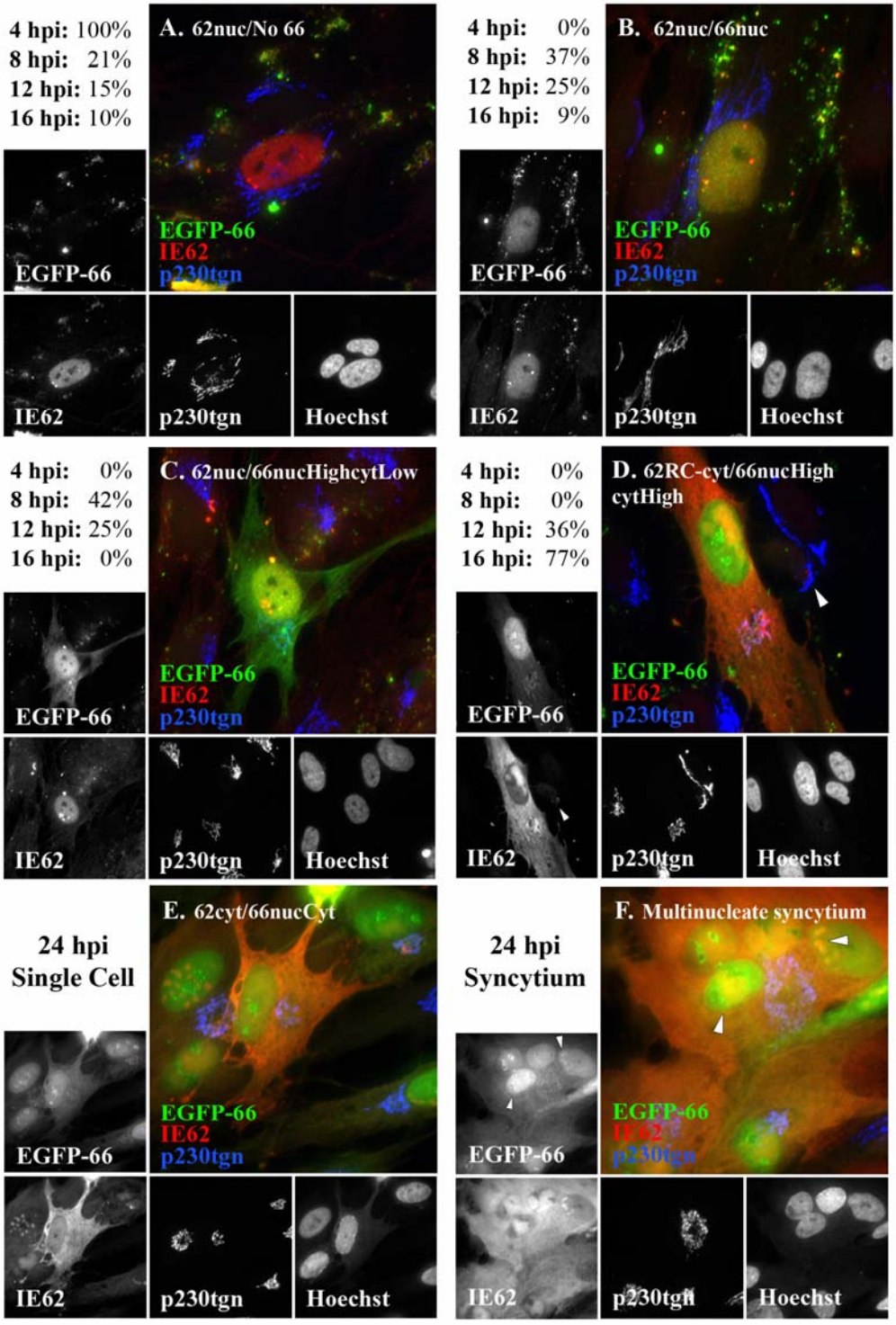
4 hpi: 100%
8 hpi: 21%
12 hpi: 15%
16 hpi: 10%
A. 62nuc/No 66
EGFP-66
EGFP-66
IE62
p230tgn
IE62
p230tgn
Hoechst
4 hpi: 0%
8 hpi: 37%
12 hpi: 25%
16 hpi: 9%
B. 62nuc/66nuc
EGFP-66
EGFP-66
IE62
p230tgn
IE62
p230tgn
Hoechst
4 hpi: 0%
8 hpi: 42%
12 hpi: 25%
16 hpi: 0%
C. 62nuc/66nucHighcytLow
EGFP-66
EGFP-66
IE62
p230tgn
IE62
p230tgn
Hoechst
4 hpi: 0%
8 hpi: 0%
12 hpi: 36%
16 hpi: 77%
D. 62RC-cyt/66nucHigh cytHigh
EGFP-66
EGFP-66
IE62
p230tgn
IE62
p230tgn
Hoechst
24 hpi Single Cell
E. 62cyt/66nucCyt
EGFP-66
EGFP-66
IE62
p230tgn
IE62
p230tgn
Hoechst
24 hpi Syncytium
F. Multinucleate syncytium
EGFP-66
EGFP-66
IE62
p230tgn
IE62
p230tgn
Hoechst

Figure 4-1 IE62 and ORF66 spatio-temporal relationship revealed by infection with cell-free VZV.GFP-66

MRC-5 fibroblasts grown on coverslips were infected with cell-free VZV.GFP-66 extracts, incubated for 4, 8, 12, 16 or 24 h and fixed with 4% paraformaldehyde for 15 minutes. Permeabilized cells were stained with polyclonal rabbit anti-IE62 and monoclonal mouse anti-p230, and staining patterns were assessed by EGFP auto-fluorescence or following staining with Alexa Fluor conjugated secondaries (goat anti-rabbit [ex 546] or goat anti-mouse [ex 647]), using epifluorescent microscopy. (A-D) Representative micrographs show the first four stages of IE62 and ORF66 spatio-temporal distribution, and images were captured of cells fixed at 4 hpi (A), 8 hpi (B-C) and 16 hpi (D). Each panel consists of an enlarged color-combined image with EGFP-66 (green), IE62 (red) and p230 (blue) fluorescence patterns; smaller black-and-white images of individual staining patterns, including Hoechst dye; and quantification of the percentage of cells displaying the depicted phenotype at 4, 8, 12, and 16 hpi. Individual infected cells exhibiting the fifth IE62 and ORF66 distribution phenotype (E), and syncytia showing varying patterns (F) were readily observed at 24 hpi, and representative micrographs are shown exactly as described for (A-D), without quantification. In all micrographs, the depicted protein is indicated in the lower left corner.

Collectively, these data indicate that several factors may be involved in triggering IE62 nuclear exclusion and eventual nuclear clearance during infection. The predominant GFP-66 nuclear localization throughout infection and its association with IE62 in early RC also suggests that ORF66-mediated IE62 phosphorylation could occur in the nucleus. Hence, IE62 likely requires a nuclear export mechanism to facilitate nuclear exclusion in late-stage VZV infected cells.

4.4.2 Interspecies heterokaryon analysis reveals IE62 nuclear shuttling capabilities

To ascertain whether IE62 undergoes nuclear export, we utilized interspecies heterokaryon analysis with human melanoma (MeWo) cells either transfected with plasmids expressing IE62 (pCMV62) or infected with VZV-S686A$_2$. VZV-S686A$_2$ encodes an IE62 serine 686 to alanine (S686A) point mutation in both copies of the IE62 gene (ORF62 and ORF71), and the IE62 protein in this virus is insensitive to ORF66-mediated nuclear exclusion (61). Co-cultures of

transfected or infected human melanoma cells (donor cells) and murine B6WT3 fibroblasts (acceptor cells) were incubated with CHX for one hour to repress IE62 translation, treated with polyethylene glycol to fuse cells and form heterokaryons, and then incubated for an additional 3-4 hours post-fusion in the presence of CHX to allow protein shuttling from donor to acceptor nuclei in the absence of new protein expression. Cells were fixed and stained with antibodies against IE62; an antibody specific for the human 86 kDa sub-unit of the heterodimeric DNA end-binding complex (huKu86), which is a non-shuttling nuclear resident protein (65); and Hoechst dye to identify nuclei. Hoechst localizes to bright punctate foci in murine nuclei, but exhibits diffuse nuclear localization in primate cells, allowing for straight-forward resolution of nuclear species in heterokaryons. Additionally, the huKu86 antibody does not recognize murine Ku86, thus providing an additional means of differentiation of donor and acceptor nuclei, as well as a specificity control for protein shuttling into acceptor nuclei.

In fusions performed with pCMV62-transfected MeWo cells, IE62 fluorescence was observed in Hoechst-punctate/huKu86-negative murine nuclei, displaying both diffuse nucleoplasmic fluorescence and some accumulation into foci at the periphery of the nucleolus. Similar staining patterns have been previously observed in cells expressing IE62 (58). These results indicate that IE62 undergoes nuclear export in heterokaryons when expressed in the absence of additional VZV proteins (Figure 4-2A). The maintenance of huKu86 in transfected Hoechst-diffuse donor human nuclei and its lack in the murine acceptor nuclei support the conclusion that IE62 nuclear export was authentic and not the result of decreased nuclear membrane integrity. Typically, the IE62 fluorescent signal was more intense in donor nuclei relative to acceptor nuclei and was present only in murine nuclei in close proximity of the donor nucleus. Importantly, we also detected IE62 nuclear shuttling in heterokaryons formed with

VZV-S686A$_2$-infected cells (Figure 4-2B). Similar results were observed in replicate experiments.

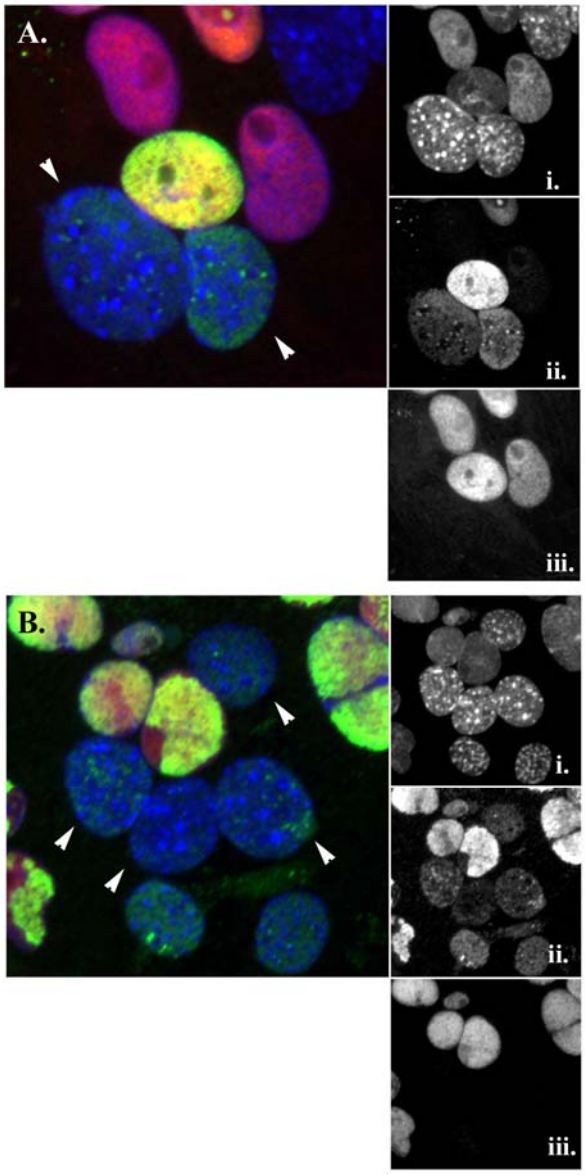

Figure 4-2 IE62 shuttles to mouse nuclei in heterokaryons formed with both transfected cells expressing IE62 and VZV-infected cells expressing IE62 that is resistant to nuclear exclusion

MeWo cells were transfected with pCMV62 (A), or infected with VZV-S686A$_2$ (B), and subjected to heterokaron formation at 48 h post-transfection or infection. Cells were overlaid with murine B6WT3 fibroblasts, incubated with 100 μg/ml CHX for 1 hour at 37ºC, fused with 50% PEG, and incubated with CHX for an additional 3-4 hours to allow for protein shuttling into murine nuclei. Cells were fixed and stained with polyclonal rabbit anti-IE62 and monoclonal mouse anti-huKu86, and proteins were detected by indirect immunofluorescence and epifluorescent microscopy following staining with Alexa Fluor-conjugated goat anti-rabbit (ex 488) and goat anti-mouse (ex 546) secondaries. In each panel, an enlarged color-combined image of Hoechst (blue), IE62 (green), and huKu86 (red) distribution in heterokaryons is shown,

with individual staining patterns for each in smaller black-and-white panels (i, ii, and iii, respectively). The depicted proteins are indicated in each micrograph panel. White arrowheads in colored panels point out murine nuclei contained within the heterokaryon.

4.4.3 IE62 uses a Crm1-independent mechanism for nuclear export

Nuclear export of large proteins occurs through karyopherin receptors called exportins. Many proteins are transported out of the nucleus by the exportin-1 protein (a.k.a. Crm1), which recognizes leucine-rich consensus motifs (φ-x_{2-3}-φ-x_{2-3}-φ-x-φ; φ=[L,I,V,F,M], x=any amino acid) (140). Amino acids that roughly conform to this consensus are interspersed throughout the IE62 primary sequence, and we hypothesized that IE62 may interact with Crm1 to facilitate nuclear export. To address this, we performed heterokaryon analysis of pCMV62-transfected MeWo cells incubated in the presence or absence of 20 ng/ml leptomycin B (LMB), a specific inhibitor of Crm1-mediated nuclear export (246). As shown in Figure 4-3A, IE62, but not huKu86, shuttling was readily observed in the presence of LMB, suggesting that IE62 nuclear export does not utilize the Crm1 export receptor. Interestingly, IE62 was more prominently localized to bright peri-nucleolar speckles in both donor and acceptor nuclei with LMB co-incubation (Figure 4-3A).

Since we did not observe IE62 shuttling in every heterokaryon, either in the presence or absence of LMB, we considered the possibility that LMB reduced the efficiency of IE62 nuclear export without completely abrogating export in all cases. To determine whether LMB partially affects IE62 shuttling or has no effect, we quantified the percentage of heterokaryons exhibiting detectable IE62 fluorescence in murine nuclei, in the presence or absence of LMB (Figure 4-3B). To eliminate bias, IE62-expressing nuclei were identified by scanning multiple regions of coverslips in straight lines, and all heterokaryons with expressing nuclei within a field of

observation were assessed for IE62 nuclear shuttling. As previously described, the integrity of the MeWo nuclear membrane was established by maintenance of huKu86 fluorescence and the lack of huKu86 fluorescence in murine nuclei. In two independent experiments, we counted a total of 54 heterokaryons incubated without LMB and 76 heterokaryons incubated with LMB, and we report that LMB induced no detrimental effects on IE62 shuttling. On average, shuttling into murine nuclei was observed in ~50% of heterokaryons in both cases. Thus, IE62 nuclear export does not rely upon Crm1, and instead utilizes a Crm1-independent mechanism to mediate IE62 clearance in late-stage VZV infections. In support of this, efficient IE62 nuclear exclusion was observed in VZV-infected cells incubated with the same amount of LMB (data not shown).

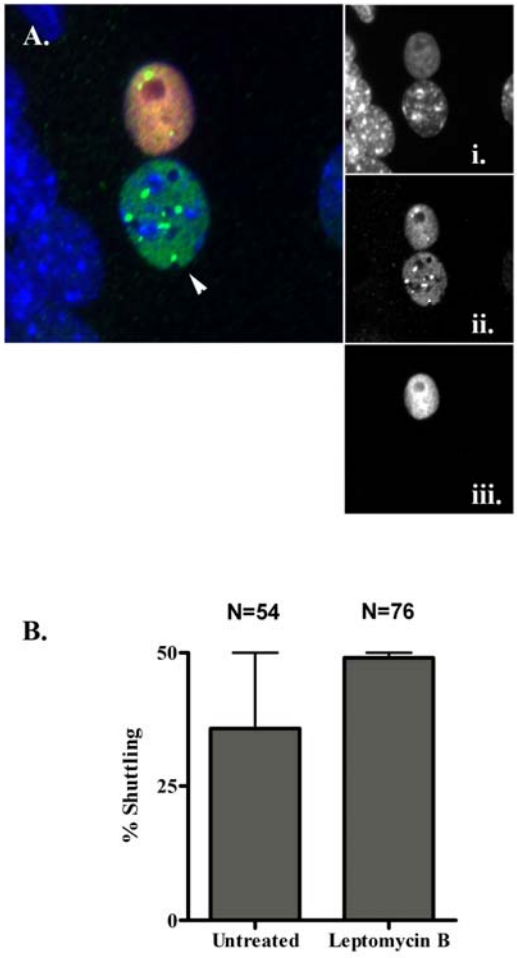

Figure 4-3 IE62 shuttling in heterokaryons incubated with the Crm1 nuclear export inhibitor, LMB

Heterokaryon analyses were performed in pCMV62-transfected MeWo cells in the presence or absence of 20 ng/ml leptomycin B (LMB). (A) A representative heterokaryon incubated with LMB, shown exactly as described in Figure 4-2, and clearly showing IE62 shuttling to a murine nucleus. In the large panel, a color-combined image is shown of Hoechst in blue, IE62 in green, and huKu86 in red; while individual staining patterns for each in smaller black-and-white panels are indicated by i, ii, and iii, respectively. The white arrowhead indicates the murine nucleus. (B) Quantification of the per cent shuttling observed in parallel cultures with and without LMB, from two independent experiments. The number of total heterokaryons quantified for each condition in two replicate experiments is shown above each bar.

4.4.4 Distinct nuclear retention and nuclear export domains map to the IE62 N and C termini

To begin to identify the IE62 regions involved in nuclear export, we performed similar heterokaryon analyses and quantifications of nuclear shuttling in cells transfected with plasmids expressing truncated IE62 peptides lacking large segments of either the N or C terminus (Figure 4-4). Surprisingly, two peptides consisting of predominantly C-terminal IE62 amino acids ($IE62_{\Delta 26\text{-}602}$ and $IE62_{\Delta 161\text{-}506}$) exhibited highly promiscuous shuttling into most surrounding nuclei, which was observed in nearly 100% of heterokaryons quantified (Figure 4-4B). An example of an $IE62_{\Delta 161\text{-}506}$ heterokaryon is shown in Figure 4-4C. Both $IE62_{\Delta 26\text{-}602}$ and $IE62_{\Delta 161\text{-}506}$ exhibited IE62 nuclear localization with punctate foci throughout the nucleoplasm, but no accumulation was observed in the nucleolar region. Importantly, both peptides were resolved at the expected molecular mass by SDS-PAGE (Figure 4-4A), and were at least two times larger than the cutoff for free diffusion across the NPC (40 kDa). Thus, it appears that the IE62 N-terminal region may be important for nuclear retention, whereas the C-terminus, or possibly the first 26 amino acids, contains sequences involved in nuclear export. We point out, however, that the enhanced expression of these peptide mutants with respect to full-length IE62 may also contribute to the observed efficient nuclear shuttling phenotype (Figure 4-4A).

C-terminal truncation mutants, $IE62_{\Delta 968\text{-}end}$ and $IE62_{\Delta 865\text{-}end}$, shuttled with similar efficiency as full-length IE62. In marked contrast, deletion of the C-terminal half of IE62 ($IE62_{\Delta 733\text{-}end}$) and an internal truncation mutant ($IE62_{\Delta 733\text{-}995}$) displayed almost no ability to shuttle to murine nuclei in heterokaryon assays. While $IE62_{\Delta 733\text{-}end}$ was detected at lower levels by polyclonal IE62 antiserum in both heterokaryons and immunoblots (Figure 4-4A and data not shown), $IE62_{\Delta 733\text{-}995}$ was expressed at least as efficiently as full-length IE62 (Figure 4-4A, D).

This supports data acquired with N-terminal truncation peptides suggesting that C-terminal motifs were involved in nuclear export, and indicates that the IE62 733-995 region is critical for this IE62 activity.

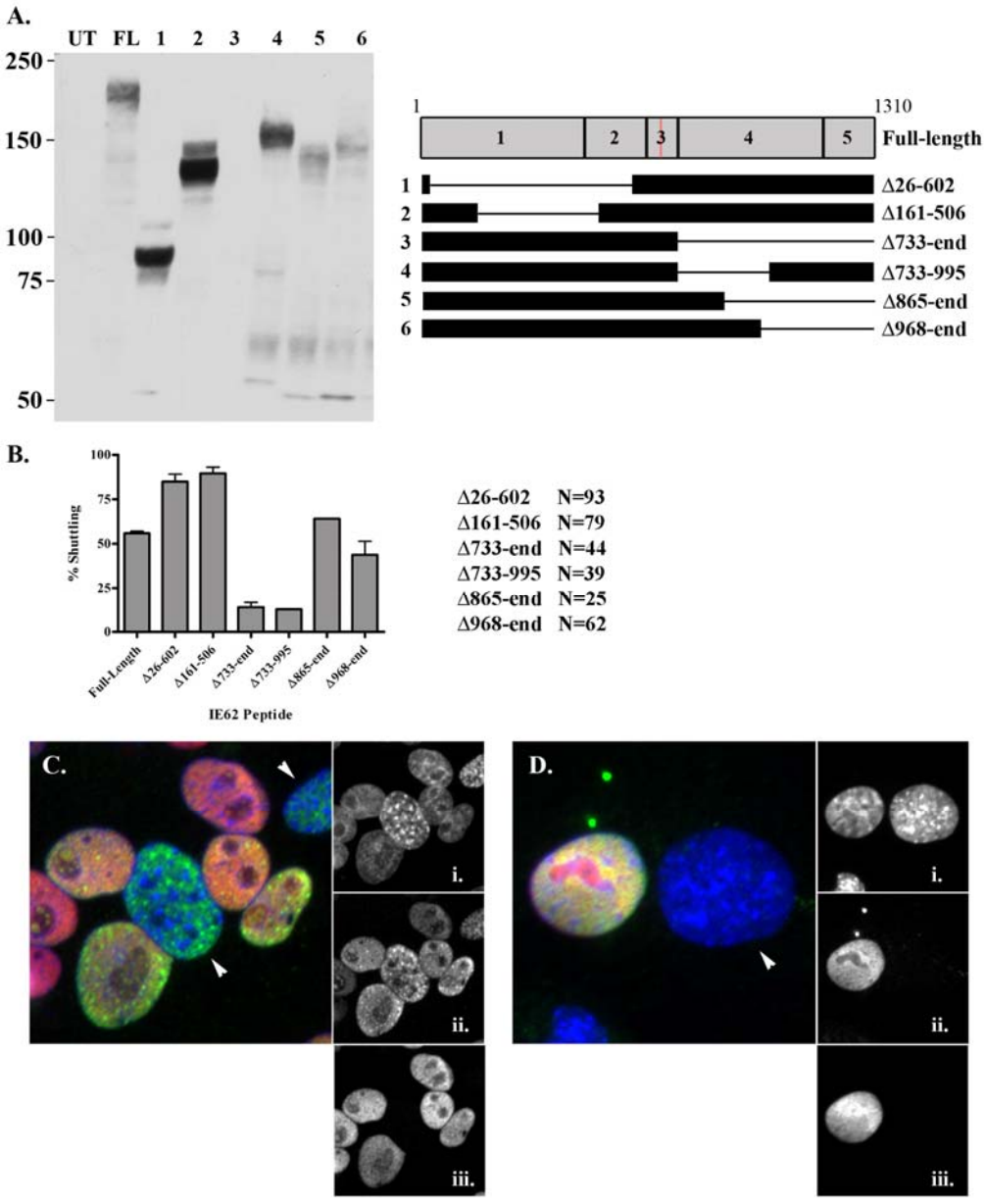

Figure 4-4 Analysis of truncated IE62 peptide shuttling in heterokaryons

(A) Immunoblot analysis of IE62 peptide sizes and expression levels. Lysates of 293T cells expressing IE62 peptides were separated by SDS-PAGE, transferred to PVDF and probed with a polyclonal rabbit anti-IE62 antibody, and peptides were detected following incubation with horseradish peroxidase conjugated goat anti-rabbit secondaries. Protein size markers (kDa) are indicated to the left of the immunoblot panel, and letters or numbers corresponding to the transfected peptide are shown above each lane. A map of full-length IE62 and truncation peptides is shown to the right of the immunoblot panel, and includes the peptide lane numbers. The red line on full-length IE62 represents the location of the NLS. (B) Bar graph of per cent

shuttling of truncated IE62 peptides in heterokaryons. Results are shown as a mean (±SEM) from two independent experiments, and the total number of heterokaryons quantitated is denoted at the right. (C and D) Representative micrographs of peptides exhibiting hyper-shuttling (C; $IE62_{\Delta 161\text{-}506}$) or reduced shuttling (D; $IE62_{\Delta 733\text{-}995}$) phenotypes. In the large panels, a color-combined image is shown of Hoechst in blue, IE62 in green, and huKu86 in red; while individual staining patterns for each in smaller black-and-white panels are indicated by i, ii, and iii, respectively. White arrowheads in colored panels point out murine nuclei contained within each heterokaryon. UT=untransfected; FL=full-length.

4.4.5 Delineation of functional N-terminal domains involved in nuclear retention

The IE62 N-terminus contains a potent activation domain within the first 83 amino acids (40, 195), a DBDD between amino acids 468 and 642 (23, 234, 235, 247), and an intervening segment involved in binding to multiple cellular transcriptional regulators and viral factors (22, 37, 157, 194, 209, 225) (see Figure 4-7). One noteworthy feature of the intervening segment is a tract of repeated serines followed by multiple acidic residues, which is a likely site for phosphorylation by both cellular casein kinase II (CKII) and the viral ORF47 protein kinase (124). Since only the activation domain remained intact in the $IE62_{\Delta 161\text{-}506}$ peptide, it was unclear whether IE62 nuclear retention occurred as a result of its interaction with cellular proteins or through its DNA binding activities. To delineate the regions responsible for nuclear retention, we developed plasmids expressing several smaller N-terminal truncations and tested peptide shuttling in heterokaryons, as described above (Figure 4-5). $IE62_{\Delta 161\text{-}272}$ and $IE62_{\Delta 272\text{-}347}$ exhibited nuclear shuttling in nearly 50% of heterokaryons, similar to full-length IE62, indicating that nuclear retention functions were not contained within these regions (Figure 4-5B). In contrast, deletion of a short N-terminal portion of the IE62 DBDD ($IE62_{\Delta 484\text{-}515}$) resulted in efficient nuclear shuttling in 100% of heterokaryons (Figure 4-5B and C). These results indicate that IE62 DNA-binding or dimerization activities are responsible for IE62 nuclear retention.

Notably, the IE62$_{\Delta 484\text{-}515}$ peptide was distributed in a manner similar to that exhibited by IE62$_{\Delta 26\text{-}602}$ and IE62$_{\Delta 161\text{-}506}$, indicating that the integrity of the DBDD is critical for the proper distribution of IE62 within the nucleus.

Unexpectedly, we observed enhanced nuclear retention and association with nucleolar foci, combined with no IE62 shuttling for a truncated peptide lacking only the N-terminal poly-serine/acidic tract (pSAT) (IE62$_{\Delta 352\text{-}375}$) (Figure 4-5B and D). Since this region includes 11 serine residues and is likely a significant target for cellular kinases (58), we postulated that its contribution to nuclear export may involve phosphorylation. To test this, we inserted a fragment into the IE62$_{\Delta 352\text{-}375}$ deletion mutant plasmid, which encoded poly-alanine (poly-A) in place of poly-serine (poly-S) but retained all the natural acidic residues (referred to as IE62$_{\Delta polyStoA}$). In heterokaryon analyses, the IE62$_{\Delta polyStoA}$ protein behaved similar to the IE62$_{\Delta 352\text{-}375}$ truncated peptide, indicating that the serine residues in this region are critical for its role in facilitating IE62 nuclear export (Figure 4-5B and E). Some nuclear shuttling ability was rescued in an IE62 insertion mutant that expressed poly-glutamic acid (E) in place of poly-S (Figure 4-5B), although it was inefficient, providing support for the conclusion that phosphorylation of the IE62 pSAT is involved in nuclear export.

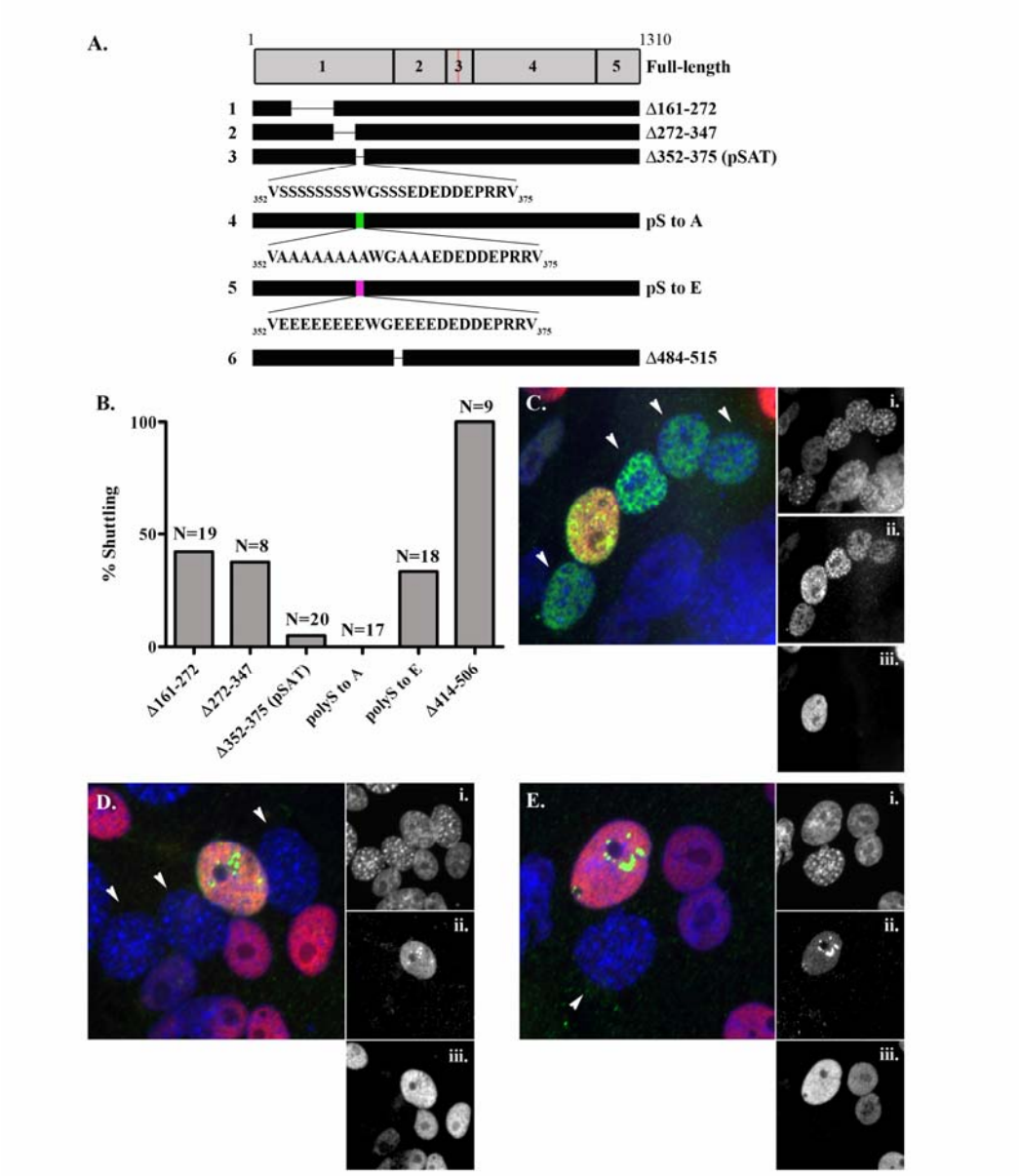

Figure 4-5 Heterokaryon analysis reveals IE62 N-terminal domains involved in both nuclear retention and nuclear shuttling

(A) A map of peptide truncation and insertion locations. For the pSAT deletion and insertion mutations, the modified regions are shown in single letter amino acid code below the respective peptide map. (B) Bar graph of per cent shuttling of each peptide, with the total number of heterokaryons quantitated for each peptide indicated above the corresponding bar. (C-E) Representative heterokaryons for $IE62_{\Delta 414\text{-}506}$, $IE62_{\Delta 352\text{-}375}$, and $IE62_{pStoA}$, respectively. In the large panels, a color-combined image is shown of Hoechst in blue, IE62 in green, and huKu86 in red; while individual staining patterns for each in smaller black-and-white panels are indicated by i, ii, and iii, respectively. White arrowheads point out murine nuclei contained in the heterokaryons.

4.4.6 Short truncations in the IE62 735-995 region reveal unexpected phenotypes in interspecies heterokaryon analyses

Two plasmids expressing IE62 with short deletions in the 735-995 region implicated in nuclear export were assessed for shuttling capabilities in heterokaryons (Figure 4-6). Curiously, an $IE62_{\Delta 735\text{-}853}$ peptide was not able to localize to the nucleus at all (Figure 4-6B), despite the presence of the IE62 NLS at aa 677-685. We suspect that deletion of amino acids near to the IE62 NLS (aa 677-685) interfered with recognition by karyopherin transport receptors. In direct contrast, deletion of a 26 amino acid segment from IE62 942-968 resulted in highly efficient IE62 nuclear export and localization in murine nuclei in every heterokaryon observed (Figure 4-6C). Additionally, $IE62_{\Delta 942\text{-}968}$ lacked the ability to form nucleolar foci, implying that nucleolar association may be involved in IE62 nuclear retention.

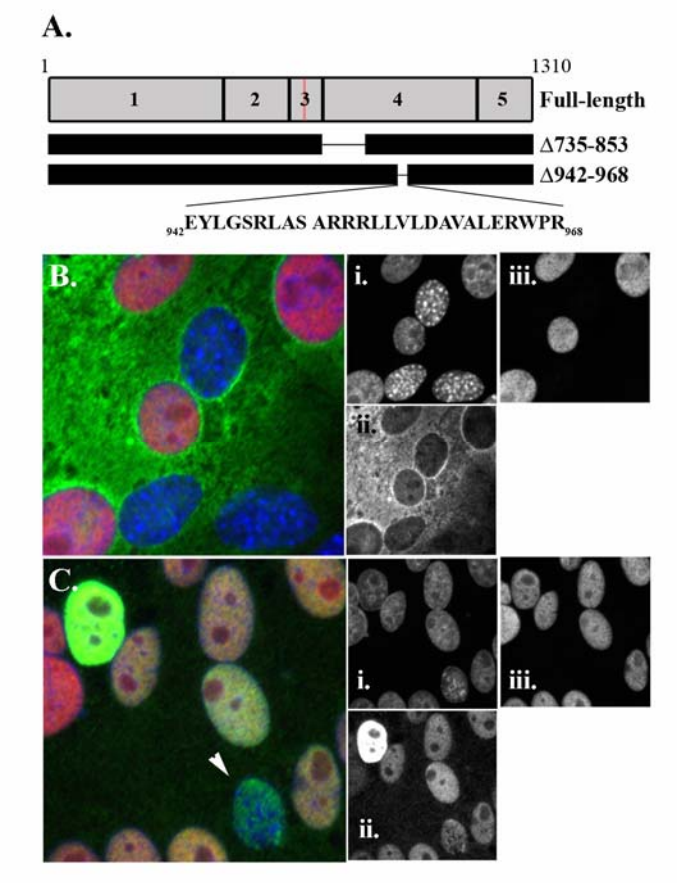

Figure 4-6 Peptides truncated within the first 250 amino acids of IE62 region 3 reveal unexpected behaviors in heterokaryon analyses

(A) Map of truncated IE62 peptides. (B and C) Representative heterokaryons for IE62$_{\Delta 735\text{-}853}$ and IE62 $_{\Delta 942\text{-}968}$, respectively, are shown. In the large panels, a color-combined image is shown of Hoechst in blue, IE62 in green, and huKu86 in red; while individual staining patterns for each in smaller black-and-white panels are indicated by i, ii, and iii, respectively.

4.5 DISCUSSION

The data presented here provide the first evidence that IE62 is a nuclear shuttling protein in VZV-infected cells, and also strongly suggest that IE62 nuclear exclusion may depend on phosphorylation by kinases in addition to ORF66. Independent deletion of two IE62 segments, including an N-terminal poly-S tract and aa 733-995, resulted in abrogation of IE62 nuclear export. The observation that poly-S to A, but not poly-S to E, substitutions resulted in a similar inability to undergo nuclear shuttling strongly argue that IE62 nuclear export was regulated by phosphorylation in the pSAT region. Minimal disruption of the IE62 DBDD or deletion of aa 942-968 induced a hyper-shuttling phenotype, suggesting that IE62 nuclear retention also contributes to its steady-state cellular distribution. These results imply that IE62 cellular localization is regulated by a complex cycle of molecular interactions involving nuclear import and retention, phosphorylation induced nuclear export, and phosphorylation-dependent nuclear exclusion.

The IE62-ORF66 spatio-temporal relationship in VZV-infected cells suggested that factors in addition to ORF66 contribute to the regulation of IE62 cellular location during VZV-infection. We demonstrated that ORF66 is expressed with early gene kinetics, as ORF66 fluorescence became visible 4-8 hpi, after IE62 was expressed and accumulated in the nucleus. Since the mechanism of ORF66-mediated nuclear exclusion likely involves inhibition of IE62 nuclear import, these data implied that IE62 must undergo nuclear export to facilitate efficient nuclear clearance during late-stage infection. Regarding the cellular site of IE62 phosphorylation, a fraction of ORF66 was observed co-localized with expanding IE62 dots in the nucleus in very early infection when both ORF66 and IE62 were exclusively nuclear, and also in pre-RC. These may represent potential sites of IE62-ORF66 interaction and phosphorylation;

and as abundant levels of cytoplasmic IE62 were not observed until 12 hpi, this further suggests that an additional switch may be required to sever IE62 tethering in the nucleus or promote IE62 nuclear export during later stages of infection. Cytoplasmic co-localizations were also observed, and thus we cannot rule out the possibility of ORF66-mediated IE62 phosphorylation in this compartment.

Consistent with the indirect immunofluorescence studies, interspecies heterokaryon analyses revealed that IE62 undergoes nuclear export both when expressed alone and in the context of VZV infection. However, IE62 nuclear export does not occur through the Crm-1 export receptor, which mediates cytoplasmic transport of protein cargoes bearing leucine-rich nuclear export motifs. Additional factors involved in mediating nuclear export of cellular proteins through the RanGTP-mediated nuclear export pathway include CAS, the specific export receptor for karyopherin α; exportin (Exp) 4, which facilitates nuclear export of eIF5a; Exp 6, the nuclear export receptor for profilin/actin; and Exp 7, which carries p50RhoGAP and 14–3–3 sigma proteins into the cytoplasm (reviewed in (140)). As no specific nuclear export consensus motif has been elucidated for any of these, it is currently unclear whether IE62 contains sequences responsible for interaction with one of these alternate export factors. Calreticulin has recently been shown to mediate export of many hormone nuclear receptors in a Ca^{2+}-dependent/Ran-independent manner through recognition of an export signal consisting of the DNA-binding domain (25, 98, 99). However, since the IE62 motifs involved in nuclear export (aa 733-995 and the N-terminal pSAT) map to regions outside of the IE62 DBDD, it seems unlikely that IE62 utilizes this pathway for nuclear clearance. Additional pathways exist for the nuclear export of RNA species, and one of these is hijacked by the herpesvirus proteins of the ICP27 family. ICP27 and its orthologs transport intronless viral mRNA out of the nucleus, and

utilize the cellular mRNA export machinery, including TAP and Aly/REF to facilitate nuclear export (36, 159, 245). IE62 is not an ICP27 ortholog, but we postulate that this pathway could be involved in IE62 nuclear export, nonetheless. The identification of the factors involved in IE62 nuclear export is currently under investigation.

Surprisingly, deletion of the N-terminal pSAT resulted in abrogation of IE62 nuclear shuttling abilities and enhanced association with nuclear subdomains that localized at the periphery of the nucleolus. Our data indicate that the serine residues contained within this motif are critical for its role in IE62 nuclear export, and IE62 proteins containing phospho-mimetic substitutions retained the ability to shuttle in heterokaryon analyses. This implies that IE62 poly-S phosphorylation may be involved in the promoting IE62 nuclear export. We conjecture that this could occur through one of three mechanisms: i) the phosphorylated pSAT may be directly recognized by a nuclear transport receptor; ii) pSAT phosphorylation may disrupt specific IE62 interactions that mediate nuclear retention; or iii) pSAT phosphorylation may induce an overall conformational change, resulting in unmasking of an IE62 nuclear export motif. In VZV-infected cells, the pSAT is likely a major substrate for phosphorylation by both cellular CKII and VZV ORF47 protein kinases (58, 120). Interestingly, VZV expressing kinase inactive forms of ORF47 induce enhanced IE62 nuclear accumulation, and it has been hypothesized that ORF47 kinase activity may be required to release IE62 from the nucleus during late stage infection (22). Thus, we postulate that ORF47-mediated phosphorylation of IE62 may function in its nuclear export. This would not explain the ability of IE62 to export in transfected cells expressing only the IE62 protein, but since CKII and ORF47 share similar consensus sequences and are known to cooperatively phosphorylate VZV protein targets during infection, CKII activity may compensate for the absence of ORF47 in transfected cells. It will be interesting to determine

whether co-expression of ORF47 in IE62 heterokaryons induces enhanced IE62 nuclear shuttling.

In addition to nuclear export activities, our studies have revealed that IE62 is retained in the nucleus in a manner dependent on the integrity of the DBDD, as IE62 peptides containing disruptions in this region exhibited enhanced shuttling in heterokaryon analyses. This suggests that dimerization-dependent protein:protein interactions or an association with DNA may either mask the IE62 nuclear export motif or simply override recognition by a nuclear export receptor due to a higher affinity interaction. The fact that the IE62 DBDD contributes to nuclear retention in transfected cells also suggests a possible association with cellular DNA in the absence of additional VZV gene expression. Given the proximity of the N-terminal pSAT to the DBDD (Figure 4-7), it is possible that pSAT phosphorylation induces a disruption of DBDD-mediated interaction in the nucleus. Surprisingly, an IE62 peptide with a short deletion at aa 942-968, within one region determined to be critical for IE62 nuclear export, was independently involved in nuclear retention. While the specific reason for enhanced nuclear export observed with this peptide was not entirely clear, it was apparent that its nucleolar targeting ability was lost. This is in direct contrast with the IE62 pSAT mutant, in which enhanced nucleolar accumulation correlated with a loss in IE62 shuttling ability. Thus, by extension this nucleolar targeting may be one determinant responsible for IE62 nuclear retention, and a nucleolar targeting sequence may exist within the aa 942-968 region.

The evidence presented here strongly indicates that IE62 undergoes nuclear export in the context of VZV infected cells, and that this activity is intrinsic to a structural motif within the IE62 protein. Initially, we identified aa 733-995 as critical for IE62 nuclear export, but subsequent deletions in this region revealed unexpected phenotypes, including lack of nuclear

import or hyper-shuttling. Unusual activities imparted by these mutations may reflect disruption of IE62 tertiary structure involved in mediating specific protein:protein interactions. Thus, future experiments aimed at further delineation of specific motifs involved in both nuclear export and nuclear retention will benefit from more specific amino acid targeting to prevent gross changes in IE62 overall structure. Studies are currently underway to determine whether aa 733-995 are sufficient for the nuclear exclusion of a constitutively nuclear heterologous control protein, and to delineate any specific residues within this region that contribute to nuclear export.

In sum, we have identified novel nuclear export and nuclear retention motifs for the VZV IE62 protein. For comparison with known IE62 regions required for specific protein:protein interactions or functional activities, these are summarized in Figure 4-7. We propose a model in which IE62 localizes to the nucleus during immediate early stages of infection and is excluded from the nucleus in late infection due to active nuclear export and cooperative phosphorylation by the VZV ORF66 and ORF47 protein kinases. These interactions ultimately regulate the switch between IE62 transcriptional regulatory processes and its subsequent re-direction to the cytoplasm for virion assembly.

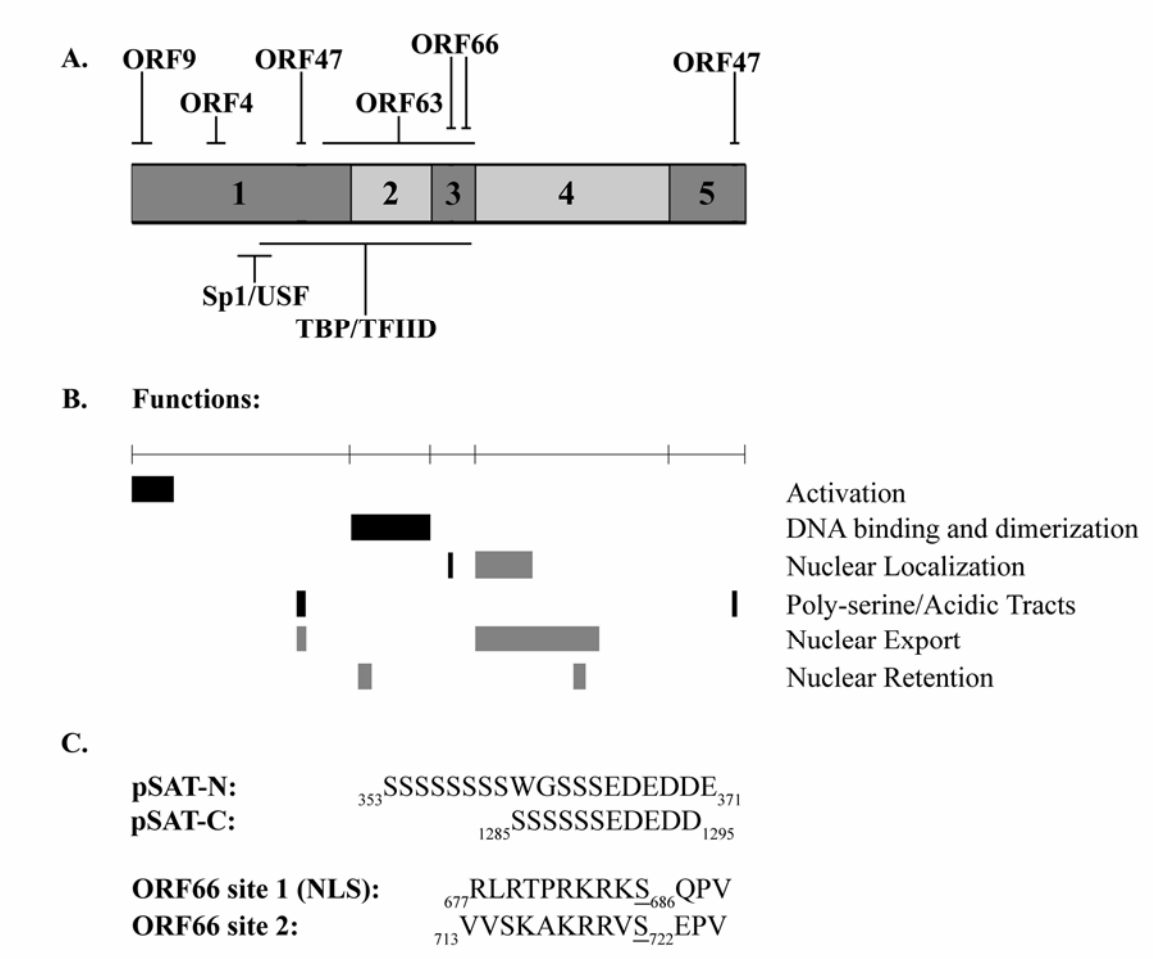

Figure 4-7 Updated schematic of IE62 protein:protein interaction and functional domains

(A) Scaled representation of the IE62 primary structure, showing regions important for interactions with viral regulatory proteins (above) and cellular transcriptional factors (below). Five regions of either low (dark gray; regions 1, 3 and 5) or high (light gray; regions 2 and 4) homology with the HSV-1 ICP4 ortholog are indicated. (B) Domains required for IE62 functional activities, depicted with respect to regions 1-5. Black boxes indicate previously defined functional motifs, while the gray boxes represent novel functional domains described herein. (C) Motifs phosphorylated by viral kinases.

5.0 DOWNREGULATION OF CLASS I MAJOR HISTOCOMPATIBILITY COMPLEX SURFACE EXPRESSION BY VARICELLA-ZOSTER VIRUS INVOLVES OPEN READING FRAME 66 PROTEIN KINASE DEPENDENT AND INDEPENDENT MECHANISMS

Amie J. Eisfeld[1,3], Michael B. Yee[1], Angela Erazo[1,3], Allison Abendroth[4,5], and Paul R. Kinchington[1,2,]

Departments of Ophthalmology[1] and Molecular Genetics & Biochemistry[2], and Graduate Program in Molecular Virology and Microbiology[3], School of Medicine, University of Pittsburgh, PA, 15213; and Center for Virus Research, Westmead Millennium Institute[4], and University of Sydney[5], P.O. Box 412, Westmead, 2145 NSW, Australia.

5.1 ABSTRACT

We show here that the varicella-zoster virus (VZV) open reading frame (ORF) 66 protein kinase is one mechanism employed to reduce class I major histocompatibility complex (MHC-I) surface expression in VZV-infected cells. Cells expressing enhanced green fluorescent protein-tagged functional and inactivated ORF66 (GFP-66 and GFP-66kd) from replication-defective adenovirus vectors revealed that ORF66 reduced MHC-I surface levels in a manner mostly dependent on kinase activity. Cells infected with recombinant VZV expressing GFP-66 exhibited a significantly greater reduction in MHC-I surface expression over that observed in cells infected with VZV disrupted in GFP-66 expression. MHC-I maturation was delayed in its transport from the endoplasmic reticulum through the Golgi in both adenovirus-transduced cells expressing only GFP-66 and in VZV-infected cells expressing high levels of GFP-66, and this was predominantly kinase-dependent. MHC-I levels were reduced in VZV-infected cells and analyses of intracellular MHC-I revealed accumulation of folded MHC-I in the Golgi region, irrespective of ORF66 expression. Thus, the ORF66 kinase is important for VZV-mediated MHC-I downregulation, but additional mechanisms also may be involved. Analyses of the VZV ORF9a protein, the ortholog of the bovine herpesvirus 1 (BHV-1) transporter associated with antigen processing (TAP) inhibitor, UL49.5, revealed no effects on MHC-I. These results establish a new role for viral protein kinases in immune evasion, and suggest that VZV utilizes unique mechanisms to inhibit antigen presentation.

5.2 INTRODUCTION

Varicella-zoster virus (VZV) is the human-restricted member of the herpesvirus subfamily, *Alphaherpesvirinae,* which causes chickenpox upon primary infection and herpes zoster (shingles) following reactivation from a prolonged period of neuronal latency in the sensory ganglia. Based on the current model of pathogenesis (137), efficient dissemination, disease and establishment of latency within the infected host requires VZV growth in multiple cell types. Following inhalation, VZV is spread to epidermal sites of replication by a T-lymphocyte-associated viremia. Infection likely occurs in the tonsils, with VZV preferentially infecting memory $CD4^+$ T lymphocytes (138). These T cells can home to and mediate infection of human skin allografts in the severe combined immunodeficient (SCID)-hu model of VZV infection (139). In humans, skin lesions occur 10-21 days following the initial inoculation, and VZV DNA is detected in peripheral blood mononuclear cells during primary infection (49, 158). VZV accesses axons of innervating sensory neurons in the skin and establishes a life-long latent infection in neurons of the dorsal root ganglia. In contrast with latency of the closely related herpes simplex virus type 1 (HSV-1), VZV latency is characterized by persistent transcription, and possibly expression, of several viral lytic genes including ORFs 4, 21, 29, 62, 63 and 66 (44, 45, 170). This does not appear to stimulate a ganglionic infiltration of T cells (106, 240). VZV may also productively or abortively infect antigen presenting cells, including immature and mature dendritic cells (3, 105, 179), monocytes, macrophages and B-lymphocytes (8, 80, 108, 133).

The lymphotrophic nature of VZV and its ability to sustain infection in multiple cell types over a prolonged period suggest that VZV pathogenesis benefits from immune evasion mechanisms that limit antigen presentation. Several reports have also indicated a possible

chronic, non-inflammatory expression of viral lytic antigens during latency (44, 45, 170, 240), which may be suggestive of ongoing virus directed immune evasion. Accordingly, VZV reduces the surface expression of $CD8^+$ T lymphocyte (CTL)-restricted class I major histocompatibility complexes (MHC-I), both in cultured cells and in thymic T cells in the SCID-hu model (2, 38). Two proteins from closely related alphaherpesviruses, HSV-1 and 2 ICP47 and bovine herpesvirus 1 (BHV-1) U_L49.5, inhibit the TAP complex using distinct mechanisms to prevent peptide transport into the lumen of the endoplasmic reticulum (ER) (4, 134, 232). VZV does not encode an ICP47 ortholog, and no function in modulation of antigen presentation has been shown for the VZV UL49.5 ortholog, ORF9a (134). Furthermore, in VZV-infected cells, it has been suggested that MHC-I is processed through the *cis*-Golgi normally, but is prevented from accessing the cell surface (2). These observations imply that VZV–encoded mechanisms of MHC-I surface downregulation may be different from those of HSV-1 and 2 and BHV-1.

A previous study reported that transient expression of the VZV ORF66 protein kinase resulted in reduced MHC-I surface expression in human foreskin fibroblasts (HFF) (2). The ORF66 protein is a serine/threonine (ser/thr)-specific protein kinase with homology to the alphaherpesvirus U_S3 kinase family. Similar to other U_S3 kinases, ORF66 recognizes and phosphorylates serines preceded by several basic amino acids (58). While VZV that does not express ORF66 is only moderately impaired for replication in most cell cultures, ORF66 expression is required for efficient replication in cultured T-lymphocytes and in thy-liv implants in the SCID-hu model (174, 220, 224). The only known target of ORF66 is the VZV major transcriptional regulatory protein, IE62. ORF66 phosphorylates IE62 adjacent to its nuclear localization signal, leading to IE62 cytoplasmic accumulation in late-stage VZV-infected cells, and allowing for IE62 inclusion into the virion tegument (58, 123, 124). However, cellular

targets of the ORF66 protein kinase have been suggested from recent studies, in that ORF66 may contribute to anti-apoptotic mechanisms and evasion of a host cell response to interferon-γ (220).

In this work, the effects of the ORF66 kinase on MHC-I surface expression were characterized both in the context of VZV infection, and in the absence of other VZV proteins. Using novel adenovirus vectors and recombinant VZV expressing functional or altered green fluorescent protein (GFP)-tagged ORF66 kinase genes, we show that MHC-I surface expression is downregulated by ORF66 in a kinase-dependent manner, and that ORF66 contributes to MHC-I downregulation during VZV infection. The ORF66 kinase activity delayed MHC-I transport through the *cis/medial*-Golgi complex. Inhibition of MHC-I surface expression by intracellular retention in the early secretory compartment is a function that has not been attributed to any other viral protein kinase, and represents a novel role for a U_S3 family kinase in regulating the cellular environment during viral infection. We also show that VZV has ORF66-independent mechanisms that contribute to reduced MHC-I surface expression.

5.3 MATERIALS AND METHODS

5.3.1 Cells

The HEK-293 and HEK-293T cell lines (ATCC, Manassas, VA), MeWo cells (kindly provided by C. Grose, University of Iowa, Iowa City) and MRC-5 human lung fibroblasts (ATCC) were maintained as described previously (58).

5.3.2 Antibodies

The monoclonal antibodies used for flow cytometric analyses were anti-human transferrin receptor (TfR1 or CD71) (clone T56/14, IgG1; Caltag Laboratories, Burlingame, CA) (purified, R-PE conjugated and used at 1:100 dilution); an antibody recognizing class I heavy chains in complex with β-2 microglobulin (β2M) (clone G46-2.6, IgG1κ; BD Biosciences Pharmingen, San Jose, CA) (purified, PE-Cy5 conjugated and used at 1:20 dilution); and isotype control antibodies consisting of R-PE-conjugated IgG1 (Caltag Laboratories) and PE-Cy5 conjugated IgG1κ (BD Biosciences Pharmingen), used at the same respective dilutions. A rabbit polyclonal antibody recognizing VZV IE62 and a mouse monoclonal antibody that recognizes the nine amino-acid epitope (YPYDVPDYA) from influenza hemagglutinin (HA) have been previously described (58). The mouse monoclonal antibody W6/32 was obtained from Santa Cruz Biotechnology (Santa Cruz, CA) and used at 1 μg/ per immunoprecipitation, or at a dilution of 1:50 for immunofluorescence. Total class I heavy chains were immunoprecipitated with a polyclonal rabbit antibody to class I heavy chain cytoplasmic tail, designated UCSF2, at 1 μl per reaction (a kind gift of R. Salter, University of Pittsburgh). Golgi complexes were identified using rabbit anti-mannosidase II (mann II) at a 1:50 dilution (Chemicon, now a part of Millipore, Temecula, CA). A mouse monoclonal anti-α-tubulin (Sigma-Aldrich, St. Louis, MO) was used at 1:2000 for western blots and at 1 μg per immunoprecipitation. Alexa Fluor conjugated Fab fragments (goat anti-mouse or goat anti-rabbit; used at 1:400; Invitrogen Corp.) were used for secondary detection in immunofluorescence as previously detailed (58).

5.3.3 Plasmids

All plasmids were purified using Qiagen columns (Qiagen, Inc., Valencia, CA), according to the manufacturer's instructions. All oligonucleotides were obtained from IDT Inc. (Coralville, IA). The proofreading polymerase Expand (Roche Applied Science, Indianapolis, IN) was used to generate all PCR fragments, and accuracy was verified by sequencing. pGK2-HA66 expressing N-terminal HA tagged ORF66, and a similar plasmid expressing ORF66 kinase inactivated by D206E and K208R mutations (pGK2-HA66kd) have been detailed elsewhere (124). A new derivative, pGK2-HA66s, was generated from pGK2-HA66 by insertion of a double-stranded oligonucleotide that placed stop codons in all three reading frames (5'-CGCGCTAGACTAGTCTAG –3') into the Mlu I site at ORF66 amino acid 84. To generate EGFP-tagged ORF66 fusion proteins, the HA-tagged ORF66 genes from pGK2-HA66, pGK2-HA66kd and pGK2-HA66s were PCR-amplified using primers that added a unique Bgl II site proximal to the initiating ATG and a Hind III site following the stop codon. Digested PCR products were cloned into pEGFP-C1 (Clontech, Mountain View, CA) and the resultant plasmids will be referred to as pGFP-66, pGFP-66kd and pGFP-66s. A plasmid expressing IE62 with an in-frame carboxyl-terminal dsRed2 fusion inserted at amino acid 1309 (pCMV62-dsRed2) was generated in the previously described pK-CMV62 backbone (124), as follows. An Mlu I-Tth111 I fragment representing the C-terminal portion of IE62 was replaced with a PCR-generated product that inserted unique Avr II and Bgl II sites at the end of the IE62 open reading frame. This allowed the in-frame insertion of an Nhe I-Bgl II fragment containing the entire dsRed2 gene from pdsRed2-N1 (Clontech), at the unique Avr II-Bgl II sites. To express VZV ORF9a and ORF50, each gene was PCR-amplified using extended oligonucleotide primers to add EcoR I and Not I over-hangs, and subsequently cloned into pCDNA3.1 (Invitrogen, Corp.) to generate

pKORF9a and pKORF50. The transfection reporter plasmid pTK-EGFP, which expresses EGFP under the control of the HSV-1 thymidine kinase (TK) promoter, has been detailed elsewhere (51). The plasmid expressing the K3 gene from Kaposi's sarcoma herpesvirus (KSHV) in the pCDNA3.1 backbone was a kind gift from F. Jenkins, University of Pittsburgh, Pittsburgh, PA.

5.3.4 Derivation of replication defective adenoviruses

Replication defective adenoviruses expressing GFP-66 or GFP-66kd (referred to as Ad.GFP-66 and Ad.GFP-66kd) were derived using the Adeno-X Tet-Off system (Clontech). Digestion of pGFP-66 and pGFP-66kd with Nhe I and Hind III released the genes for cloning into the adenovirus intermediate vector pTRE-Shuttle2. Genes were shuttled into the Adeno-X genome as detailed in the manufacturer's instructions, and recombinant adenoviruses were obtained following transfection into HEK-293 cells. All viruses were assayed for the absence of functional replication competent viruses.

5.3.5 Derivation of recombinant VZV

Recombinant VZV expressing GFP-66 or GFP-66s were constructed using the VZV parent Oka (pOka) cosmid system (Figure 5-1C). To derive pvSpe23 cosmids in which the native ORF66 gene (nt 113142-114323) was replaced by the fluorescent versions, a modified pUC19 vector was made in which the poly-linker between Hind III and EcoR I was replaced by a double-stranded oligonucleotide encoding Avr II and Sgr AI sites. This enabled sub-cloning of the Avr II-SgrA I fragment from the pvSpe23 cosmid (nt 112957 to 117458; pUC19-pvSpe23; Figure 1D). Within this construct, the unique Avr II and Bam HI (nt 114147) sites were used to remove

the native ORF66 promoter and part of the gene. Next, the CMV IE promoter in pGFP-66 and pGFP-66s was replaced with a PCR-generated DNA fragment of the ORF66 promoter from the Avr II site to the ORF66 ATG, to give plasmid p66prom-EGFP.C1-HA66 or 66s (Figure 5-1D). Avr II and Bam HI digestion of these constructs released the ORF66 promoter-GFP/HA tagged partial ORF66 gene, which was then used to replace the Avr II- Bam HI fragment in pUC19-pvSpe23 (Figure 5-1D). The entire Avr II-SgrA I fragments were then cloned back into pvSpe23, and recombinant VZV were generated using the three additional pOka cosmids in MeWo cells, as detailed previously (187). VZV plaques exhibiting GFP fluorescence were grown into stocks, and assessed for purity and correct insertion.

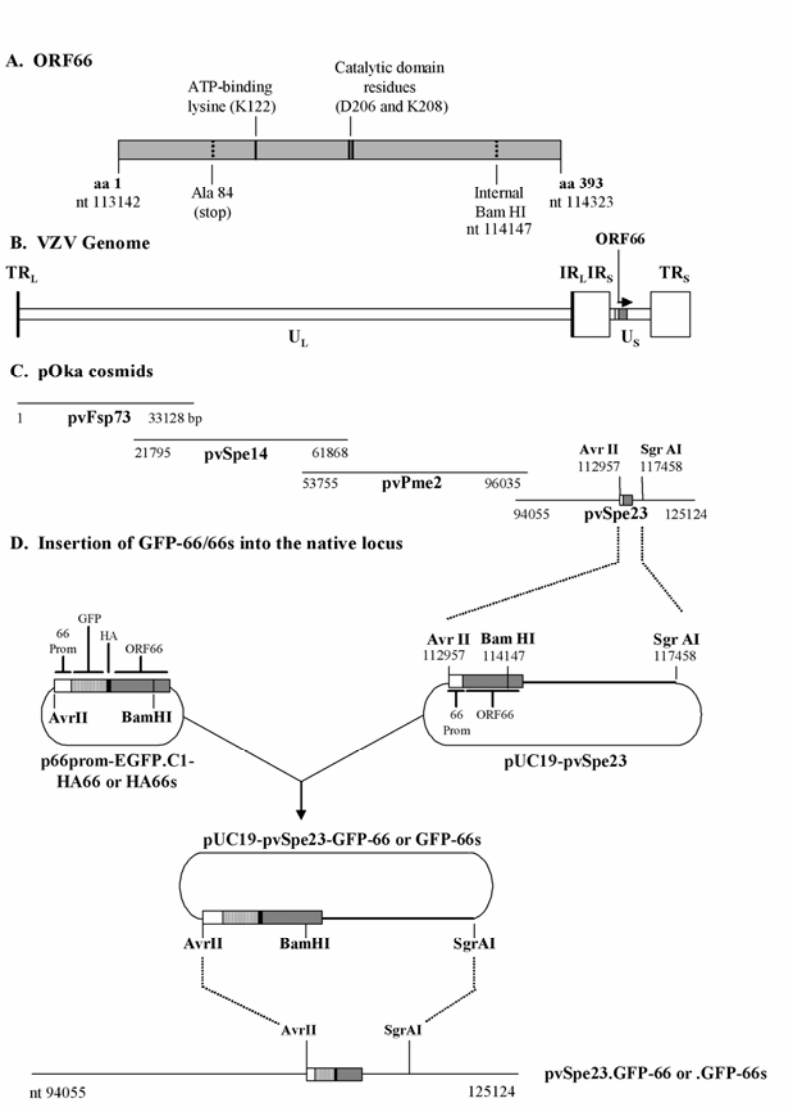

Figure 5-1 Schematic for creation of VZV containing GFP-66 or GFP-66s in the native ORF66 locus

(A) Representation of the domains of the 393 amino acid ORF66 protein showing the positions of key amino acid residues and a Bam HI restriction site, as detailed in the text. (B) Relative position of the ORF66 gene in the structure of the VZV genome. Shown are the Unique long (U_L) and Unique short (U_S) regions as well as the terminal (TR_L and TR_S) and internal (IR_L and IR_S) repeats. (C) The relative positions of the four pOka cosmids used to construct recombinant VZV. Genome co-ordinates are given with respect to the VZV pOka sequence. (D) Strategy for derivation of recombinant VZV expressing the ORF66 gene as an EGFP-tagged fusion protein. The ORF66 promoter and ORF are fully contained within a unique Avr II – SgrA I fragment of pvSpe23, and this fragment was sub-cloned into a modified pUC19 vector. The ORF66 promoter-GFP-66 cassette was inserted into this sub-fragment using Avr II-Bam HI, and then the Avr II-SgrA I sub-fragment was re-cloned into pvSpe23 as described in the Materials and Methods.

5.3.6 Transfections and infections

Transfections of MeWo, HEK-293 and HEK-293T cells were performed using Lipofectamine 2000 reagent (Invitrogen Corp.), according to the manufacturer's instructions and as detailed previously (58). Replication defective adenovirus-mediated expression of ORF66 was achieved by infecting MRC-5 cells with 5 plaque forming units (pfu)/cell of trans-gene expressing virus (Ad.GFP-66 or Ad.GFP-66kd) and 2.5 pfu/cell of Ad-Tet-Off, which expresses the tetracycline regulated transactivator. Where indicated, 2 μg/ml doxycycline (Sigma-Aldrich) were added to the media to fully repress trans-gene expression.

VZV growth curves were performed as detailed in similar studies (220). The exact infection level of the previously frozen input viruses was confirmed by titration on MeWo cells (inocula) in duplicate. Following fixation in 1% paraformaldehyde, plaques were visualized using GFP auto-fluorescence, or following immunofluorescent detection of IE62. For VZV flow cytometry analyses, inoculants of VZV.GFP-66 and VZV.GFP-66s were prepared in MRC-5 cells to >75% GFP fluorescence (as gauged by UV microscopy), and mixed with uninfected cells at a ratio of 1 to 10. Cells were gently co-pelleted by low speed centrifugation, incubated for 30 min at 25ºC, plated and placed at 37ºC. For metabolic labeling studies, trypsinized VZV-infected MRC-5 cells were used to infect confluent fibroblast monolayers at a ratio of 1 infected cell to 3 uninfected cells, to yield 100% GFP fluorescence by 36 hpi. Studies using [^{35}S] labeling components were initiated as detailed in the text.

5.3.7 Flow cytometry and immunoblotting

Cells for flow cytometry were harvested by dislodging following brief exposure to trypsin (MRC-5 cells) or 1X PBS/1 mM EDTA (293T cells). Cells were washed in FACS staining buffer (FSB) (2) and Fc-blocked with 15 μg of normal mouse IgG (Caltag Laboratories) for 10 minutes on ice. Cells were stained in FSB containing fluorophore-conjugated antibodies, washed, and fixed in freshly prepared 1% paraformaldehyde in 1X PBS. Isotype control staining was performed for each antibody and each condition. Stained cells were analyzed using a Becton Dickinson FACSAria cell sorter and data was analyzed using FACSDiva and WinMDI-2.8 software. Surface protein-negative and GFP-negative gates were set using isotype control antibodies and non-GFP expressing cells. To determine the mean fluorescence intensity (MFI) value for a cell population, the isotype control MFI was subtracted from the test MFI within corresponding GFP-negative or positive gates. MFI ratios were calculated by dividing the MFI of the test population (adenovirus-infected, VZV-infected) by the MFI of the control population (mock-infected or vector plasmid-transfected) after isotype control background values had been subtracted. Ratio values were converted to log values before statistical analysis using paired Student's *t*-test. For analysis of protein expression in infected or transfected cells, lysates of equivalent numbers of cells from each condition were separated by 7.5% sodium-dodecyl-sulfate polyacrylamide gel electrophoresis (SDS-PAGE), and analyzed by immunoblotting as previously described (58). Where indicated, membranes were stripped with 0.2 M NaOH for 5 minutes, rinsed with dH_2O and re-blotted. Digital images were acquired in the linear range of the film using an Epson Perfection 4990 photo scanner with Silver Fast Ai and Adobe Photoshop CS imaging software.

5.3.8 Immunofluorescence and microscopy

For immunofluorescence, cells grown on glass coverslips were fixed in 4% paraformaldehyde for 15 minutes, permeabilized with 0.2% triton-X-100 for 2 minutes and stained with the indicated antibodies as described previously (124). Cells for MHC-I localization studies were fixed with 2% paraformaldehyde for 10 minutes and permeabilized as just described. Where indicated, internal specific MHC-I was detected following a thirty second pre-fixation treatment with an acid elution buffer (50 mM glycine, 100 mM NaCl, pH 3.3) to remove β2M from surface class I. Nuclei were stained using Hoechst 33258 (Sigma-Aldrich). Immunofluorescence in fixed cells was observed using a Nikon Eclipse TE2000-E epifluorescent microscope, equipped with a xenon lamp and a 40X 1.3 numerical aperture oil objective, and recorded with Metamorph 7 software. Where indicated, Z-stacks were acquired at the recommended spacing for each fluorescent channel and AutoQuant 9.2 was used to deconvolve Z stacks in ten iterations using a blind deconvolution algorithm. Confocal analyses were performed as previously described (58, 124).

5.3.9 Metabolic labeling and immunoprecipitations

Pulse-labeling of cells and immunoprecipitations were carried out as previously described (115), with some modifications. Cells were first incubated with complete media containing 1% FBS and lacking cysteine and methionine (cys/met) for 20 minutes at 37ºC, and then pulsed for 15 minutes with 0.5 mCi/ml of [^{35}S]-labeled cys/met in cys/met-free media (Expre^{35}S^{35}S Mix, Perkin Elmer, Waltham, MA). Protein labeling was terminated by incubation in growth media containing 10-fold excess cold methionine and 10% FBS, and where indicated cells were chased

in the same media. Immunoprecipitations were obtained from soluble cell lysates using an ice-cold NP40 lysis buffer (115) containing a protease inhibitor cocktail (Complete, EDTA-free, Roche Diagnostics). Soluble fractions were equalized for trichloroacetic acid (TCA) precipitable radio-incorporation, and then pre-cleared with an unconjugated mix of proteins A and G sepharose (Sigma-Aldrich). Immunoprecipitations were collected using protein A/G-sepharose; washed in ice-cold radio-immunoprecipitation assay buffer (115) containing protease inhibitors; and then once in ice-cold 1X PBS. Precipitates were divided and one aliquot was subjected to endoglycosidase H (endo H) digestion, according to the manufacturer's suggestions (New England Biolabs). Immunoprecipitates were resolved on 10-20% gradient Criterion SDS-PAGE gels (Bio-Rad Laboratories, Hercules, CA), transferred to PVDF, and analyzed on a Bio Rad Molecular Imager FX using Quantity One software. In some cases, gels were dried and the signals were enhanced using En^{3}hance solution (Perkin-Elmer, Waltham, MA), captured by autoradiography with Kodak Biomax MP film and Kodak Biomax LE Transcreens, and quantified using ImageJ software.

5.4 RESULTS

5.4.1 Expression of functional and point inactivated GFP-tagged ORF66 kinase proteins in VZV-permissive cell types

An earlier study reported that HFF cells transfected with plasmids expressing ORF66 showed reduced surface MHC-I (2). In this study, it was unclear if the ORF66-induced downregulation of MHC-I surface expression was specific to ORF66 expressing cells, as the protein expression

and transfection efficiency were not determined. In particular, HFF cells and lines such as VZV-permissive MRC-5 fibroblasts are considered highly refractory to efficient transfection. To address this issue, we developed EGFP-tagged forms of ORF66 in plasmids, in replication defective adenoviruses and in recombinant VZV.

To assess the functionality of an amino-terminally EGFP-tagged ORF66 (GFP-66), we examined its cellular distribution and ability to exclude IE62 from the nucleus in live cells. IE62 nuclear exclusion is dependent on the integrity of ORF66 kinase activity, and is induced by a direct ORF66-mediated phosphorylation event adjacent to the IE62 nuclear localization signal (58, 124). We also tested a GFP-66 fusion protein in which two key residues in the ORF66 catalytic domain, which are absolutely conserved in all ser/thr kinases, were conservatively mutated (D206E, K208R; referred to as GFP-66kd). The HA-tagged version of ORF66-D206E/K208R has been previously shown to lack the ability to exclude IE62 from the nucleus and phosphorylate IE62 peptides (58, 124). For this live-cell assay, we developed a plasmid expressing IE62 with a carboxyl-terminal dsRed2 tag (IE62-dsRed2). In transfected MeWo cells, both GFP-66 and GFP-66kd accumulated in the nucleus, but also displayed cytoplasmic forms (Figure 5-2A, panels *i*-*ii*). When expressed alone, IE62-dsRed2 showed a distribution pattern identical to untagged IE62 and was predominantly nuclear (Figure 5-2A, panel *iii*) (58, 124). When GFP-66 was co-expressed with IE62-dsRed2, most co-expressing cells exhibited strong nuclear exclusion of IE62-dsRed2, which partially overlapped with GFP-66 in the cytoplasm (Figure 5-2B). IE62-dsRed2 nuclear exclusion did not occur in cells expressing GFP-66kd, indicating the activity was kinase dependent, as expected from previous studies (Figure 5-2C). These results established that amino-terminal EGFP-tagging of ORF66 did not interfere with its ability to affect IE62 cellular distribution, and that ORF66 kinase activity was intact.

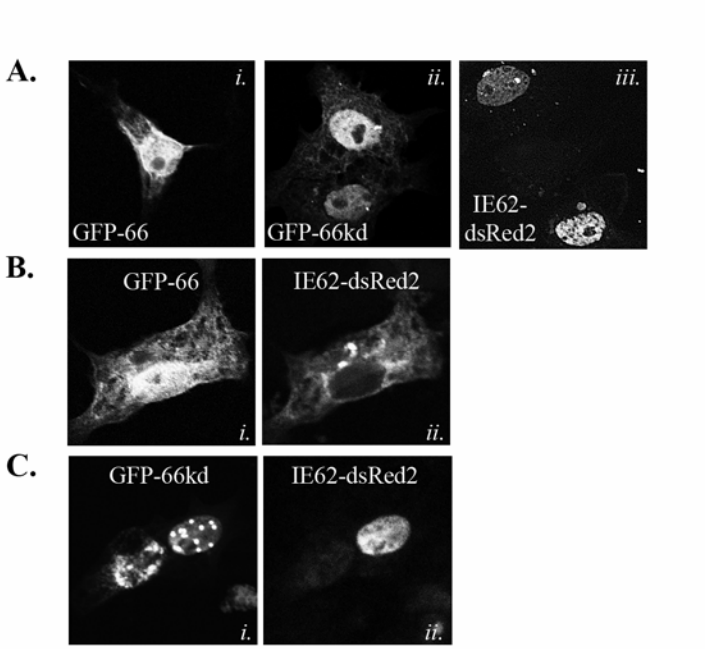

Figure 5-2 Live cell imaging to show that GFP-tagged ORF66 retains the ability to exclude IE62 from the nucleus

(A) Single panels showing cellular distributions of individually transfected GFP-66 (*i*), GFP-66kd (*ii*) and IE62-dsRed (*iii*). (B and C) Images of cells co-expressing IE62-dsRed2 and either GFP-66 (B) or GFP66kd (C). Panel *i* shows auto-fluorescence of GFP-66 and GFP-66kd, while panel *ii* shows IE62-dsRed2 auto-fluorescence from the same cell. All transfections were performed in MeWo cells, and auto-fluorescence was visualized and captured at 24 hours post-transfection by confocal microscopy. Cells were transfected with expression plasmids at a 1:1 ratio.

The GFP-66 and GFP-66kd genes were subsequently inserted into replication defective adenovirus vectors under the control of the doxycycline (dox)-repressible promoter (Ad.GFP-66 and Ad.GFP-66kd, respectively) to enable efficient expression in VZV-permissive fibroblasts. The adenovirus vector used lacked large portions of the E1 and E3 genome regions, including the MHC-I modulating genes E1A and E3/gp19K (20, 73, 205, 258), and does not have any intrinsic effects on MHC-I surface expression. MRC-5 cells required relatively low multiplicities of infection (2-5 pfu/cell) to obtain efficient trans-gene expression in over 80% of cells. Expression

was dependent on co-infection with adenovirus expressing the tetracycline tTa transactivator, and the absence of dox. Immunoblot analyses of Ad.GFP-66 and Ad.GFP-66kd cell lysates revealed proteins of the expected size (~75 kDa), which reacted with both anti-HA and anti-GFP antibodies (Figure 5-3C) (anti-GFP blot not shown). The GFP-66kd protein displayed a slightly faster mobility in SDS-PAGE compared to GFP-66, as reported previously for HA-tagged ORF66kd protein (124, 219). We also verified that adenovirus transduction and GFP-66 or GFP-66kd expression did not result in increased levels of apoptotic cells using flow cytometric analysis of annexin V surface staining and 7-AAD uptake (data not shown). These vectors allow for both efficient expression and quantitative assessment of ORF66 expression in multiple cell types.

5.4.2 GFP-66 induces kinase dependent downregulation of MHC-I surface expression

The Ad.GFP-66 and Ad.GFP-66kd viruses were next employed to assess the role of ORF66 kinase activity in downregulation of MHC-I surface expression. We report the studies here in VZV-permissive MRC-5 fibroblasts, but have found similar effects in MeWo cells and 293T cells. Surface levels of MHC-I were compared to transferrin receptor (TfR1 or CD71), a control that is widely used in MHC-I surface studies.

MRC-5 fibroblasts infected with Ad.GFP-66 or Ad.GFP-66kd in the presence or absence of 2 μg/ml dox were assessed for surface MHC-I and TfR1 levels at 36 hours post infection (hpi) (Figure 5-3A). Representative histograms showing MHC-I fluorescence in GFP-positive cells from the Ad.GFP-66 infection revealed that MHC-I surface expression was reduced when GFP-66 was expressed. Parallel infected cells grown in media containing dox showed no MHC-I downregulation, and GFP-66kd expression did not significantly downregulate MHC-I surface

expression in the absence or presence of dox. From three independent and identical experiments, GFP-66 expression induced an average of ~40% reduction of MHC-I surface levels compared to a minor 5-11% reduction in GFP-66kd expressing cells (Figure 5-3B). Analysis of surface TfR1 revealed no significant downregulation under any conditions (Figure 5-3A and B). Immunoblot analyses of equal numbers of Ad.GFP-66 and Ad.GFP-66kd infected cells from the same experiment shown in Figure 5-3A indicated that similar levels of GFP-66 and GFP-66kd were expressed (Figure 5-3C). These data indicate that functional kinase activity is required for efficient ORF66-mediated MHC-I downregulation, and implies that ORF66 phosphorylates a cellular target to induce the reduction in MHC-I surface expression.

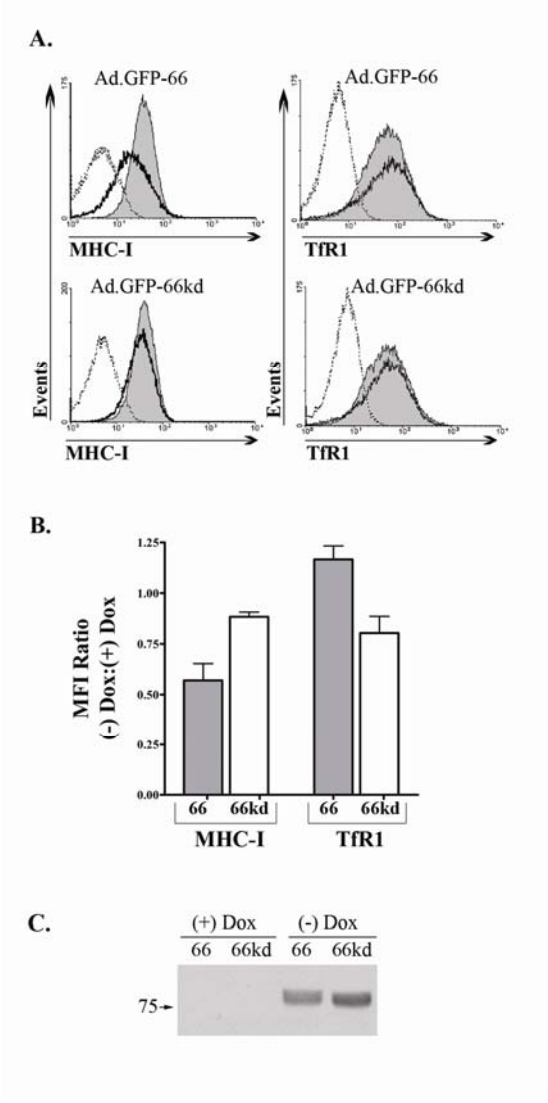

Figure 5-3 GFP-66 induces a kinase dependent and specific downregulation of surface MHC-I

(A) MRC-5 cells were infected with Ad.GFP-66 or Ad.GFP-66kd in conjunction with Ad.Tet-Off, grown in the presence or absence of 2 μg/ml of doxycycline, and harvested at 36 h post infection. Cells were stained with fluorophore-conjugated antibodies to MHC-I and TfR1 or isotype controls, and analyzed using a Becton Dickinson FACSAria. Histograms of surface fluorescence for MHC-I and TfR1 are shown with the infection condition indicated above each. The shaded gray histograms represent infected cells that were incubated with 2 μg/ml doxycycline. Cells incubated in the absence of dox were gated on GFP positivity and are represented by the solid black line histograms. The isotype controls antibody levels are shown by dotted lines. (B) Graph depicting the average (+/- SEM) MFI ratios of MHC-I and TfR1 surface fluorescence from three independent and identical experiments. (C) Western blot analysis of an equal number of cells from the Ad.GFP-66 and Ad.GFP-66kd infections under the four experimental conditions were probed with antibodies to the HA epitope, and the proteins reacting in the size range expected are shown.

5.4.3 Development of recombinant VZV expressing GFP-66 proteins

In previous studies of VZV and its effects on MHC-I surface expression, the identification of VZV infected cells required indirect immunofluorescent detection of surface VZV glycoproteins. To more accurately assess infection and correlate the levels of ORF66 expression with levels of surface MHC-I during VZV infection, we generated recombinant VZV expressing GFP-66 (VZV.GFP-66) or one in which protein kinase expression was halted by stop codon insertion at ORF66 amino acid 84 (VZV.GFP-66s). Recombinant viruses were created using wild-type VZV (pOka) cosmids (Figure 5-1) and were designed so that GFP-66 or GFP-66s was expressed at the native locus and under the natural ORF66 promoter. Each recombinant was successfully generated twice from cosmid-transfected MeWo cells, yielding green fluorescent plaques with no visible differences in size, morphology or GFP auto-fluorescence distribution (data not shown). The GFP tag enabled VZV infected cells expressing ORF66 to be differentiated in mixed populations of infected and uninfected cells, and also reported the relative amounts of ORF66 expression. Growth curve analysis in MRC-5 fibroblasts of these viruses indicated that VZV.GFP-66 grew with similar kinetics as pOka and achieved equivalent maximal titers (~1 x 10^5 infectious foci by 96 hpi; Figure 5-4A). This suggests that the addition of EGFP to ORF66 had only minimal effects, if any, on virus growth. VZV.GFP-66s infections were marginally impaired, similar to observations from a previous study (220), yielding a 3-4 fold reduction in infectious cell titers with respect to pOka and VZV.GFP-66.

The functionality of the GFP-66 kinase in VZV.GFP-66 and the disruption of ORF66 kinase expression in VZV.GFP-66s were assessed by examining IE62 localization in infected MRC-5 cells (Figure 5-4B). Consistent with functional ORF66 kinase activity, IE62 was predominantly cytoplasmic in late-stage VZV.GFP-66-infected plaques and most nuclei showed

only low-levels of IE62 staining (Figure 5-4B, panels *ii*-*iii*). Nuclear IE62 was observed at plaque edges where GFP-66 expression was low or absent, as was found for pOka-infected cells (219). GFP-66 exhibited both nuclear and cytoplasmic distributions and was often concentrated in discrete nuclear foci that appeared to surround the nucleolus (Figure 5-4B, panel *i*). In contrast, IE62 in VZV.GFP-66s-infected MRC-5 cells remained strictly nuclear, even in late-stage infected plaques and syncytia (Figure 5-4B, panels *iv*-*vi*), consistent with the lack of ORF66 kinase domain expression. Despite including only the first 83 residues of ORF66, we noted a significant overlap between GFP-66s auto-fluorescence and IE62 immunofluorescence in the nucleus. Together, the growth curve analysis and IE62 nuclear exclusion assay validates the use of VZV.GFP-66 and VZV.GFP-66s to assess the correlation of ORF66 expression with the downregulation of MHC-I surface expression in VZV-infected cells.

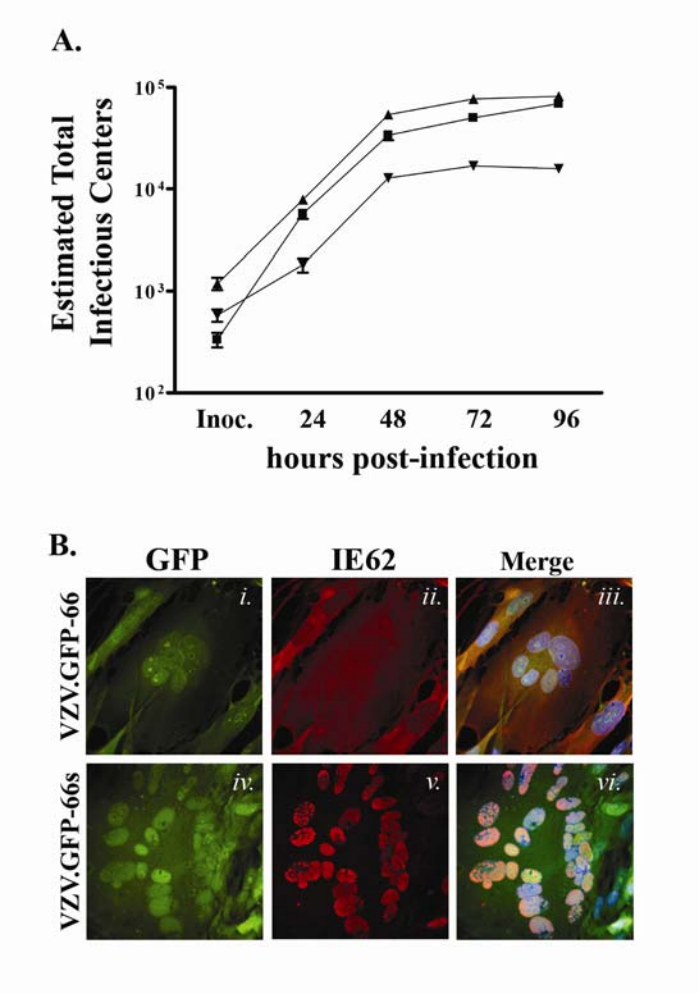

Figure 5-4 Characterization of recombinant VZV expressing GFP-66 and GFP-66s

(A) Growth curve analyses of VZV.GFP-66 (▲), VZV.GFP-66s (▼) and pOka (■). Parallel infections were established on confluent monolayers in MRC-5 fibroblasts, and the amount of virus infected cells in each culture produced by each VZV was titrated on MeWo cells after 24, 48, 72, and 96 hpi. Mean titers and standard error were deduced from duplicate wells of duplicate titrations. (B) Images showing GFP expression and IE62 cellular localization in fixed VZV.GFP-66 (*i-iii*) and VZV.GFP-66s (*iv-vi*) infected MRC-5 cells at 48 hpi. Cells were fixed with 4% paraformaldehyde and stained with rabbit anti-62 and Alexa Fluor 546 conjugated anti-rabbit Fab fragments, and Hoechst dye to identify nuclei. The depicted auto-fluorescence or stained protein is indicated above the panels, and the infection condition is on the left. Images were selected to represent the center of VZV syncytia at approximately the same stage of infection.

5.4.4 VZV has ORF66-dependent and independent effects on MHC-I and TfR1 surface expression

The cell-associated nature of VZV precludes large-scale synchronous infection, so MHC-I and TfR1 surface levels were compared in MRC-5 cells infected with VZV.GFP-66 and VZV.GFP-66s at a moderate multiplicity of infection (uninfected to VZV-infected fibroblasts at a ratio of 10:1) over a 72-hour time course. At 24, 48 and 72 hpi, MHC-I and TfR1 surface expression were analyzed by flow cytometry (Figure 5-5). Mock-infected cells stained with isotype control antibodies were used to define the GFP-negative quadrant gate at each time point (Figure 5-5A and D, panels a-c). Uniform levels of surface MHC-I and TfR1 were consistently displayed in mock-infected cells (Figure 5-5A and D, panels d-f). We note that MHC-I level in mock-infected cells showed a slight increase in over time in culture, but we cannot rule out that this is a consequence of experimental variability. At 24 hpi VZV.GFP-66 infected cells exhibited a range of GFP expression levels (Figure 5-5A, panel g). The GFP-negative population had MHC-I surface levels similar to that of uninfected cell controls, whereas most (but not all) cells expressing the higher levels of GFP had reduced MHC-I surface expression. This indicates that ORF66 expression did not have an immediate effect on MHC-I surface levels. At 48 and 72 hpi, most cells expressed high amounts of GFP in VZV.GFP-66 infections, and showed more downregulation of MHC-I surface fluorescence (Figure 5-5A, panel h-i). The greatest reduction in MHC-I surface expression was consistently observed in high GFP expressers at 72 hpi (Figure 5-5A, panel i). Regarding VZV.GFP-66s infections, while fewer cells were infected at 24 hpi, MHC-I was still reduced in a fraction of GFP positive cells (Figure 5-5A, panel j). At later times in very high GFP expressers, reduced MHC-I surface expression was also observed (Figure 5-5A, panels k-l). These data show that VZV can downregulate MHC-I in the absence of the

expression of the ORF66 kinase domain. We note that the GFP signal in GFP-66s was expressed with similar timing and to greater levels compared to that from GFP-66 during VZV infection (Figure 5-5F). The basis of the reduced levels of ORF66 kinase at 72 hours is not yet clear, but it is conceivable that the functional kinase has possible auto-regulatory effects on its own expression.

We assume that similar levels of GFP represent similar stages of infection, since the native ORF66 promoter controls both GFP-66 and GFP-66s expression. To determine if there were differences in the abilities of VZV.GFP-66 and VZV.GFP-66s to mediate MHC-I downregulation, we examined cells exhibiting similar relative GFP intensities. The same high GFP gate was used for all infections at all time points and was defined as cells with 10-fold or greater GFP fluorescence compared to mock-infected cells (indicated in each representative infection dot-plot; Figure 5-5A, panels g-l). Similar approaches were recently used to compare apoptosis and Stat1 phosphorylation in pOka and pOka66S infected cells (220). Our data were accumulated in three independent experiments. GFP-high cells in VZV.GFP-66 infections consistently exhibited a more negative MHC-I surface expression phenotype compared to GFP-high cells from VZV.GFP-66s infections (Figure 5-5B). On average, ~75% of GFP-66-high cells fell below the MHC-I positive gate at both 48 and 72 hpi, while similar GFP-66s-high cells were ~55-60% MHC-I negative. We also calculated the average MHC-I MFI ratio (relative to mock-infected cells) of GFP-high cells from these three experiments and found that GFP-high cells in VZV.GFP-66 infections had a lower average MHC-I MFI ratio at all time points compared to similar cells in VZV.GFP-66s infections (Figure 5-5C). This difference was statistically significant at 72 hpi ($p \leq 0.05$). These analyses indicate that while ORF66-independent processes negatively influence MHC-I surface expression, more efficient MHC-I

surface downregulation in VZV infection requires expression of the functional ORF66 kinase domain.

Surprising results were obtained with TfR1. Both VZV.GFP-66 and VZV.GFP-66s induced an increase in TfR1 surface expression compared to mock-infected cells, with more up-regulation occurring when the ORF66 kinase activity was intact (Figure 5-5D and E). A 2.5-fold increase in TfR1 expression over mock-infection was observed in the VZV.GFP-66 infection at 72 hpi, compared to a 1.8-fold increase in VZV.GFP-66s infection. At all times, the difference was statistically significant. These data indicate that the surface expression of TfR1 is also regulated by both ORF66-dependent and independent mechanisms during VZV infection, but is affected in an opposite manner compared to surface MHC-I. The differential regulation of outcomes for surface MHC-I and TfR1 implies that ORF66 may have multiple effects on other cell surface protein trafficking patterns.

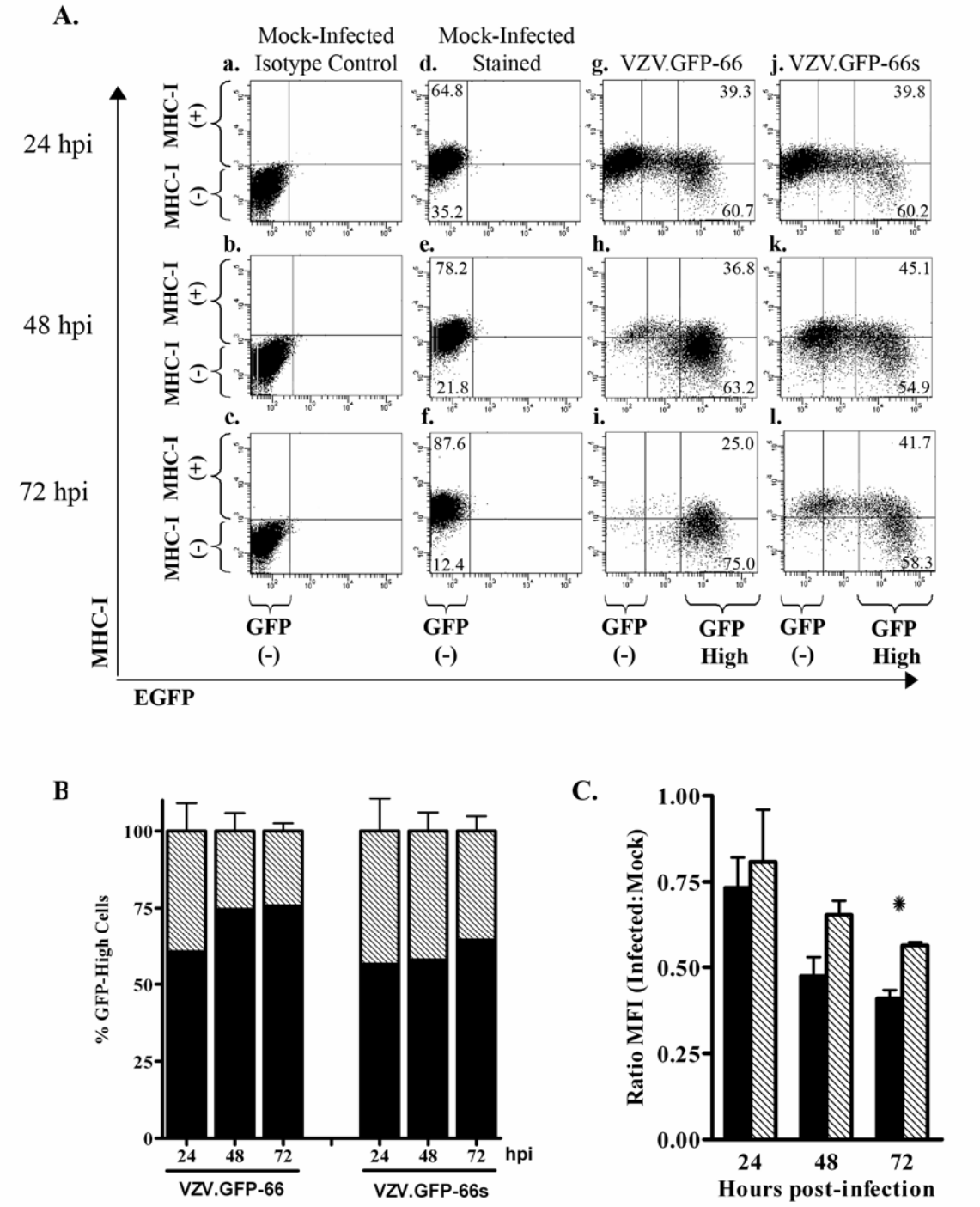
A.
Mock-Infected Isotype Control
Mock-Infected Stained
a.
d.
g. VZV.GFP-66
j. VZV.GFP-66s
24 hpi
48 hpi
72 hpi
MHC-I (+)
MHC-I (-)
64.8
35.2
39.3
60.7
39.8
60.2
78.2
21.8
36.8
63.2
45.1
54.9
87.6
12.4
25.0
75.0
41.7
58.3
GFP (-)
GFP High
MHC-I
EGFP
B
% GFP-High Cells
100
75
50
25
0
24
48
72
hpi
VZV.GFP-66
VZV.GFP-66s
C.
Ratio MFI (Infected:Mock)
1.00
0.75
0.50
0.25
0.00
Hours post-infection

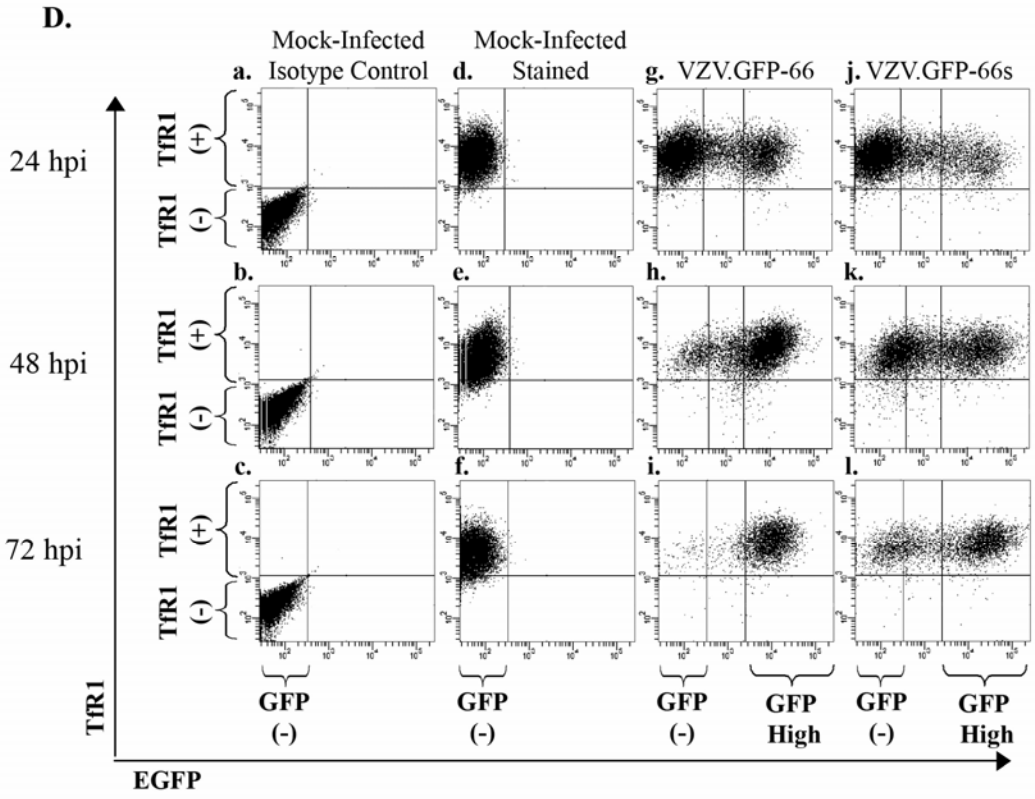
D.
Mock-Infected Isotype Control
Mock-Infected Stained
VZV.GFP-66
VZV.GFP-66s
24 hpi
48 hpi
72 hpi
TfR1 (+)
TfR1 (-)
TfR1
EGFP
GFP (-)
GFP High

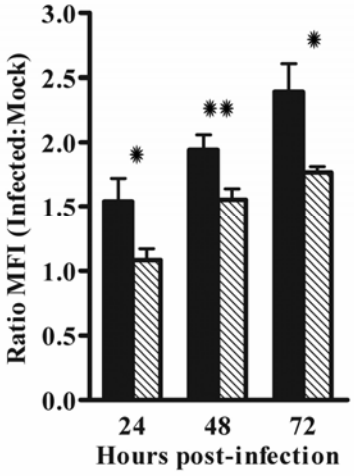
E
Ratio MFI (Infected:Mock)
Hours post-infection

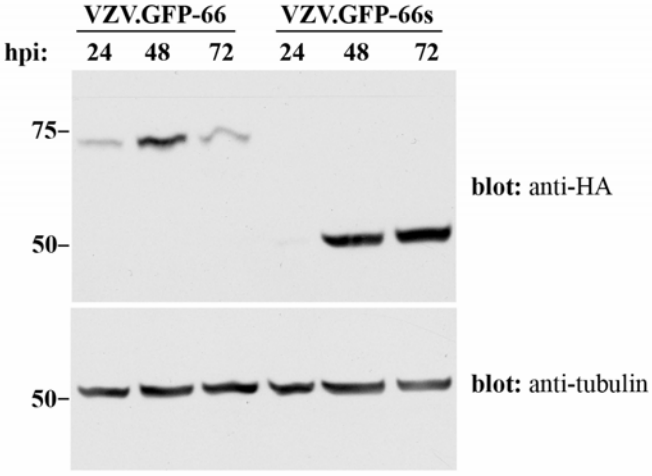
F.
VZV.GFP-66
VZV.GFP-66s
hpi:
blot: anti-HA
blot: anti-tubulin

Figure 5-5 MHC-I downregulation in VZV infection with and without expression of functional kinase

MRC-5 cells were infected with VZV.GFP-66 or VZV.GFP-66s at a ratio of 10:1, surface-stained for MHC-I and TfR1 at 24, 48 and 72 hpi, and analyzed by flow cytometry. (A) Dot-plots from a representative experiment depicting MHC-I surface expression as a function of GFP-66 or GFP-66s expression. The analysis time-point is shown to the left of each row, and the infection condition is shown above each column. Quadrant gates to identify MHC-I negative and MHC-I positive cell populations were established at each time point using mock-infected isotype control stained cells (a-c). The same quadrant gate was used for mock (d-e), VZV.GFP-66 (g-i) and VZV.GFP-66s (j-l) infections. To quantitatively assess differences between VZV.GFP-66 and VZV.GFP-66s infections, cells were gated on high GFP fluorescence, represented as the right-most vertical line in infected cell dot-plots (g-l). The GFP negative and GFP-high (where relevant) cell populations for each column are indicated below panels c, f, i, and l. The percentage of mock-infected cells exhibiting an MHC-I negative and MHC-I positive phenotype is indicated in the upper left and lower left quadrants in panels d-f. Similar MHC-I negative and MHC-I positive cell percentages in GFP-high cells are indicated in the upper right and lower right quadrants of panels g-l. (B) The average percentage (+/- SEM) of MHC-I positive (gray) and MHC-I negative (black) cells in the GFP-high gate in each infection condition was calculated from three independent experiments. (C) MFIs of GFP-high cells in VZV.GFP-66 (black) and VZV.GFP-66s (gray) infections were expressed as a ratio of the MFI of mock-infected cells. Average ratios (+/- SEM) from three independent experiments were compared at each time point, and we found that VZV.GFP-66 exhibited a significant reduction in MHC-I surface expression over VZV.GFP-66s at 72 hpi. (D) TfR1 surface expression dot-plots and (E) MFI ratios are shown exactly as described for MHC-I. (F) Lysates of aliquots of equal numbers of cells from each infection condition at each time point were separated by SDS-PAGE and analyzed by immunoblot sequentially with mouse anti-HA and then anti α-tubulin antibodies. $*p \leq 0.05$, $** p \leq 0.005$

5.4.5 ORF66 kinase delays the biosynthetic maturation of MHC-I

Molecular mechanisms underlying downregulation of MHC-I by VZV infection and ORF66 have not been well resolved. While one study reported no change in MHC-I synthesis levels or rate of acquisition of endo H resistance in VZV-infected fibroblasts (2), another study observed a modest effect on total class I heavy chain and β2M synthesis at 48 hpi (38). Our data shows that most MHC-I surface downregulation occurred after 24 hpi. To clearly elucidate the mechanism, we undertook an analysis of MHC-I biogenesis in cells expressing the ORF66 kinase independently of other proteins, as well as in the context of VZV infection.

Pulse-chase studies combined with endo H cleavage analysis were used to address MHC-I synthesis and maturation in MRC-5 cells infected with Ad.GFP-66 or Ad.GFP-66kd. Endo H resistance is acquired when *cis/medial*-Golgi enzymes mediate replacement of high mannose groups with more complex N-linked glycans on glycoproteins. Mock or adenovirus infected MRC-5 cells were subjected to an [^{35}S] cys/met 15-min pulse and harvested or chased to allow maturation of labeled protein. Equivalent amounts of labeled protein from each infection condition were subjected to immunoprecipitation with the W6/32 antibody, which only recognizes folded MHC-I molecules that have associated with β2M. Immunoprecipitations performed with non-specific isotype control antibodies did not result in significant amounts of precipitated radio-labeled protein (data not shown).

Comparison of the SDS-PAGE resolution of immunoprecipitates obtained at the end of the pulse (0 min) revealed that expression of functional or kinase inactive ORF66 had no effect on the levels of MHC-I complexes, as compared to that obtained from mock-infected cells, and that MHC-I from all conditions was completely sensitive to endo H cleavage (Figure 5-6A-C, lanes 1 and 2). These observations indicate that ORF66 does not modulate expression of MHC-I components or its initial assembly into heavy chain (HC)-β2M heterodimers. The amount of MHC-I HC was also found to remain relatively stable in chase conditions up to 120 min, indicating that ORF66 does not induce MHC-I degradation. However, ORF66 expression clearly delayed MHC-I acquisition of endo H resistance. In mock-infected cells, heavy chains were ~53% resistant to endo H cleavage at 30 minutes, ~78% at 60 minutes, and 98% resistant by 120 minutes of chase (Figure 5-6A and D). In contrast, MHC-I from Ad-GFP-66 infected cells demonstrated only ~11% and 16% endo H resistance at 30 and 60 min of chase, respectively (Figure 5-6B and D). By 120 minutes of chase, most heavy chains remained sensitive to

cleavage, with only 26% exhibiting resistance. In Ad.GFP-66kd infected cells, MHC-I acquired endo H resistance at a rate more similar to that observed in mock infections, with 35% resistance at 30 min, 52% at 60 min, and 74% at 120 min (Figure 5-6C and D). In a similar experiment, Ad.GFP-66 infection induced a comparable reduction in MHC-I maturation relative to mock infection, but no impairment was observed when infections were incubated in the presence of 2 μg/ml dox (data not shown). These data indicate that MHC-I maturation through the *cis/medial*-Golgi compartment is impaired predominantly as a result of ORF66 kinase activity.

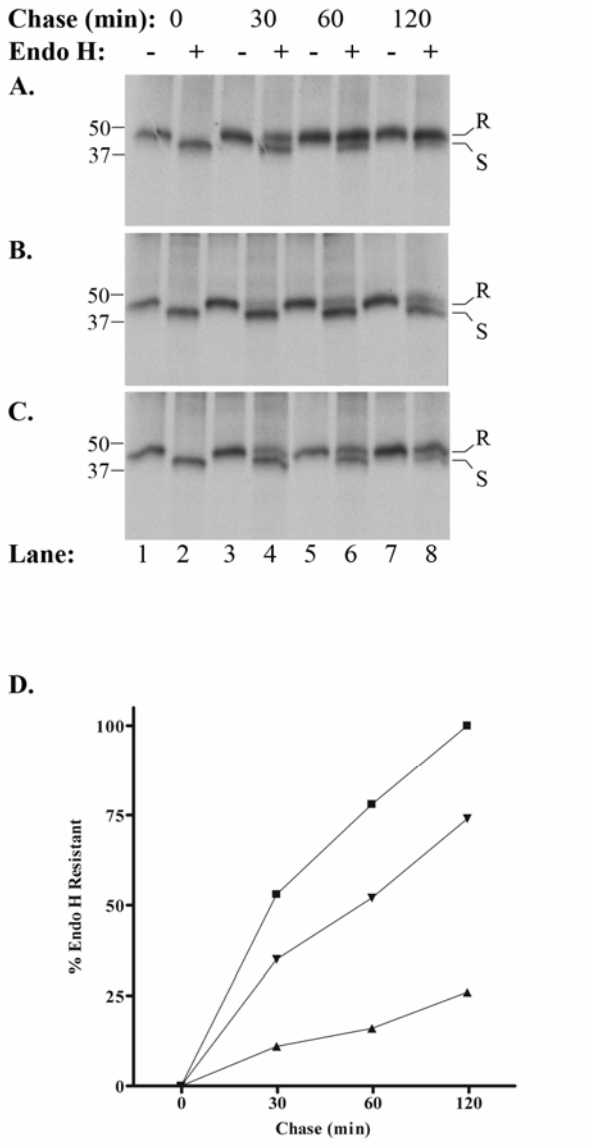

Figure 5-6 GFP-66 expression induces a delay in MHC-I maturation in MRC-5 fibroblasts

(A) Mock-infected, (B) Ad.GFP-66-infected or (C) Ad.GFP-66kd-infected cells were pulse-labeled with [^{35}S] cys/met, chased in media containing cold cys/met, and folded MHC-I was immunoprecipitated and subjected to endo H digestion. Autoradiographs of proteins separated by SDS-PAGE are shown. The chase time and presence (+) or absence (-) of endo H is indicated above each lane, and lane numbers are shown at the bottom. Class I molecules that are resistant to endo H cleavage migrate more slowly through the gel, and are designated by the letter R to the side of each radiograph. Sensitive molecules migrate more quickly and are indicated by the letter S. Protein size standards were run with each gel and are shown (in kDa) to the left. (D) The rate of acquisition of endo H resistance was quantified for mock infections (■), Ad.GFP-66 infections (▲) and Ad.GFP-66kd infections (▼) using autoradiography. The percent of the total MHC-I molecules exhibiting resistance was plotted as a function of time.

5.4.6 VZV affects early events in MHC-I biogenesis

The ORF66-mediated delay of MHC-I maturation prompted a reassessment of MHC-I maturation in VZV-infected cells. Infection conditions for the two VZV were carefully normalized to be equivalent, and VZV-infected MRC-5 fibroblasts were established at relatively high VZV-infected cell multiplicity (3 uninfected cells to 1 infected cell) to ensure efficient infection. Cells were pulse labeled at 36 hours post infection, when all cells were GFP-positive. Immunoblot analysis of infection lysate supernatants indicated that GFP-66s was expressed to a greater level compared to GFP-66 under these conditions (see Figure 5-8A).

In two independent and identical experiments, SDS-PAGE separated immunoprecipitates for each infection condition revealed that pulse-labeled class I heavy chains in uninfected cells were completely sensitive to endo H cleavage at 0 minutes, but became almost fully resistant by 180 minutes of chase (Figure 5-7A). Labeled MHC-I levels remained relatively stable for the duration of the experiment, suggesting there was no turnover. In VZV-infected cells, there was a consistent reduction in the rate of class I maturation compared to uninfected cells, with a greater degree of delay in VZV-infected cells expressing the functional ORF66 kinase (Figure 5-7B-D). On average, after 30 minutes of chase only 31% of the total precipitated MHC-I heavy chains from VZV.GFP-66-infected cells exhibited endo H resistance, whereas greater than 60% were resistant in uninfected cells. VZV.GFP-66-infected cells were 51% and 72% resistant at 60 and 180 minutes of chase, respectively, compared to 78% and 85% resistance in uninfected cells at the same times. MHC-I in VZV.GFP-66s-infected cells was marginally delayed in acquisition of endo H resistance, but not to the level seen in VZV.GFP-66 infection, showing an average 58% resistance at 30 min, 67% at 60 min, and 82% after 180 min of chase. These data indicate that the greatest delay in acquisition of endo H resistance for MHC-I occurs when the ORF66 kinase

is expressed and functional. This correlates with the observed delay in cells expressing the ORF66 kinase in the absence of other VZV proteins. Thus, the ORF66 kinase delays MHC-I maturation in a predominantly kinase-dependent manner and contributes to the reduced MHC-I phenotype seen in VZV-infected cells.

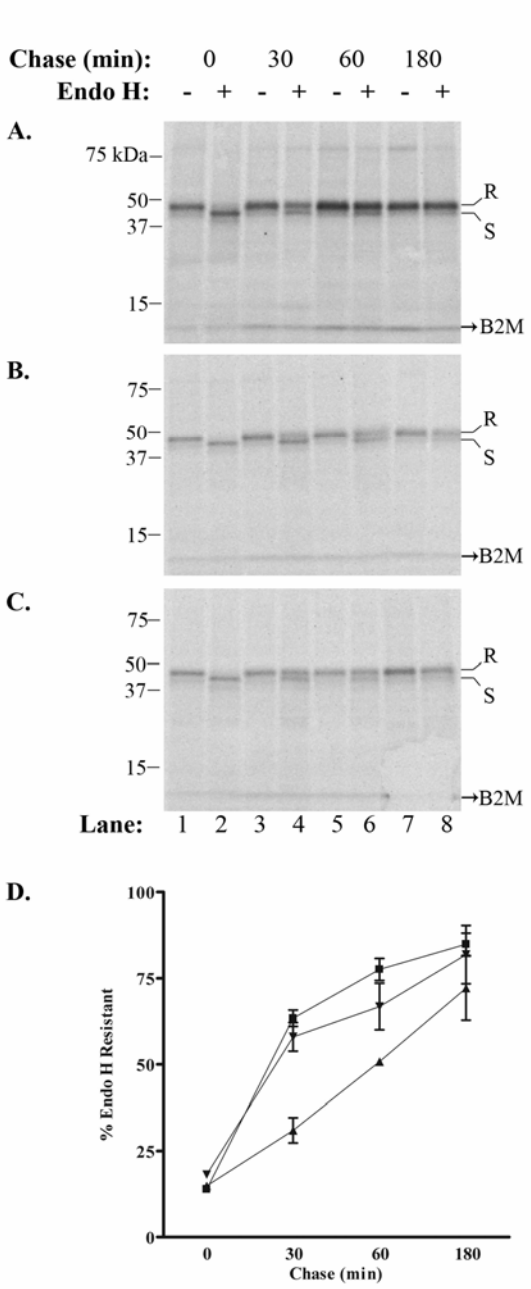

Figure 5-7. GFP-66 mediates a delay in MHC-I maturation in the context of VZV infection

Endo H resistance analysis was performed for MHC-I molecules from (A) Mock-infected, (B) VZV.GFP-66-infected and (C) VZV.GFP-66s infected cells. Chase times and treatment with endo H are shown above each radiograph and lane numbers are shown below. Protein size markers are specified in kDa to the left, and endo H resistant (R) or sensitive (S) forms are indicated to the right. (D) The rate of MHC-I maturation was determined by phosphorimager analysis from two independent but identical experiments, and is plotted as a function of time for mock infections (■), VZV.GFP-66 infections (▲) and VZV,GFP-66s infections (▼).

Additional VZV activities contributing to the delay of MHC-I on cell surface were also indicated in these studies. Specifically, we noted that the levels of β2M associated class I immunoprecipitated by the W6/32 antibody from both VZV.GFP-66 and VZV.GFP-66s infections were greatly reduced at all time points compared to that from uninfected cells, even though all immunoprecipitations were normalized for equal amounts of labeled protein in the cleared lysates. The TCA-precipitable material was substantially reduced in both VZV.GFP-66 and VZV.GFP-66s infected cells, over that in uninfected cells (data not shown). This likely reflects a VZV-induced global reduction in host protein synthesis that may affect MHC-I component expression. To determine if VZV induces a specific reduction in MHC-I synthesis, we performed parallel immunoprecipitations from longer-term radio-labeled (6 hour) extracts of uninfected cells or cells equally infected with VZV.GFP-66 or VZV.GFP-66s, using antibodies that recognized folded MHC-I (W6/32), total class I heavy chains or α-tubulin. Equivalent levels of TCA-precipitable counts were used for each immunoprecipitation. The SDS-PAGE resolved immunoprecipitates revealed that α-tubulin synthesis was reduced in both infection conditions compared to uninfected cells, consistent with global reduction in host protein expression (Figure 5-8B, lanes 1-3). Quantification of total MHC-I heavy chain synthesis by phosphorimager analysis revealed a 45-50% reduction relative to uninfected cells in both infections (Figure 5-8B, lanes 4-6). However, folded MHC-I heavy chains precipitated with W6/32 were more reduced (~65%) than that predicted by heavy chain levels in both VZV-infected cell populations (Figure 5-8B, lanes 7-9). While modest, this difference was consistently detected in replicate experiments, suggesting an additional impairment in the formation of the heavy chain-β2M heterodimer. Altogether, the biochemical analyses of MHC-I from VZV-infected cells strongly indicated that VZV uses multiple processes to impede MHC-I surface levels.

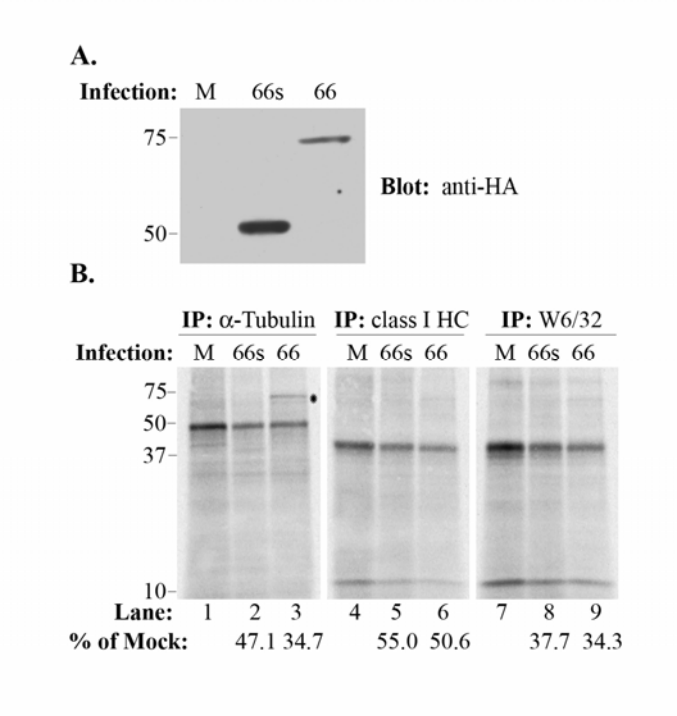

Figure 5-8 VZV infection reduces class I synthesis and impairs the association of class I heavy chains with β2M

Total α-tubulin and class I heavy chain, as well as folded class I heavy chain levels were compared by parallel immunoprecipitation from either mock-infected cells (M) or cells infected with VZV.GFP-66 (66) or VZV.GFP-66s (66s), following a 6-hour [^{35}S] cys/met label. (A) Western blot analysis of cleared infected cell lysates showing the level of GFP-66 and GFP-66s protein expressed in each infection condition. The infection condition is indicated at the top. (B) Autoradiographs of each set of parallel immunoprecipitations. The antibody used and infection condition are labeled above the radiograph, and lane numbers are shown below. Protein size markers (in kDa) are shown to the left. The relative amounts (%) of proteins expressed in infected cells compared to uninfected cells for both VZV.GFP-66 and VZV.GFP-66s are shown under lane numbers 2-3, 5-6, and 8-9. The * indicates a reproducible co-precipitating band of ~75 kDa, which was apparent in the α-tubulin immunoprecipitation of VZV.GFP-66 infected cells. This band did not react with antibodies to HA; its identity is currently unknown.

5.4.7 Intracellular retention of MHC-I in VZV-infected cells

A previous study suggested that MHC-I is processed correctly, but retained in the Golgi apparatus in VZV-infected HFF cells (2). Given our new observations that VZV delays MHC-I early maturation, we re-evaluated the distribution of MHC-I in VZV infections in both the

presence and absence of the ORF66 kinase. Immunolocalization of MHC-I and its association with *cis/medial*-Golgi in MRC-5 fibroblasts was determined using the conformation dependent W6/32 antibody and anti-mannosidase II (mann II) antibodies. To facilitate specific detection of intracellular MHC-I, cells were treated briefly with a mild acid buffer (228) prior to fixation and permeabilization, to dissociate β2M from surface class I heavy chains and render surface MHC-I unrecognizable by W6/32. In uninfected, untreated cells, surface MHC-I displayed finely punctate distribution with more concentrated staining at cellular boundaries (Figure 5-9A, panel *i*). Uninfected cells subjected to acid treatment lacked a similar pattern of surface staining and had a characteristic peri-nuclear distribution of MHC-I that was proximal to, but did not completely overlap, mann II staining. There were also obvious peripheral vesicular cytoplasmic foci, which may represent MHC-I *en route* to or recycling from the cell surface (Figure 5-9A, panels *ii*-*iv*).

For comparison of MHC-I localization in VZV.GFP-66 and VZV.GFP-66s infections, we assessed late-stage multi-nucleate syncytia, which expressed abundant levels of GFP-66 or GFP-66s and retained clear cellular morphology. Syncytia were randomly selected and mann II and MHC-I staining patterns were documented. Representative VZV.GFP-66 and VZV.GFP-66s syncytia are shown in Figure 5-9B, with high-level GFP fluorescence indicating similar late infection stages (panels *i* and *v*). Surface MHC-I in VZV.GFP-66 and VZV.GFP-66s infections were distributed similar to uninfected cells, although the signal was clearly consistently reduced (data not shown). In the VZV.GFP-66 syncytium, nuclei were arranged in central clusters and the Golgi apparatus was significantly rearranged, consistent with previous observations (79, 89, 172). Two populations of mann II became disjointed: some localized to foci closely apposed to the nucleus, while the remainder was distributed in a ringed structure in the center of the syncytia

(Figure 5-9B, panel *ii*). Golgi rearrangement resulted in a central pool of intracellular MHC-I, which partially overlapped the mann II staining, but also showed independent accumulation at the center of the mann II ring (Figure 5-9B, panels *iii*-*iv*). Little or no MHC-I was observed outside of the mann II staining region, in contrast to the abundance of punctate foci observed throughout the periphery of uninfected cell cytoplasm. In VZV.GFP-66s syncytia, a similar central mann II ring formed (Figure 5-9B, panel *vi*). MHC-I showed accumulation in this region, but was disorganized and exhibited a remarkable lack of overlap with mann II staining (Figure 5-9B, panels *vi*-*viii*). Additional undefined populations of MHC-I were consistently observed throughout the VZV.GFP-66s cytoplasm (Figure 5-9B, panel *vii*). These did not co-localize with mann II or other cytoplasmic organelle markers for *cis*-Golgi (GM130), *trans*-Golgi network (p230), ER (Erp29), early endosomes (EEA-1), or lysosomes (Lamp-1) (data not shown). The localization and organization of MHC-I in infected cells supports a role for ORF66 in MHC-I retention in the *cis/medial*-Golgi, and indicate that other factors may influence the distribution of intracellular MHC-I during VZV infection.

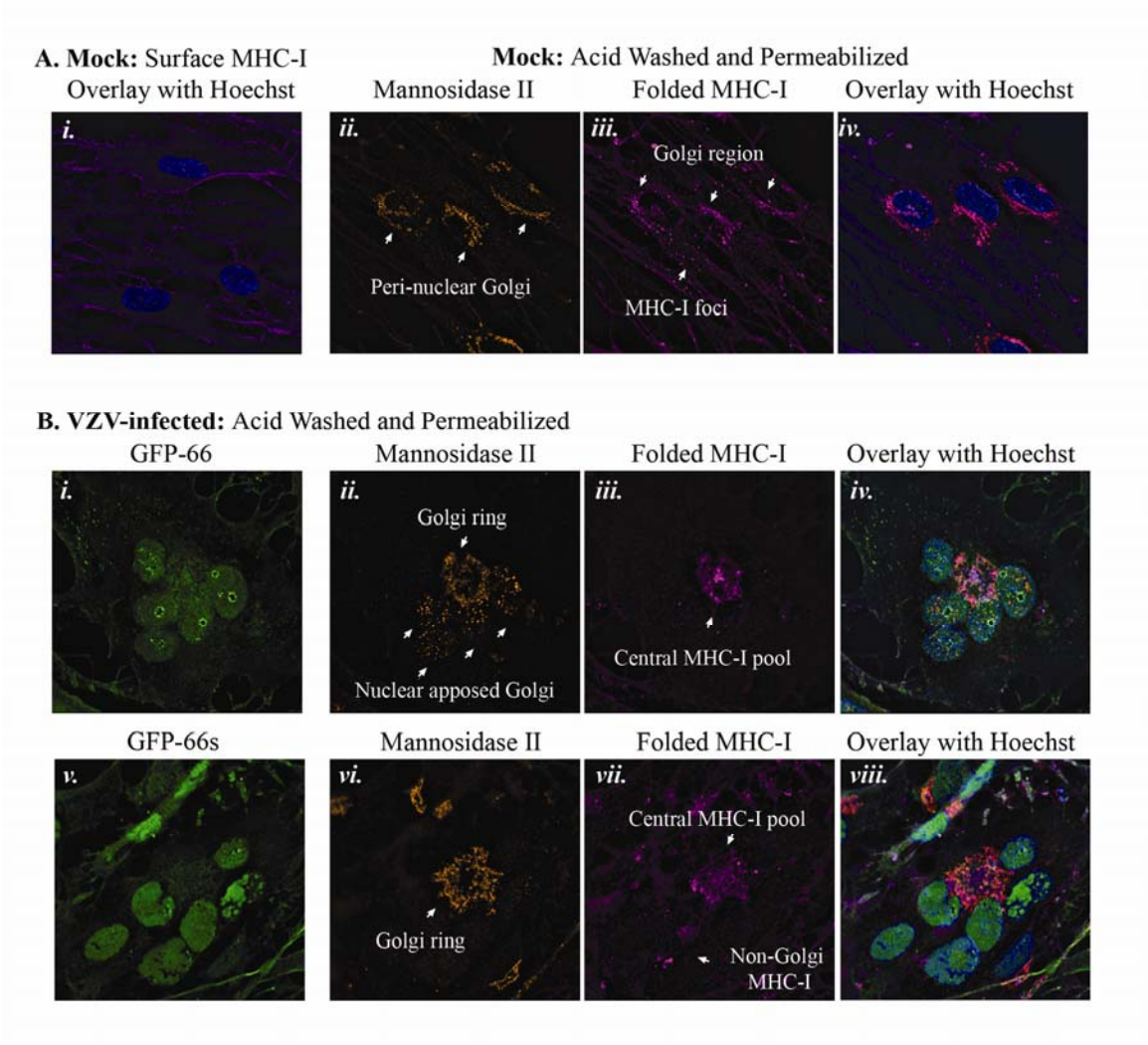

Figure 5-9 MHC-I localization in VZV infection with and without ORF66 expression

Cells on cover-slips were either surface stained for MHC-I or stripped of surface β2M, permeabilized and stained for intracellular folded MHC-I (W6/32) and rabbit anti-mann II combined with anti-mouse Alexa-Fluor 647 and anti-rabbit Alexa-Fluor 546, respectively. All cells were stained with Hoechst 33258 to identify nuclei. Z-stacks were acquired and deconvolved for each fluorescent channel. MHC-I, mann II and Hoechst stains were pseudo-colored to promote simultaneous observance of each channel in the merged images. (A) MHC-I expression profile in uninfected MRC-5 fibroblasts. MHC-I surface fluorescence is shown as an image merged with Hoechst (*i*). A similar staining pattern was not observed in β2M-stripped cells, which exhibited low levels of peri-nuclear MHC-I that partially overlapped with mannosidase II staining (*ii-iv*). Individual stains are indicated above each micrograph panel. (B) Comparison of intracellular MHC-I distribution in late-stage VZV.GFP-66 (*i-iv*) and VZV.GFP-66s (*v-viii*) infected syncytia. Each set of panels shows a representative syncytium. Stains are indicated above each micrograph. In both (A) and (B), arrows highlight specific features that are discussed in the text.

5.4.8 Assessment of expression of additional VZV ORFs on MHC-I surface expression

As our data clearly indicate that ORF66-independent mechanisms regulate MHC-I surface levels, we evaluated select VZV genes for abilities to affect MHC-I. A panel of plasmids expressing VZV ORFs 0, 1, 2, 7, 9, 11, 17, 21, 23, 32, 40, 44, 46, 58, 64 and 65 revealed no ability for any gene to downregulate MHC-I (data not shown). VZV encodes an ortholog to the BHV-1 U_L49.5 TAP inhibitor (VZV ORF9a) (134), and we also addressed the ability of ORF9a protein to downregulate MHC-I in VZV-permissive cells (Figure 5-10). For this study, test plasmids were co-transfected in 293T cells with an equal amount of a plasmid expressing low levels of EGFP under the control of the weakly constitutive HSV-1 thymidine kinase promoter (pTK-EGFP), and MHC-I surface expression was analyzed in EGFP-positive cells by flow cytometry. Cells transfected with plasmid vector lacking any viral ORF were considered the negative control, and we utilized plasmids expressing either ORF66 or the KSHV K3 protein as independent positive controls. EGFP-positive cells from both ORF66 and K3 transfections yielded significantly reduced MHC-I surface levels ($p<0.05$) relative to vector control transfections, indicating that the pTK-EGFP co-transfection successfully reported test plasmid uptake. No significant MHC-I downregulation was observed in ORF9a transfections, supporting data from a previous study in which ORF9a failed to mediate MHC-I downregulation in human melanoma (Mel JuSo) cells (134). This indicates that the ability of ORF9a to inhibit TAP either may not be conserved or may require the expression of additional VZV genes. Little is known of the functions of VZV ORF9a during infection, but the pseudorabies virus (PrV) ORF9a ortholog (gN) is disulfide-linked to PrV gM (VZV ortholog: ORF50) in infected cells (113). We considered the potential ORF9a:ORF50 interaction as the most likely to affect ORF9a's functions, and we thus assessed the effect of combined ORF9a and ORF50 expression on MHC-I surface expression. Neither

ORF50 alone nor ORF9a and ORF50 in combination resulted in significant MHC-I downregulation, either. While we could not confirm the expression of ORF9a due to lack of an ORF9a antibody, similar negative results were observed in cells transfected with an EGFP-tagged version of ORF9a (data not shown). Therefore, VZV genes other than the ORF66 kinase and ORF9a are likely involved in the regulation of MHC-I surface expression.

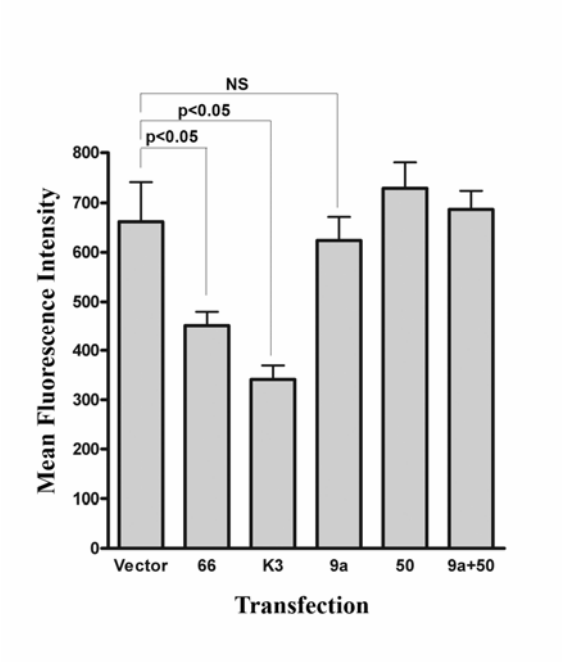

Figure 5-10 The VZV ortholog to BHV-1 UL49.5, ORF9a, does not mediate downregulation of MHC-I surface expression

HEK-293T cells were co-transfected with an EGFP-expressing marker plasmid (pTK-EGFP) and plasmids expressing untagged versions of ORF9a, ORF50 or ORF9a and ORF50 in combination. Empty vector co-transfection was used as a negative control, and co-transfections with plasmids encoding the KSHV K3 MHC-I downregulator or VZV ORF66 served as the positive controls. At 48 h post-transfection, cells were stained for MHC-I and analyzed by flow cytometry. The average MFIs (+/- SEM) of GFP-positive cells from four independent experiments are shown. MFI data from each test transfection condition was compared against that of the negative control using the paired Student's *t*-test, and the results are indicated above corresponding bars. An equal level of pTK-EGFP was maintained in all transfection conditions. *NS*=not significant.

5.5 DISCUSSION

The data presented here indicate a new role for the VZV ORF66 protein kinase in inhibition of MHC-I surface presentation, and also strongly suggest that VZV possesses additional ORF66-independent mechanisms to modulate surface MHC-I in VZV-infected cells. Novel recombinant VZV expressing GFP-66 proteins allowed highly accurate measurement of VZV infection and clearly demonstrated that the most efficient MHC-I downregulation was concurrent with extensive ORF66 expression at later stages of VZV infection. VZV reduced the rate of MHC-I transport from the ER to the *cis/medial*-Golgi, induced a reduction in MHC-I heavy chain synthesis, and caused a moderate but consistent decrease in levels of folded hetero-dimerized class I heavy chains. ORF66 appeared to act predominantly by inducing a delay in MHC-I transport from the ER to the *cis/medial*-Golgi. While two previous studies have reported that VZV inhibits MHC-I surface expression, our study provides a more coherent portrait of MHC-I regulation during VZV infection and begins to clarify the VZV genes that are involved.

Abendroth, et. al. (2) reported no decrease in MHC-I synthesis or transport through the *cis/medial*-Golgi at 24 hpi, but indicated that the major bulk of intracellular MHC-I was retained in the more peripheral stacks of the Golgi complex. It is clear from studies presented here that VZV infection does not immediately induce a surface downregulation of MHC-I, as is seen with ICP47 expression during the immediate early stage of HSV infection. Rather the modulation of MHC-I surface expression correlates more closely with later stages of infection and high levels of ORF66 expression. While we did observe intracellular accumulation of MHC-I in the Golgi region, we also detected an ORF66-dependent retention preceding the *cis/medial*-Golgi complex, which was concomitant with the lowest levels of MHC-I surface expression in VZV-infected

cells. Since the former study was performed at 24 hpi, ORF66 expression most likely did not reach significant enough levels to affect MHC-I processing. The data from a second study suggested that MHC-I heavy chain and β2M synthesis were lower at 48 hpi (38), and our data are in agreement with this, since we observed an ORF66-independent reduction in MHC-I synthesis in cells expressing high levels of GFP. While a non-specific mechanism of global protein synthesis reduction is almost certainly involved, our data also suggest that VZV may impair MHC-I heavy chain and β2M association, since levels of folded hetero-dimerized heavy chains were consistently lower than total class I heavy chains. The consistent upregulation of TfR1 surface expression in VZV-infected cells was unexpected, and contrasts with data from the two previous studies (2, 38). We suspect that differences in the experimental approaches used may account for this. For example, Abendroth, et. al. (2) reported no effects on TfR1 surface expression in VZV-infected fibroblasts analyzed at 24 hpi. While we observed some effect on TfR1 at 24 hpi, the greatest upregulation was observed at 48 and 72 hpi, indicating that this is predominantly a late-stage infection phenomenon. This adds to the complexity of the VZV program for controlling surface protein expression in infected cells.

The specific mechanism by which ORF66 affects MHC-I surface levels remains unclear at this time. Expression of functional ORF66 kinase resulted in impaired MHC-I maturation, but did not affect MHC-I synthesis, degradation or association with β2M. The successful association of class I heavy chains with β2M suggests that ER-resident chaperone machinery (including calnexin, calreticulin and Erp57) may function normally in the presence of ORF66 expression. Our evidence do not suggest a close association of ORF66 with either folded MHC-I or total class I heavy chains, as ORF66 did not co-precipitate with MHC-I and did not co-localize with MHC-I in VZV-infected cells. Inactivation of the ORF66 kinase domain abrogated most of its

ability to mediate MHC-I downregulation, suggesting that phosphorylation of a host cell protein is involved. However, the slight reductions in MHC-I maturation and surface expression observed in the presence of the GFP-66kd protein do imply a possible dominant-negative interaction with a cellular protein involved in MHC-I biosynthesis. Two commonly used viral mechanisms that inhibit MHC-I maturation in the early secretory compartment are inhibition of the TAP complex (68, 93, 96, 134, 148), which transports proteasomally-derived peptides into the ER; and inhibition of tapasin (20, 191), which bridges TAP to MHC-I and mediates the transfer of peptides from TAP to the MHC-I binding groove. While neither TAP nor tapasin exhibits motifs similar to those phosphorylated by the ORF66 kinase (58), we hypothesize that ORF66 may activate host kinase cascades with downstream effects that dysregulate TAP or tapasin function. Interestingly, it has been reported that phosphorylated TAP complexes bind peptides and ATP but cannot transport peptides without being dephosphorylated (152). We speculate that ORF66 induces a hyper-phosphorylated state of the TAP that may lock the complex in a peptide-bound state. An alternative scenario is that ORF66 causes aberrant phosphorylation of MHC-I cytoplasmic tails or the cellular machinery involved in vesicular transport between the ER and the *cis/medial*-Golgi. This is prompted by the observations that cellular protein kinase A (PKA) is known to phosphorylate MHC-I tails (85, 200), and the U_S3 kinase of HSV-1 (orthologous to ORF66) has been shown to induce phosphorylation of some cellular PKA targets (19). Known ORF66 targets are highly similar to the optimized target motif of HSV-1 U_S3 kinase (145), suggesting that some PKA targets could also be targets of ORF66. MHC-I cytoplasmic tail phosphorylation normally occurs at the cell surface or in late or recycling endosomes (30, 57, 115, 154). Thus, aberrant phosphorylation of pre-Golgi MHC-I could result in deviations from normal trafficking early in its secretory transport. Studies to

address ORF66-mediated effects on the peptide loading complex and ORF66-directed phosphorylation of MHC-I are in progress.

The ORF66 kinase modulates several aspects of the cellular environment to facilitate VZV infection, but cellular proteins that are targeted for direct phosphorylation by ORF66 remain unknown. In VZV-infected T lymphocytes, ORF66 inhibits activation of caspase 3 and interferon γ (IFNγ)-mediated Stat1 phosphorylation (220). One consequence of IFNγ signaling is the upregulation of MHC-I surface expression, through increased transcription from the human leukocyte antigen (HLA) locus (160). Here, we demonstrate that ORF66 modulates MHC-I surface expression independently of IFNγ signaling. However, it will be interesting to address the effects of ORF66 on both induced MHC-I transcription and post-translational membrane trafficking in response to both type I and type II IFN treatment. The identification of host cell proteins phosphorylated in the presence of the ORF66 kinase and the effects of ORF66 expression on the cellular transcriptome are currently under investigation.

VZV lacking ORF66 expression maintains the ability to induce MHC-I downregulation, and therefore VZV must encode one or more additional genes that affect MHC-I surface expression. Several alphaherpesviruses, including HSV-1, negatively regulate MHC-I through the virion host shutoff (vhs) gene, which mediates a global reduction of cellular protein expression (82, 97, 135, 231). VZV also causes a reduction in cellular protein synthesis that may contribute to the reduction in MHC-I surface levels in infected cells. The VZV vhs ortholog (ORF17) is known to induce mRNA degradation, albeit to a lesser extent compared to its HSV-1 counterpart, but its role in silencing cellular protein expression during VZV infection remains unclear (217). VZV ORF9a, the ortholog of the BHV-1 UL49.5 TAP inhibitor, was previously assessed for effects on MHC-I surface expression in a human melanoma cell line (Mel JuSo) and

was found to have no effect (134). Our analyses also indicated no ability to induce MHC-I surface downregulation, even when ORF9a was expressed with its possible chaperone ORF50. However, we note that the HCMV U_S10 protein is able to bind MHC-I and impede its maturation through the Golgi, but does not affect the surface expression of MHC-I detected by pan-specific HLA antibodies (69). The identities of additional VZV genes involved in MHC-I downregulation remain to be elucidated.

We conjecture that ORF66-induced MHC-I downregulation could be important at multiple stages of VZV pathogenesis. Viruses lacking ORF66 expression show only minor reductions in growth in several VZV-permissive cell types in culture, but are growth-restricted in T-lymphocytes in the SCID-hu model of VZV infection (174, 220, 224). This restriction has been attributed to, at least in part, ORF66-mediated inhibition of apoptosis, as a greater percentage of cells showed increased caspase 3 activation when ORF66 expression was lacking (220). Thus, one role for the ORF66 kinase is to promote T-lymphocyte survival and the subsequent transfer of infectious virus to skin cells during the viremic stage of VZV infection. While we do not know whether ORF66 induces MHC-I downregulation in T cells, we suggest that this ORF66 function could serve to further enhance T cell survival by allowing avoidance of immune surveillance. The ORF66 induced downregulation of MHC-I surface expression may also be critical during VZV growth in skin cell layers. ORF66 is not required for pathogenesis in human skin implants in the SCID-hu mouse (174, 220), but this model lacks a fully competent immune system. Recent evidence suggests that epidermal cells are infected shortly after inoculation and undergo a prolonged infection period before producing infectious lesions at the skin surface (139). Since VZV-specific-immunity may become well developed during later parts of the skin infection phase, evasion of adaptive immunity could be important for survival of

infected skin cells. Finally, ORF66 may affect MHC-I presentation in VZV-infected sensory neurons during latency. Several VZV lytic antigens, in addition to ORF66, are transcribed and may be expressed during latent infection, and these include ORFs 4, 21, 29, 62, and 63 (45, 170). Memory CTL that recognize ORFs 4, 10, 29, and 62 can be detected in VZV immune subjects (12), but human ganglia have been found to lack VZV specific CTL infiltration (106, 240). The latter study also shows that human ganglia harboring latent HSV-1 contain HSV-1 specific CTL, clearly implying that antigens can be properly presented in neurons. Hence, the expression of ORF66 may be required for two roles during VZV latency: one may be to suppress the nuclear localization and nuclear functions of the major VZV transcriptional transactivator by promoting cytoplasmic location (58), and the other may be to prevent antigen presentation of latency associated VZV antigens.

In summary, VZV appears to attack MHC-I using a multi-faceted approach that includes the ORF66 kinase. Similar functions have not been described for orthologous U_S3 kinase family proteins, and as no other viral kinase has been shown to impair MHC-I transport through the Golgi complex, this represents a novel role for kinases in viral immune evasion. ORF66's ability to delay MHC-I maturation in VZV-infected cells may contribute to VZV pathogenesis by promoting efficient dissemination, survival during the extended incubation period and persistence in latently infected ganglia.

6.0 THE VARICELLA-ZOSTER VIRUS (VZV) ORF66 PROTEIN KINASE EXHIBITS DYNAMIC INTRANUCLEAR TRAFFICKING AND NOVEL ASSOCIATIONS WITH ND10 DOMAINS, THE NUCLEOLUS AND THE VZV MAJOR CAPSID PROTEIN

Amie J. Eisfeld[1,2], Kira Lathrop[2], and Paul R. Kinchington[2,3]

Graduate Program in Molecular Virology and Microbiology[1] and Departments of Ophthalmology[2] and Molecular Genetics and Biochemistry[3], School of Medicine, University of Pittsburgh, PA, 15213.

6.1 ABSTRACT

In this study, we utilized recombinant varicella-zoster virus (VZV) expressing enhanced green fluorescent protein (EGFP)-tagged ORF66 kinase proteins to investigate novel ORF66 trafficking behavior in relation to catalytic activity and time. EGFP-66 localized to bright foci (i.e. "speckles") at the periphery of the nucleolus and throughout the nucleoplasm in early and late stages of infection. Using live-cell time lapse imaging, we showed that the nucleolar speckles remained mostly immobile, while nucleoplasmic speckles exhibited high-velocity trajectories that moved throughout nucleoplasm in a directed manner. Nucleoplasmic speckles exhibited fusion and the ability to traffic to the nucleolus. Cytoplasmic speckles were also observed in some cells expressing high levels of ORF66, but these moved more slowly and less erratically. A sub-population of ORF66 speckles associated with ND10 domains during very early infection, but most were associated with the surfaces of VZV replication or capsid assembly compartments. In contrast, VZV expressing a kinase inactivated version of ORF66 (EGFP-66kd) failed to form nucleoplasmic speckles and exhibited abnormal accumulation in both RC and nuclear regions containing mislocalized major capsid protein (MCP). Furthermore, EGFP-66kd was recruited from RC at very late times post-infection and accrued with the MCP at the periphery of the nucleus, suggesting a high-affinity association with a capsid component. EGFP-66 nuclear speckles were efficiently formed in the absence of additional VZV protein expression, and these were also juxtaposed to ND10 domains, indicating that speckle formation and ND10 association are intrinsic properties of ORF66. Together, these results demonstrate highly novel nuclear interactions for the VZV ORF66 protein kinase, and suggest that ORF66 may use nucleoplasmic trafficking and sequential localization to mediate multiple functions in VZV-infected nuclei, including a potential role in capsid morphogenesis.

6.2 INTRODUCTION

The human herpesvirus, varicella-zoster virus (VZV), causes chickenpox in naïve individuals, establishes latency in sensory neurons, and can reactivate in response to immunosuppressive stimuli to induce herpes zoster (shingles). VZV is classified among the herpesvirus subfamily *Alphaherpesvirinae*, which includes two additional human pathogens, herpes simplex virus type 1 and 2 (HSV-1 and HSV-2). Alphaherpesviruses uniquely encode a serine/threonine (Ser/Thr) protein kinase gene within the unique short (U_S) region of the genome and collectively, these are referred to as the U_S3 kinase family. The VZV U_S3 ortholog is the ORF66 protein kinase. U_S3 kinases are multi-functional and are known to phosphorylate cellular factors to prevent apoptosis (53, 71, 74, 112, 149, 188); alter the actin cytoskeleton to promote cell-to-cell spread (63, 221, 237); modify the cellular histone deacetylase (HDAC) machinery, possibly to promote viral gene expression (84, 201); modulate interferon signaling (198); and facilitate capsid egress through the nuclear lamina by phosphorylation of multiple laminar proteins (131, 144, 178, 181, 212, 215, 221, 241). In VZV-infected cells, ORF66 has been shown to prevent activation of caspases and phosphorylation of Stat1 in response to γ-interferon, implying that ORF66 may prevent apoptosis and immune-mediated cellular signaling (219, 220). However, the effects of ORF66 on other U_S3 kinase targets have not been reported.

VZV lacking ORF66 expression replicate in many cell types in culture, but are attenutated in T lymphocytes both in culture and in thy-liv implants from the severe combined immunodeficient (SCID)-hu model of *in vivo* VZV infection (174, 220, 224). VZV expressing point-inactivated versions of ORF66 do not compensate replication in T cells, and this suggests that phosphorylation of either a viral or host cell target is critical (219). Two unique functions have been described for the ORF66 kinase in VZV infected cells: phosphorylation and nuclear

exclusion of the VZV major transcriptional regulator, IE62, in late-stage infection (58, 124); and downregulation of class I major histocompatibility complex surface expression (59). IE62 is an essential viral transactivator, which uniquely exhibits abundant association with the viral tegument (125). To facilitate IE62 tegument incorporation, ORF66 directly phosphorylates IE62 immediately adjacent to its nuclear localization signal, resulting in IE62 nuclear exclusion and accumulation in the *trans*-Golgi network (TGN) (58, 127) (see also Chapter 4). Regarding MHC-I, ORF66 modulates the host cell environment in a kinase activity-dependent manner, such that MHC-I trafficking through the Golgi complex is impaired, resulting in a reduction in the total MHC-I surface levels (59). Since MHC-I is crucial for the activation of $CD8^+$ T cells (CTL) and subsequent elimination of infected cells, this may represent a highly novel means of evasion of adaptive immunity. The cellular targets involved in MHC-I downregulation have not been determined.

We have recently reported the derivation of recombinant VZV expressing functional or catalytically inactive EGFP-tagged ORF66 kinase proteins (VZV.GFP-66 and VZV.GFP-66kd, respectively), which are regulated by the native ORF66 promoter (59, 61). Using these, we have demonstrated for the first time that ORF66 is expressed with typical U_S3 kinetics, beginning at 4-8 h post-infection, and exhibits diffuse nuclear and cytoplasmic localization (Chapter 4). In addition, highly unique nuclear distributions were observed at later times, including accumulation in bright foci (i.e., "speckles") throughout the nucleoplasm and formation of ringed structures that surrounded the putative nucleolus ((59) and Chapter 4). Since ORF66 does not co-localize with IE62 in nuclear speckles (Chapter 4), this suggests an alternate nuclear function for ORF66 during late-stage VZV infection. Similar distributions have not been reported for any other U_S3 kinase.

In this study, we utilized the EGFP-66 viruses in fixed and live cell microscopy assays to investigate ORF66 speckle trafficking as a function of kinase activity and time during VZV infection. We reveal novel ORF66 associations with cellular and viral nuclear domains, as well as dynamic trafficking throughout the nucleus and to the nucleolus. These results suggest a high level of multi-functionality for ORF66 during VZV infection, and imply that ORF66 may be involved in capsid maturation, similar to other U_S3 kinases.

6.3 MATERIALS AND METHODS

6.3.1 Cells and chemicals

MRC-5 human lung fibroblasts (ATCC, Manassas, VA) and human melanoma cells (kindly provided by C.Grose, University of Iowa, Iowa City, IA) were maintained as previously described (59). To completely repress *trans*-gene expression from replication defective adenovirus vectors, we used doxycycline at a concentration of 0.5 μg/ml**.**

6.3.2 Viruses

Recombinant VZV-pOka and VZV expressing EGFP-tagged ORF66 (VZV.GFP-66) or ORF66kd (VZV.GFP-66kd) have been previously described (59, 61). VZV.GFP-66 and VZV.GFP-66kd were derived from pOka cosmids and express in-frame EGFP-ORF66 or ORF66kd (EGFP-66, EGFP-kd) fusion proteins in place of the wild-type ORF, and under the control of the natural promoter. In VZV.GFP-66kd, the ORF66 gene encodes point mutations at

two critical kinase domain residues (D206E and K208R), which render the kinase inactive (59, 124). VZV expressing kinase active ORF66 with an N-terminal hemagglutinin (HA) epitope tag (YPYDVPDYA) (referred to as VZV.HA-66) was derived in a manner similar to that of VZV.GFP-66 (59). For this, we created a modified pGK2-HA66 plasmid (124), in which the human cytomegalovirus (HCMV) IE promoter was replaced with PCR-amplified native ORF66 promoter, from the Avr II site (nt 112957) through the natural ORF66 ATG, with Hind III and Pst I restriction endonuclease overhangs (p66prom-HA66). The 66prom-HA66 cassette was digested out of this plasmid backbone using unique Avr II and Bam HI restriction sites, and used to replace the corresponding ORF66 fragment in the pUC19-pvSpe23 shuttling vector (59). The entire Avr II-SgrAI fragment from pUC19-pvSpe23, containing HA-66, was cloned into the pvSpe23 cosmid (pvSpe23.HA-66), and isogenic viruses were obtained after co-transfection of pvSpe23.HA-66 with the remaining VZV pOka cosmids (pvFsp73, pvSpe14, and pvPme2) and pCMV62 (expresses the VZV transactivator IE62) in MeWo cells. All VZV infections for live and fixed cell microscopy were initiated with active MRC-5 cultures of cell-associated VZV, at a ratio of one infected cell to 50 uninfected cells, and were incubated for 48 h preceding fixation. A replication defective adenovirus vector expressing EGFP-66 from a tet/DOX-repressible promoter was used to infect MRC-5 cells as previously described (59).

6.3.3 Antibodies, immunofluorescence and microscopy of fixed specimens

Indirect immunofluorescence was performed as previously described (59). A monoclonal mouse antibody to the VZV ORF66 protein was kindly provided by A. Baiker (Ludwig-Maximilians-Universität München, München, Germany). Polyclonal rabbit antiserum to VZV IE62 (1:800) and ORF29 (1:500), and monoclonal mouse anti-HA antibodies (1:400) have been previously

described (58, 124, 126). A mouse monoclonal antibody to the VZV major capsid protein (MCP, ORF40; Virusys Corporation, Sykesville, MD) was used at 1:400. In some studies, we used a mouse monoclonal antibody against VZV IE62 (Advanced Biotechnologies, Inc., Columbia, MD). Antibodies for detection of host cell nuclear antigens were as follows: monoclonal mouse anti-C23-nucleolin (nucleolus; used at 1:1000), rabbit anti-coilin (Cajal bodies; used at 1:200), and mouse anti-PML (ND10 domains; used at 1:500) (Santa Cruz Biotechnology, Inc., Santa Cruz, CA). For secondary detection of cellular and VZV antigens, Alexa Fluor (AF) conjugated goat anti-mouse or goat anti-rabbit Fab fragments (Invitrogen Corporation, Carlsbad, CA) were used at 1:400. Excitation (ex) spectra are indicated in the Figure Legends. Nuclei were stained using Hoechst 33258 (Sigma-Aldrich). Epifluorescent microscopy was performed as previously described (59).

6.3.4 Live-cell time-lapse microscopy and object tracking analysis

MRC-5 cells were seeded to confluency on glass-bottomed culture plates (Bioptechs, Butler, PA) and allowed to equilibrate for 24-48 h, at which time they were infected with cell-associated VZV.GFP-66 or VZV.GFP-66kd. For time-lapse imaging of live infected cells, dishes were placed on a Delta T Stage open heating system (Bioptechs), which was mounted on a Nikon TE2000 epifluorescent microscope. This heating system was modified by the manufacturer to be semi-closed by the addition of a water-tight gasket in the system lid. Cells were maintained at 37ºC with continuous medium recycling and an atmosphere of 5% humidified CO_2. Metamorph 7.2 software was used to control time-lapse imaging, and micrographs of equal exposure were acquired every 5 minutes using a 20X air objective with a correction collar, and image stacks were converted into AVI files for visualization.

For object tracking analysis, time-lapse stacks were manually aligned in Metamorph using the nucleolus as a reference point. Fluorescence images were inverted, corrected for shading, and the background flattened to facilitate observance of individual EGFP-66 foci (speckles). The trajectories and velocities of 12 independent nuclear speckles and 17 independent cytoplasmic speckles were quantified using the Track Objects algorithm and analyzed using GraphPad Prism 4 software.

6.4 RESULTS

6.4.1 VZV ORF66 localizes to the nucleolar periphery

In VZV.GFP-66-infected cells, we have reported a high proportion of EGFP-66 in the nucleus, as well as novel speckles in the nucleoplasm and in ring-shaped structures that surround the putative nucleolus (59) (see also Chapter 4). A similar distribution has not been reported for any other U_S3 kinase. To ensure that this EGFP-66 distribution resulted from specific ORF66 activities and to assess any relationship with the nucleolus, we performed indirect immunofluorescence analyses in cells infected with VZV.GFP-66, VZV expressing an HA-tagged version of ORF66 (VZV.HA-66) and VZV pOka. Infected MRC-5 cells were left unstained or stained with an antibodies to C23-nucleolin (VZV.GFP-66), the HA epitope tag (VZV.GFP-HA), or a monoclonal antibody recognizing the wild-type untagged ORF66 protein (VZV pOka). All cells were stained with Hoechst to identify nuclei. Protein localizations were determined by epifluorescent microscopy.

As expected, EGFP-66 was highly nuclear in most cells and often exhibited both nucleoplasmic speckles and speckles that associated in a ring at the periphery of the nucleolus (Figure 6-1A and B). Nucleolar speckles did not localize within the nucleolus, as determined by Z-section analysis (Figure 6-1B). Nucleoplasmic speckles varied in size and number and were often distributed unevenly throughout the nucleus (Figure 6-1A and B). HA-66 detected by indirect immunofluorescence was similarly distributed, with predominant nuclear localization, nucleoplasmic speckles and ORF66 accumulation at the nucleolus (Figure 6-1C). HA-66 nucleolar rings consisted of independent speckles, similar to those observed for EGFP-66. Importantly, wild-type ORF66 detected by a monoclonal antibody was more abundantly localized to the nucleus compared with the cytoplasm, and accumulated preferentially in the nucleolar regions (Figure 6-1D), but high resolution identification of individual speckles was impeded by high background staining. These results indicate that the determinants within the ORF66 kinase protein and not the EGFP epitope tag are responsible for novel ORF66 nuclear distributions in VZV-infected cells.

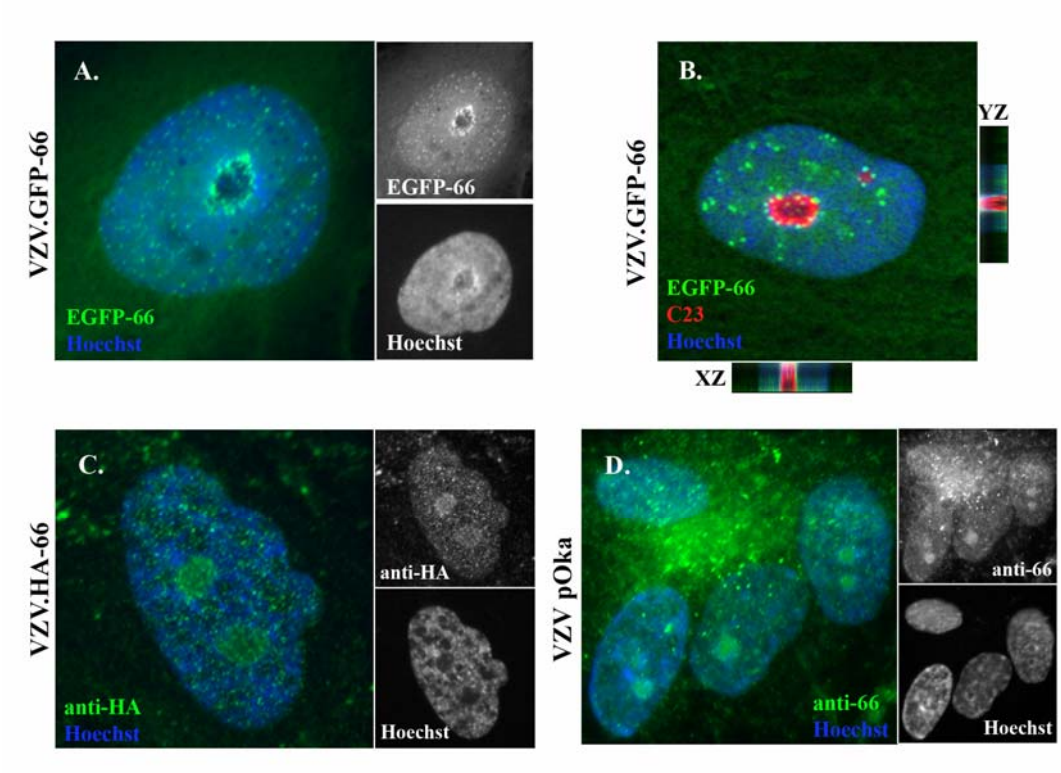

Figure 6-1 Wild-type and epitope-tagged ORF66 localize to the nucleolar periphery in VZV infected cells

MRC-5 cells grown on coverslips were inoculated with VZV.GFP-66 (A and B), VZV.HA-66 (C), or VZV-pOka (D) and fixed at 48 hpi. In (A), no indirect immunofluorescence was performed. In the remaining panels, cells were stained with monoclonal mouse anti-C23 and Alexa-Fluor 647 conjugated secondaries (AF 647) (B); anti-HA and AF 488 (C); or anti-ORF66 and AF 488. In A, C, and D, the enlarged micrograph depicts a color combined image of ORF66 expression in green and Hoechst 33258-stained nuclear chromatin in blue. Smaller black and white panels show individual ORF66 and Hoechst staining patterns. In B, a color combined image of EGFP-66 (green), C23 (red), and Hoechst (blue) fluorescence is depicted, with YZ and XZ orthogonal planes through the nucleolar region of a partial Z-stack of a VZV.GFP-66-infected cell, to the right and at the bottom, respectively.

6.4.2 Intranuclear EGFP-66 speckles exhibit dynamic trafficking including fusion, association with the nucleolus and directed trajectories

The unique nuclear speckles exhibited by ORF66 prompted an investigation of ORF66 trafficking in VZV infection. We reasoned that a better definition of ORF66 activities may provide clues into the nature of ORF66 speckle functions. For this, we exploited the intrinsic

auto-fluorescent property of EGFP-66 and live-cell time-lapse imaging to assess changes in ORF66 distribution over time. The cell-associated nature of VZV does not allow the establishment of high multiplicity synchronous infections. Thus, to facilitate time-dependent visualization of EGFP-66 in infected MRC-5 fibroblasts, autofluorescence was captured at the edges of established VZV.GFP-66 plaques for an extended time-course of >24 hours. Similar studies were performed with VZV.EGFP-66kd to determine any role in ORF66 trafficking that could be attributed to kinase activity. Movies of EGFP fluorescence in representative cells infected with VZV.GFP-66 or VZV.GFP-66kd are shown in Supplemental Figs. 1 and 2, respectively: VZV-GFP66.AVI and VZV-GFP66kd.AVI. An overview of the EGFP-66 and EGFP-66kd localization patterns is exhibited in Figure 6-2. For clarity, we note that many VZV.GFP-66-infected cells exhibited reduced levels of EGFP-66 fluorescence relative to that shown, although trafficking patterns were similar. We believe these differences are likely due to differences in the relative multiplicity of infection for each cell.

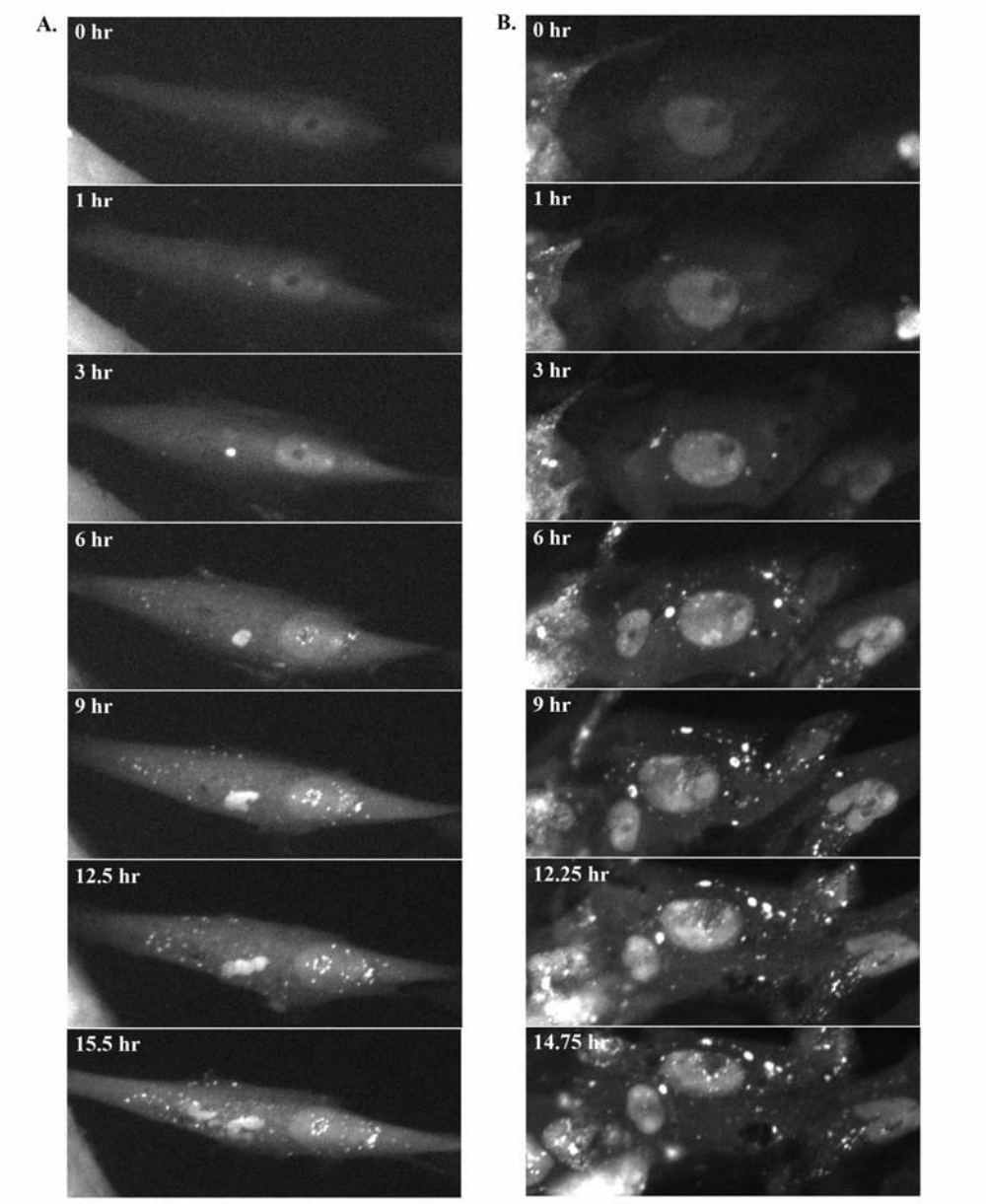

Figure 6-2 Overview of EGFP-66 and EGFP-66kd localizations in VZV-infected cells imaged by live-cell time-lapse microscopy

MRC-5 fibroblasts were plated on Bioptechs glass-bottomed dishes and infected with cell-associated VZV.GFP-66 (A-C) or VZV.GFP-66kd (D) at a ratio of 1 infected cell to 50 uninfected cells. At 24 hpi, a dish was placed on heated stage system, and medium was maintained at 37ºC with a continuous 5% humidified CO_2 perfusion. Micrographs of equal exposure were captured at the edge of a developing plaque every 5 minutes for 26-27 h. EGFP-66 and EGFP-66kd localizations are shown for single cells that began to exhibit nuclear and cytoplasmic fluorescence at approximately the same time after initiation of time-lapse capture. The time elapsed is indicated in the upper left of each panel.

In VZV.GFP-66 infections, EGFP-66 initially exhibited diffuse nuclear and cytoplasmic fluorescence, although nuclear fluorescence was more prominent (Figure 6-2A). This is consistent with the EGFP-66 fluorescence pattern exhibited in fixed cells at the edges of VZV-infected plaques (i.e., early stage infection), as well as the EGFP-66 distribution pattern observed from 4-8 hpi in low multiplicity "cell-free" VZV infections (Chapter 4). The next significant feature we observed was a peri-nuclear cytoplasmic dot, which exhibited higher fluorescence compared to the surrounding cytoplasm and the nucleus. Again, this was consistent with peri-nuclear dots observed in cell-free infections, which co-localized with the VZV IE62 protein (Chapter 4). EGFP-66 then accumulated in several areas in the nucleoplasm, and this was followed by the appearance of nucleolar speckles. Nucleoplasmic speckles were apparent thereafter, and many exhibited rapid and erratic trafficking patterns with trajectories that covered large areas of the nucleus. Concurrent with the appearance of motile nucleoplasmic speckles, EGFP-66 was also observed in speckles in the distal areas of the cytoplasm; in the previously described cytoplasmic dot, which was significantly larger and more amorphous; and in a juxtanuclear region on the opposite side of the nucleus. The latter distribution patterns are consistent with a late infection stage, as cell-free infections exhibited this phenotype at only >12 hpi. Notably, EGFP-66 nucleolar speckles appeared to remain relatively stationary throughout the time course. Time-lapse analysis of EGFP-66kd in infected cells established that the absence of functional kinase activity resulted in a lack of motile nucleoplasmic speckles and faulty accumulation in expanding nuclear compartments (Figure 6-2). Similar results were observed in independent cells at other stage positions in the same experiment and in replicate experiments.

To emphasize specific features of ORF66 nucleoplasmic trafficking, we have shown enlarged sequential frames of the VZV.GFP-66 infected nucleus over a 55 minute period beginning ~14 h after the initiation of the time-lapse capture (Figure 6-3A). Two speckles that began on opposite sides of the nucleolus exhibited high motility (Figure 6-3A, frames 0, 5, 10, and 15; white and black arrows) and fused near the nuclear boundary at the top of the nucleus (Figure 6-3A, frame 20, white arrow with black border). Fusion was confirmed by the increased size and brighter fluorescence of the remaining speckle. Within 10 minutes, the fused speckle trafficked into the periphery of the nucleolus, remained stationary for an additional 10 minutes, and subsequently began a slow ascent away from the nucleolus and into the nucleoplasm (Figure 6-3A frame 30, 35, 40, 45, 50 and 55). Fusion among cytoplasmic speckles was less obvious, and some of these may have been derived from the amorphous ORF66 cytoplasmic structure (Figure 6-3B).

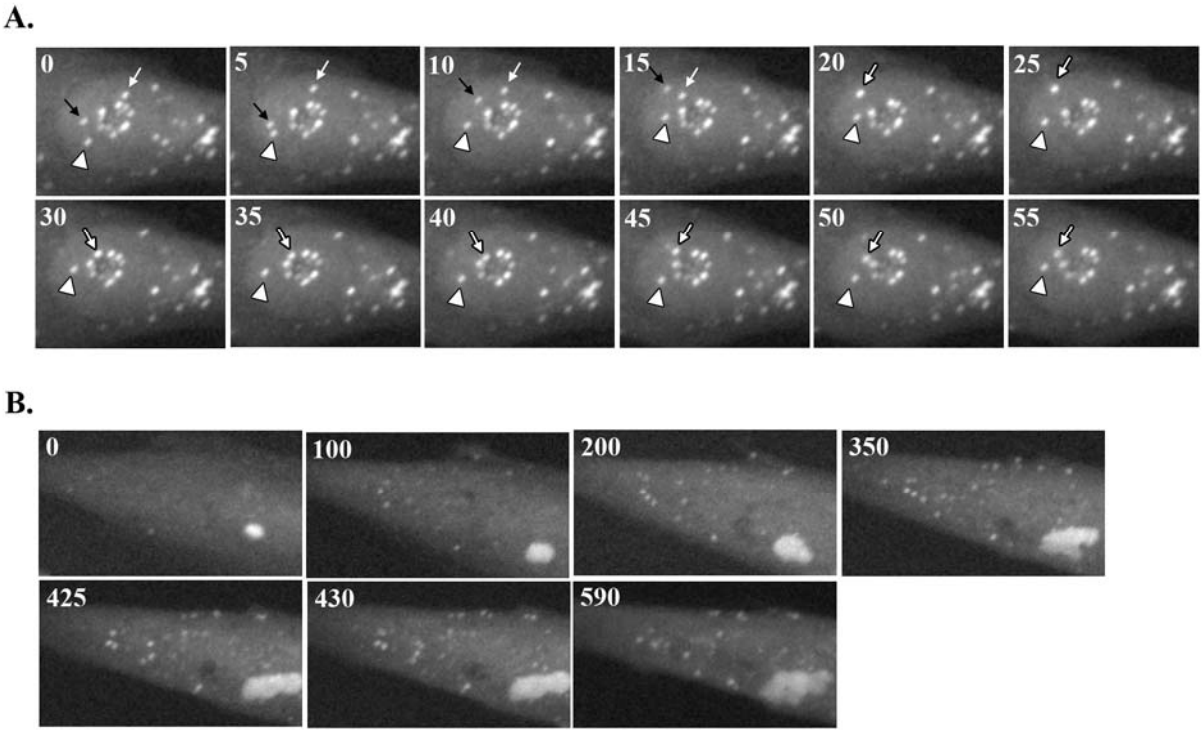

Figure 6-3 EGFP-66 speckles are highly dynamic

(A) Trafficking of specific EGFP-66 nucleoplasmic speckles over a 1 h time-frame. The first frame (0) is an enlarged image of the nucleus shown in Figure 6-2A, and each subsequent frame shows the same nucleus 5 minutes later. The total number of elapsed minutes is shown in the upper left corner. White and black arrows point to individual motile EGFP-66 speckles in each frame. These two speckles fused after 20 minutes, and were subsequently demarcated by a white arrow with a black border. Arrowheads point to a relatively stationary speckle. (B) EGFP-66 cytoplasmic speckles. The first frame (0) is an enlarged image of the left-most cytoplasm shown in Figure 6-2A, and each subsequent frame shows the same region, with the elapsed minutes shown in the upper left corner.

To more quantitatively characterize EGFP-66 nuclear and cytoplasmic trafficking, we tracked the trajectories of 12 independent nuclear speckles representing nucleolar and nucleoplasmic populations, as well as 17 individual cytoplasmic speckles. Speckle trajectories for each are shown in Figure 6-4A and B. Sample trajectories of representative nuclear speckles

and several cytoplasmic speckles were plotted as a function of time (Figure 6-4C and D). Clearly, nucleolar speckles were relatively stationary and did not appreciably move away from their points of origin (Figure 6-4C, green trajectory). In contrast, nucleoplasmic speckles exhibited a variety of motions and some of these appeared to be directed, since bursts of high velocity movement away from the points of origin were readily detected (Figure 6-4C, majenta trajectory). Nucleoplasmic speckles also exhibited some retrograde movements, suggesting they may interact intermittently with nuclear structures that obstruct forward motion. The maximum velocity observed among nucleoplasmic speckles was 0.01454 μm/sec (0.8724 μm/min). EGFP-66kd cytoplasmic speckles collectively moved away from points of origin, and did not generally exhibit trajectories suggestive of directed motion (Figure 6-4B and D). The maximum velocity observed for a cytoplasmic speckle was 0.002127 μm/sec (0.12762 μm/min).

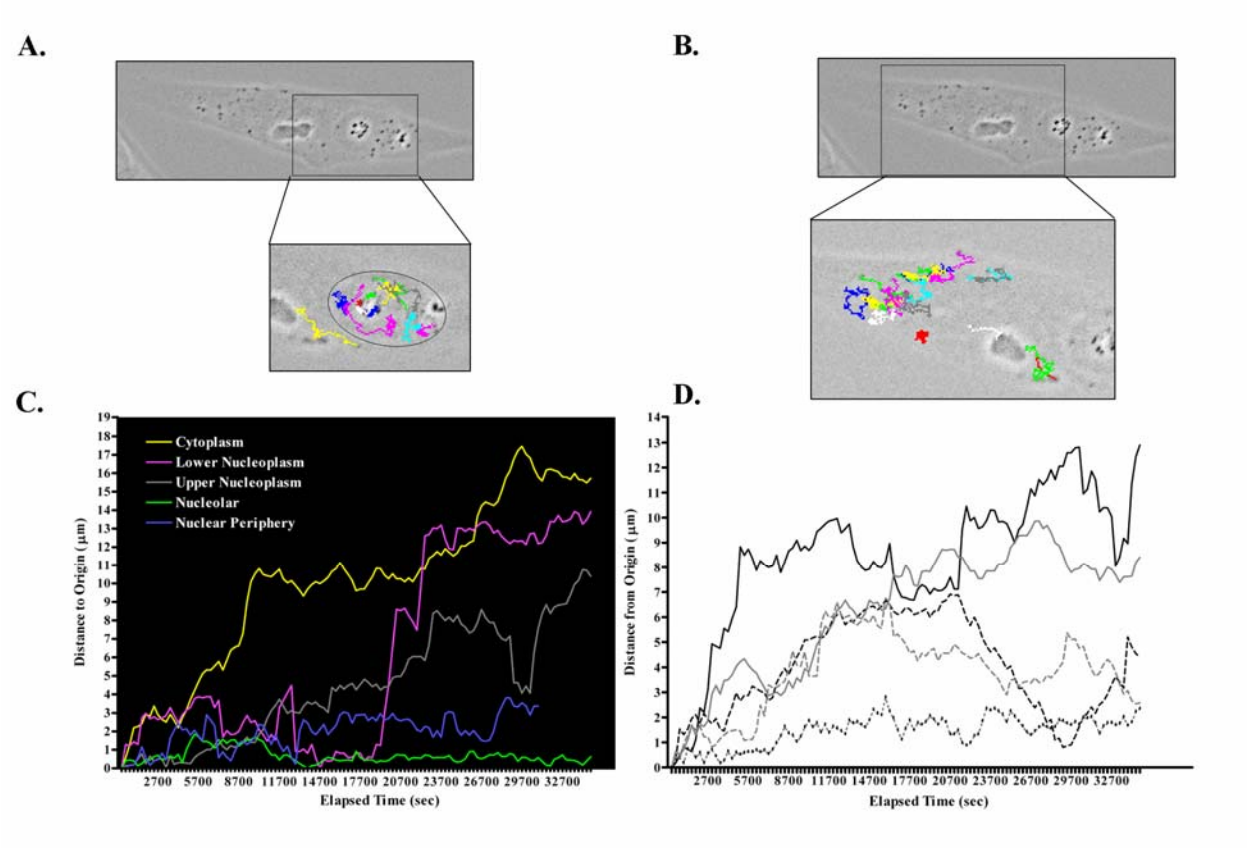

Figure 6-4 Quantitative analysis of ORF66 speckle trafficking

Frames representing the last 117 images (9.75 h or 585 min) from the VZV.GFP-66 time-lapse experiment shown in Figure 6-2 were inverted, corrected for shading, and flattened; and then aligned by hand with Metamorph 7.2 software, using the nucleolus as a reference. Speckle trajectories and velocities were quantified for the nucleus (A) or the cytoplasm (B) using the Metamorph Track Objects function. Enlarged images show individual speckle trajectories in multiple colors, as well as the region of the cell that was mapped. In (A), an outline of the nuclear boundary was artificially added for ease of reference. (C) The displacement of 4 sample nuclear speckles and 1 cytoplasmic speckle with respect to their origins were plotted as a function of time, and are color-coded to match the corresponding speckle trajectories in (A). Nuclear speckles were selected to represent distinct areas of the nucleus, and these are indicated on the legend. In (D), 5 sample cytoplasmic speckles were analyzed as described in (C), except that displacement curves are not color coded.

These data indicate a highly dynamic nature for ORF66 nucleoplasmic speckles, emphasize a high level of ORF66 multi-functionality, and are suggestive of a new role for

ORF66 in regulating aspects of the nuclear environment in VZV-infected cells. In addition, ORF66 kinase activity is clearly critical for its proper localization and trafficking.

6.4.3 A sub-population of ORF66 nuclear speckles associates with ND10 domains, but not Cajal bodies

Cellular Cajal bodies (CB), a nuclear sub-domain implicated in the storage and trafficking of small nuclear ribonucleoproteins (snRNP) and formation of transcriptosomes are known to associate with the nucleolus; have the ability to join to form larger CBs or split into smaller CBs; and exhibit high velocity directed trafficking patterns at a rate of up to 0.9 μm/min (199, 262). Given the similarity with the observed trafficking patterns of EGFP-66, we assessed the possibility that EGFP-66 speckles associated with CB in VZV-infected cells. For this, we infected MRC-5 fibroblasts with cell-associated VZV.GFP-66 and stained fixed cells with antibodies against a major CB component, p80 coilin. The previously established time-dependent localization pattern for EGFP-66 was utilized to identify cells at specific stages of infection in mixed cultures. Uninfected MRC-5 cells exhibited coilin staining in a speckled pattern evenly distributed throughout the nucleus, with some brighter foci apparent in the region around the nucleolus (Figure 6-5A). As expected, there was no specific accumulation in the nucleolar interior. In marked contrast, coilin was drastically redistributed in VZV-infected cells, initially accumulating in the nucleolus (Figure 6-5B), followed by exclusive localization in 5-20 nucleoplasmic speckles (Figure 6-5C). Some nucleoplasmic speckles were observed at the nucleolar periphery, but none of the coilin-positive speckles co-localized with EGFP-66 speckles. Coilin speckles remained in late-stage infections, although their number and size was reduced (Figure 6-5D). Thus, EGFP-66 speckles are not CB. Notably, there was no difference

coilin localization in VZV.GFP-66kd-infected cells, indicating that coilin redistribution was induced by viral factors other than the ORF66 kinase.

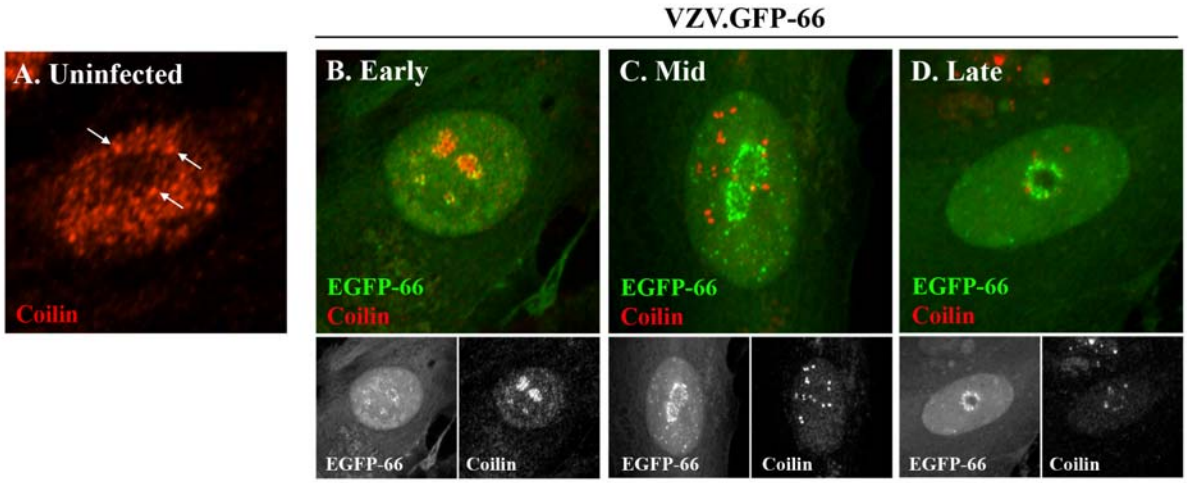

Figure 6-5 ORF66 speckles are not Cajal bodies

MRC-5 fibroblasts were left uninfected or infected with VZV.GFP-66 and fixed as described above, and stained with antibodies against the major CB component, p80 coilin. (A) Mock-infected cells with typical coilin staining pattern. Arrows poin out coilin foci in the region of the nucleolus. (B-D) Coilin localization at different stages of VZV infection. Stages are indicated at the top. Large color-combined panels depict EGFP-66 in green and coilin in red. Smaller black and white images show individual staining patterns, which are indicated for each panel.

We also assessed any possible EGFP-66 co-localization with ND10 domains, as these are known to associate ICP4 foci that eventually expand into replication compartments (RC) (62). For this, we performed similar infections, but stained cells with antibodies against the ND10 constituent, PML, and the VZV IE62 protein, which is the ortholog to HSV-1 ICP4. Abundant PML-reactive nuclear domains similar to those in mock-infected cells were observed at early times post-infection, when ORF66 was expressed at low levels and was predominantly nucleoplasmic. In these cells, minute EGFP-66 speckles were observed in association with IE62 foci at the nuclear edge and also juxtaposed to PML independently of IE62 staining (Figure 6-6B). However, co-localization was not observed between PML and EGFP-66 nucleoplasmic or

nucleolar speckles. Later, PML was observed adjacent to expanding IE62 nuclear staining (Figure 6-6C), and EGFP-66 speckles were also associated with IE62 in these regions. No juxtaposition or co-localization was observed between PML and EGFP-66 in more prominent nuclear dots in other cells (data not shown). PML-positive foci persisted into late stage infection, albeit to reduced levels (Figure 6-6D). These results indicate that EGFP-66 speckles may be involved in the subversion of host processes regulated by ND10 domains or in the formation of VZV replication compartments. However, the the failure of these two proteins to exhibit any co-localization in later stages of infection imply that EGFP-66 speckles have additional, unrelated functions.

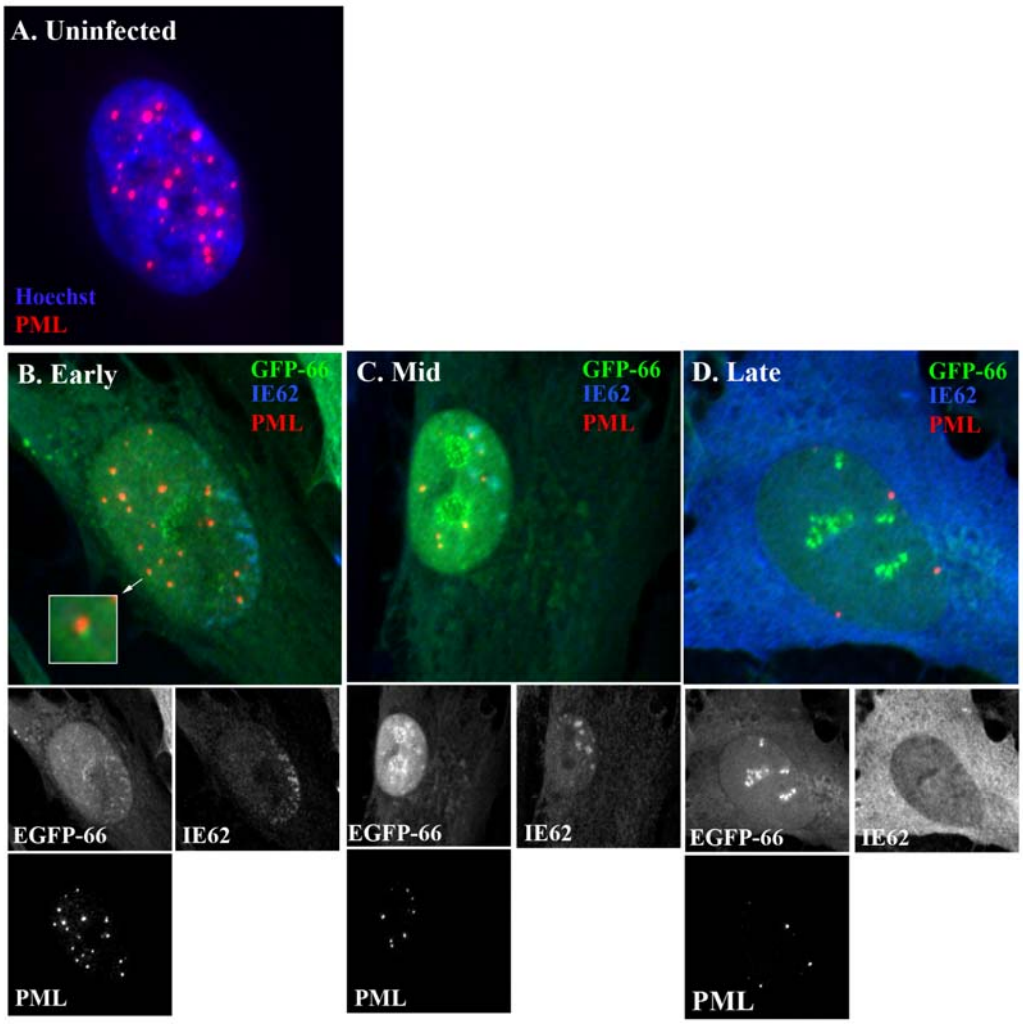

Figure 6-6 A sub-population of EGFP-66 speckles localize adjacent to ND10 domains

MRC-5 fibroblasts were left uninfected or infected with VZV.GFP-66 and fixed as described above, and stained with antibodies against the major ND10 component, PML (AF 647), and VZV IE62 (AF 546). (A) Uninfected cells exhibit many bright PML foci throughout the nucleus. Image depicts a coolr combine overlay of PML and Hoechst. (B-D) PML distribution in VZV.GFP-66-infected cells at different stages. Stages are indicated at the top. Large color-combined panels depict EGFP-66 in green, PML in red and IE62 in blue. Smaller black and white images show individual staining patterns, which are indicated for each panel.

6.4.4 ORF66 decorates the surface of VZV replication compartments (RC) in early infection, but aberrantly accumulates within RC in the absence of kinase activity

The above studies did not identify EGFP-66 speckles in association with cellular nuclear bodies, but did imply a possible association with RC. The HSV-1 ICP4 protein is a major component of RC, and here we observed IE62 nuclear staining reminiscent of this type of localization (Chapter 4). In addition, some EGFP-66 speckles appeared to associate with IE62 exhibiting RC-like staining patterns. To more specifically delineate the level of EGFP-66 association with VZV RC, we performed similar indirect immunofluorescence analyses in VZV.GFP-66-infected cells stained for both the IE62 protein and the VZV ORF29 protein. ORF29 is the VZV single stranded DNA-binding protein and a putative early gene involved in VZV genome replication (126). ORF29 exhibits punctate nuclear localization within structures nearly identical in appearance to HSV-1 RC (46). As we observed EGFP-66kd accumulation in large nuclear structures in live-cell analysis, we also performed VZV.GFP-66kd infections to assess any kinase activity dependent associations with this compartment.

As described in previous studies (Chapter 4) (127), IE62 was predominantly nuclear during early infection stages, exhibiting diffuse nucleoplasmic fluorescence and accumulation in multiple foci. Here, we demonstrate that IE62 foci co-localize with ORF29, suggesting they represent pre-replicative compartments (pre-RC) (Figure 6-7A). Faint EGFP-66 speckles were observed in the putative pre-RC region; but EGFP-66 was also observed in low levels at the nucleolar periphery, throughout the nucleoplasm and in the cytoplasm. Later, when abundant levels of cytoplasmic IE62 were detected, VZV RC expanded, coalesced and contained the majority of nuclear IE62 (Figure 6-7B). ORF66 speckles decorated the outer surface of RC but did not co-localize with punctate ORF29 staining or diffuse IE62 staining. Small ORF66

speckles were observed throughout the nucleoplasm and some were also distributed at the nucleolar periphery. As the RC continued to expand, EGFP-66 accumulated at the nucleolus, but also continued to decorate the RC (Figure 6-7C). Finally, in very late-stage infected cells, the RC occluded most of the nucleus and lacked high levels of IE62 staining (Figure 6-7D). EGFP-66 often appeared to be restricted to the nucleolar area and usually did not decorate the RC surface. These results indicate that EGFP-66 associates with $IE62^{+}$ RC in VZV-infected nuclei during intermediate stages of development, and with nucleoli at both early and later stages of infection, and suggests ORF66 performs overlapping functions in each of these locations.

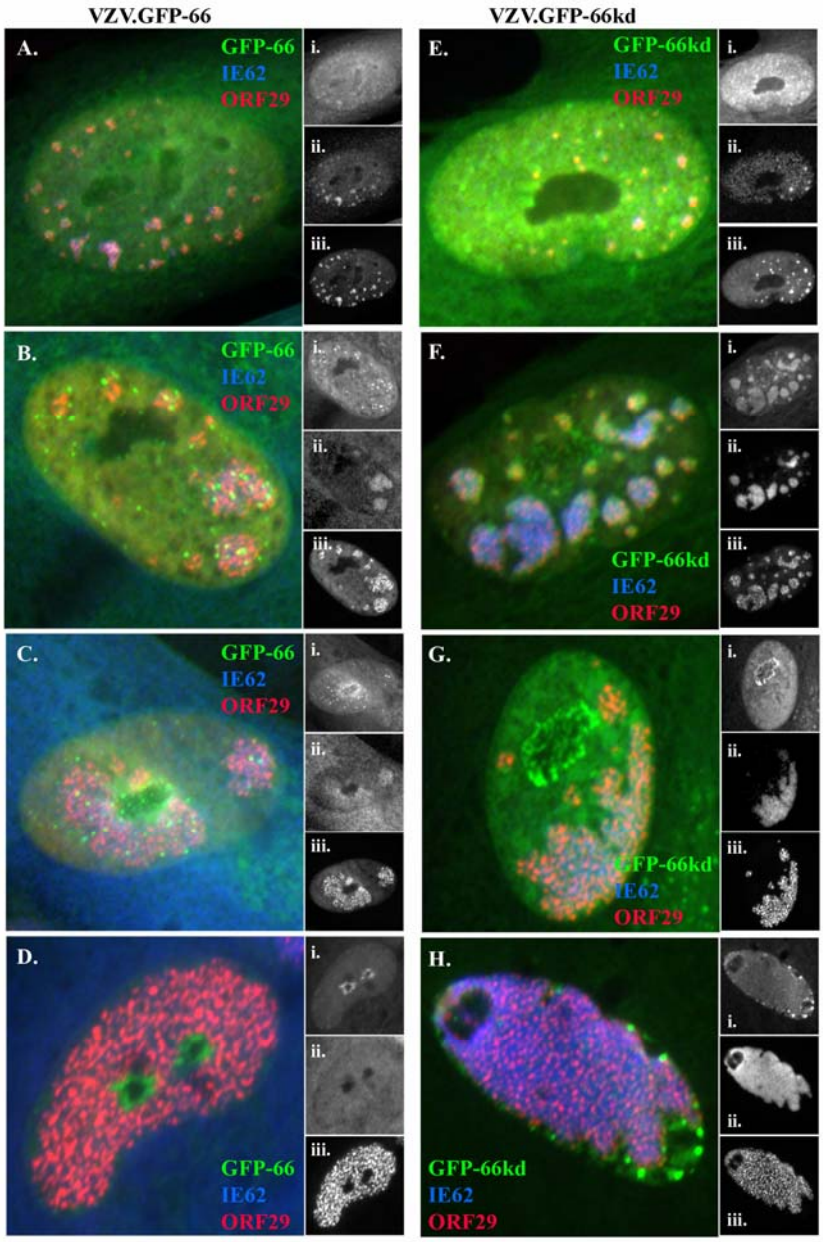

Figure 6-7 ORF66 associates with VZV nuclear replication compartments during early stages of VZV infection

MRC-5 fibroblasts grown on coverslips were infected with VZV.GFP-66 (A-D) or VZV.GFP-66kd (E-H) at a ratio of 1 infected cell to 50 uninfected cells. At 48 hpi, cells were fixed with 4% paraformaldehyde and stained with a rabbit polyclonal antibody to VZV ORF29 protein and a mouse monoclonal antibody to VZV IE62. Viral protein localizations were visualized by indirect immunofluorescence after staining with secondary Alexa Fluor-conjugated antibodies (goat anti-rabbit 546 and goat anti-mouse 647). For each micrograph grouping, the enlarged merged image depicts pseudocolored fluorescence for EGFP-66 (green), ORF29 (red) and IE62 (blue). Smaller panels show individual protein distributions in black and white: i) GFP-66 or GFP-66kd, ii) IE62, and iii) ORF29. The infection condition is indicated at the top of each column of panels.

EGFP-66kd in VZV.GFP-66kd infections exhibited marked differences in localization compared with the functional EGFP-66. Specifically, EGFP-66kd did not exhibit nucleoplasmic speckles that decorated the RC surface, and instead aberrantly accumulated in a diffuse manner similar to that of IE62 in expanding RC (Figure 6-7F and G). At a later stage, EGFP-66kd was often prominently observed in nucleolar-associated foci, indicating that this was not dependent on functional kinase activity. Additional nuclear accumulations independent of ORF29 and IE62 also suggested that EGFP-66kd may associate with other structures in VZV-infected nuclei (Figure 6-7G). In very late-stage infection, EGFP-66kd aberrantly accumulated at the edges of ORF29/IE62-defined RC near the nuclear membrane and did not appear to be significantly localized in the nucleolar region (Figure 6-7H). The aberrant accumulations were either in the form of discrete circular foci in several areas or massive accumulations to one side of the nucleus. These results clearly demonstrate that ORF66 lacking kinase activity exhibited atypical trafficking in VZV-infected cells: initially accumulating within RC rather than to speckles at RC surface, and later accumulating at the nuclear periphery rather than at the nucleolus. In particular, the aberrant accumulation in RC indicated a possible protein:protein interaction that could not be interrupted in the absence of kinase activity.

6.4.5 ORF66 lacking kinase activity exhibits specific co-localization with the VZV major capsid protein in large nuclear inclusions and at the nuclear periphery

Since EGFP-66 and EGFP-66kd in VZV-infected cells were not always associated with RC or the nucleolus, we also investigated the possibility that these proteins associated with nuclear compartments involved in capsid morphogenesis. For this, we performed indirect

immunofluorescence and epifluorescent microscopy analyses of VZV.GFP-66 and VZV.GFP-66kd-infected cells stained with antibodies against IE62 and the VZV major capsid protein (MCP). In late-stage infected nuclei exhibiting only low levels of IE62 expression, MCP could be observed distributed in large lobes throughout the nucleus (Figure 6-8A). In this example cell, several minute MCP foci are apparent at the extreme top of the nucleus, and these may represent capsids budding from the nuclear membrane (upper arrowheads). EGFP-66 speckles were largely accumulated in the nucleolar region, but small EGFP-66 foci were also observed at the edges of MCP-containing compartments, and one EGFP-66 speckle on the lower side of the nucleus was co-localized with a putative budding nucleocapsid (lower arrowhead). However, no significant co-localization was observed between EGFP-66 and MCP. In direct contrast, VZV expressing EGFP-66kd exhibited aberrant MCP accumulation at the edge of the nucleus, nearly perfectly overlapping with EGFP-66kd autofluorescence (Figure 6-8B). Less EGFP-66kd was observed in other regions of the nucleus, suggesting that EGFP-66kd interacts with MCP or another capsid related factor, and that this interaction may be involved in aberrant EGFP-66kd trafficking to the RC periphery in late stages of infection.

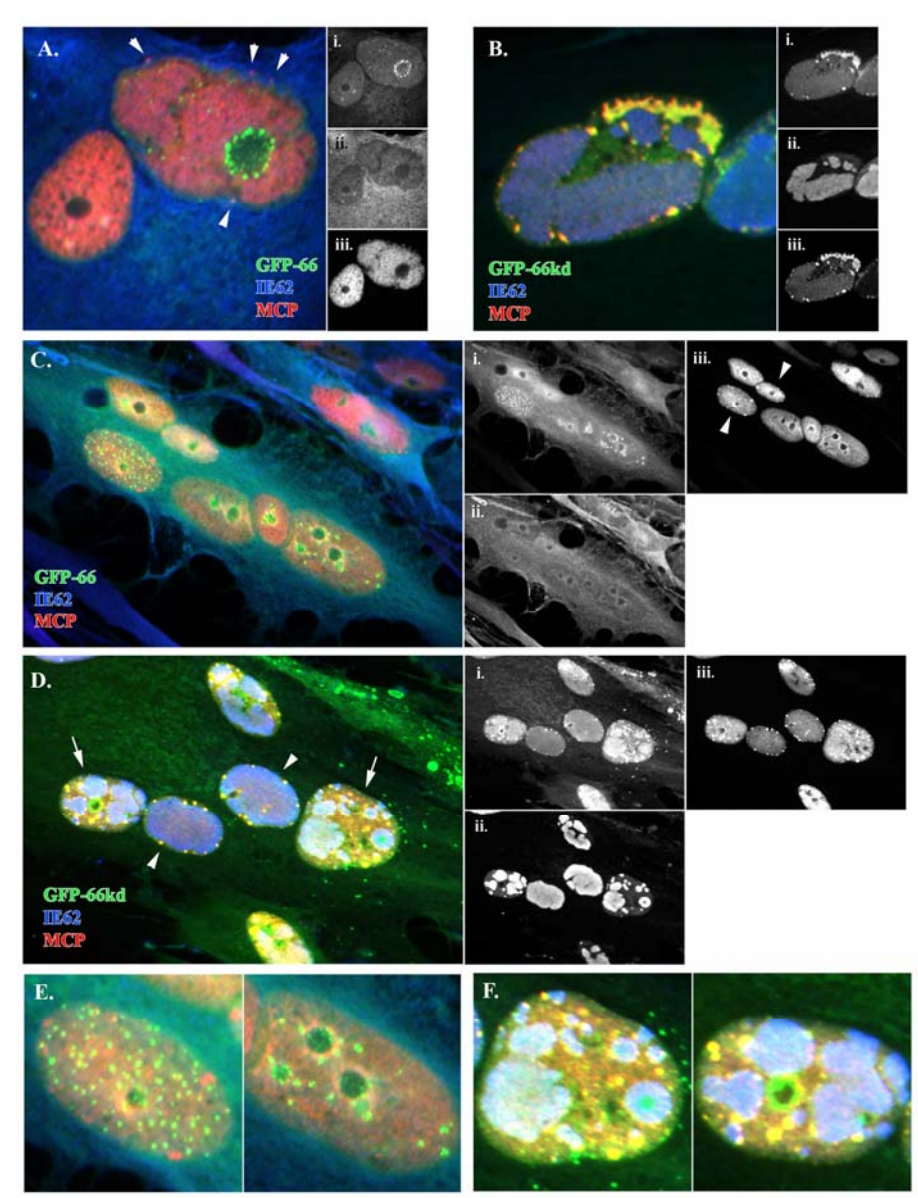

Figure 6-8 VZV major capsid protein is aberrantly distributed in fibroblasts infected with VZV.GFP-66kd
MRC-5 cells were infected with VZV.GFP-66 or VZV.GFP-66kd and fixed as described above. Cells were stained with rabbit poly-clonal anti-IE62 (goat-anti-rabbit 546) and mouse monoclonal antibody to the VZV MCP (goat-anti-mouse 647), and visualized by epifluorescent microscopy. Close-up images of VZV.GFP-66 (A) and VZV.GFP-66kd (B) late-stage nuclei show marked differences in MCP localization and co-localization with GFP-66kd. Late-stage VZV.GFP-66 (C) and VZV.GFP-66kd (D) syncytia exhibit nuclei with varying ORF66 and MCP localizations. In all cases, the color-combined panel shows pseudo-colored EGFP-66 or EGFP-66kd in green, MCP in red and IE62 in blue. Individual staining profiles for (A-D) are shown in black in white to the right of each colored panel: i) EGFP-66 or EGFP-66kd; ii) IE62; iii) MCP. Enlarged nuclei from VZV.GFP-66 and VZV.GFP-66kd syncytia are shown in (E) and (F), respectively.

VZV.GFP-66 and VZV.GFP-66kd-infected syncytia were imaged to highlight the myriad of nuclear distributions observed for the EGFP-66 kinase proteins and MCP in late-stage infected cells (Figure 6-8C and D). IE62 cellular distribution was predominantly cytoplasmic in a representative micrograph depicting VZV.GFP-66 (Figure 6-8C, panel ii) and localized to large nuclear RC in VZV.GFP-66kd infections (Figure 6-8D, panel ii), indicating these cells were indeed in late-stage infection (panel ii for both). Interestingly, MCP was distributed throughout the nucleus with accumulation at the nucleolus in many VZV.GFP-66-infected cells (Figure 6-8C, panel iii), suggesting a possible role for the nucleolus in capsid assembly and egress. Occasionally, in cells expressing high levels of MCP, accumulations were observed at the nuclear edge, in structures reminiscent of "assemblons" observed in HSV-1-infected cells (Figure 6-8C, panel iii) (244). EGFP-66 displayed bright foci that accumulated in the nucleoplasm and at the nucleolus, but never co-localized with MCP in these structures. Two VZV.GFP-66-infected nuclei from the syncytium in Figure 6-8C are enlarged for enhanced viewing of EGFP-66 and MCP localizations (Figure 6-8E). In VZV.GFP-66kd syncytia (Figure 6-8D), many late-stage nuclei exhibited EGFP-66 and MCP co-localization at the nuclear edge (arrowheads), similar to the micrograph shown in Figure 6-8B. However, cells at an earlier infection stage, as indicated by only partial occlusion of the nucleus by RC-associated IE62, also displayed significant co-localization between EGFP-66kd and MCP in many structures throughout the nucleoplasm (Figure 6-8D, arrows), and this did not usually occur at the nucleolus. These nuclei were enlarged for better visualization of EGFP-66kd/MCP co-localization and are shown in Figure 6-8F. Interestingly, abundant levels of EGFP-66kd remained associated with RC at these times, and thus ORF66 may interact with multiple nuclear

compartments simultaneously during VZV infection. Of note, we also observed bright EGFP-66kd autofluorescence in cytoplasmic foci in close proximity to some nuclei in syncytia (Figure 6-8D, far right; also in Figure 6-8F). As postulated for EGFP-66kd association with RC, the aberrant accumulation in capsid assembly compartments indicated a novel protein:protein interaction that was enhanced in the absence of kinase activity. Furthermore, as EGFP-66kd staining in VZV RC was reduced in favor of association with MCP in late-stage infected cells, this implies that EGFP-66kd may have been recruited directly from RC, possibly through interactions with the MCP or another capsid assembly component.

6.4.6 EGFP-66 nuclear speckle formation does not require expression of additional VZV proteins

To determine whether ORF66 speckles could form in the absence of additional VZV gene expression, we analyzed EGFP-66 distribution in MRC-5 cells infected with replication defective adenoviruses expressing EGFP-66 from a DOX-repressible promoter. Control infections were performed in the presence of DOX to assess any affects induced by the adenovirus vector. For these studies, we also stained cells for antigens that localize to CB and ND10 domains, as just described for VZV-infected cells. EGFP-66 formed nuclear speckles that localized at the periphery of the nucleolus (nucleolar stain not shown) and throughout the nucleoplasm when expressed in the absence of additional VZV gene expression, indicating that the ability to localize in this manner was an intrinsic property of the ORF66 protein (Figure 6-9). Speckles were more prominent in cells expressing high levels of ORF66 (as determined by EGFP fluorescence) and were less apparent with lower expression. In many cells, prominent EGFP-66 speckles were juxtaposed to ND10 domains, and PML appeared to be highly distributed in

grainy speckles throughout the nucleus. This suggests a subtle disbursement of PML in the presence of ORF66 expression. Of note, many EGFP-66 speckles were also observed independently in the nucleoplasm (Figure 6-9A). As was the case for VZV-infected cells, EGFP-66 displayed no co-localization with CB (Figure 6-9B). Importantly, distal cytoplasmic speckles were not observed in cells expressing only EGFP-66. Thus, EGFP-66 nuclear speckles either associated with a currently unknown cellular nuclear structure or formed *de novo* following EGFP-66 accumulation, while cytoplasmic speckles were a derivative of some process of VZV infection.

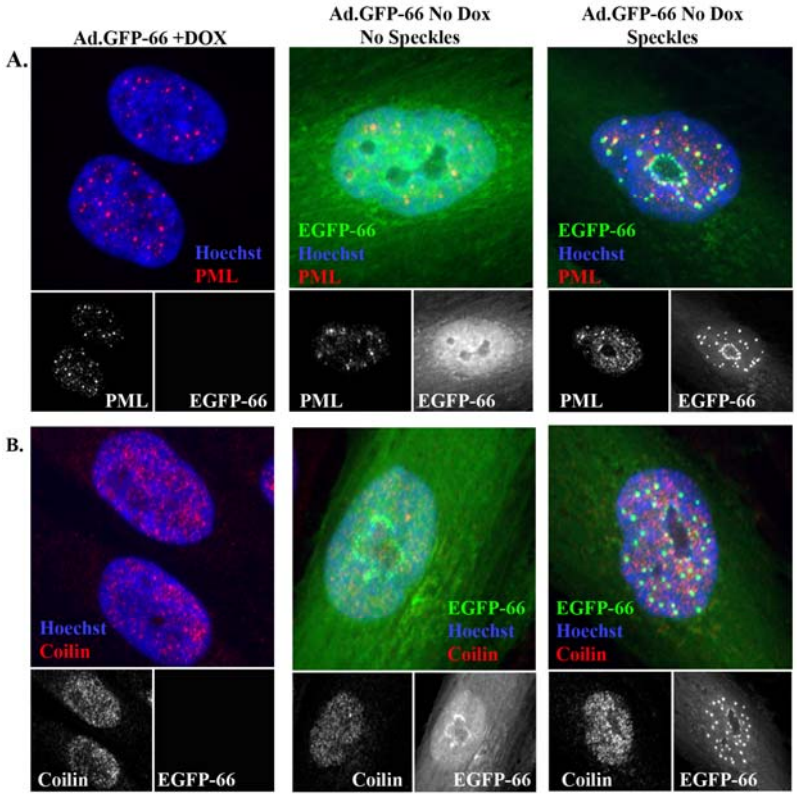

Figure 6-9 ORF66 expressed in the absence of other VZV genes associates with the nucleolus and forms nuclear foci that partially overlap with ND10 domains

MRC-5 cells were mock-infected or infected with 2 pfu/cell of Ad.GFP-66 and Ad.tTa and incubated in the presence or absence of 0.5 μg/ml DOX. At 24 hpi, cells were fixed and stained with antibodies to PML (AF 647) (A), or Cajal bodies (AF 647) (B). In both (A) and (B), mock-infected and infected cells that either lack or show nuclear speckles are displayed. In all

panels, the enlarged micrographs depict a color combined image of EGFP-66 (green), PML or coilin as indicated (red), and Hoechst-stained chromatin (blue). Smaller black and white panels show individual fluorescence patterns as indicated.

6.5 DISCUSSION

In this study, we have extended previous observations indicating novel nuclear distributions for the VZV ORF66 protein kinase, and we provide evidence to suggest that ORF66 associates in a temporally-defined manner with specific nuclear sub-domains to coordinately affect multiple aspects of the VZV replication cycle.

In very early stages of infection, nuclear EGFP-66 was predominantly diffusely localized, but minute speckles were consistently observed adjacent to ND10 domains, independent of the asymmetrically distributed IE62 foci at the periphery of the nucleus. At a slightly later time-point, IE62 foci coalesced into pre-RC/RC, and EGFP-66 speckles were observed decorating the pre-RC surface while ND10 domains were associated with its boundary. Thus, one possible function for ORF66 could be to facilitate ND10 trafficking to sites of viral transcription and genome replication, either by dispersing ND10 components or actively inducing ND10 transport. In HSV-1 infected fibroblasts, ND10 are formed *de novo* adjacent to RC from components in the nuclear milieu in response to HSV-1 genomes, rather than by active ND10 trafficking to sites of viral transcription and replication (62). Our immunofluorescence analyses of ND10 structures in cells expressing only the ORF66 protein suggest that ORF66 may function to disperse ND10 components, thus providing some circumstantial support for the former possibility. Interestingly, PML is also essential for type I and II interferon-mediated programmed cell death (243). As it is known that ORF66 inhibits caspase activation in VZV-infected T-lymphocytes treated with type

II interferon (220), it is possible that ORF66 association with ND10 is related to this function. A similar association with ND10 has not been described for the HSV-1 U_S3 kinase, and cellular distribution studies using antibodies against U_S3 have revealed only nuclear membrane, and not nucleoplasmic, association (212). Thus, this observation may be representative of a unique function for the ORF66 protein kinase in VZV-infected cells.

EGFP-66 nucleolar association was observed during very early stages of infection and persisted even when IE62 was completely excluded from the nucleus, implying involvement in a critical function independent of IE62 in the VZV replication cycle. This function may be distinct from that of nucleoplasmic speckles, as nucleolar speckles remained relatively immobile at the nucleolar periphery. Under normal physiological conditions, the nucleolus functions in transcription and processing of ribosomal RNA, biogenesis and nuclear export of pre-ribosomal particles, and intranuclear and nucleocytoplasmic transport of nuclear proteins (262). As a result of the primary role in formation of ribosomes, many nucleolar proteins have RNA recognition motifs. The EGFP-66 association with the nucleolus was astonishingly reproducible, and independent of both ORF66 kinase activity and the expression of additional VZV proteins. However, it is not yet clear whether ORF66 binds RNA or participates in modulation of any of the normal nucleolar processes.

In a previous study, cell-free VZV infections clearly demonstrated that ORF66 expression and nuclear localization was not sufficient for IE62 nuclear exclusion, and these two proteins did not co-localize in VZV-infected nuclei before RC formed (Chapter 4). In the more detailed studies we presented here, EGFP-66 speckles were observed decorating the surface of VZV pre-RC and RC, where abundant levels of IE62 accumulated, and this association was concurrent with IE62 nuclear exclusion. However, ORF66 did not appear to associate with RC

at very late times post-infection when IE62 was completely cytoplasmic. This suggests that EGFP-66 specifically localizes to RC to mediate IE62 phosphorylation. In support of this, VZV lacking kinase activity abnormally accumulated in RC and co-localized with the diffusely distributed IE62 there. We suggest this occurs due to enhanced affinity for IE62 in the absence of the ability of ORF66 to mediate phosphorylation, similar to what is observed in cells infected with VZV expressing point-inactivated ORF47 (22). Interestingly, the HSV-1 ICP4 NLS is a phosphorylation target for the U_S3 kinase in transfected cells (unpublished observations, M. B. Yee and P. R. Kinchington) but ICP4 is not an abundant cytoplasmic protein in HSV-1 infection, suggesting that specific compartmentalization of ICP4 (nucleoplasmic) and U_S3 (nuclear membrane) may preclude U_S3-mediated ICP4 phosphorylation and nuclear exclusion. These observations provide support for the idea that ORF66 nuclear distribution patterns are reflective of unique ORF66 functions during VZV infection. While we suggest that IE62 is the major target for the ORF66 protein kinase in VZV RC, we cannot rule out the possibility that additional VZV proteins may be phosphorylated there, as well.

Similar to the situation in RC, EGFP-66 speckles decorated capsid assembly compartments demarcated by the VZV MCP, while the EGFP-66kd protein aberrantly accumulated in this region. Interestingly, EGFP-66kd was simultaneously associated with RC, MCP and nucleoli when RC only partially occluded the nucleus (early infection); but was exclusively associated with mislocalized MCP near the nuclear membrane when RC completely occluded the nucleus (late-stage infection). This implied that a high-affinity association occurred between EGFP-66kd and MCP or another capsid component, and further suggested that VZV capsids may associate with both RC and nucleoli before proceeding to the nuclear membrane for export. In support of this, some MCP accumulation was observed at the periphery of the

nucleolus in VZV.GFP-66-infected cells, and to a lesser extent in VZV.GFP-66kd infected cells. The VZV ORF33.5 capsid scaffolding protein contains an ORF66 consensus motif ($_{176}$RRRRVSPS$_{184}$), which is also an exact match to the optimal consensus for HSV-1 and 2 U_S3 kinases (47, 206, 207). We suggest that the ORF33.5 protein may be a novel target for the ORF66 kinase, and that interaction with this motif may override other interactions in the RC or the nucleolus. Small, motile EGFP-66 foci reminiscent of nucleocapsids were also present in the distal cytoplasm of VZV-infected cells, and importantly, these were not observed in cells expressing only EGFP-66. Thus, we consider it possible that these may represent cytoplasmic virion particles. In support of this, it has been previously reported that ORF66 is a tegument protein (123). Collectively, these observations imply a possible association between ORF66 and the VZV capsid that is enhanced by ablation of ORF66 kinase activity, and suggest a role for ORF66 in capsid morphogenesis. Lastly, the accumulation of EGFP-66kd and MCP at the nuclear periphery may imply that ORF66 kinase activity is important for nucleocapsid egress. In particular, MCP often appeared to accumulate in clusters, similar to what has been observed for HSV-1 capsids with viruses lacking U_S3 expression. Electron microscopy (EM) performed in T cells and melanoma cells infected with VZV lacking ORF66 expression did not show any nucleocapsid accumulation in the peri-nuclear space (219, 220), but comparative nucleocapsid egress studies have not been performed in fibroblasts. Thus, it is possible that the methods of nucleocapsid exit in each cell type are different.

The question remains: how and why are ORF66 speckles trafficking around the nucleus? At this time there is no clear explanation, but several relevant points may provide some insight into potential future experiments aimed at answering these questions:

i) The ability of ORF66 to traffic around the nucleus and associate with multiple nuclear sub-domains suggests it may be involved in communication between these compartmentalized regions, or function in delivery of cargoes from one nuclear region to another. We hypothesize that one cargo could be VZV nucleocapsids, and we are currently deriving recombinant, dual-fluorescent VZV (mRFP-ORF66/ORF23-EGFP) to address this possibility. Alternatively, nucleoplasmic trafficking may be a simple means for ORF66 to travel to different sub-domains where it can mediate phosphorylation of specific compartmentalized targets.

ii) The high velocity and directed manner in which EGFP-66 speckles traffic in the nucleoplasm is suggestive of an energy-dependent process. We are currently testing this hypothesis using live-cell imaging studies combined with ATP depletion and temperature reductions.

iii) ORF66 may utilize the nucleoskeletal network for nucleoplasmic trafficking. By electron microscopy (EM), the nucleoskeleton has been suggested to consist of the nuclear lamina at the nuclear edge, core filaments which radiate from the nucleolus to the nuclear periphery near the nuclear pore complex, and a diffuse meshwork skeleton that interconnects each of the components (104, 262). Recently, an EGFP-tagged version of the cell cycle regulatory phosphatase, CDC14b, was reported to exhibit this type of nuclear localization in live cells, confirming that observations made by EM were not artefactual (184). The nucleoskeleton is involved in nuclear compartmentalization and is probably critical for both DNA replication and RNA polymerase II transcription. These functions are all important for efficient viral replication, and thus modulation of the nucleoskeleton could prove to be a major determinant of the efficiency of VZV replication. HSV-1 is known to regulate components of the nuclear lamina (144, 178, 181), but no role in regulation of the interior nucleoskeleton has been reported.

In sum, these data provide a platform for understanding the complex interactions between ORF66, the cellular environment, and other VZV proteins. We propose a model in which ORF66 localizes to the nucleus and initially interacts with ND10 domains to either promote their association with RC or inhibit an antiviral response; subsequently associates with RC to mediate IE62 phosphorylation and nuclear exclusion; and finally facilitates either nucleocapsid morphogenesis or egress from the nucleus. Future efforts aimed at understanding the nature of ORF66 nuclear localizations will provide important insights into the mechanisms of VZV pathogenesis and the molecular differences between HSV-1 and VZV infection.

7.0 PERSPECTIVE AND DISCUSSION OF FUTURE DIRECTIONS

Overall, the results described herein represent a significant contribution to VZV biology and expand our understanding of a critical mediator of VZV pathogenesis, the ORF66 protein kinase. Previous to this work, the role of the ORF66 kinase in VZV pathogenesis had been well-characterized, but the molecular functions of the ORF66 molecule were mostly unknown. I have described the first ORF66 *in vitro* kinase assay; the first ORF66 viral protein target, IE62; and the first ORF66 substrate motifs (within IE62), which appear to resemble the optimum phosphorylation consensus for the related HSV-1 and 2 (47, 206, 207). In addition, my work has identified mechanisms in addition to ORF66 that regulate IE62 nuclear versus cytoplasmic localization in VZV-infected cells. Since IE62 nuclear exclusion may involve phosphorylation by ORF47 for nuclear release, this is the first indication of specific, cooperative activities by the VZV kinases in promoting a single outcome. I have also extended a previous observation that ORF66 contributes to immune evasion by inducing downregulation of MHC-I. These studies not only identified the general mechanism whereby ORF66 influences MHC-I, but also significantly enhanced our understanding of the regulation of MHC-I surface presentation in VZV-infected cells, and further suggested that additional VZV genes may be involved. I have used VZV expressing EGFP-tagged ORF66 kinase proteins to demonstrate novel nuclear distribution and trafficking for ORF66, and I reveal a potential new role for ORF66 in capsid morphogenesis during VZV infection. Thus, ORF66 affects multiple, seemingly unrelated proteins during

infection that are both viral and cellular in nature, in line with the multi-functionality of orthologous U_S3 kinase proteins.

My *in vitro* kinase assay not only established that ORF66 was a functional protein kinase, but also identified the first substrate for ORF66 phosphorylation, and delineated two specific target motifs within the IE62 protein. The IE62 motifs phosphorylated by ORF66 include RKRKS_{686}QPVand KRRVS_{722}EPV, and these were phosphorylated with similar efficiency in *in vitro* reactions. Based on this, I define a minimum consensus for ORF66 phosphorylation as: R/K_3-X-S, where X=Val or R/K (or potentially other amino acids). In the IE62 genome, there are six additional proteins (ORFs 1, 4, 9, 22, 33.5 and 49) that carry at least three consecutive basic amino acids upstream of serine or threonine residues, which represent putative targets for ORF66-mediated phosphorylation and regulation in VZV-infected cells (Figure 7-1). Potential phosphorylations of these proteins are currently being assessed by other members of the laboratory utilizing *in vitro* kinase assays based on the conditions derived in this study. Of particular interest will be the ORF33.5 capsid scaffold protein, as ORF66 was implicated as potentially affecting nucleocapsid morphogenesis in ORF66 nuclear trafficking studies reported here. In addition to assessing potential VZV protein targets, the kinase assay may also be used to assess phosphorylation of putative cellular phosphorylation candidates.

VZV ORF	Putative ORF66 Phosphorylation Site
ORF1	R-R-K-A-$\underline{S}_{65}$-A-Q-L
ORF4	R-R-R-R-P-$\underline{T}_{145}$-T-P-A
ORF9	R-R-K-T-$\underline{T}_{20}$-P-S-Y
ORF22	R-R-R-R-R-P-$\underline{S}_{337}$-W-T-P
ORF33.5	R-R-R-R-V-$\underline{S}_{181}$-P-S-Y
ORF49	K-R-K-P-$\underline{S}_{70}$-G-K-S
Known Targets	
IE62	R-K-R-K-$\underline{S}_{686}$-Q-P-V
IE62	K-R-R-V-$\underline{S}_{722}$-E-P-V

Figure 7-1 Comparison of known ORF66 phosphorylation motifs with predicted viral target motifs

ORF66 phosphorylates two residues in the IE62 sequence. Based on a loose consensus of R/K_3-X-S/T, six other VZV ORFs are predicted to have ORF66 phosphorylation motifs, and these are shown in single letter amino acid code. The phosphorylated IE62 targets are included for reference. The predicted phosphorylation site is underlined, and the placement in the context of the primery amino acid sequence is indicated.

Given the importance of ORF66 kinase expression and catalytic activity for VZV survival in T lymphocytes, small molecule inhibitors of ORF66 could pose a potential novel avenue for development of a specific VZV antiviral. The purification of the ORF66 kinase and identification of an ORF66 substrate and autophosphorylation activity presented here provide the basis for the development of an ORF66 inhibition screening assay. However, the implications of ORF66's biological activities and the potential effects on VZV pathogenesis must be carefully considered before such an inhibitor could be implemented. T lymphocytes are likely infected shortly after VZV infection (137, 139), and thus an ORF66 inhibitor would have to be utilized upon exposure to prevent T-cell mediated dissemination to the skin, where such an inhibitor would likely be less effective in controlling VZV replication. Since ORF66 expression may be important for the maintenance of latency by maintaining IE62 nuclear exclusion, inhibition of ORF66 kinase activity could potentially instigate VZV reactivation in individuals where it would

normally not occur. Thus, an ORF66 inhibitor would not be appropriate for use in controlling zoster infections. One controlled situation where an ORF66 inhibitor may be beneficial is if used in combination with the varicella vaccine. The vaccine consists of live virus, which is known to infect T lymphocytes and cause severe disseminated disease in some at-risk individuals (78). Thus, simultaneous vaccination and ORF66-based anti-VZV treatment could significantly minimize the risks associated with vaccine-associated disease.

ORF66-mediated IE62 phosphorylation represents an unprecedented interaction that has not been reported for any other alphaherpesvirus. We hypothesized that this may be critical for regulation of the viral transcriptional program; efficient transactivation of VZV gene expression immediately upon infection and especially in the absence of the α-TIF ortholog, ORF10; and potentially for the maintenance of VZV latency. The generation of VZV mutants lacking both ORF10 expression and the IE62 S868 residue, the critical determinant of ORF66-mediated IE62 nuclear exclusion, should allow us to test the hypothesis that IE62 tegument association compensates for the lack of ORF10 expression and tegument association in cell culture. However, it will be much more difficult to test the hypothesis that ORF66-mediated phosphorylation of IE62 is involved in maintaining cytoplasmic IE62, and possibly latency, in VZV-infected ganglia. One would expect to see an increased capacity for reactivation in viruses lacking ORF66 expression if this is the case, but such studies require a model for both VZV latency and VZV reactivation, and this is not currently available.

We have hypothesized that ORF66-directed IE62 phosphorylation results in the impairment of importin α binding to the IE62 NLS through steric inhibition of the protein:protein interaction. While intramolecular masking by phosphorylation is a commonly used mechanism in the regulation of nuclear import and export, few proteins have been shown to be nuclear

import impaired upon phosphorylation downstream of the NLS (88). Thus, the ability of IE62 to interact with importin proteins should be assessed not only to clarify the mechanism for nuclear exclusion, but also because this ORF66-mediated IE62 phosphorylation event could provide a model of nuclear exclusion by C-terminal NLS phosphorylation. An alternative explanation for IE62 nuclear exclusion is that the NLS becomes masked by an intermolecular interaction with a cytoplasmic anchor, which recognizes the ORF66-phosphorylated/NLS motifs, thereby preventing importin α recognition. Support for this stems from the observation that both ORF66 phosphorylation motifs are an exact match for the 14-3-3 recognition consensus (R-X-X-X-pS/T-X-P, where pS=phospho-serine or threonine and X= any amino acid) (28). Thus, the ability of phosphorylated IE62 to bind 14-3-3 proteins should also be assessed.

Additional investigations of the nucleocytoplasmic trafficking of IE62 revealed that a complex interplay likely regulates IE62 cellular distribution, dependent upon ORF66 phosphorylation-mediated inhibition of nuclear import, IE62 nuclear export through a nuclear export motif, and a possible novel coordinate ORF47 or CKII phosphorylation; which collectively result in IE62 nuclear exclusion. We were particularly intrigued by the possibility of ORF47 poly-S phosphorylation-induced nuclear exclusion, since it may represent a novel, cooperative effort by the ORF66 and ORF47 kinases in contributing to a common outcome. Future experiments will be aimed at determining specific IE62 residues phosphorylated by the ORF47 protein kinase, and the effects of N-terminal poly-S mutation in the context of VZV infection. Since the poly-S tract is likely phosphorylated by cellular CKII as well, a CKII inhibitor should be utilized in the context of wild-type VZV infection to determine if CKII contributes to IE62 nuclear exclusion, or if this is primarily a function of the combined activities of ORF47 and ORF66 protein kinases. Furthermore, it will be interesting to determine any

effects of the C-terminal poly-S tract on IE62 cellular location. Interestingly, ORF47-mediated phosphorylation of the VZV gE protein facilitates the recruitment of gE into the TGN (119), the site of virion assembly. Thus, I speculate that IE62 poly-S phosphorylation by ORF47 could also result in TGN recruitment once IE62 has been excluded from the nucleus.

I have clearly demonstrated a kinase activity-dependent role for ORF66 in modulation of MHC-I surface expression in VZV-infected cells, but the mechanism is not entirely resolved. Potential pathways through which this could occur have already been discussed (i.e., through inhibition of the TAP complex or inhibition of MHC-I vesicular transport). Alphaherpesvirus proteins that specifically affect MHC-I biogenesis (as opposed to global effects induced by host protein shutoff) are involved in inhibition of the TAP complex, but it is not known whether VZV affects TAP activity. TAP inhibition would result in a delay in MHC-I maturation, and I consider this as the most likely mechanism for MHC-I subversion induced by the ORF66 protein. Future experiments aimed at more specifically elucidating the mechanism of ORF66-mediated MHC-I downregulation should assess TAP function using the peptide transport assay originally described for the determining ICP47's role in MHC-I downregulation (96). However, as multiple effects on the PLC could potentially lead to the delay in MHC-I transport, the overall components of the PLC and early events in the assembly of MHC-I heavy chain molecules should be assessed in parallel, complimentary experiments using metabolic labeling and co-immunoprecipitation analyses of individual PLC components. MHC-I thermostability can also be assessed by incubating lysates at 37°C for one hour preceding immunoprecipitation with the conformationally-dependent W6/32 antibody: peptide-loaded MHC-I will remain folded and will immunoprecipitate, while MHC-I lacking peptides will dissociate from MHC-I heavy chains and fail to precipitate. This experiment will assist in determining if the delay in MHC-I maturation is

due to faulty assembly by the peptide loading complex (PLC) or aberrant trafficking through the *cis*/medial-Golgi.

Of particular interest for the role of ORF66 in VZV pathogenesis is the ability of ORF66 to mediate MHC-I downregulation in the context of VZV-infected T lymphocytes. Interestingly, the human immunodeficiency virus (HIV) nef protein, which is a well-established mediator of MHC-I downregulation, can induce MHC-I downregulation in several transformed cell lines, but functions significantly more efficiently in T lymphocytes, which are also one of the HIV natural reservoir cell types (114). ORF66 expression and kinase activity is known to promote T-lymphocyte survival in the face of type II interferon treatment (219, 220), but MHC-I downregulation could confer enhanced survival for VZV-infected T lymphocytes trafficking through lymphoid tissues in the presence of many additional immune cells. It will be difficult, however, to assess the role of ORF66-mediated MHC-I downregulation for *in vivo* VZV pathogenesis in T lymphocytes or any other VZV-permissive cell type, as the only well-established model of VZV infection is the SCID-hu mouse, which lacks an adaptive immune system.

Viral proteins that mediate MHC-I downregulation are known to impair CTL-mediated lysis of infected cells, and this establishes functional significance in viral immune evasion. It will be important to establish a functional role for the ORF66 protein in protecting VZV-infected cells from CTL-mediated lysis. The highly restricted human tropism of VZV is a severe limitation in testing this function of ORF66 in the context of infection. However, VZV-specific human T-cell clones have been created and used with autologous B cells to study the immune recognition of specific VZV antigens expressed by vaccinia virus vectors (167, 168). This system could be utilized to determine the ability of ORF66 to prevent T-cell activation in

response to specific VZV antigens in the absence of additional VZV gene expression. Importantly, it should be noted that the orthologous HSV-1 U_S3 kinase inactivates CTL and prevents apoptosis induced by cytolytic granule release (13, 223). While it is unknown whether this function is conserved for the ORF66 kinase, this possibility should be considered when evaluating any results from this assay.

Additional VZV genes may be involved in mediating MHC-I downregulation, but these have not yet been identified. The vast majority of herpesvirus proteins that induce MHC-I downregulation are relatively small membrane proteins. Thus, candidate screening analysis for additional VZV mediators of MHC-I subversion should include VZV glycoproteins, especially those for which no known function has been described. A potential major obstacle in this approach may occur if the VZV protein involved in MHC-I downregulation works only in concert with other VZV proteins. Thus, another approach to identifying the additional genes involved could include random mutagenesis of the VZV genome using the VZV bacterial artificial chromosome, combined with a large-scale screen of mutants for any differences in their abilities to affect MHC-I surface expression. Our studies and those of others have indicated that the VZV ORF9a protein, the ortholog of the varicellovirus TAP inhibitor, does not appear to be functional when expressed alone in transformed cells (59, 136). While this may be due to lack of conservation of MHC-I modulatory activity or inability to affect MHC-I in the absence of an unknown viral protein, an additional explanation for this observation is that ORF9a affects specific MHC-I allotypes. If this were the case, downregulation may not be observed if MHC-I surface expression is assessed with pan-specific anti-MHC-I antibodies. Thus, an assessment of ORF9a's ability to mediate downregulation of specific MHC-I allotypes could potentially lead to identification of an immunomodulatory activity. Notably, herpesviruses are known to more

efficiently target MHC-I allotypes that present peptides to CTL (e.g., HLA-A and HLA-B), rather than those that are dominant natural killer (NK) cell ligands (e.g. HLA-C) (155).

ORF66 trafficking studies indicated a possible novel role for nucleocapsid morphogenesis in VZV-infected fibroblasts. Orthologous U_S3 kinases have been implicated in faciliting nucleocapsid egress from the nucleus through phosphorylation of several components of the cellular nuclear lamina (144, 178, 181). Given the unique distribution of ORF66 in VZV-infected cells, I propose that ORF66 mediates this effect through novel intranuclear interactions and phosphorylation activities. Interestingly, while the ORF66 and HSV-1 U_S3 kinase domains are >40% identical and >60% similar, a BLAST query of the ORF66 N-terminal domain against that of the HSV-1 U_S3 kinase revealed no significant homology (unpublished results). In addition, ORF66 encodes a unique C-terminal 15 amino acid motif ($_{379}$PDPYPNPMEVGD$_{393}$). These unique regions may confer different cellular localization abilities or interactions with unique protein targets to facilitate specific ORF66 functions during VZV infection. Future experiments should be aimed at identifying specific interactions between ORF66 and VZV capsid proteins, as well as any effects ORF66 has on trafficking of nucleocapsids in VZV-infected nuclei.

Since the ORF66 protein is ~48 kDa and larger than the size constraint for free diffusion across the nuclear pore complex, active nuclear import is implied. While no classical R/K-rich nuclear import motifs are present in the ORF66 sequence, this does not exclude the possibility that ORF66 utilizes an importin β-specific import pathway, or potentially binds to another protein to piggy-back a ride into the nucleus. Interestingly, ORF66 encodes a putative nuclear export motif ($_{178}$LPICDILAI$_{186}$), implying potential nuclear shuttling activities; this is supported by the abundant ORF66 nuclear and cytoplasmic localization in VZV-infected cells. The

availability of EGFP-tagged ORF66 kinase proteins will allow the assessment of ORF66 nucleocytoplasmic trafficking by physiologically relevant approaches such as fluorescence recovery after photobleaching (FRAP) methodologies.

While several properties of ORF66 have been clearly defined by the studies presented here, a more comprehensive understanding of the roles of ORF66 in VZV pathogenesis will require identification of cellular protein interaction partners and phosphorylation substrates. For this reason, intensive future efforts should be aimed at identifying these interactions and assessing the role of the ORF66 protein kinase on the cellular phospho-proteome.

8.0 REFERENCES

1. **Abele, R., and R. Tampe.** 2004. The ABCs of immunology: structure and function of TAP, the transporter associated with antigen processing. Physiology (Bethesda) **19:**216-24.
2. **Abendroth, A., I. Lin, B. Slobedman, H. Ploegh, and A. M. Arvin.** 2001. Varicella-zoster virus retains major histocompatibility complex class I proteins in the Golgi compartment of infected cells. J Virol **75:**4878-88.
3. **Abendroth, A., G. Morrow, A. L. Cunningham, and B. Slobedman.** 2001. Varicella-zoster virus infection of human dendritic cells and transmission to T cells: implications for virus dissemination in the host. J Virol **75:**6183-92.
4. **Ahn, K., T. H. Meyer, S. Uebel, P. Sempe, H. Djaballah, Y. Yang, P. A. Peterson, K. Fruh, and R. Tampe.** 1996. Molecular mechanism and species specificity of TAP inhibition by herpes simplex virus ICP47. Embo J **15:**3247-55.
5. **Ambagala, A. P., R. S. Gopinath, and S. Srikumaran.** 2003. Inhibition of TAP by pseudorabies virus is independent of its vhs activity. Virus Res **96:**37-48.
6. **Ambagala, A. P., R. S. Gopinath, and S. Srikumaran.** 2004. Peptide transport activity of the transporter associated with antigen processing (TAP) is inhibited by an early protein of equine herpesvirus-1. J Gen Virol **85:**349-53.
7. **Ambagala, A. P., S. Hinkley, and S. Srikumaran.** 2000. An early pseudorabies virus protein down-regulates porcine MHC class I expression by inhibition of transporter associated with antigen processing (TAP). J Immunol **164:**93-9.
8. **Arbeit, R. D., J. A. Zaia, M. A. Valerio, and M. J. Levin.** 1982. Infection of human peripheral blood mononuclear cells by varicella-zoster virus. Intervirology **18:**56-65.
9. **Arvin, A. M.** 2002. Antiviral therapy for varicella and herpes zoster. Semin Pediatr Infect Dis **13:**12-21.
10. **Arvin, A. M.** 2006. Investigations of the pathogenesis of Varicella zoster virus infection in the SCIDhu mouse model. Herpes **13:**75-80.
11. **Arvin, A. M.** 1996. Varicella-zoster virus: overview and clinical manifestations. Semin Dermatol **15:**4-7.
12. **Arvin, A. M., M. Sharp, M. Moir, P. R. Kinchington, M. Sadeghi-Zadeh, W. T. Ruyechan, and J. Hay.** 2002. Memory cytotoxic T cell responses to viral tegument and regulatory proteins encoded by open reading frames 4, 10, 29, and 62 of varicella-zoster virus. Viral Immunol **15:**507-16.

13. **Aubert, M., E. M. Krantz, and K. R. Jerome.** 2006. Herpes simplex virus genes Us3, Us5, and Us12 differentially regulate cytotoxic T lymphocyte-induced cytotoxicity. Viral Immunol **19:**391-408.
14. **Baiker, A., C. Bagowski, H. Ito, M. Sommer, L. Zerboni, K. Fabel, J. Hay, W. Ruyechan, and A. M. Arvin.** 2004. The immediate-early 63 protein of Varicella-Zoster virus: analysis of functional domains required for replication in vitro and for T-cell and skin tropism in the SCIDhu model in vivo. J Virol **78:**1181-94.
15. **Baudoux, L., P. Defechereux, S. Schoonbroodt, M. P. Merville, B. Rentier, and J. Piette.** 1995. Mutational analysis of varicella-zoster virus major immediate-early protein IE62. Nucleic Acids Res **23:**1341-9.
16. **Bechtel, J., A. Grundhoff, and D. Ganem.** 2005. RNAs in the virion of Kaposi's sarcoma-associated herpesvirus. J Virol **79:**10138-46.
17. **Bechtel, J. T., R. C. Winant, and D. Ganem.** 2005. Host and viral proteins in the virion of Kaposi's sarcoma-associated herpesvirus. J Virol **79:**4952-64.
18. **Benetti, L., J. Munger, and B. Roizman.** 2003. The herpes simplex virus 1 US3 protein kinase blocks caspase-dependent double cleavage and activation of the proapoptotic protein BAD. J Virol **77:**6567-73.
19. **Benetti, L., and B. Roizman.** 2004. Herpes simplex virus protein kinase US3 activates and functionally overlaps protein kinase A to block apoptosis. Proc Natl Acad Sci U S A **101:**9411-6.
20. **Bennett, E. M., J. R. Bennink, J. W. Yewdell, and F. M. Brodsky.** 1999. Cutting edge: adenovirus E19 has two mechanisms for affecting class I MHC expression. J Immunol **162:**5049-52.
21. **Besser, J., M. Ikoma, K. Fabel, M. H. Sommer, L. Zerboni, C. Grose, and A. M. Arvin.** 2004. Differential requirement for cell fusion and virion formation in the pathogenesis of varicella-zoster virus infection in skin and T cells. J Virol **78:**13293-305.
22. **Besser, J., M. H. Sommer, L. Zerboni, C. P. Bagowski, H. Ito, J. Moffat, C. C. Ku, and A. M. Arvin.** 2003. Differentiation of varicella-zoster virus ORF47 protein kinase and IE62 protein binding domains and their contributions to replication in human skin xenografts in the SCID-hu mouse. J Virol **77:**5964-74.
23. **Betz, J. L., and S. G. Wydoski.** 1993. Functional interaction of varicella zoster virus gene 62 protein with the DNA sequence bound by herpes simplex virus ICP4 protein. Virology **195:**793-7.
24. **Bibor-Hardy, V., and F. Sakr.** 1989. A 165 kd protein of the herpes simplex virion shares a common epitope with the regulatory protein, ICP4. Biochem Biophys Res Commun **163:**124-30.
25. **Black, B. E., J. M. Holaska, F. Rastinejad, and B. M. Paschal.** 2001. DNA binding domains in diverse nuclear receptors function as nuclear export signals. Curr Biol **11:**1749-58.
26. **Boyle, W. J., P. van der Geer, and T. Hunter.** 1991. Phosphopeptide mapping and phosphoamino acid analysis by two-dimensional separation on thin-layer cellulose plates. Methods Enzymol **201:**110-49.
27. **Bresnahan, W. A., and T. Shenk.** 2000. A subset of viral transcripts packaged within human cytomegalovirus particles. Science **288:**2373-6.
28. **Bridges, D., G. B. Moorhead.** 2004. 14-3-3 proteins: a number of functions for a numbered protein. Sci STKE **242:**re10.

29. **Brisson, M., W. J. Edmunds, and N. J. Gay.** 2003. Varicella vaccination: impact of vaccine efficacy on the epidemiology of VZV. J Med Virol **70 Suppl 1:**S31-7.
30. **Capps, G. G., and M. C. Zuniga.** 2000. Phosphorylation of class I MHC molecules in the absence of phorbol esters is an intracellular event and may be characteristic of trafficking molecules. Mol Immunol **37:**59-71.
31. **Carrozza, M. J., and N. A. DeLuca.** 1996. Interaction of the viral activator protein ICP4 with TFIID through TAF250. Mol Cell Biol **16:**3085-93.
32. **Cartier, A., T. Komai, and M. G. Masucci.** 2003. The Us3 protein kinase of herpes simplex virus 1 blocks apoptosis and induces phosporylation of the Bcl-2 family member Bad. Exp Cell Res **291:**242-50.
33. **CDC.** 2007. Varicella. *In* H. J. Atkinson W, McIntyre L, Wolfe S (ed.), Epidemiology and Prevention of Vaccine-Preventable Diseases. Public Health Foundation, Washington DC.
34. **Che, X., L. Zerboni, M. H. Sommer, and A. M. Arvin.** 2006. Varicella-zoster virus open reading frame 10 is a virulence determinant in skin cells but not in T cells in vivo. J Virol **80:**3238-48.
35. **Chee, A. V., and B. Roizman.** 2004. Herpes simplex virus 1 gene products occlude the interferon signaling pathway at multiple sites. J Virol **78:**4185-96.
36. **Chen, I. H., K. S. Sciabica, and R. M. Sandri-Goldin.** 2002. ICP27 interacts with the RNA export factor Aly/REF to direct herpes simplex virus type 1 intronless mRNAs to the TAP export pathway. J Virol **76:**12877-89.
37. **Cilloniz, C., W. Jackson, C. Grose, D. Czechowski, J. Hay, and W. T. Ruyechan.** 2007. The varicella-zoster virus (VZV) ORF9 protein interacts with the IE62 major VZV transactivator. J Virol **81:**761-74.
38. **Cohen, J. I.** 1998. Infection of cells with varicella-zoster virus down-regulates surface expression of class I major histocompatibility complex antigens. J Infect Dis **177:**1390-3.
39. **Cohen, J. I.** 2001. Mutagenesis of the varicella-zoster virus genome: lessons learned. Arch Virol Suppl**:**91-7.
40. **Cohen, J. I., D. Heffel, and K. Seidel.** 1993. The transcriptional activation domain of varicella-zoster virus open reading frame 62 protein is not conserved with its herpes simplex virus homolog. J Virol **67:**4246-51.
41. **Cohen, J. I., S. E. Straus, A. M. Arvin.** 2007. Varicella-Zoster Virus, p. 2773-2818. *In* D. M. Knipe, P.M. Howley (ed.), Fields Virology, vol. 2. Wolters Kluwer/Lippincott Williams & Wilkens, Philadelphia.
42. **Cohen, J. I., and K. Seidel.** 1994. Varicella-zoster virus (VZV) open reading frame 10 protein, the homolog of the essential herpes simplex virus protein VP16, is dispensable for VZV replication in vitro. J Virol **68:**7850-8.
43. **Cohen, J. I., and K. E. Seidel.** 1993. Generation of varicella-zoster virus (VZV) and viral mutants from cosmid DNAs: VZV thymidylate synthetase is not essential for replication in vitro. Proc Natl Acad Sci U S A **90:**7376-80.
44. **Cohrs, R. J., and D. H. Gilden.** 2007. Prevalence and abundance of latently transcribed varicella-zoster virus genes in human ganglia. J Virol **81:**2950-6.
45. **Cohrs, R. J., D. H. Gilden, P. R. Kinchington, E. Grinfeld, and P. G. Kennedy.** 2003. Varicella-zoster virus gene 66 transcription and translation in latently infected human Ganglia. J Virol **77:**6660-5.

46. **Cohrs, R. J., J. Wischer, C. Essman, and D. H. Gilden.** 2002. Characterization of varicella-zoster virus gene 21 and 29 proteins in infected cells. J Virol **76:**7228-38.
47. **Daikoku, T., Y. Yamashita, T. Tsurumi, K. Maeno, and Y. Nishiyama.** 1993. Purification and biochemical characterization of the protein kinase encoded by the US3 gene of herpes simplex virus type 2. Virology **197:**685-94.
48. **Davison, A. J., and J. E. Scott.** 1986. The complete DNA sequence of varicella-zoster virus. J Gen Virol **67 (Pt 9):**1759-816.
49. **de Jong, M. D., J. F. Weel, T. Schuurman, P. M. Wertheim-van Dillen, and R. Boom.** 2000. Quantitation of varicella-zoster virus DNA in whole blood, plasma, and serum by PCR and electrochemiluminescence. J Clin Microbiol **38:**2568-73.
50. **Debrus, S., C. Sadzot-Delvaux, A. F. Nikkels, J. Piette, and B. Rentier.** 1995. Varicella-zoster virus gene 63 encodes an immediate-early protein that is abundantly expressed during latency. J Virol **69:**3240-5.
51. **Decman, V., P. R. Kinchington, S. A. Harvey, and R. L. Hendricks.** 2005. Gamma interferon can block herpes simplex virus type 1 reactivation from latency, even in the presence of late gene expression. J Virol **79:**10339-47.
52. **Defechereux, P., S. Debrus, L. Baudoux, B. Rentier, and J. Piette.** 1997. Varicella-zoster virus open reading frame 4 encodes an immediate-early protein with posttranscriptional regulatory properties. J Virol **71:**7073-9.
53. **Deruelle, M., K. Geenen, H. J. Nauwynck, and H. W. Favoreel.** 2007. A point mutation in the putative ATP binding site of the pseudorabies virus US3 protein kinase prevents Bad phosphorylation and cell survival following apoptosis induction. Virus Res.
54. **Disney, G. H., and R. D. Everett.** 1990. A herpes simplex virus type 1 recombinant with both copies of the Vmw175 coding sequences replaced by the homologous varicella-zoster virus open reading frame. J Gen Virol **71 (Pt 11):**2681-9.
55. **Disney, G. H., T. A. McKee, C. M. Preston, and R. D. Everett.** 1990. The product of varicella-zoster virus gene 62 autoregulates its own promoter. J Gen Virol **71 (Pt 12):**2999-3003.
56. **Duerst, R. J., and L. A. Morrison.** 2004. Herpes simplex virus 2 virion host shutoff protein interferes with type I interferon production and responsiveness. Virology **322:**158-67.
57. **Eichholtz, T., P. Vossebeld, M. van Overveld, and H. Ploegh.** 1992. Activation of protein kinase C accelerates internalization of transferrin receptor but not of major histocompatibility complex class I, independent of their phosphorylation status. J Biol Chem **267:**22490-5.
58. **Eisfeld, A. J., S. E. Turse, S. A. Jackson, E. C. Lerner, and P. R. Kinchington.** 2006. Phosphorylation of the varicella-zoster virus (VZV) major transcriptional regulatory protein IE62 by the VZV open reading frame 66 protein kinase. J Virol **80:**1710-23.
59. **Eisfeld, A. J., M. B. Yee, A. Erazo, A. Abendroth, and P. R. Kinchington.** 2007. Downregulation of Class I Major Histocompatibility Complex Surface Expression by Varicella-Zoster Virus Involves Open Reading Frame 66 Protein Kinase Dependent and Independent Mechanisms. J Virol.
60. **Elgadi, M. M., and J. R. Smiley.** 1999. Picornavirus internal ribosome entry site elements target RNA cleavage events induced by the herpes simplex virus virion host shutoff protein. J Virol **73:**9222-31.
61. **Erazo, A., M. B. Yee, N. Osterreider, P. R. Kinchington.** In preparation.

62. **Everett, R. D., and J. Murray.** 2005. ND10 components relocate to sites associated with herpes simplex virus type 1 nucleoprotein complexes during virus infection. J Virol **79:**5078-89.
63. **Favoreel, H. W., G. Van Minnebruggen, D. Adriaensen, and H. J. Nauwynck.** 2005. Cytoskeletal rearrangements and cell extensions induced by the US3 kinase of an alphaherpesvirus are associated with enhanced spread. Proc Natl Acad Sci U S A **102:**8990-5.
64. **Felser, J. M., P. R. Kinchington, G. Inchauspe, S. E. Straus, and J. M. Ostrove.** 1988. Cell lines containing varicella-zoster virus open reading frame 62 and expressing the "IE" 175 protein complement ICP4 mutants of herpes simplex virus type 1. J Virol **62:**2076-82.
65. **Fenaroli, A., M. Vujanac, D. De Cesare, and V. Zimarino.** 2004. A small-scale survey identifies selective and quantitative nucleo-cytoplasmic shuttling of a subset of CREM transcription factors. Exp Cell Res **299:**209-26.
66. **Feng, P., D. N. Everly, Jr., and G. S. Read.** 2005. mRNA decay during herpes simplex virus (HSV) infections: protein-protein interactions involving the HSV virion host shutoff protein and translation factors eIF4H and eIF4A. J Virol **79:**9651-64.
67. **Forghani, B., R. Mahalingam, A. Vafai, J. W. Hurst, and K. W. Dupuis.** 1990. Monoclonal antibody to immediate early protein encoded by varicella-zoster virus gene 62. Virus Res **16:**195-210.
68. **Fruh, K., K. Ahn, H. Djaballah, P. Sempe, P. M. van Endert, R. Tampe, P. A. Peterson, and Y. Yang.** 1995. A viral inhibitor of peptide transporters for antigen presentation. Nature **375:**415-8.
69. **Furman, M. H., N. Dey, D. Tortorella, and H. L. Ploegh.** 2002. The human cytomegalovirus US10 gene product delays trafficking of major histocompatibility complex class I molecules. J Virol **76:**11753-6.
70. **Galluzzi, K. E.** 2007. Management strategies for herpes zoster and postherpetic neuralgia. J Am Osteopath Assoc **107:**S8-S13.
71. **Galvan, V., and B. Roizman.** 1998. Herpes simplex virus 1 induces and blocks apoptosis at multiple steps during infection and protects cells from exogenous inducers in a cell-type-dependent manner. Proc Natl Acad Sci U S A **95:**3931-6.
72. **Garcia-Valcarcel, M., W. J. Fowler, D. R. Harper, D. J. Jeffries, and G. T. Layton.** 1997. Cloning, expression, and immunogenicity of the assembly protein of varicella-zoster virus and detection of the products of open reading frame 33. J Med Virol **53:**332-9.
73. **Ge, R., X. Liu, and R. P. Ricciardi.** 1994. E1A oncogene of adenovirus-12 mediates trans-repression of MHC class I transcription in Ad5/Ad12 somatic hybrid transformed cells. Virology **203:**389-92.
74. **Geenen, K., H. W. Favoreel, L. Olsen, L. W. Enquist, and H. J. Nauwynck.** 2005. The pseudorabies virus US3 protein kinase possesses anti-apoptotic activity that protects cells from apoptosis during infection and after treatment with sorbitol or staurosporine. Virology **331:**144-50.
75. **Geer, L. Y., M. Domrachev, D. J. Lipman, and S. H. Bryant.** 2002. CDART: protein homology by domain architecture. Genome Res **12:**1619-23.

76. **Geiss, B. J., T. J. Smith, D. A. Leib, and L. A. Morrison.** 2000. Disruption of virion host shutoff activity improves the immunogenicity and protective capacity of a replication-incompetent herpes simplex virus type 1 vaccine strain. J Virol **74:**11137-44.
77. **Gershon, A. A.** 2001. Prevention and treatment of VZV infections in patients with HIV. Herpes **8:**32-36.
78. **Gershon, A. A.** 2003. Varicella vaccine: rare serious problems--but the benefits still outweigh the risks. J Infect Dis **188:**945-7.
79. **Gershon, A. A., D. L. Sherman, Z. Zhu, C. A. Gabel, R. T. Ambron, and M. D. Gershon.** 1994. Intracellular transport of newly synthesized varicella-zoster virus: final envelopment in the trans-Golgi network. J Virol **68:**6372-90.
80. **Gilden, D. H., A. R. Hayward, J. Krupp, M. Hunter-Laszlo, J. C. Huff, and A. Vafai.** 1987. Varicella-zoster virus infection of human mononuclear cells. Virus Res **7:**117-29.
81. **Goldman, G. S.** 2005. Universal varicella vaccination: efficacy trends and effect on herpes zoster. Int J Toxicol **24:**205-13.
82. **Gopinath, R. S., A. P. Ambagala, S. Hinkley, and S. Srikumaran.** 2002. Effects of virion host shut-off activity of bovine herpesvirus 1 on MHC class I expression. Viral Immunol **15:**595-608.
83. **Grinfeld, E., and P. G. Kennedy.** 2004. Translation of varicella-zoster virus genes during human ganglionic latency. Virus Genes **29:**317-9.
84. **Gu, H., Y. Liang, G. Mandel, and B. Roizman.** 2005. Components of the REST/CoREST/histone deacetylase repressor complex are disrupted, modified, and translocated in HSV-1-infected cells. Proc Natl Acad Sci U S A **102:**7571-6.
85. **Guild, B. C., and J. L. Strominger.** 1984. HLA-A2 antigen phosphorylation in vitro by cyclic AMP-dependent protein kinase. Sites of phosphorylation and segmentation in class i major histocompatibility complex gene structure. J Biol Chem **259:**13504-10.
86. **Hanks, S. K., and A. M. Quinn.** 1991. Protein kinase catalytic domain sequence database: identification of conserved features of primary structure and classification of family members. Methods Enzymol **200:**38-62.
87. **Hanks, S. K., A. M. Quinn, and T. Hunter.** 1988. The protein kinase family: conserved features and deduced phylogeny of the catalytic domains. Science **241:**42-52.
88. **Harreman, M. T., T. M. Kline, H. G. Milford, M. B. Harben, A. E. Hodel, and A. H. Corbett.** 2004. Regulation of nuclear import by phosphorylation adjacent to nuclear localization signals. J Biol Chem **279:**20613-21.
89. **Harson, R., and C. Grose.** 1995. Egress of varicella-zoster virus from the melanoma cell: a tropism for the melanocyte. J Virol **69:**4994-5010.
90. **Heineman, T. C., and J. I. Cohen.** 1995. The varicella-zoster virus (VZV) open reading frame 47 (ORF47) protein kinase is dispensable for viral replication and is not required for phosphorylation of ORF63 protein, the VZV homolog of herpes simplex virus ICP22. J Virol **69:**7367-70.
91. **Heineman, T. C., K. Seidel, and J. I. Cohen.** 1996. The varicella-zoster virus ORF66 protein induces kinase activity and is dispensable for viral replication. J Virol **70:**7312-7.
92. **Heininger, U., and J. F. Seward.** 2006. Varicella. Lancet **368:**1365-76.
93. **Hengel, H., J. O. Koopmann, T. Flohr, W. Muranyi, E. Goulmy, G. J. Hammerling, U. H. Koszinowski, and F. Momburg.** 1997. A viral ER-resident glycoprotein inactivates the MHC-encoded peptide transporter. Immunity **6:**623-32.

94. **Hengel, H., U. Reusch, A. Gutermann, H. Ziegler, S. Jonjic, P. Lucin, and U. H. Koszinowski.** 1999. Cytomegaloviral control of MHC class I function in the mouse. Immunol Rev **168:**167-76.
95. **Hewitt, E. W.** 2003. The MHC class I antigen presentation pathway: strategies for viral immune evasion. Immunology **110:**163-9.
96. **Hill, A., P. Jugovic, I. York, G. Russ, J. Bennink, J. Yewdell, H. Ploegh, and D. Johnson.** 1995. Herpes simplex virus turns off the TAP to evade host immunity. Nature **375:**411-5.
97. **Hill, A. B., B. C. Barnett, A. J. McMichael, and D. J. McGeoch.** 1994. HLA class I molecules are not transported to the cell surface in cells infected with herpes simplex virus types 1 and 2. J Immunol **152:**2736-41.
98. **Holaska, J. M., B. E. Black, D. C. Love, J. A. Hanover, J. Leszyk, and B. M. Paschal.** 2001. Calreticulin Is a receptor for nuclear export. J Cell Biol **152:**127-40.
99. **Holaska, J. M., B. E. Black, F. Rastinejad, and B. M. Paschal.** 2002. Ca2+-dependent nuclear export mediated by calreticulin. Mol Cell Biol **22:**6286-97.
100. **Honess, R. W., and B. Roizman.** 1974. Regulation of herpesvirus macromolecular synthesis. I. Cascade regulation of the synthesis of three groups of viral proteins. J Virol **14:**8-19.
101. **Honess, R. W., and B. Roizman.** 1975. Regulation of herpesvirus macromolecular synthesis: sequential transition of polypeptide synthesis requires functional viral polypeptides. Proc Natl Acad Sci U S A **72:**1276-80.
102. **Hope-Simpson, R. E.** 1965. The Nature of Herpes Zoster: a Long-Term Study and a New Hypothesis. Proc R Soc Med **58:**9-20.
103. **Horton, R. M., Z. L. Cai, S. N. Ho, and L. R. Pease.** 1990. Gene splicing by overlap extension: tailor-made genes using the polymerase chain reaction. Biotechniques **8:**528-35.
104. **Hozak, P.** 1996. The nucleoskeleton and attached activities. Exp Cell Res **229:**267-71.
105. **Hu, H., and J. I. Cohen.** 2005. Varicella-zoster virus open reading frame 47 (ORF47) protein is critical for virus replication in dendritic cells and for spread to other cells. Virology **337:**304-11.
106. **Hufner, K., T. Derfuss, S. Herberger, K. Sunami, S. Russell, I. Sinicina, V. Arbusow, M. Strupp, T. Brandt, and D. Theil.** 2006. Latency of alpha-herpes viruses is accompanied by a chronic inflammation in human trigeminal ganglia but not in dorsal root ganglia. J Neuropathol Exp Neurol **65:**1022-30.
107. **Ito, H., M. H. Sommer, L. Zerboni, A. Baiker, B. Sato, R. Liang, J. Hay, W. Ruyechan, and A. M. Arvin.** 2005. Role of the varicella-zoster virus gene product encoded by open reading frame 35 in viral replication in vitro and in differentiated human skin and T cells in vivo. J Virol **79:**4819-27.
108. **Ito, Y., H. Kimura, S. Hara, S. Kido, T. Ozaki, Y. Nishiyama, and T. Morishima.** 2001. Investigation of varicella-zoster virus DNA in lymphocyte subpopulations by quantitative PCR assay. Microbiol Immunol **45:**267-9.
109. **Jans, D. A., M. J. Ackermann, J. R. Bischoff, D. H. Beach, and R. Peters.** 1991. p34cdc2-mediated phosphorylation at T124 inhibits nuclear import of SV-40 T antigen proteins. J Cell Biol **115:**1203-12.
110. **Jans, D. A., and S. Hubner.** 1996. Regulation of protein transport to the nucleus: central role of phosphorylation. Physiol Rev **76:**651-85.

111. **Jans, D. A., C. Y. Xiao, and M. H. Lam.** 2000. Nuclear targeting signal recognition: a key control point in nuclear transport? Bioessays **22:**532-44.
112. **Jerome, K. R., R. Fox, Z. Chen, A. E. Sears, H. Lee, and L. Corey.** 1999. Herpes simplex virus inhibits apoptosis through the action of two genes, Us5 and Us3. J Virol **73:**8950-7.
113. **Jons, A., J. M. Dijkstra, and T. C. Mettenleiter.** 1998. Glycoproteins M and N of pseudorabies virus form a disulfide-linked complex. J Virol **72:**550-7.
114. **Kasper, M. R., and K. L. Collins.** 2003. Nef-mediated disruption of HLA-A2 transport to the cell surface in T cells. J Virol **77:**3041-9.
115. **Kasper, M. R., J. F. Roeth, M. Williams, T. M. Filzen, R. I. Fleis, and K. L. Collins.** 2005. HIV-1 Nef disrupts antigen presentation early in the secretory pathway. J Biol Chem **280:**12840-8.
116. **Katan, M., W. S. Stevely, and D. P. Leader.** 1985. Partial purification and characterization of a new phosphoprotein kinase from cells infected with pseudorabies virus. Eur J Biochem **152:**57-65.
117. **Kato, A., M. Yamamoto, T. Ohno, H. Kodaira, Y. Nishiyama, and Y. Kawaguchi.** 2005. Identification of proteins phosphorylated directly by the Us3 protein kinase encoded by herpes simplex virus 1. J Virol **79:**9325-31.
118. **Kennedy, P. G.** 2002. Key issues in varicella-zoster virus latency. J Neurovirol **8 Suppl 2:**80-4.
119. **Kenyon, T. K., J. I. Cohen, and C. Grose.** 2002. Phosphorylation by the varicella-zoster virus ORF47 protein serine kinase determines whether endocytosed viral gE traffics to the trans-Golgi network or recycles to the cell membrane. J Virol **76:**10980-93.
120. **Kenyon, T. K., E. Homan, J. Storlie, M. Ikoma, and C. Grose.** 2003. Comparison of varicella-zoster virus ORF47 protein kinase and casein kinase II and their substrates. J Med Virol **70 Suppl 1:**S95-102.
121. **Kenyon, T. K., J. Lynch, J. Hay, W. Ruyechan, and C. Grose.** 2001. Varicella-zoster virus ORF47 protein serine kinase: characterization of a cloned, biologically active phosphotransferase and two viral substrates, ORF62 and ORF63. J Virol **75:**8854-8.
122. **Kinchington, P. R., D. Bookey, and S. E. Turse.** 1995. The transcriptional regulatory proteins encoded by varicella-zoster virus open reading frames (ORFs) 4 and 63, but not ORF 61, are associated with purified virus particles. J Virol **69:**4274-82.
123. **Kinchington, P. R., K. Fite, A. Seman, and S. E. Turse.** 2001. Virion association of IE62, the varicella-zoster virus (VZV) major transcriptional regulatory protein, requires expression of the VZV open reading frame 66 protein kinase. J Virol **75:**9106-13.
124. **Kinchington, P. R., K. Fite, and S. E. Turse.** 2000. Nuclear accumulation of IE62, the varicella-zoster virus (VZV) major transcriptional regulatory protein, is inhibited by phosphorylation mediated by the VZV open reading frame 66 protein kinase. J Virol **74:**2265-77.
125. **Kinchington, P. R., J. K. Hougland, A. M. Arvin, W. T. Ruyechan, and J. Hay.** 1992. The varicella-zoster virus immediate-early protein IE62 is a major component of virus particles. J Virol **66:**359-66.
126. **Kinchington, P. R., G. Inchauspe, J. H. Subak-Sharpe, F. Robey, J. Hay, and W. T. Ruyechan.** 1988. Identification and characterization of a varicella-zoster virus DNA-binding protein by using antisera directed against a predicted synthetic oligopeptide. J Virol **62:**802-9.

127. **Kinchington, P. R., J. I. Cohen.** 2000. Varicella zoster virus proteins, p. 74-104. *In* A. M. Arvin, A. A. Gershon (ed.), Varicella zoster virus: virology and clinical management. Oxford Press, Oxford, United Kingdom.
128. **Kinchington, P. R., W. C. Reinhold, T. A. Casey, S. E. Straus, J. Hay, and W. T. Ruyechan.** 1985. Inversion and circularization of the varicella-zoster virus genome. J Virol **56:**194-200.
129. **Kinchington, P. R., and S. E. Turse.** 1998. Regulated nuclear localization of the varicella-zoster virus major regulatory protein, IE62. J Infect Dis **178 Suppl 1:**S16-21.
130. **Kleinschmidt-DeMasters, B. K., and D. H. Gilden.** 2001. The expanding spectrum of herpesvirus infections of the nervous system. Brain Pathol **11:**440-51.
131. **Klupp, B. G., H. Granzow, and T. C. Mettenleiter.** 2001. Effect of the pseudorabies virus US3 protein on nuclear membrane localization of the UL34 protein and virus egress from the nucleus. J Gen Virol **82:**2363-71.
132. **Koch, J., and R. Tampe.** 2006. The macromolecular peptide-loading complex in MHC class I-dependent antigen presentation. Cell Mol Life Sci **63:**653-62.
133. **Koenig, A., and M. H. Wolff.** 2003. Infectibility of separated peripheral blood mononuclear cell subpopulations by varicella-zoster virus (VZV). J Med Virol **70 Suppl 1:**S59-63.
134. **Koppers-Lalic, D., E. A. Reits, M. E. Ressing, A. D. Lipinska, R. Abele, J. Koch, M. Marcondes Rezende, P. Admiraal, D. van Leeuwen, K. Bienkowska-Szewczyk, T. C. Mettenleiter, F. A. Rijsewijk, R. Tampe, J. Neefjes, and E. J. Wiertz.** 2005. Varicelloviruses avoid T cell recognition by UL49.5-mediated inactivation of the transporter associated with antigen processing. Proc Natl Acad Sci U S A **102:**5144-9.
135. **Koppers-Lalic, D., F. A. Rijsewijk, S. B. Verschuren, J. A. van Gaans-Van den Brink, A. Neisig, M. E. Ressing, J. Neefjes, and E. J. Wiertz.** 2001. The UL41-encoded virion host shutoff (vhs) protein and vhs-independent mechanisms are responsible for down-regulation of MHC class I molecules by bovine herpesvirus 1. J Gen Virol **82:**2071-81.
136. **Koppers-Lalic, D., M. Rychlowski, D. van Leeuwen, F. A. Rijsewijk, M. E. Ressing, J. J. Neefjes, K. Bienkowska-Szewczyk, and E. J. Wiertz.** 2003. Bovine herpesvirus 1 interferes with TAP-dependent peptide transport and intracellular trafficking of MHC class I molecules in human cells. Arch Virol **148:**2023-37.
137. **Ku, C. C., J. Besser, A. Abendroth, C. Grose, and A. M. Arvin.** 2005. Varicella-Zoster virus pathogenesis and immunobiology: new concepts emerging from investigations with the SCIDhu mouse model. J Virol **79:**2651-8.
138. **Ku, C. C., J. A. Padilla, C. Grose, E. C. Butcher, and A. M. Arvin.** 2002. Tropism of varicella-zoster virus for human tonsillar CD4(+) T lymphocytes that express activation, memory, and skin homing markers. J Virol **76:**11425-33.
139. **Ku, C. C., L. Zerboni, H. Ito, B. S. Graham, M. Wallace, and A. M. Arvin.** 2004. Varicella-zoster virus transfer to skin by T Cells and modulation of viral replication by epidermal cell interferon-alpha. J Exp Med **200:**917-25.
140. **Kutay, U., and S. Guttinger.** 2005. Leucine-rich nuclear-export signals: born to be weak. Trends Cell Biol **15:**121-4.
141. **Kwong, A. D., J. A. Kruper, and N. Frenkel.** 1988. Herpes simplex virus virion host shutoff function. J Virol **62:**912-21.

142. **Lam, M. H., L. J. Briggs, W. Hu, T. J. Martin, M. T. Gillespie, and D. A. Jans.** 1999. Importin beta recognizes parathyroid hormone-related protein with high affinity and mediates its nuclear import in the absence of importin alpha. J Biol Chem **274:**7391-8.
143. **Lange, A., R. E. Mills, C. J. Lange, M. Stewart, S. E. Devine, and A. H. Corbett.** 2007. Classical nuclear localization signals: definition, function, and interaction with importin alpha. J Biol Chem **282:**5101-5.
144. **Leach, N., S. L. Bjerke, D. K. Christenson, J. M. Bouchard, F. Mou, R. Park, J. Baines, T. Haraguchi, and R. J. Roller.** 2007. Emerin is hyperphosphorylated and redistributed in herpes simplex virus type 1-infected cells in a manner dependent upon both UL34 and US3. J Virol.
145. **Leader, D. P., A. D. Deana, F. Marchiori, F. C. Purves, and L. A. Pinna.** 1991. Further definition of the substrate specificity of the alpha-herpesvirus protein kinase and comparison with protein kinases A and C. Biochim Biophys Acta **1091:**426-31.
146. **Lehner, P. J., and P. Cresswell.** 2004. Recent developments in MHC-class-I-mediated antigen presentation. Curr Opin Immunol **16:**82-9.
147. **Lehner, P. J., S. Hoer, R. Dodd, and L. M. Duncan.** 2005. Downregulation of cell surface receptors by the K3 family of viral and cellular ubiquitin E3 ligases. Immunol Rev **207:**112-25.
148. **Lehner, P. J., J. T. Karttunen, G. W. Wilkinson, and P. Cresswell.** 1997. The human cytomegalovirus US6 glycoprotein inhibits transporter associated with antigen processing-dependent peptide translocation. Proc Natl Acad Sci U S A **94:**6904-9.
149. **Leopardi, R., C. Van Sant, and B. Roizman.** 1997. The herpes simplex virus 1 protein kinase US3 is required for protection from apoptosis induced by the virus. Proc Natl Acad Sci U S A **94:**7891-6.
150. **Li, Q., M. A. Ali, and J. I. Cohen.** 2006. Insulin degrading enzyme is a cellular receptor mediating varicella-zoster virus infection and cell-to-cell spread. Cell **127:**305-16.
151. **Li, Q., T. Krogmann, M. A. Ali, W. J. Tang, and J. I. Cohen.** 2007. The amino terminus of varicella-zoster virus (VZV) glycoprotein E is required for binding to insulin-degrading enzyme, a VZV receptor. J Virol **81:**8525-32.
152. **Li, Y., L. Salter-Cid, A. Vitiello, T. Preckel, J. D. Lee, A. Angulo, Z. Cai, P. A. Peterson, and Y. Yang.** 2000. Regulation of transporter associated with antigen processing by phosphorylation. J Biol Chem **275:**24130-5.
153. **Lilley, B. N., and H. L. Ploegh.** 2005. Viral modulation of antigen presentation: manipulation of cellular targets in the ER and beyond. Immunol Rev **207:**126-44.
154. **Lippe, R., E. Luke, Y. T. Kuah, C. Lomas, and W. A. Jefferies.** 1991. Adenovirus infection inhibits the phosphorylation of major histocompatibility complex class I proteins. J Exp Med **174:**1159-66.
155. **Lodoen, M. B., and L. L. Lanier.** 2005. Viral modulation of NK cell immunity. Nat Rev Microbiol **3:**59-69.
156. **Lungu, O., C. A. Panagiotidis, P. W. Annunziato, A. A. Gershon, and S. J. Silverstein.** 1998. Aberrant intracellular localization of Varicella-Zoster virus regulatory proteins during latency. Proc Natl Acad Sci U S A **95:**7080-5.
157. **Lynch, J. M., T. K. Kenyon, C. Grose, J. Hay, and W. T. Ruyechan.** 2002. Physical and functional interaction between the varicella zoster virus IE63 and IE62 proteins. Virology **302:**71-82.

158. **Mainka, C., B. Fuss, H. Geiger, H. Hofelmayr, and M. H. Wolff.** 1998. Characterization of viremia at different stages of varicella-zoster virus infection. J Med Virol **56:**91-8.
159. **Malik, P., D. J. Blackbourn, and J. B. Clements.** 2004. The evolutionarily conserved Kaposi's sarcoma-associated herpesvirus ORF57 protein interacts with REF protein and acts as an RNA export factor. J Biol Chem **279:**33001-11.
160. **Malmgaard, L.** 2004. Induction and regulation of IFNs during viral infections. J Interferon Cytokine Res **24:**439-54.
161. **McGeoch, D. J.** 1989. The genomes of the human herpesviruses: contents, relationships, and evolution. Annu Rev Microbiol **43:**235-65.
162. **McGeoch, D. J., M. A. Dalrymple, A. J. Davison, A. Dolan, M. C. Frame, D. McNab, L. J. Perry, J. E. Scott, and P. Taylor.** 1988. The complete DNA sequence of the long unique region in the genome of herpes simplex virus type 1. J Gen Virol **69 (Pt 7):**1531-74.
163. **McGeoch, D. J., A. Dolan, S. Donald, and D. H. Brauer.** 1986. Complete DNA sequence of the short repeat region in the genome of herpes simplex virus type 1. Nucleic Acids Res **14:**1727-45.
164. **McKee, T. A., G. H. Disney, R. D. Everett, and C. M. Preston.** 1990. Control of expression of the varicella-zoster virus major immediate early gene. J Gen Virol **71 (Pt 4):**897-906.
165. **McMillan, D. J., J. Kay, and J. S. Mills.** 1997. Characterization of the proteinase specified by varicella-zoster virus gene 33. J Gen Virol **78 (Pt 9):**2153-7.
166. **Meggio, F., Pinna L.A.** 2003. One-thousant-and-one substrates of protein kinase CK2? FASEB J **17:**349-368.
167. **Milikan, J. C., P. R. Kinchington, G. S. Baarsma, R. W. Kuijpers, A. D. Osterhaus, and G. M. Verjans.** 2007. Identification of viral antigens recognized by ocular infiltrating T cells from patients with varicella zoster virus-induced uveitis. Invest Ophthalmol Vis Sci **48:**3689-97.
168. **Milikan, J. C., R. W. Kuijpers, G. S. Baarsma, A. D. Osterhaus, and G. M. Verjans.** 2006. Characterization of the varicella zoster virus (VZV)-specific intra-ocular T-cell response in patients with VZV-induced uveitis. Exp Eye Res **83:**69-75.
169. **Miserocchi, E., N. K. Waheed, E. Dios, W. Christen, J. Merayo, M. Roque, and C. S. Foster.** 2002. Visual outcome in herpes simplex virus and varicella zoster virus uveitis: a clinical evaluation and comparison. Ophthalmology **109:**1532-7.
170. **Mitchell, B. M., D. C. Bloom, R. J. Cohrs, D. H. Gilden, and P. G. Kennedy.** 2003. Herpes simplex virus-1 and varicella-zoster virus latency in ganglia. J Neurovirol **9:**194-204.
171. **Mo, C., J. Lee, M. H. Sommer, and A. M. Arvin.** 2003. Varicella-zoster virus infection facilitates VZV glycoprotein E trafficking to the membrane surface of melanoma cells. J Med Virol **70 Suppl 1:**S56-8.
172. **Moffat, J., C. Mo, J. J. Cheng, M. Sommer, L. Zerboni, S. Stamatis, and A. M. Arvin.** 2004. Functions of the C-terminal domain of varicella-zoster virus glycoprotein E in viral replication in vitro and skin and T-cell tropism in vivo. J Virol **78:**12406-15.
173. **Moffat, J. F., M. D. Stein, H. Kaneshima, and A. M. Arvin.** 1995. Tropism of varicella-zoster virus for human CD4+ and CD8+ T lymphocytes and epidermal cells in SCID-hu mice. J Virol **69:**5236-42.

174. **Moffat, J. F., L. Zerboni, M. H. Sommer, T. C. Heineman, J. I. Cohen, H. Kaneshima, and A. M. Arvin.** 1998. The ORF47 and ORF66 putative protein kinases of varicella-zoster virus determine tropism for human T cells and skin in the SCID-hu mouse. Proc Natl Acad Sci U S A **95:**11969-74.
175. **Momburg, F., and H. Hengel.** 2002. Corking the bottleneck: the transporter associated with antigen processing as a target for immune subversion by viruses. Curr Top Microbiol Immunol **269:**57-74.
176. **Moriuchi, H., M. Moriuchi, and J. I. Cohen.** 1995. Proteins and cis-acting elements associated with transactivation of the varicella-zoster virus (VZV) immediate-early gene 62 promoter by VZV open reading frame 10 protein. J Virol **69:**4693-701.
177. **Moriuchi, M., H. Moriuchi, S. E. Straus, and J. I. Cohen.** 1994. Varicella-zoster virus (VZV) virion-associated transactivator open reading frame 62 protein enhances the infectivity of VZV DNA. Virology **200:**297-300.
178. **Morris, J. B., H. Hofemeister, and P. O'Hare.** 2007. Herpes simplex virus infection induces phosphorylation and delocalization of emerin, a key inner nuclear membrane protein. J Virol **81:**4429-37.
179. **Morrow, G., B. Slobedman, A. L. Cunningham, and A. Abendroth.** 2003. Varicella-zoster virus productively infects mature dendritic cells and alters their immune function. J Virol **77:**4950-9.
180. **Mosammaparast, N., and L. F. Pemberton.** 2004. Karyopherins: from nuclear-transport mediators to nuclear-function regulators. Trends Cell Biol **14:**547-56.
181. **Mou, F., T. Forest, and J. D. Baines.** 2007. US3 of herpes simplex virus type 1 encodes a promiscuous protein kinase that phosphorylates and alters localization of lamin A/C in infected cells. J Virol **81:**6459-70.
182. **Munger, J., and B. Roizman.** 2001. The US3 protein kinase of herpes simplex virus 1 mediates the posttranslational modification of BAD and prevents BAD-induced programmed cell death in the absence of other viral proteins. Proc Natl Acad Sci U S A **98:**10410-5.
183. **Murphy, J. A., R. J. Duerst, T. J. Smith, and L. A. Morrison.** 2003. Herpes simplex virus type 2 virion host shutoff protein regulates alpha/beta interferon but not adaptive immune responses during primary infection in vivo. J Virol **77:**9337-45.
184. **Nalepa, G., and J. W. Harper.** 2004. Visualization of a highly organized intranuclear network of filaments in living mammalian cells. Cell Motil Cytoskeleton **59:**94-108.
185. **Ng, T. I., and C. Grose.** 1992. Serine protein kinase associated with varicella-zoster virus ORF 47. Virology **191:**9-18.
186. **Ng, T. I., L. Keenan, P. R. Kinchington, and C. Grose.** 1994. Phosphorylation of varicella-zoster virus open reading frame (ORF) 62 regulatory product by viral ORF 47-associated protein kinase. J Virol **68:**1350-9.
187. **Niizuma, T., L. Zerboni, M. H. Sommer, H. Ito, S. Hinchliffe, and A. M. Arvin.** 2003. Construction of varicella-zoster virus recombinants from parent Oka cosmids and demonstration that ORF65 protein is dispensable for infection of human skin and T cells in the SCID-hu mouse model. J Virol **77:**6062-5.
188. **Ogg, P. D., P. J. McDonell, B. J. Ryckman, C. M. Knudson, and R. J. Roller.** 2004. The HSV-1 Us3 protein kinase is sufficient to block apoptosis induced by overexpression of a variety of Bcl-2 family members. Virology **319:**212-24.

189. **Osborne, A. R., T. A. Rapoport, and B. van den Berg.** 2005. Protein translocation by the Sec61/SecY channel. Annu Rev Cell Dev Biol **21:**529-50.
190. **Oxman, M. N., M. J. Levin, G. R. Johnson, K. E. Schmader, S. E. Straus, L. D. Gelb, R. D. Arbeit, M. S. Simberkoff, A. A. Gershon, L. E. Davis, A. Weinberg, K. D. Boardman, H. M. Williams, J. H. Zhang, P. N. Peduzzi, C. E. Beisel, V. A. Morrison, J. C. Guatelli, P. A. Brooks, C. A. Kauffman, C. T. Pachucki, K. M. Neuzil, R. F. Betts, P. F. Wright, M. R. Griffin, P. Brunell, N. E. Soto, A. R. Marques, S. K. Keay, R. P. Goodman, D. J. Cotton, J. W. Gnann, Jr., J. Loutit, M. Holodniy, W. A. Keitel, G. E. Crawford, S. S. Yeh, Z. Lobo, J. F. Toney, R. N. Greenberg, P. M. Keller, R. Harbecke, A. R. Hayward, M. R. Irwin, T. C. Kyriakides, C. Y. Chan, I. S. Chan, W. W. Wang, P. W. Annunziato, and J. L. Silber.** 2005. A vaccine to prevent herpes zoster and postherpetic neuralgia in older adults. N Engl J Med **352:**2271-84.
191. **Park, B., Y. Kim, J. Shin, S. Lee, K. Cho, K. Fruh, S. Lee, and K. Ahn.** 2004. Human cytomegalovirus inhibits tapasin-dependent peptide loading and optimization of the MHC class I peptide cargo for immune evasion. Immunity **20:**71-85.
192. **Pellet, P. E., B. Roizman.** 2007. The Family: Herpesviridae A Brief Introduction, p. 2479-2500. *In* D. M. Knipe, P.M. Howley (ed.), Fields Virology, vol. 2. Wolters Kluwer/Lippincott Williams & Wilkins, Philadelphia.
193. **Pemberton, L. F., and B. M. Paschal.** 2005. Mechanisms of receptor-mediated nuclear import and nuclear export. Traffic **6:**187-98.
194. **Peng, H., H. He, J. Hay, and W. T. Ruyechan.** 2003. Interaction between the varicella zoster virus IE62 major transactivator and cellular transcription factor Sp1. J Biol Chem **278:**38068-75.
195. **Perera, L. P., J. D. Mosca, W. T. Ruyechan, G. S. Hayward, S. E. Straus, and J. Hay.** 1993. A major transactivator of varicella-zoster virus, the immediate-early protein IE62, contains a potent N-terminal activation domain. J Virol **67:**4474-83.
196. **Perera, L. P., J. D. Mosca, M. Sadeghi-Zadeh, W. T. Ruyechan, and J. Hay.** 1992. The varicella-zoster virus immediate early protein, IE62, can positively regulate its cognate promoter. Virology **191:**346-54.
197. **Perry, L. J., and D. J. McGeoch.** 1988. The DNA sequences of the long repeat region and adjoining parts of the long unique region in the genome of herpes simplex virus type 1. J Gen Virol **69 (Pt 11):**2831-46.
198. **Piroozmand, A., A. H. Koyama, Y. Shimada, M. Fujita, T. Arakawa, and A. Adachi.** 2004. Role of Us3 gene of herpes simplex virus type 1 for resistance to interferon. Int J Mol Med **14:**641-5.
199. **Platani, M., I. Goldberg, J. R. Swedlow, and A. I. Lamond.** 2000. In vivo analysis of Cajal body movement, separation, and joining in live human cells. J Cell Biol **151:**1561-74.
200. **Pober, J. S., B. C. Guild, and J. L. Strominger.** 1978. Phosphorylation in vivo and in vitro of human histocompatibility antigens (HLA-A and HLA-B) in the carboxy-terminal intracellular domain. Proc Natl Acad Sci U S A **75:**6002-6.
201. **Poon, A. P., H. Gu, and B. Roizman.** 2006. ICP0 and the US3 protein kinase of herpes simplex virus 1 independently block histone deacetylation to enable gene expression. Proc Natl Acad Sci U S A **103:**9993-8.

202. **Poon, A. P., and B. Roizman.** 2005. Herpes simplex virus 1 ICP22 regulates the accumulation of a shorter mRNA and of a truncated US3 protein kinase that exhibits altered functions. J Virol **79:**8470-9.
203. **Poon, I. K., and D. A. Jans.** 2005. Regulation of nuclear transport: central role in development and transformation? Traffic **6:**173-86.
204. **Preston, V. G., J. Kennard, F. J. Rixon, A. J. Logan, R. W. Mansfield, and I. M. McDougall.** 1997. Efficient herpes simplex virus type 1 (HSV-1) capsid formation directed by the varicella-zoster virus scaffolding protein requires the carboxy-terminal sequences from the HSV-1 homologue. J Gen Virol **78 (Pt 7):**1633-46.
205. **Proffitt, J. L., E. Sharma, and G. E. Blair.** 1994. Adenovirus 12-mediated down-regulation of the major histocompatibility complex (MHC) class I promoter: identification of a negative regulatory element responsive to Ad12 E1A. Nucleic Acids Res **22:**4779-88.
206. **Purves, F. C., A. D. Deana, F. Marchiori, D. P. Leader, and L. A. Pinna.** 1986. The substrate specificity of the protein kinase induced in cells infected with herpesviruses: studies with synthetic substrates [corrected] indicate structural requirements distinct from other protein kinases. Biochim Biophys Acta **889:**208-15.
207. **Purves, F. C., M. Katan, W. S. Stevely, and D. P. Leader.** 1986. Characteristics of the induction of a new protein kinase in cells infected with herpesviruses. J Gen Virol **67 (Pt 6):**1049-57.
208. **Quensel, C., B. Friedrich, T. Sommer, E. Hartmann, and M. Kohler.** 2004. In vivo analysis of importin alpha proteins reveals cellular proliferation inhibition and substrate specificity. Mol Cell Biol **24:**10246-55.
209. **Rahaus, M., N. Desloges, M. Yang, W. T. Ruyechan, and M. H. Wolff.** 2003. Transcription factor USF, expressed during the entire phase of varicella-zoster virus infection, interacts physically with the major viral transactivator IE62 and plays a significant role in virus replication. J Gen Virol **84:**2957-67.
210. **Reits, E., A. Griekspoor, and J. Neefjes.** 2002. Herpes viral proteins manipulating the peptide transporter TAP. Curr Top Microbiol Immunol **269:**75-83.
211. **Ressing, M. E., S. E. Keating, D. van Leeuwen, D. Koppers-Lalic, I. Y. Pappworth, E. J. Wiertz, and M. Rowe.** 2005. Impaired transporter associated with antigen processing-dependent peptide transport during productive EBV infection. J Immunol **174:**6829-38.
212. **Reynolds, A. E., E. G. Wills, R. J. Roller, B. J. Ryckman, and J. D. Baines.** 2002. Ultrastructural localization of the herpes simplex virus type 1 UL31, UL34, and US3 proteins suggests specific roles in primary envelopment and egress of nucleocapsids. J Virol **76:**8939-52.
213. **Rihs, H. P., D. A. Jans, H. Fan, and R. Peters.** 1991. The rate of nuclear cytoplasmic protein transport is determined by the casein kinase II site flanking the nuclear localization sequence of the SV40 T-antigen. Embo J **10:**633-9.
214. **Ruyechan, W., P. Ling, P. Kinchington, J. Hay.** 1991. The correlation between varicella zoster virus transcription and the sequence of the viral genome, p. 301-318. *In* E. K. Wagner (ed.), Herpesvirus transcription and its regulation. CRC Press, Boca Raton, Fla.

215. **Ryckman, B. J., and R. J. Roller.** 2004. Herpes simplex virus type 1 primary envelopment: UL34 protein modification and the US3-UL34 catalytic relationship. J Virol **78:**399-412.
216. **Saper, M. A., P. J. Bjorkman, and D. C. Wiley.** 1991. Refined structure of the human histocompatibility antigen HLA-A2 at 2.6 A resolution. J Mol Biol **219:**277-319.
217. **Sato, H., L. D. Callanan, L. Pesnicak, T. Krogmann, and J. I. Cohen.** 2002. Varicella-zoster virus (VZV) ORF17 protein induces RNA cleavage and is critical for replication of VZV at 37 degrees C but not 33 degrees C. J Virol **76:**11012-23.
218. **Sato, H., L. Pesnicak, and J. I. Cohen.** 2003. Varicella-zoster virus ORF47 protein kinase, which is required for replication in human T cells, and ORF66 protein kinase, which is expressed during latency, are dispensable for establishment of latency. J Virol **77:**11180-5.
219. **Schaap-Nutt, A., M. Sommer, X. Che, L. Zerboni, and A. M. Arvin.** 2006. Orf66 Protein Kinase Function Is Required for T Cell Tropism of Varicella-Zoster Virus in Vivo. J Virol.
220. **Schaap, A., J. F. Fortin, M. Sommer, L. Zerboni, S. Stamatis, C. C. Ku, G. P. Nolan, and A. M. Arvin.** 2005. T-cell tropism and the role of ORF66 protein in pathogenesis of varicella-zoster virus infection. J Virol **79:**12921-33.
221. **Schumacher, D., B. K. Tischer, S. Trapp, and N. Osterrieder.** 2005. The protein encoded by the US3 orthologue of Marek's disease virus is required for efficient de-envelopment of perinuclear virions and involved in actin stress fiber breakdown. J Virol **79:**3987-97.
222. **Sciortino, M. T., M. Suzuki, B. Taddeo, and B. Roizman.** 2001. RNAs extracted from herpes simplex virus 1 virions: apparent selectivity of viral but not cellular RNAs packaged in virions. J Virol **75:**8105-16.
223. **Sloan, D. D., G. Zahariadis, C. M. Posavad, N. T. Pate, S. J. Kussick, and K. R. Jerome.** 2003. CTL are inactivated by herpes simplex virus-infected cells expressing a viral protein kinase. J Immunol **171:**6733-41.
224. **Soong, W., J. C. Schultz, A. C. Patera, M. H. Sommer, and J. I. Cohen.** 2000. Infection of human T lymphocytes with varicella-zoster virus: an analysis with viral mutants and clinical isolates. J Virol **74:**1864-70.
225. **Spengler, M. L., W. T. Ruyechan, and J. Hay.** 2000. Physical interaction between two varicella zoster virus gene regulatory proteins, IE4 and IE62. Virology **272:**375-81.
226. **Stevenson, D., K. L. Colman, and A. J. Davison.** 1994. Characterization of the putative protein kinases specified by varicella-zoster virus genes 47 and 66. J Gen Virol **75 (Pt 2):**317-26.
227. **Stevenson, D., K. L. Colman, and A. J. Davison.** 1994. Delineation of a sequence required for nuclear localization of the protein encoded by varicella-zoster virus gene 61. J Gen Virol **75 (Pt 11):**3229-33.
228. **Storkus, W. J., H. J. Zeh, 3rd, R. D. Salter, and M. T. Lotze.** 1993. Identification of T-cell epitopes: rapid isolation of class I-presented peptides from viable cells by mild acid elution. J Immunother **14:**94-103.
229. **Tagawa, T., T. Kuroki, P. K. Vogt, and K. Chida.** 1995. The cell cycle-dependent nuclear import of v-Jun is regulated by phosphorylation of a serine adjacent to the nuclear localization signal. J Cell Biol **130:**255-63.

230. **Terhune, S. S., J. Schroer, and T. Shenk.** 2004. RNAs are packaged into human cytomegalovirus virions in proportion to their intracellular concentration. J Virol **78:**10390-8.
231. **Tigges, M. A., S. Leng, D. C. Johnson, and R. L. Burke.** 1996. Human herpes simplex virus (HSV)-specific CD8+ CTL clones recognize HSV-2-infected fibroblasts after treatment with IFN-gamma or when virion host shutoff functions are disabled. J Immunol **156:**3901-10.
232. **Tomazin, R., A. B. Hill, P. Jugovic, I. York, P. van Endert, H. L. Ploegh, D. W. Andrews, and D. C. Johnson.** 1996. Stable binding of the herpes simplex virus ICP47 protein to the peptide binding site of TAP. Embo J **15:**3256-66.
233. **Trgovcich, J., C. Cebulla, P. Zimmerman, and D. D. Sedmak.** 2006. Human cytomegalovirus protein pp71 disrupts major histocompatibility complex class I cell surface expression. J Virol **80:**951-63.
234. **Tyler, J. K., K. E. Allen, and R. D. Everett.** 1994. Mutation of a single lysine residue severely impairs the DNA recognition and regulatory functions of the VZV gene 62 transactivator protein. Nucleic Acids Res **22:**270-8.
235. **Tyler, J. K., and R. D. Everett.** 1993. The DNA binding domain of the varicella-zoster virus gene 62 protein interacts with multiple sequences which are similar to the binding site of the related protein of herpes simplex virus type 1. Nucleic Acids Res **21:**513-22.
236. **Vafai, A., Z. Wroblewska, and L. Graf.** 1990. Antigenic cross-reaction between a varicella-zoster virus nucleocapsid protein encoded by gene 40 and a herpes simplex virus nucleocapsid protein. Virus Res **15:**163-74.
237. **Van Minnebruggen, G., H. W. Favoreel, L. Jacobs, and H. J. Nauwynck.** 2003. Pseudorabies virus US3 protein kinase mediates actin stress fiber breakdown. J Virol **77:**9074-80.
238. **van Zijl, M., H. van der Gulden, N. de Wind, A. Gielkens, and A. Berns.** 1990. Identification of two genes in the unique short region of pseudorabies virus; comparison with herpes simplex virus and varicella-zoster virus. J Gen Virol **71 (Pt 8):**1747-55.
239. **Varnum, S. M., D. N. Streblow, M. E. Monroe, P. Smith, K. J. Auberry, L. Pasa-Tolic, D. Wang, D. G. Camp, 2nd, K. Rodland, S. Wiley, W. Britt, T. Shenk, R. D. Smith, and J. A. Nelson.** 2004. Identification of proteins in human cytomegalovirus (HCMV) particles: the HCMV proteome. J Virol **78:**10960-6.
240. **Verjans, G. M., R. Q. Hintzen, J. M. van Dun, A. Poot, J. C. Milikan, J. D. Laman, A. W. Langerak, P. R. Kinchington, and A. D. Osterhaus.** 2007. Selective retention of herpes simplex virus-specific T cells in latently infected human trigeminal ganglia. Proc Natl Acad Sci U S A **104:**3496-501.
241. **Wagenaar, F., J. M. Pol, B. Peeters, A. L. Gielkens, N. de Wind, and T. G. Kimman.** 1995. The US3-encoded protein kinase from pseudorabies virus affects egress of virions from the nucleus. J Gen Virol **76 (Pt 7):**1851-9.
242. **Wang, Z., M. D. Gershon, O. Lungu, C. A. Panagiotidis, Z. Zhu, Y. Hao, and A. A. Gershon.** 1998. Intracellular transport of varicella-zoster glycoproteins. J Infect Dis **178 Suppl 1:**S7-12.
243. **Wang, Z. G., D. Ruggero, S. Ronchetti, S. Zhong, M. Gaboli, R. Rivi, and P. P. Pandolfi.** 1998. PML is essential for multiple apoptotic pathways. Nat Genet **20:**266-72.

244. **Ward, P. L., W. O. Ogle, and B. Roizman.** 1996. Assemblons: nuclear structures defined by aggregation of immature capsids and some tegument proteins of herpes simplex virus 1. J Virol **70:**4623-31.
245. **Williams, B. J., J. R. Boyne, D. J. Goodwin, L. Roaden, G. M. Hautbergue, S. A. Wilson, and A. Whitehouse.** 2005. The prototype gamma-2 herpesvirus nucleocytoplasmic shuttling protein, ORF 57, transports viral RNA through the cellular mRNA export pathway. Biochem J **387:**295-308.
246. **Wolff, B., J. J. Sanglier, and Y. Wang.** 1997. Leptomycin B is an inhibitor of nuclear export: inhibition of nucleo-cytoplasmic translocation of the human immunodeficiency virus type 1 (HIV-1) Rev protein and Rev-dependent mRNA. Chem Biol **4:**139-47.
247. **Wu, C. L., and K. W. Wilcox.** 1991. The conserved DNA-binding domains encoded by the herpes simplex virus type 1 ICP4, pseudorabies virus IE180, and varicella-zoster virus ORF62 genes recognize similar sites in the corresponding promoters. J Virol **65:**1149-59.
248. **Wysocka, J., and W. Herr.** 2003. The herpes simplex virus VP16-induced complex: the makings of a regulatory switch. Trends Biochem Sci **28:**294-304.
249. **Xia, K., N. A. DeLuca, and D. M. Knipe.** 1996. Analysis of phosphorylation sites of herpes simplex virus type 1 ICP4. J Virol **70:**1061-71.
250. **Xia, K., D. M. Knipe, and N. A. DeLuca.** 1996. Role of protein kinase A and the serine-rich region of herpes simplex virus type 1 ICP4 in viral replication. J Virol **70:**1050-60.
251. **Yao, F., and R. J. Courtney.** 1992. Association of ICP0 but not ICP27 with purified virions of herpes simplex virus type 1. J Virol **66:**2709-16.
252. **Yao, F., and R. J. Courtney.** 1989. A major transcriptional regulatory protein (ICP4) of herpes simplex virus type 1 is associated with purified virions. J Virol **63:**3338-44.
253. **Zabierowski, S., and N. A. DeLuca.** 2004. Differential cellular requirements for activation of herpes simplex virus type 1 early (tk) and late (gC) promoters by ICP4. J Virol **78:**6162-70.
254. **Zerboni, L., S. Hinchliffe, M. H. Sommer, H. Ito, J. Besser, S. Stamatis, J. Cheng, D. Distefano, N. Kraiouchkine, A. Shaw, and A. M. Arvin.** 2005. Analysis of varicella zoster virus attenuation by evaluation of chimeric parent Oka/vaccine Oka recombinant viruses in skin xenografts in the SCIDhu mouse model. Virology **332:**337-46.
255. **Zerboni, L., C. C. Ku, C. D. Jones, J. L. Zehnder, and A. M. Arvin.** 2005. Varicella-zoster virus infection of human dorsal root ganglia in vivo. Proc Natl Acad Sci U S A **102:**6490-5.
256. **Zhang, F., R. L. White, and K. L. Neufeld.** 2000. Phosphorylation near nuclear localization signal regulates nuclear import of adenomatous polyposis coli protein. Proc Natl Acad Sci U S A **97:**12577-82.
257. **Zhang, Y., and D. B. Williams.** 2006. Assembly of MHC class I molecules within the endoplasmic reticulum. Immunol Res **35:**151-62.
258. **Zhao, B., and R. P. Ricciardi.** 2006. E1A is the component of the MHC class I enhancer complex that mediates HDAC chromatin repression in adenovirus-12 tumorigenic cells. Virology **352:**338-44.
259. **Zhou, Z. H., D. H. Chen, J. Jakana, F. J. Rixon, and W. Chiu.** 1999. Visualization of tegument-capsid interactions and DNA in intact herpes simplex virus type 1 virions. J Virol **73:**3210-8.

260. **Zhu, Z., M. D. Gershon, Y. Hao, R. T. Ambron, C. A. Gabel, and A. A. Gershon.** 1995. Envelopment of varicella-zoster virus: targeting of viral glycoproteins to the trans-Golgi network. J Virol **69:**7951-9.
261. **Zhu, Z., Y. Hao, M. D. Gershon, R. T. Ambron, and A. A. Gershon.** 1996. Targeting of glycoprotein I (gE) of varicella-zoster virus to the trans-Golgi network by an AYRV sequence and an acidic amino acid-rich patch in the cytosolic domain of the molecule. J Virol **70:**6563-75.
262. **Zimber, A., Q. D. Nguyen, and C. Gespach.** 2004. Nuclear bodies and compartments: functional roles and cellular signalling in health and disease. Cell Signal **16:**1085-104.